International Journal of
Molecular Sciences

Chromatin, Epigenetics and Plant Physiology

Edited by
Jiří Fajkus and Miloslava Fojtová

Printed Edition of the Special Issue Published in
International Journal of Molecular Sciences

www.mdpi.com/journal/ijms

MDPI

Chromatin, Epigenetics and Plant Physiology

Chromatin, Epigenetics and Plant Physiology

Special Issue Editors

Jiří Fajkus
Miloslava Fojtová

MDPI • Basel • Beijing • Wuhan • Barcelona • Belgrade

Special Issue Editors

Jiří Fajkus
Masaryk University, CEITEC
Mendel Centre for Plant
Genomics and Proteomics Brno
Czech Republic

Miloslava Fojtová
Masaryk University, CEITEC,
Mendel Centre for Plant
Genomics and Proteomics Brno
Czech Republic

Editorial Office
MDPI
St. Alban-Anlage 66
4052 Basel, Switzerland

This is a reprint of articles from the Special Issue published online in the open access journal *International Journal of Molecular Sciences* (ISSN 1422-0067) from 2019 to 2020 (available at: https://www.mdpi.com/journal/ijms/special_issues/plant_chromatin).

For citation purposes, cite each article independently as indicated on the article page online and as indicated below:

LastName, A.A.; LastName, B.B.; LastName, C.C. Article Title. *Journal Name* **Year**, *Article Number*, Page Range.

ISBN 978-3-03936-028-4 (Hbk)
ISBN 978-3-03936-029-1 (PDF)

Contents

About the Special Issue Editors

Jiří Fajkus: In 1987, he achieved MSc. and RNDr. titles from Biochemistry, J. E. Purkinje University Brno (now Masaryk University), Czech Republic. He was a research fellow and then a PhD student at the Institute of Biophysics, Czech Academy of Sciences. After completing his PhD in Biophysics in 1992 (thesis title 'Domains in the Eukaryotic Genomes'), he worked as a postdoctoral fellow at the Laval University Cancer Research Centre, Quebec, Canada (1992–1993, 1995, Lab. of Prof. Ronald Hancock). In 1996, he established his own research group at the Institute of Biophysics, Czech Academy of Sciences. In 1998, he also started a new research laboratory at the Faculty of Science, Masaryk University (MU), which now continues as the Laboratory of Functional Genomics and Proteomics, National Centre for Biomolecular Research, Faculty of Science, MU. In 2003, he became an Associate Professor of Molecular Biology and Genetics, and in 2010, a Full Professor of Molecular Biology and Genetics, MU, Brno, Czech Republic. In 2011, he became the Head of the Mendel Centre for Plant Genomics and Proteomics at CEITEC—Central European Institute of Technology, MU. His research interests cover the biology of telomeres, chromatin structure and function, epigenetics, DNA repair and plant molecular biology. The major achievements of his research group include the first description of telomerase activity in plant cells (1996), stable telomere maintenance during plant ontogenesis and the reversible regulation of telomerase in plant cells (1998), the evolutionary variability of plant telomeres (2003), characterisation of a novel type of genome instability in plant CAF-1 mutants—specific and progressive loss of telomeres and rDNA, epigenetic reprogramming of rRNA genes (2010), characterization of AtTRB proteins as components of a plant shelterin-like telomere complex and epigenetic factor (2014, 2016), determination of unknown/non-canonical telomeres in plants of the genera Genlisea, Cestrum and Allium using the original BAL31-NGS method to identify telomere DNA, even in giant genomes with a small number of chromosomes for this purpose (2015–2017). The major recent achievement of his laboratory is the identification of the first bona fide telomerase RNA subunits across land plants with canonical and non-canonical telomeres, and the demonstration of their monophyletic origin (2019).

Miloslava Fojtová: In 1991, she achieved an MSc. title at Biochemistry, Charles University, Prague, Czech Republic. She was a research fellow and then a PhD student of Biophysics at the Institute of Biophysics, Czech Academy of Sciences. After completing her PhD in 2000 (thesis title 'Genetic and Epigenetic Changes of Plant Genomes'), she continued at the Institute of Biophysics, Department of Molecular Epigenetics as a postdoc. In 2010, she moved to Masaryk University, Brno, and joined Jiří Fajkus' research group. In 2017, she became an Associate Professor of Biomolecular Chemistry, MU. Now, she works as a senior scientist and principal investigator at the Mendel Centre for Plant Genomics and Proteomics, CEITEC—Central European Institute of Technology, MU, and the Laboratory of Functional Genomics and Proteomics, National Centre for Biomolecular Research, Faculty of Science, MU. Her research interests include plant telomeres and telomerase, epigenetic regulations and the impact of developmental and stress factors on plant genome and epigenome. She actively participates in the teaching and supervision of undergraduate and graduate students and significantly contributes to most research activities of J. Fajkus' research group.

International Journal of
Molecular Sciences

MDPI

Editorial

Chromatin, Epigenetics and Plant Physiology

Miloslava Fojtová [1,2,3] and Jiří Fajkus [1,2,3,*]

[1] Mendel Centre for Plant Genomics and Proteomics, CEITEC, Masaryk University, CZ-62500 Brno, Czech Republic; fojtova@sci.muni.cz
[2] Laboratory of Functional Genomics and Proteomics, NCBR, Faculty of Science, Masaryk University, CZ-61137 Brno, Czech Republic
[3] Department of Cell Biology and Radiobiology, Institute of Biophysics of the Czech Academy of Sciences, v.v.i., CZ-61265 Brno, Czech Republic
* Correspondence: fajkus@sci.muni.cz

Received: 7 April 2020; Accepted: 14 April 2020; Published: 16 April 2020

The ever-increasing interest in epigenetics comes from the fact that in the diverse life situations of organisms, e.g., in cell differentiation, developmental decisions, or responses to biotic and abiotic stresses, it is primarily the reprogramming of the regulation of the existing genetic information, rather than its direct change, that solves the problem. Epigenetic mechanisms allow the organism to channel the appropriate response through diverse particular molecular tools modifying distinct levels of the structure of chromatin. Chromatin is thus marked with certain signals, for example, DNA methylation, posttranslational modifications of histones, incorporation of specific histone variants, or chromatin remodeling. These signals, written by respective enzymes and complexes, termed as epigenetic writers (e.g., DNA methyltransferases, histone methyltransferases, and histone acetyltransferases) have to find their readers—biomolecules recognizing the specific mark, and erasers which are capable of resetting the program. Recent data suggest a deep interconnection of individual epigenetic players, which frequently act together as components of the same multi-subunit complexes. For example, methylcytosine binding protein MeCP2 (a reader) recruits histone deacetylase (an eraser) and H3K9 histone methyltransferase Suv39h1 (a writer), and in this way reinforces the repressive state of a chromatin region [1,2]. Recent research in plants brings many novel findings elucidating the interdependence of diverse epigenetic mechanisms and their crosstalk with various signaling pathways, including the action of phytohormones and reactive oxygen and nitrogen species. Using these molecular tools, chromatin structure decides which particular set of genes will be active in a particular physiological process.

The special issue "Chromatin, Epigenetics and Plant Physiology" in the International Journal of Molecular Sciences comprises two review articles and eight original research papers (Table 1). All contributions deal with important aspects of epigenetic regulations of crucial cellular processes involved in plant growth and development.

Four articles, one review, and three research papers deal with chromatin remodeling complexes. Wang et al. [3] provide a review on the role of Arabidopsis SWR1 and INO80 chromatin remodeling complexes involved in the regulation of the replacement of nucleosomal H2A/H2B dimers with H2A.Z/H2B. The authors describe the composition of the SWR1/INO80-c complex and discuss its diverse nuclear roles ranging from repair processes to regulation of gene expression. Guo et al. [4] report on the involvement of the chromatin remodeler encoded by the *OsCHR4* gene in regulation of rice leaf morphology, via modulation of accumulation of cuticle wax on leaf surfaces and auxin biosynthesis. Expression profiles and subcellular localizations of tomato SWI3-like proteins were studied by Zhao et al. [5]. The authors further identify interactions of these subunits of the chromatin remodeling complex with proteins participating in the reproductive development. Their observations support the idea of evolutionary conservation of SWI3 physiological functions in different plant species. Similarly, the involvement of the SWI subunits of the chromatin remodeling complex in

temperature-dependent regulation of plant growth and developmental responses in Arabidopsis is reported by Gratkowska-Zmuda et al. [6]. Altogether, these results demonstrate the importance of the proper chromatin remodeling in crucial cellular processes, including gene expression, cell cycle regulation, DNA replication and repair, and hormone signaling.

Table 1. Contributors to the special issue "Chromatin, Epigenetics and Plant Physiology".

Authors	Title	Type
Wang et al. [3]	Roles of the INO80 and SWR1 Chromatin Remodeling Complexes in Plants	Review
Guo et al. [4]	Mutations in the Rice OsCHR4 Gene, Encoding a CHD3 Family Chromatin Remodeler, Induce Narrow and Rolled Leaves with Increased Cuticular Wax	Original Research
Zhao et al. [5]	Identification and Characterization of Tomato SWI3-Like Proteins: Overexpression of SlSWIC Increases the Leaf Size in Transgenic Arabidopsis	Original Research
Gratkowska-Zmuda et al. [6]	The SWI/SNF ATP-Dependent Chromatin Remodeling Complex in Arabidopsis Responds to Environmental Changes in Temperature-Dependent Manner	Original Research
Krispil et al. [7]	The Position and Complex Genomic Architecture of Plant T-DNA Insertions Revealed by 4SEE	Original Research
Lochmanová et al. [8]	Different Modes of Action of Genetic and Chemical Downregulation of Histone Deacetylases with Respect to Plant Development and Histone Modifications	Original Research
Koláčková et al. [9]	Nuclear Disposition of Alien Chromosome Introgressions into Wheat and Rye Using 3D-FISH	Original Research
Zhang et al. [10]	Identification and Characterization of circRNAs Responsive to Methyl Jasmonate in Arabidopsis thaliana	Original Research
Boudichevskaia et al. [11]	Depletion of KNL2 Results in Altered Expression of Genes Involved in Regulation of the Cell Cycle, Transcription, and Development in Arabidopsis	Original Research
R.M.S. et al. [12]	Redox Components: Key-Regulators of Epigenetic Modifications in Plants	Review

Results presented in two papers within the special issue "Chromatin, Epigenetics, and Plant Physiology" were obtained using specific advanced methodical approaches. Circular chromosome conformation capture (4C)-based method was utilized by Krispil et al. [7] for the detection of the entire scope of T-DNA insertions, by capturing the local enrichment of spatial chromosomal associations in their genomic proximity without prior knowledge of their genomic locations in Arabidopsis transgenic lines. This approach enables the identification of previously unmapped T-DNA insertions and related chromosomal rearrangements and is applicable to any plant with a sequenced genome. Lochmanová et al. [8] studied the acetylation of histone proteins by a mass spectrometry-based proteomic approach. They conclude that the effect of epigenetically active drugs on early plant development is complex and is not restricted to the ability of these compounds to modulate the levels of histone acetylation marks.

Koláčková et al. [9] solved an interesting problem of the spatial organization of parental genomes in the somatic nuclei of interspecific plant hybrids. They demonstrate that domains of introgressed chromosomes are highly stable among the tissue types and during the cell cycle phases. High-throughput sequencing of Arabidopsis seedlings exposed to methyl jasmonic acid was performed by Zhang et al. [10] to identify differentially expressed circular RNAs. Based on their data, differentially expressed circular RNAs are involved in metabolic and developmental processes and are supposed to play important roles in methyl jasmonic acid-mediated signaling. Boudichevskaia et al. [11] dealt with the characterization of the role of Arabidopsis KNL2 (kinetochore null 2), which is important for deposition of CENH3 at centromeric regions. Transcriptomic analysis of mutant plants reveals that the *KNL2* gene loss of function affects processes of cell cycle regulation, transcription, development, and DNA repair. In the review article by R.M.S. et al. [12], the impact of redox components on activities of important epigenetic regulators was described. Authors provide an integrated view on the roles

of oxidants (reactive oxygen species and nitric oxide) and antioxidants (pyridine nucleotides and glutathione) in the modulation of DNA methylation and histone modifications in plants.

Together, this collection offers diverse insights into the current plant epigenetics to allow readers to update their knowledge on the described phenomena and mechanisms in this highly complex and quickly evolving field.

Funding: M.F. and J.F. are supported by the European Regional Development Fund-Project 'SINGING PLANT' (CZ.02.1.01/0.0/0.0/16_026/0008446) and the Ministry of Education, Youth and Sports of the Czech Republic—project CEITEC 2020 (LQ1601).

Conflicts of Interest: The authors declare no conflict of interest.

References

1. Fuks, F.; Hurd, P.J.; Wolf, D.; Nan, X.S.; Bird, A.P.; Kouzarides, T. The Methyl-CpG-binding protein MeCP2 links DNA methylation to histone methylation. *J. Biol. Chem.* **2003**, *278*, 4035–4040. [CrossRef] [PubMed]
2. Jones, P.L.; Veenstra, G.J.C.; Wade, P.A.; Vermaak, D.; Kass, S.U.; Landsberger, N.; Strouboulis, J.; Wolffe, A.P. Methylated DNA and MeCP2 recruit histone deacetylase to repress transcription. *Nat. Genet.* **1998**, *19*, 187–191. [CrossRef] [PubMed]
3. Wang, J.; Gao, S.; Peng, X.; Wu, K.; Yang, S. Roles of the INO80 and SWR1 Chromatin Remodeling Complexes in Plants. *Int. J. Mol. Sci.* **2019**, *20*, 4591. [CrossRef] [PubMed]
4. Guo, T.; Wang, D.; Fang, J.; Zhao, J.; Yuan, S.; Xiao, L.; Li, X. Mutations in the Rice OsCHR4 Gene, Encoding a CHD3 Family Chromatin Remodeler, Induce Narrow and Rolled Leaves with Increased Cuticular Wax. *Int. J. Mol. Sci.* **2019**, *20*, 2567. [CrossRef] [PubMed]
5. Zhao, Z.; Li, T.; Peng, X.; Wu, K.; Yang, S. Identification and Characterization of Tomato SWI3-Like Proteins: Overexpression of SlSWIC Increases the Leaf Size in Transgenic Arabidopsis. *Int. J. Mol. Sci.* **2019**, *20*, 5121. [CrossRef] [PubMed]
6. Gratkowska-Zmuda, D.; Kubala, S.; Sarnowska, E.; Cwiek, P.; Oksinska, P.; Steciuk, J.; Rolicka, A.; Zaborowska, M.; Bucior, E.; Maassen, A.; et al. The SWI/SNF ATP-Dependent Chromatin Remodeling Complex in Arabidopsis Responds to Environmental Changes in Temperature-Dependent Manner. *Int. J. Mol. Sci.* **2020**, *21*, 762. [CrossRef] [PubMed]
7. Krispil, R.; Tannenbaum, M.; Sarusi-Portuguez, A.; Loza, O.; Raskina, O.; Hakim, O. The Position and Complex Genomic Architecture of Plant T-DNA Insertions Revealed by 4SEE. *Int. J. Mol. Sci.* **2020**, *21*, 2373. [CrossRef] [PubMed]
8. Lochmanová, G.; Ihnatová, I.; Kuchaříková, H.; Brabencová, S.; Zachová, D.; Fajkus, J.; Zdráhal, Z.; Fojtová, M. Different Modes of Action of Genetic and Chemical Downregulation of Histone Deacetylases with Respect to Plant Development and Histone Modifications. *Int. J. Mol. Sci.* **2019**, *20*, 5093. [CrossRef]
9. Koláčková, V.; Perničková, K.; Vrána, J.; Duchoslav, M.; Jenkins, G.; Phillips, D.; Turkosi, E.; Šamajová, O.; Sedlářová, M.; Šamaj, J.; et al. Nuclear Disposition of Alien Chromosome Introgressions into Wheat and Rye Using 3D-FISH. *Int. J. Mol. Sci.* **2019**, *20*, 4143. [CrossRef]
10. Zhang, J.; Liu, R.; Zhu, Y.; Gong, J.; Yin, S.; Sun, P.; Feng, H.; Wang, Q.; Zhao, S.; Wang, Z.; et al. Identification and Characterization of circRNAs Responsive to Methyl Jasmonate in Arabidopsis thaliana. *Int. J. Mol. Sci.* **2020**, *21*, 792. [CrossRef] [PubMed]
11. Boudichevskaia, A.; Houben, A.; Fiebig, A.; Prochazkova, K.; Pecinka, A.; Lermontova, I. Depletion of KNL2 Results in Altered Expression of Genes Involved in Regulation of the Cell Cycle, Transcription, and Development in Arabidopsis. *Int. J. Mol. Sci.* **2019**, *20*, 5726. [CrossRef] [PubMed]
12. Saravana Kumar, R.M.; Wang, Y.; Zhang, X.; Cheng, H.; Sun, L.; He, S.; Hao, F. Redox Components: Key Regulators of Epigenetic Modifications in Plants. *Int. J. Mol. Sci.* **2020**, *21*, 1419. [CrossRef]

International Journal of
Molecular Sciences

MDPI

Review

Roles of the INO80 and SWR1 Chromatin Remodeling Complexes in Plants

Jianhao Wang [1,2], Sujuan Gao [3], Xiuling Peng [1,2], Keqiang Wu [4,*] and Songguang Yang [1,*]

1 Key Laboratory of South China Agricultural Plant Molecular Analysis and Genetic Improvement, Guangdong Provincial Key Laboratory of Applied Botany, South China Botanical Garden, Chinese Academy of Sciences, Guangzhou 510650, China; xn2112wjh@163.com (J.W.); m13203206354_2@163.com (X.P.)
2 University of Chinese Academy of Sciences, Chinese Academy of Sciences, Beijing 100049, China
3 College of Light Industry and Food Science, Zhongkai University of Agriculture and Engineering, Guangzhou 510225, China; gaoshj@126.com
4 Institute of Plant Biology, National Taiwan University, Taipei 106, Taiwan
* Correspondence: kewu@ntu.edu.tw (K.W.); yangsongguang@scbg.ac.cn (S.Y.)

Received: 21 August 2019; Accepted: 13 September 2019; Published: 17 September 2019

Abstract: Eukaryotic genes are packed into a dynamic but stable nucleoprotein structure called chromatin. Chromatin-remodeling and modifying complexes generate a dynamic chromatin environment that ensures appropriate DNA processing and metabolism in various processes such as gene expression, as well as DNA replication, repair, and recombination. The INO80 and SWR1 chromatin remodeling complexes (INO80-c and SWR1-c) are ATP-dependent complexes that modulate the incorporation of the histone variant H2A.Z into nucleosomes, which is a critical step in eukaryotic gene regulation. Although SWR1-c has been identified in plants, plant INO80-c has not been successfully isolated and characterized. In this review, we will focus on the functions of the SWR1-c and putative INO80-c (SWR1/INO80-c) multi-subunits and multifunctional complexes in *Arabidopsis thaliana*. We will describe the subunit compositions of the SWR1/INO80-c and the recent findings from the standpoint of each subunit and discuss their involvement in regulating development and environmental responses in *Arabidopsis*.

Keywords: chromatin remodeling; INO80/SWR1 complexes; NuA4 complex; histone variant H2A.Z; gene regulation; plant development

1. Introduction

Eukaryotic DNA is packaged with histones to form an inherently stable complex structure known as chromatin. The basic repeating unit of chromatin is the nucleosome, which consists of approximately 146 base pairs of DNA wrapped on a histone octamer containing two molecules each of histone H2A, H2B, H3, and H4 [1]. Therefore, to allow DNA processing, such as DNA replication, repair, and recombination, a dynamic chromatin environment is needed. Two main players, histone post-translational modifications by histone-modifying enzymes and nucleosome positioning by ATP-dependent chromatin-remodeling complexes (CRCs) are involved in the regulation of chromatin dynamics [2,3]. In general, CRCs can destabilize the interactions between histone octamers and DNA by using the energy derived from ATP hydrolysis [4], thus increasing the binding efficiency of transcription factors.

The catalytic subunit (ATPase) of CRCs belongs to the SWI/SNF family [5], which is part of a large superfamily of helicases and translocases called superfamily 2 (SF2). The SWI/SNF family is named after the first identified CRC from *S. cerevisiae* by the examination of mating type switching (*SWI*) and sucrose nonfermenting (*SNF*) mutants [6]. Further studies conducted with *Drosophila*, mammals, and plants revealed that CRCs widely exist in eukaryotes. Based on the evolutionarily conserved central

ATPase subunit, CRCs are currently classified into four subfamilies: SWI/SNF, ISWI (imitation SWI), INO80 (Inositol Requiring 80) and CHD (chromo and DNA-binding domain) [7]. CRCs of the INO80 family include the yeast INO80 complex (INO80-c) and its orthologues in humans and plants, the yeast SWR1 (SWi2/snf2-Related 1) complex (SWR1-c) and its orthologues SRCAP (SNF2-RELATED CBP ACTIVATOR PROTEIN) (human) and SWR1 (*Arabidopsis*) (Table 1). Among those families, SWR1/INO80-c plays essential roles in DNA repair, checkpoint regulation, DNA replication, telomere maintenance and chromosome segregation [8,9].

Table 1. Compositions of INO80, SWR1 and NuA4 Complexes in *Arabidopsis.*

Complex									
Organism	**Yeast**			**Human**			***Arabidopsis***		
Family and Composition	**INO80**	**SWR1**	**NuA4**	**INO80**	**SWR1/SRCAP**	**NuA4/Tip60**	**INO80**	**SWR1**	**NuA4**
ATPase or Acetyltransferase	Ino80	Swr1	Eaf1 **, Esa1 *	hIno80	SRCAP	p400 **, Tip60 *	INO80	PIE1	HAM1/2 *, EAF1 **
Noncatalytic homologous subunits	Rvb1, Rvb2			Tip49a, Tip49b			RVB1/RIN1		
							RVB2A, RVB2B		
	Arp4, Actin1			BAF53a			ARP4, ACT1		
	Arp5, Arp8	Arp6		Arp5, Arp8	Arp6	Actin	ARP5, ARP9	ARP6	
	Taf14	Yaf9		GAS41			GAS41/YAF9A, TAF14/YAF9B		
	Ies2, Ies6			hIes2, hIes6					
	Swc4/Eaf2			DMAP1			SWC4		
	Swc2/Vps72			YL-1			SWC2		
	Swc6/Vps71			ZnF-HIT1			SWC6		
	Bdf1			Brd8/TRCp120					
	H2A.Z, H2B			H2A.Z, H2B			H2A.Z, H2B		
			Tra1			TRRAP			TRA1
			Epl1			EPC1			
			Yng2			ING3			ING1, ING2
			Eaf3			MRG15			MRG1, MRG2
			Eaf5						
			Eaf7			MRGBP			
			Eaf6			hEaf6			
Unique	Ies1, Ies3, Ies 4, Ies5, Nhp10	Swc3,5,7		Amida, NFRKB, MCRS1, FLJ90652, FLJ20309		MRGX, FLJ11730, MRGBP, EPC1, EPC-like	MBD9, AL5-7		

* and ** represent the acetyltransferase and ATPase subunits of NuA4-c, respectively. The subunits of INO80 and NuA4 complexes in *Arabidopsis* are based on the sequence homology and protein-protein interacting data.

Although the molecular mechanisms of SWR1/INO80-c are largely unknown, a large body of genetic and biochemical evidence strongly suggests that SWR1/INO80-c are also present in plants. In this review, we compare the functions and subunit compositions of the SWR1/INO80-c of plants and other organisms including yeasts and mammals. We also discuss the recent investigations underpinning the involvement of SWR1/INO80-c subunits in regulating key plant growth and development processes, as well as environmental responses.

2. Chromatin Remodeling Functions of INO80 and SWR1 CRCs

Biochemical analyses indicated that SWR1-c promotes the replacement of nucleosomal H2A/H2B dimers with H2A.Z/H2B [10], while INO80-c catalyzes the reverse dimer exchange reaction [11–13]. Further studies demonstrated that H3-K56Ac (H3K56 acetylation) or H3-K56Q (substitution H3-K56 for glutamine) switches the substrate specificity of SWR1-c, inhibiting H2A.Z deposition [13]. Consistently, it was observed that H2A.Z deposition is inhibited by H3-K56Q but not by SWR1-c or INO80-c [14]. However, recent direct EMSA assays indicated that INO80-c catalyzes the replacement of H2A.Z/H2B with H2A/H2B on an H2A.Z/H3-K56Q substrate [15]. The structural analysis of the core INO80-c from

the fungus *Chaetomium thermophilum* showed that the two AAA$^+$ ATPases, Rvb1 (RuvB-like protein 1) and Rvb2, form heterohexamers, acting as a 'stator' for the motor (ATPase) and nucleosome-gripping subunits [16]. The ATPase of INO80-c binds to nucleosomal DNA at superhelical location 6 (SHL6), unwraps approximately 15 base pairs, disrupts the H2A–DNA contacts and is poised to pump entry DNA into the nucleosome [16]. Arp5 (Actin-Related Protein 5)–Ies6 (Ino Eighty Subunit 6) binds at SHL2 and SHL 3 acting as a counter grip for the motor on the other side of the H2A–H2B dimer. On the other hand, yeast SWR1-c is also assembled around a heterohexameric core of the Rvb1 and Rvb2 subunits, and the motor subunit binds at SHL2, a position it shares in common with other remodelers [17].

In yeast, the histone variant H2A.Z (Htz1) is enriched in intergenic regions compared with coding regions, and it is involved in the activation of a subset of genes [18]. Meanwhile, incorporation of Htz1 into nucleosomes influences histone modifications and chromatin remodeling, supporting a role for Htz1 at inactive promoters [18]. In *Arabidopsis*, the high-resolution ChIP-exo assay showed that SWR1 and INO80-c are targeted selectively to the +1 nucleosome of essentially all genes via their subunits [19]. For instance, Swc4 (SWR complex subunit 4) and Swc5 occupy nucleosome positions in the body of genes in addition to +1, while Rvb1 and Swc2 have correlated co-occupancy levels that span a wide range over different promoters [19]. Interestingly, a previous study showed that SWR1/INO80-c may be involved in DNA methylation, since a strong anti-correlation between DNA methylation and H2A.Z deposition was observed [20]. However, the H2A.Z deposition at gene bodies is correlated with a lower transcription level, presumably by destabilizing constitutive gene expression rather than promoting gene body DNA methylation [21]. The genomic binding maps of the subunits of SWR1/INO80-c suggested that many subunits have a rather plastic organization that allows their subunits to exchange between the two complexes [19].

3. The Subunits of INO80 and SWR1 CRCs

yIno80, the ATPase of yeast INO80 complex, was identified in a screen for regulators of phospholipid biosynthesis [22]. Further studies found that yIno80 associates with 14 other proteins including Rvb1, Rvb2, Arp4, Arp5, Arp8, actin1, Taf14 (TATA binding protein-Associated Factor 14), Ies1-6, and Nhp10 (Non-Histone Protein 10) to form a complex (INO80 complex) of 1.2 Mda [22,23] (Table 1). ySwr1, the homolog of yIno80, was subsequently identified and found to catalyze the exchange of H2A for Htz1 [10,24]. Proteomic data indicated that SWR1-c consists of 14 subunits sharing 4 components (Rvb1, Rvb2, Arp4, Act1) with the INO80 complex (Table 1). Interestingly, 4 subunits (Arp4, Yaf9-YEAST ALL1-FUSED GENE FROM CHROMOSOME 9, Swc4, and Act1) of SWR1-c are also part of the NuA4 (Nucleosome Acetyltransferase of H4) complex that is a key regulator of transcription, cellular response to DNA damage and cell cycle control [25,26]. In addition to acetylation of histone H4, histone H2A and histone H2A variant Htz1 [27–29], the yeast NuA4 complex also targets non-histone proteins, which encompass metabolism, RNA processing and stress response [30]. In human, Tip60 (Tat-interactive protein 60), the homolog of acetyltransferase subunit of yNuA4 complex (Esa1, Essential for *SAS* Family Acetyltransferase), was originally identified as an interacting partner of the HIV1-tat protein [31]. Subsequently, the purified Tip60 complex contains at least 16 subunits harboring HAT activity towards histone H4, H2A and H2A.Z in chromatin [32–34]. The subunit composition analysis indicates that the Tip60 (NuA4) complex is a fusion form of yeast NuA4 and SWR1 complexes since it also has the enzymatic activity of ATP-dependent H2A.Z-H2B histone dimer exchange [35] (Table 1). A recent report showed that a dynamic merge and separation of NuA4 and SWR1 complexes control cell fate plasticity in *C. albicans* [36]. Indeed, the YEATS domain of Yaf9 can recognize the acetylation of Eaf1 K173 and mediate the Yaf9-Eaf1 interaction. Furthermore, the reversible acetylation and deacetylation of Eaf1 by Esa1 and Hda1 control the merge and separation of NuA4 and SWR1 complexes, and this regulation is triggered by Brg1 recruitment of Hda1 to chromatin in response to nutritional signals that sustain hyphal elongation [36].

To date, the structural insights into the plant SWR1/INO80-c are largely unknown. Based on sequence homology and protein-protein interacting data, the possible subunits orthologues of yeast and human SWR1/INO80-c were identified in *Arabidopsis* (Table 1). The plant ATPase of SWR1-c, PHOTOPERIOD-INDEPENDENT EARLY FLOWERING 1 (PIE1), was first characterized as an activator of *FLOWERING LOCUS C* (*FLC*) in flowering [37]. Further affinity purification followed by tandem mass spectrometry (TAP-MS) assays showed that SWR1-c contains at least 12 subunits, including RVB2A/B, YAF9A/B, and SWC6 in *Arabidopsis* [38]. Furthermore, a more recent study identified 11 conserved SWR1-c subunits in *Arabidopsis* using the conserved SWR1 subunit ARP6 as a bait in tandem affinity purification experiments [39]. Unlike SWR1-c, the compositions of *Arabidopsis* INO80-c are based on the sequence homology and protein-protein interacting data. The homologue of yINO80 was found in *Arabidopsis* as a factor in homologous recombination [40]. These data suggested that plants may also have the INO80 complex. Interestingly, recent studies indicated that the NuA4 complex may exist in *Arabidopsis*, since YAF9A, the yYAF9 homologue (a subunit of yeast NuA4 complex), targets to *FLC* chromatin and regulates the acetylation of H2A.Z and H4 [41]. The multiplication of the subunits in yeast, human and plant suggest that INO80/SWR1 CRCs are conserved in eukaryotes.

4. Involvement of INO80/SWR1-c in DNA Repair

In yeast, the *ino80* and *swr1* mutants are hypersensitive to DNA damage-inducing agents [42,43], suggesting a direct role for INO80 and SWR1 CRCs in DNA repair. Indeed, *ino80* mutants have defects in both the homologous recombination (HR) and nonhomologous end-joining (NHEJ), two pathways for the repair of DNA double-strand breaks (DSBs), while *swr1* mutants have defects in NHEJ alone [44]. Similarly, *Arabidopsis INO80* also plays a role in DSBs (Table 2, Figure 1). Under standard growth conditions, the *ino80* mutants show a reduction of the HR frequency compared with wild-type plants [40,45]; however, after genotoxic treatment, HR in the mutant increased, accompanied by more DNA double-strand breaks and stronger cellular responses [45]. Further analyses show that *INO80* promotes HR downstream of the chaperone NRP1 (NAP1-RELATED PROTEIN 1) after the formation of γ-H2A.X foci during DNA damage repair [46]. Nevertheless, the functional coordination of *INO80* and *NRP1/2* was also observed in apical meristems during plant growth and development [47]. In addition to INO80, ARP5, the conserved subunit of the INO80-c, also plays key roles in the DNA repair. Indeed, ARPs are highly similar to actin, but they cannot polymerize and do not have ATPase activity. Currently, ARPs are classified into 11 subfamilies, and ARP4-ARP9 are predominantly localized in the nucleus [48]. As dedicated conserved subunits of SWI/SNF and INO80 CRCs, ARPs associate directly with ATPases via the conserved N-terminal HSA (helicase-SANT-associated) domain [49]. The *arp5* plants were hypersensitive to DNA-damaging reagents [50], and the transcription levels of DNA repair genes *RAD51*/*RAD54* were up-regulation in mutant plants [51].

Table 2. The Functions of core SWR1/INO80-c Subunits in *Arabidopsis*.

	Gene	Interacting Proteins *	Functions	Reference
The common subunits of INO80/SWR1-c	SWC2		unknown	
	SWC4		Flowering time control; Leaf cell proliferation and expansion	[38]
	SWC6/SEF	SUF4, FLX, TAF14	Flowering time control	[52,53]
			MicroRNA expression	[54,55]
		HAM1, EAF1		[38,56]
			Immunity response	[57]
	RVB1/RIN1	FLX, SUF4, FES1, FRI		[52]
		RPM1, RPP5	Sporophyte and female gametophyte; Disease resistance	[58]
	RVB2A, RVB2B	EAF1		[56]
	ARP4		Multiple effects on plant development	[59]
			Core subunit of SWR1, NuA4, INO80 and SWI/SNF complexes	[56]
Unique subunits of INO80-c	INO80		Controls homologous recombination	[40,45,46,51]
			Flowering time control	[45,51]
			Apical meristems maintenance	[47]
	ARP5		organ development; DNA repair	[50,51]
	ARP9		unknown	
Unique subunits of SWR1-c	PIE1		Flowering time control	[37,60–62]
			Immunity response	[57,63]
			MicroRNA expression	[54]
			Anthocyanin biosynthesis	[64]
			Maintenance of H3K27me3	[65]
	ARP6		Flowering time control	[61,62,66,67]
			MicroRNA expression	[54,55]
			Immunity response	[57]
			DNA repair	[68]
			Female meiosis regulation; Germ-line specification	[69,70]
			Osmotic stress; Phosphate starvation response	[71,72]
	YAF9A	CCA1, HAM1	Flowering time control	[41,73,74]
	YAF9B			

* The interactions among the core subunits of SWR1/INO80-c are shown in Figure 1.

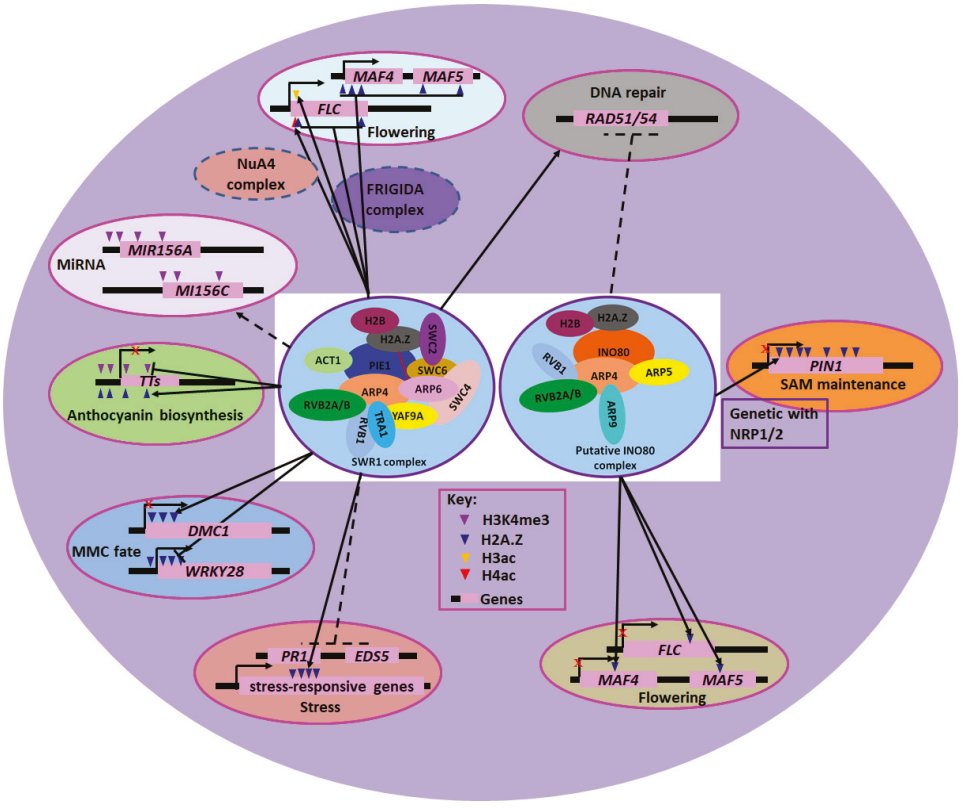

Figure 1. INO80 and SWR1 Chromatin Remodeling Complexes in Cellular Processes and Plant Development. The compositions of putative INO80 and SWR1 complex are indicated. The purple oval represents the nucleus of plant cells. The overlapped ovals and red lines represent interacting subunits of the INO80 and SWR1 complex. Lines with perpendicular bars and red cross denote repression, while arrows indicate enhancement or activation. Broken lines indicate relationships not proven to be direct.

Similar to *INO80* and *ARP5*, SWR1-c is also important for DNA repair in *Arabidopsis*. Since mutations in genes for SWR1-c subunits *PIE1*, *ARP6* and *SWC6* cause hypersensitivity to various DNA damaging agents [68]. The reduced DNA repair capacity of those mutants is connected with impaired HR, in contrast with the hyper-recombinogenic phenotype of yeast SWR1 mutants [44,68]. This suggests functional diversification of SWR1-c between lower and higher eukaryotes. The *arp5 arp6* double mutants displayed a higher percentage of DNA in tails than that of individual single mutants, suggesting that function of ARP5 in the INO80-c acts independently and/or synergistically with the ARP6-containing SWR1-c in DNA repair [51].

5. Functions of INO80/SWR1-c in Flowering

Successful reproduction in plants requires the coordinated transition from vegetative growth to reproductive development. Complex and intricate gene-regulatory networks of transcription factors and chromatin remodelers guide flowering time and flower development, while integrating both internal and external signals [75]. In *Arabidopsis*, two MADS box transcription factors *MADS AFFECTING FLOWERING 4/5* (*MAF4/5*), *FLC* and *SHORT VEGETATIVE PHASE* (*SVP*) act as negative regulators of

flowering time via directly repressing the expression of the floral pathway integrators *FLOWERING LOCUS T* (*FT*) and *SUPPRESSOR OF OVEREXPRESSION OF CONSTANS 1* (*SOC1*) [76–78].

The core subunit components of the *Arabidopsis* SWR1-c, including PIE1, ARP6, ARP4, SWC6/SERRATED LEAVES AND EARLY FLOWERING (SEF), SWC4 and YAF9A/B have been shown to play important roles in regulating the proper growth and flowering. The *Arabidopsis* ATPase of SWR1-c, PIE1, was first identified as an activator of *FLC* [37]. Mutations in *PIE1* repress the *FLC*-mediated delay of flowering, as a result of the presence of *FRIGIDA* [37]. Further research demonstrated that PIE1 associates with the SWR1-c subunits ARP6 (also known as EARLY IN SHORT DAYS 1 [ESD1] and SUPPRESSOR OF FRI 3 [SUF3]) and SWC6 in repression of flowering [53,60,61,66,67]. Indeed, loss of H2A.Z from chromatin in *arp6* and *pie1* mutants results in reduced *FLC* expression and premature flowering, indicating that H2A.Z is required for the expression of *FLC* [62], which suggested a link between PIE1 and H2A.Z incorporation.

Next to ARP6, ARP4 (present in both INO80-c and SWR1-c, Table 1) has also been shown to act in plant reproductive development. Knockdown of *ARP4* results in strong pleiotropic phenotypes such as altered organization of plant organs, early flowering, delayed flower senescence and high levels of sterility, indicating its important roles in plant development [59]. Besides, TAP-MS assays showed that the multiple subunits of SWR1, NuA4, INO80 and SWI/SNF complexes copurified with ARP4, suggesting that ARP4 may be a core subunit of those complexes [56].

In yeast, Swc2 together with Swc6 and Arp6 forms SWR1 complex 2, which handles binding to the histone variant H2A.Z associated with the nucleosome and facilitating histone exchange [79]. To date, three SWCs including SWC2, SWC4 and SWC6 were found in *Arabidopsis*. *SWC4*-deficient mutants are embryo-lethal, while *SWC4* knockdown lines display acceleration of flowering time, indicating that SWC4 controls post-embryonic processes [38]. However, unlike PIE1, SWC4 represses flowering via repressing *FT* [38]. Indeed, SWC4 mediates the recruitment of SWR1-c to the target chromatin regions through recognizing AT-rich DNA elements that are over-represented in the promoters of a subset of genes (*FT*, *FUL*, *IAA19* and *ERF9*) where H2A.Z incorporation impairs transcription [38]. Intriguingly, like yeast SWC4, recent data demonstrated that SWC4 also associates with YAF9s in *Arabidopsis* by TAP-MS assays [41]. *SWC6* was originally identified from *sef* mutants. The *sef* plants present a pleiotropic phenotype including serrated leaves, frequent absence of inflorescence internodes, bushy aspect, and early flowering [53,60]. Like PIE1, SWC6 also activates the transcription of *FLC* via interacting with SUF4 and FLX, two subunits of the FRIGIDA transcription activator complex [52]. Meanwhile, defects in the splicing of *SWC6* pre-mRNA mediated by SKIP (SNW/SKI-INTERACTING PROTEIN) reduce H2A.Z enrichment at *FLC*, *MAF4*, and *MAF5*, resulting in reduced expression of these genes [80]. Interestingly, SWC6 interacts with HAM1 [38], a Myst family histone acetyltransferase of the putative *Arabidopsis* NuA4 complex (NuA4-c) [81]. Although yeast two-hybrid assays showed that SWC2 interacts with H2A.Z and SWC6, the function of *SWC2* in *Arabidopsis* has not been characterized so far [61].

Yeast Yaf9 (YEAST ALL1-FUSED GENE FROM CHROMOSOME 9) contains an N-terminal YEATS domain and a C-terminal predicted coiled-coil sequence [82]. The YEATS domain proteins are conserved from yeast to human, and function as transcriptional regulators as a part of chromatin-modifying complexes [83]. Indeed, as a selective reader of H3K27ac, the YEATS domain of Yaf9 is essential for deposition of H2A.Z, gene transcription and the DNA-damage response [84]. Deletion of *Yaf9* shows reduced telomere-proximal gene expression and sensitivity to DNA-damaging agents [85]. Additionally, *Yaf9* has involved chromosome segregation, telomere silencing and response to spindle stress [82]. Moreover, SWR1-c and NuA4-c share 4 subunits (Act1, Arp4, Swc4, Yaf9), indicating a possible functional link between these two complexes in yeast [86]. The *Arabidopsis* Yaf9 homolog YAF9A acts as a negative regulator of flowering by controlling the H4 acetylation levels in *FLC* and *FT* chromatin [41,73]. Furthermore, CCA1 (CIRCADIAN CLOCK ASSOCIATED1) recruits YAF9A to the promoter region of *GI* (*GIGANTEA*), resulting in accumulation of H2A.Z and the acetylation of H4, thus increasing *GI* expression [74]. Indeed, recent data demonstrated that YAF9A and YAF9B have unequally

redundant functions, and they regulate flowering time by both *FLC*-dependent and independent mechanisms [41]. Moreover, YAF9A interacts with HAM1, a putative catalytic subunit of NuA4-c, causing high level acetylation of H2A.Z and H4 of *FLC* chromatin without affecting the deposition of H2A.Z at the *FLC* locus [41]. YAF9 proteins also associate with other speculative SWR1-c subunits in *Arabidopsis* [38,56]. Together, these data suggest functional conservation of the SWR1-c-NuA4-c module in plants and yeast. In addition to flowering, SWR1-c subunit loss-of-function mutants also exhibit pleiotropic flower phenotypes including frequent absence of inflorescence internodes, bushy growth and flowers with altered organ number and size [37,60,62,66,69].

Unlike the SWR1-c, *Arabidopsis* INO80-c plays a positive role in flowering. INO80, the ATPase of INO80-c is involved in flowering time control via interacting with H2A.Z. Indeed, INO80 binds within the gene body, enhances H2A.Z enrichment and maintains low expression levels of the key flowering repressor genes *FLC* and *MAF4/5*, thus *ino80* mutants displaying late flowering phenotype [45]. Recent analysis demonstrated that INO80 interacts with ARP5 and acts in concert with ARP5 during plant cellular proliferation and replication stress response [51]. Nevertheless, ARP5 is not required for INO80-mediated control of flowering time and related transcriptional regulation of *FLC* and *MAF4*/*MAF5* [51]. Taken together, these data indicated that SWR1-c and INO80-c may play an opposite role in flowering, which is consistent with the biochemical activity of SWR1-c and INO80-c.

6. Functions of INO80/SWR1-c in Immunity Response

Plants need to precisely coordinate defense with growth and development to optimize environmental conditions. A previous study showed that 65% of the differentially expressed genes in *hta9 hta11* mutants (loss of two major H2A.Z encoding genes out of the possible three in *Arabidopsis*) were also misregulated in *pie1* plants, and the majority of misregulated genes were related to systemic acquired resistance (SAR) [63]. These data indicated that SWR1-c plays a role in maintaining a repressive state of the SAR response. However, further phenotypic analysis showed that *pie1*, *swc6*, and *hta9 hta11* mutants displayed more macroscopic disease symptoms and increased susceptibility toward *Pst* DC3000 compared with the wild-type, whereas the *arp6* mutant showed increased resistance [57]. These observations suggest that H2A.Z, PIE1, and SWC6 are essential for basal resistance in *Arabidopsis*, whereas ARP6 has an opposite function. Moreover, although the *arp6* and *swc6* mutants have similar morphological and developmental phenotypes (early flowering and serrated leaves), and ARP6 and SWC6 have been shown to physically interact in *Arabidopsis* [53,60], the RNA-seq data did not show a strong correlation in these mutants [57]. This observation is consistent with the defense phenotypes, suggesting that ARP6 and SWC6 could have distinct functions in *Arabidopsis*.

To data, little is known about INO80-c in plant immunity response. However, *Arabidopsis* RVB1/RIN1 (RESISTANCE TO PSEUDOMONAS SYRINGAE PV MACULICOLA INTERACTOR 1), the common subunit of INO80/SWR1-c, interacts with both RPM1 (CC-NB-LRR) and RPP5 (TIR-NB-LRR) proteins to negatively regulate the expression of disease resistance (R) genes [58]. Indeed, RVB1 belongs to the members of a larger family of proteins known as the AAA^+ class chaperone-like ATPases [87]. In bacteria, Rvb1 and Rvb2 form a double hexamer around Holliday junctions to promote their migration during homologous recombination in DSB repair [88]. In yeast, Rvb1 and Rvb2 are present in both SWR1/INO80-c and are homologous to *Arabidopsis* RVB1and RVB2A/B. *RVB1* is essential for *Arabidopsis* development during both female gametophyte and sporophyte development [58]. Meanwhile, ectopic expression of *RVB1* in yeast *yRvb1* deletion alleles can rescue yeast viability [58]. Intriguingly, although TAP-MS experiments showed that RVB1 may not be the subunit of *Arabidopsis* SWR1-c [39], the interaction between RVB1 and YAF9A still suggested that RVB1 associates with SWR1-c [41]. Compared with yeast, little is known about RVB2A/B functions in plants. Recent data showed that RVB2A/B physically interact with the EAF1 subunit of the NuA4 complex [56], which is a homolog of yeast Eaf1. Further research is required to investigate the molecular mechanism of how INO80-c is involved in plant defense.

7. Involvement of INO80/SWR1-c in the Regulation of MicroRNA Expression

MicroRNAs (miRNAs) repress protein production post-transcriptionally. In flowering plants, modules of miRNAs and their target transcription factors, such as the miR156-SPLs/miR172-AP2 LIKEs and miR319-TCPs/miR164-CUCs modules, control diverse developmental processes including phase transitions, leaf shape, and floral organ identity [89,90]. Previous studies suggest that SWR1-c contributes to the fine control of plant development by generating a balance between miRNAs and target mRNAs at the transcriptional level. In the mutants of *arp6*, *sef*, and *pie1*, miR156 and miR164 levels are reduced at the transcriptional level, which results in the accumulation of target mRNAs and associated morphological changes [54]. Further investigation showed that *arp6*, *sef*, and *hta9 hta11* mutant plants reduce the expression of *MIR156A* and *MIR156C* via facilitating the deposition of H3K4me3, rather than decreasing nucleosome occupancy [55].

The functions of INO80-c in miRNA regulation are largely unknown. However, in mammals, *INO80* is a target gene of miR148a in the cancer stem cells (CSCs) of anaplastic thyroid carcinoma (ATC) [91]. The expression of *INO80* was upregulated in ATC-CSCs and downregulated upon miRNA148 overexpression. Moreover, overexpression of miRNA148a and knockdown of *INO80* acted synergistically to decrease the expression of stem cell marker genes as well as to attenuate stem cell-specific properties including the ability to form tumors [91]. These results suggested that in addition to miRNA regulation, miRNA may also affect the functions of INO80-c or SWR1-c.

8. Other Functions of Core Subunits of INO80/SWR1-c

In addition to the functions of INO80/SWR1-c described above, the core subunits of INO80/SWR1-c have other roles in plants development. For instance, the accumulation of anthocyanin in H2A.Z deposition-deficient mutants such as *pie1* is associated with increased H3K4me3 of anthocyanin biosynthetic genes, which is negatively associated with the presence of H2A.Z [64]. These results reveal an antagonistic relationship between H2A.Z and H3K4me3 in the regulation of anthocyanin biosynthesis genes. However, genome-wide occupancy assays of H2A.Z, H3K4me3 and H3K27me3 showed that H2A.Z preferentially associates with H3K4me3 at promoters and H3K27me3 at enhancers in *Arabidopsis* inflorescence. Moreover, H2A.Z represses enhancer activity by promoting H3K27me3 and preventing H3K4me3 histone modifications [92]. A recent study demonstrated that H3K27me3-enriched chromatin is dependent on the prior action of PIE1 and H2A.Z. Indeed, the H2A.Z- and H3K27me3-enriched chromatin is subsequently stabilized during transcription by the CHD remodeler PICKLE and the histone methyltransferase CURLY LEAF [65]. Collectively, these data suggested that there is a cross-talk between H2A.Z deposition and histone modifications.

Moreover, *ARP6* also regulates the female meiosis of prophase I by activating the expression of meiotic recombination related genes such as *DMC1* (*DISRUPTED MEIOTIC cDNA1*) [69]. Subsequent research revealed that ARP6 associates with SWR1-c and promotes the expression of *WRKY28* through H2A.Z deposition in megaspore mother cells (MMC) [70]. Intriguingly, *arp6* null alleles exhibit a delayed germination rate in osmotic stress conditions, suggesting a positive role of ARP6 in osmotic stress responses [71]. Meanwhile, *arp6* plants also display an apparent phosphate starvation response (PSR), when grown in a phosphate replete medium, since ARP6 is required for proper H2A.Z deposition at a number of *PSR* genes [72]. Moreover, overexpressing *ARP6s* from other plant species such as *Physcomitrella patens* and rice (*Oryza sativa*) could rescue the early flowering phenotype of *Arabidopsis arp6* mutants, suggesting that the function of ARP6 is conserved in plants [93].

9. Concluding Remarks and Future Perspectives

The roles of SWR1/INO80-c in nuclear activities are quite diverse ranging from DSB repair to the regulation of gene expression. The mutants of *INO80-c* and *SWR1-c* subunits display a variety of organism-specific phenotypes. Moreover, phenotypic differences among the single and double mutants of *INO80-c* and *SWR1-c* subunit genes are also observed. For instance, the phenotype of

pie1 plants is more severe than that of other SWR1 component mutants, suggesting that PIE1 may be a scaffolding component of different complexes. Indeed, like human p400, PIE1 contains HSA, ATPase, and SANT domains, which are found separately in the Swr1 and Eaf1 proteins, implying that PIE1 may also be an ortholog of p400. TAP-MS data showed that *Arabidopsis* TRA1 (also a subunit of Spt-Ada-Gcn5-acetyltransferase [SAGA] complex), the homolog of the yeast NuA4 subunit Tra1 and the mammalian Tip 60 subunit TRRAP, also presents in SWR1-c. Collectively, these data suggest that the same subunit (like PIE1) may exist in different distinct complexes. The SWR1-c components also play different roles in resistance to different pathogens. For instance, *pie1* and *swc6* plants display reduced basal resistance, while loss of *ARP6* fucntion results in enhanced resistance [57]. Further in-depth analyses are needed to uncover the functional specificity of SWR1/INO80-c and NuA4-c subunits and their interaction in plants.

Although SWR1/INO80-c are associated with histone variants in vivo [45,63] (Table 2; Figure 1), the precise chromatin-remodeling mechanisms of these complexes in diverse cellular processes are largely unknown. For instances, the mechanism of how SWR1/INO80-c are recruited to their target loci such as *FLC* is still unclear [37,45,60,61]. It is possible that there is a cross-talk between chromatin modifications and histone variant exchange. In yeast, the NuA4-c mediated acetylation of specific histones in the nucleosome is important for SWR1-c targeting to chromatin and H2A.Z incorporation [28,94]. Moreover, it was shown that Bdf1, a bromodomain-containing subunit of yeast SWR1-c, recruits the complex to chromatin by recognizing acetylated H4 tails [28,95]. Consistently, loss-of-function of Bdf1 results in global reduction of H2A.Z in chromatin [96]. Indeed, the Yaf9 subunit of SWR1-c (also a subunit of NuA4-c) targets histone H3K27ac through its YEATS domain in yeast [84]. The *Arabidopsis* Yaf9 homologs YAF9A and YAF9B are also novel histone readers that bind to unmodified and acetylated histone H3 [41]. Meanwhile, MBD9, a bromodomain and homeodomains (PHD)-containing unique subunit of *Arabidopsis* SWR1-c, also recognizes the acetylated histones [97]. Further studies demonstrated that in *mbd9* plants, the level of H2A.Z incorporation is significantly reduced, and H2A.Z sites depending on MBD9 has higher levels of H3K9Ac and lower levels of H3K4me3 and H3K36me3 [39]. These data suggest that MBD9, like Bdf1 in yeast, could target SWR1-c via its bromodomain by recognizing acetylated histone marks, such asH3K9Ac. Further research is required to investigate whether acetylated residues on histones can directly recruit SWR1-c to facilitate distinct nuclear processes. In addition, genome-wide binding analyses of INO80/ SWR1-c combined with transcriptome analysis will be useful for the identification of the direct target genes regulated by SWR1/INO80-c, which may provide a comprehensive understanding of how SWR1/INO80-c control plant development and stress responses.

Author Contributions: J.W. and S.G. conceived the idea and wrote the manuscript. X.P. and S.Y. designed and organized the tables and figure. S.Y. and K.W. conceived the idea and revised and organized the manuscript.

Funding: This work was supported by the Guangdong Natural Science Funds for Distinguished Young Scholars (2016A030306047); Pearl River S&T Nova Program of Guangzhou (201610010138); the Youth Innovation Promotion Association, CAS (2017398), and the National Natural Science Foundation of China (No. 31771423). This work was also supported by the Ministry of Science and Technology of Taiwan (105-2311-B-002-012-MY3 and 106-2313-B-002-003) and National Taiwan University (NTU-AS- 108L104310).

Conflicts of Interest: The authors declare no conflict of interest.

Abbreviations

Act1	Actin1
ARP4	Actin-Related Protein 4
ARP5	Actin-Related Protein 5
ARP6	Actin-Related Protein 6
ARP8	Actin-Related Protein 8
ARP9	Actin-Related Protein 9
ATC	anaplastic thyroid carcinoma
ATP	adenosine triphosphate

ATPases	adenosine triphosphatase
Bdf1	Bromodomain factor 1
Brg1	brahma-related gene 1
CCA1	CIRCADIAN CLOCK ASSOCIATED1
CHD	chromo and DNA-binding domain
CRCs	chromatin-remodeling complexes
CSCsCUCs	cancer stem cellsCUP SHAPED COTYLEDONs
DMC1	DISRUPTED MEIOTIC cDNA1
DNA	DeoxyriboNucleic Acid
DSBs	DNA double-strand breaks
EAF1	Esa1-associated factor 1
ERF9	ethylene response factor 9
Esa1	Essential for SAS Family Acetyltransferase 1
ESD1	EARLY IN SHORT DAYS 1
FLC	FLOWERING LOCUS C
FLX	FLC EXPRESSOR
FT	FLOWERING LOCUS T
FUL	FRUITFULL
GI	GIGANTEA
HAM1	HAIRY MERISTEM 1
Hda1	Histone deacetylase 1
HR	homologous recombination
HSA	helicase/SANT-associated
hta11	HISTONE H2A 11
hta9	HISTONE H2A 9
IAA19	AUXIN-RESPONSIVE PROTEIN 19
Ies1-6	Ino Eighty Subunit 1-6
INO80	Inositol Requiring 80
INO80-c	INO80 complex
ISWI	imitation SWI
MAF4/5	MADS AFFECTING FLOWERING 4/5
MBD9	Methyl-CpG-binding domain 9
miRNAs	MicroRNAs
MMC	megaspore mother cells
NHEJ	nonhomologous end-joining
Nhp10	Non-Histone Protein 10
NRP1	NAP1-RELATED PROTEIN 1
NuA4	nucleosome acetyltransferase of H4
NuA4-c	NuA4 complex
PHD	plant homeodomain
PIE1	PHOTOPERIOD-INDEPENDENT EARLY FLOWERING 1
PSR	phosphate starvation responses
RAD51/RAD54	RADiation sensitive 51/54
RPM1	RESISTANCE TO P. SYRINGAE PV MACULICOLA 1
RPP5	RECOGNITION OF PERONOSPORA PARASITICA 5
Rvb1	RuvB-like protein 1
RVB1/RIN1	RESISTANCE TO PSEUDOMONAS SYRINGAE PV MACULICOLA INTERACTOR 1
Rvb2	RuvB-like protein 2
RVB2A/B	RuvB-like protein 2A/B
SAGA	Spt-Ada-Gcn5-acetyltransferase
SANT	Swi3-Ada2-NCoR-TFIIIB
SAR	systemic acquired resistance
SEF	SERRATED LEAVES AND EARLY FLOWERING

SF2	superfamily 2
SHL 3	superhelical location 3
SHL2	superhelical location 2
SHL6	superhelical location 6
SKIP	SNW/SKI-INTERACTING PROTEIN
SOC1	SUPPRESSOR OF OVEREXPRESSION OF CONSTANS 1
SPLs	SQUAMOSA PROMOTER BINDING PROTEIN (SBP)-DOMAIN TRANSCRIPTION FACTORs
SRCAP	SNF2-RELATED CBP ACTIVATOR PROTEIN (human)
SUF3	SUPPRESSOR OF FRI 3
SUF4	SUPPRESSOR OF FRI 4
SVP	SHORT VEGETATIVE PHASE
Swc2-6	SWR complex subunit 2-6
SWI	mating type switching
SWR1	SWi2/snf2-Related 1
SWR1-c	SWR1 complex
Taf14	TATA binding protein-Associated Factor 14
TAP-MS	tandem mass spectrometry
TCPs	TEOSINTE BRANCHED 1, CYCLOIDEA AND PCF TRANSCRIPTION FACTORs
Tip60	Tat-interactive protein 60
Tra1	transfer region 1
TRRAP	transformation/transcription domain-associated protein
Yaf9	YEAST ALL1-FUSED GENE FROM CHROMOSOME 9
YAF9A	YEAST ALL1-FUSED GENE FROM CHROMOSOME 9A
YAF9A/B	YEAST ALL1-FUSED GENE FROM CHROMOSOME 9A/B
YAF9B	YEAST ALL1-FUSED GENE FROM CHROMOSOME 9B

References

1. Luger, K.; Mader, A.W.; Richmond, R.K.; Sargent, D.F.; Richmond, T.J. Crystal structure of the nucleosome core particle at 2.8 a resolution. *Nature* **1997**, *389*, 251–260. [CrossRef] [PubMed]
2. Henikoff, S.; Shilatifard, A. Histone modification: Cause or cog? *Trends Genet.* **2011**, *27*, 389–396. [CrossRef] [PubMed]
3. Jerzmanowski, A. Swi/snf chromatin remodeling and linker histones in plants. *Biochim. Biophys. Acta* **2007**, *1769*, 330–345. [CrossRef] [PubMed]
4. Imbalzano, A.N. Energy-dependent chromatin remodelers: Complex complexes and their components. *Crit. Rev. Eukar. Gene* **1998**, *8*, 225–255. [CrossRef]
5. Gorbalenya, A.E.; Koonin, E.V. Helicases-amino-acid-sequence comparisons and structure-function-relationships. *Curr. Opin. Struc. Biol.* **1993**, *3*, 419–429. [CrossRef]
6. Abrams, E.; Neigeborn, L.; Carlson, M. Molecular analysis of snf2 and snf5, genes required for expression of glucose-repressible genes in saccharomyces-cerevisiae. *Mol. Cell Biol.* **1986**, *6*, 3643–3651. [CrossRef] [PubMed]
7. Clapier, C.R.; Cairns, B.R. The biology of chromatin remodeling complexes. *Annu Rev. Biochem.* **2009**, *78*, 273–304. [CrossRef]
8. Morrison, A.J.; Shen, X.T. Chromatin remodelling beyond transcription: The ino80 and swr1 complexes. *Nat. Rev. Mol. Cell Biol.* **2009**, *10*, 373–384. [CrossRef] [PubMed]
9. Gerhold, C.B.; Gasser, S.M. Ino80 and swr complexes: Relating structure to function in chromatin remodeling. *Trends Cell Biol.* **2014**, *24*, 619–631. [CrossRef] [PubMed]
10. Mizuguchi, G.; Shen, X.; Landry, J.; Wu, W.H.; Sen, S.; Wu, C. Atp-driven exchange of histone h2az variant catalyzed by swr1 chromatin remodeling complex. *Science* **2004**, *303*, 343–348. [CrossRef]
11. Papamichos-Chronakis, M.; Watanabe, S.; Rando, O.J.; Peterson, C.L. Global regulation of h2a.Z localization by the ino80 chromatin-remodeling enzyme is essential for genome integrity. *Cell* **2011**, *144*, 200–213. [CrossRef] [PubMed]

12. Watanabe, S.; Tan, D.; Lakshminarasimhan, M.; Washburn, M.P.; Hong, E.J.; Walz, T.; Peterson, C.L. Structural analyses of the chromatin remodelling enzymes ino80-c and swr-c. *Nat. Commun.* **2015**, *6*, 7108. [CrossRef] [PubMed]
13. Watanabe, S.; Radman-Livaja, M.; Rando, O.J.; Peterson, C.L. A histone acetylation switch regulates h2a.Z deposition by the swr-c remodeling enzyme. *Science* **2013**, *340*, 195–199. [CrossRef] [PubMed]
14. Wang, F.; Ranjan, A.; Wei, D.B.; Wu, C. Comment on "a histone acetylation switch regulates h2a.Z deposition by the swr-c remodeling enzyme". *Science* **2016**, *353*, 358. [CrossRef] [PubMed]
15. Watanabe, S.; Peterson, C.L. Response to comment on "a histone acetylation switch regulates h2a.Z deposition by the swr-c remodeling enzyme". *Science* **2016**, *353*, 358. [CrossRef] [PubMed]
16. Eustermann, S.; Schall, K.; Kostrewa, D.; Lakomek, K.; Strauss, M.; Moldt, M.; Hopfner, K.P. Structural basis for atp-dependent chromatin remodelling by the ino80 complex. *Nature* **2018**, *556*, 386–390. [CrossRef]
17. Willhoft, O.; Ghoneim, M.; Lin, C.L.; Chua, E.Y.D.; Wilkinson, M.; Chaban, Y.; Ayala, R.; McCormack, E.A.; Ocloo, L.; Rueda, D.S.; et al. Structure and dynamics of the yeast swr1-nucleosome complex. *Science* **2018**, *362*, eaat7716. [CrossRef]
18. Li, B.; Pattenden, S.G.; Lee, D.; Gutierrez, J.; Chen, J.; Seidel, C.; Gerton, J.; Workman, J.L. Preferential occupancy of histone variant h2az at inactive promoters influences local histone modifications and chromatin remodeling. *Proc. Natl. Acad. Sci. USA* **2005**, *102*, 18385–18390. [CrossRef]
19. Yen, K.; Vinayachandran, V.; Pugh, B.F. Swr-c and ino80 chromatin remodelers recognize nucleosome-free regions near +1 nucleosomes. *Cell* **2013**, *154*, 1246–1256. [CrossRef]
20. Zilberman, D.; Coleman-Derr, D.; Ballinger, T.; Henikoff, S. Histone h2a.Z and DNA methylation are mutually antagonistic chromatin marks. *Nature* **2008**, *456*, 125–129. [CrossRef]
21. Coleman-Derr, D.; Zilberman, D. Deposition of histone variant h2a.Z within gene bodies regulates responsive genes. *PLoS Genet.* **2012**, *8*, e1002988. [CrossRef] [PubMed]
22. Ebbert, R.; Birkmann, A.; Schuller, H.J. The product of the snf2/swi2 paralogue ino80 of saccharomyces cerevisiae required for efficient expression of various yeast structural genes is part of a high-molecular-weight protein complex. *Mol. Microbiol.* **1999**, *32*, 741–751. [CrossRef] [PubMed]
23. Shen, X.; Mizuguchi, G.; Hamiche, A.; Wu, C. A chromatin remodelling complex involved in transcription and DNA processing. *Nature* **2000**, *406*, 541–544. [CrossRef] [PubMed]
24. Wu, W.H.; Wu, C.H.; Ladurner, A.; Mizuguchi, G.; Wei, D.; Xiao, H.; Luk, E.; Ranjan, A.; Wu, C. N terminus of swr1 binds to histone h2az and provides a platform for subunit assembly in the chromatin remodeling complex. *J. Biol. Chem.* **2009**, *284*, 6200–6207. [CrossRef] [PubMed]
25. Allard, S.; Utley, R.T.; Savard, J.; Clarke, A.; Grant, P.; Brandl, C.J.; Pillus, L.; Workman, J.L.; Cote, J. Nua4, an essential transcription adaptor/histone h4 acetyltransferase complex containing esa1p and the atm-related cofactor tra1p. *Embo J.* **1999**, *18*, 5108–5119. [CrossRef] [PubMed]
26. Doyon, Y.; Cote, J. The highly conserved and multifunctional nua4 hat complex. *Curr. Opin. Genet. Dev.* **2004**, *14*, 147–154. [CrossRef] [PubMed]
27. Mitchell, L.; Lambert, J.P.; Gerdes, M.; Al-Madhoun, A.S.; Skerjanc, I.S.; Figeys, D.; Baetz, K. Functional dissection of the nua4 histone acetyltransferase reveals its role as a genetic hub and that eaf1 is essential for complex integrity. *Mol. Cell Biol.* **2008**, *28*, 2244–2256. [CrossRef] [PubMed]
28. Altaf, M.; Auger, A.; Monnet-Saksouk, J.; Brodeur, J.; Piquet, S.; Cramet, M.; Bouchard, N.; Lacoste, N.; Utley, R.T.; Gaudreau, L.; et al. Nua4-dependent acetylation of nucleosomal histones h4 and h2a directly stimulates incorporation of h2a.Z by the swr1 complex. *J. Biol. Chem.* **2010**, *285*, 15966–15977. [CrossRef] [PubMed]
29. Babiarz, J.E.; Halley, J.E.; Rine, J. Telomeric heterochromatin boundaries require nua4-dependent acetylation of histone variant h2a.Z in saccharomyces cerevisiae. *Gene Dev.* **2006**, *20*, 700–710. [CrossRef] [PubMed]
30. Lin, Y.Y.; Lu, J.Y.; Zhang, J.M.; Walter, W.; Dang, W.W.; Wan, J.; Tao, S.C.; Qian, J.; Zhao, Y.M.; Boeke, J.D.; et al. Protein acetylation microarray reveals that nua4 controls key metabolic target regulating gluconeogenesis. *Cell* **2009**, *136*, 1073–1084. [CrossRef] [PubMed]
31. Kamine, J.; Elangovan, B.; Subramanian, T.; Coleman, D.; Chinnadurai, G. Identification of a cellular protein that specifically interacts with the essential cysteine region of the hiv-1 tat transactivator. *Virology* **1996**, *216*, 357–366. [CrossRef] [PubMed]

32. Ikura, T.; Ogryzko, V.V.; Grigoriev, M.; Groisman, R.; Wang, J.; Horikoshi, M.; Scully, R.; Qin, J.; Nakatani, Y. Involvement of the tip60 histone acetylase complex in DNA repair and apoptosis. *Cell* **2000**, *102*, 463–473. [CrossRef]
33. Legube, G.; Linares, L.K.; Lemercier, C.; Scheffner, M.; Khochbin, S.; Trouche, D. Tip60 is targeted to proteasome-mediated degradation by mdm2 and accumulates after uv irradiation. *Embo J.* **2002**, *21*, 1704–1712. [CrossRef] [PubMed]
34. Giaimo, B.D.; Ferrante, F.; Vallejo, D.M.; Hein, K.; Gutierrez-Perez, I.; Nist, A.; Stiewe, T.; Mittler, G.; Herold, S.; Zimmermann, T.; et al. Histone variant h2a.Z deposition and acetylation directs the canonical notch signaling response. *Nucleic Acids Res.* **2018**, *46*, 8197–8215. [CrossRef] [PubMed]
35. Auger, A.; Galarneau, L.; Altaf, M.; Nourani, A.; Doyon, Y.; Utley, R.T.; Cronier, D.; Allard, S.; Cote, J. Eaf1 is the platform for nua4 molecular assembly that evolutionarily links chromatin acetylation to atp-dependent exchange of histone h2a variants. *Mol. Cell Biol.* **2008**, *28*, 2257–2270. [CrossRef] [PubMed]
36. Wang, X.; Zhu, W.; Chang, P.; Wu, H.; Liu, H.; Chen, J. Merge and separation of nua4 and swr1 complexes control cell fate plasticity in candida albicans. *Cell Discov.* **2018**, *4*, 45. [CrossRef] [PubMed]
37. Noh, Y.S.; Amasino, R.M. Pie1, an iswi family gene, is required for flc activation and floral repression in arabidopsis. *Plant Cell* **2003**, *15*, 1671–1682. [CrossRef] [PubMed]
38. Gómez-Zambrano, Á.; Crevillén, P.; Franco-Zorrilla, J.M.; López, J.A.; Santos-González, J.; Roszak, P.; Santos-Gonzalez, J.; Jurado, S.; Vázquez, J.; Köhler, C.; et al. Arabidopsis swc4 binds DNA and recruits the swr1 complex to modulate histone h2a.Z deposition at key regulatory genes. *Mol. Plant* **2018**, *11*, 815–832. [CrossRef] [PubMed]
39. Sijacic, P.; Holder, D.H.; Bajic, M.; Deal, R.B. Methyl-cpg-binding domain 9 (mbd9) is required for h2a.Z incorporation into chromatin at a subset of h2a.Z-enriched regions in the arabidopsis genome. *PLoS Genet.* **2019**, *15*, e1008326. [CrossRef] [PubMed]
40. Fritsch, O.; Benvenuto, G.; Bowler, C.; Molinier, J.; Hohn, B. The ino80 protein controls homologous recombination in arabidopsis thaliana. *Mol. Cell* **2004**, *16*, 479–485. [CrossRef] [PubMed]
41. Crevillén, P.; Gómez-Zambrano, Á.; López, J.A.; Vázquez, J.; Piñeiro, M.; Jarillo, J.A. Arabidopsis yaf9 histone readers modulate flowering time through nua4-complex-dependent h4 and h2a.Z histone acetylation at flc chromatin. *NEW Phytol.* **2019**, *222*, 1893–1908. [CrossRef] [PubMed]
42. Van Attikum, H.; Fritsch, O.; Hohn, B.; Gasser, S.M. Recruitment of the ino80 complex by h2a phosphorylation links atp-dependent chromatin remodeling with DNA double-strand break repair. *Cell* **2004**, *119*, 777–788. [CrossRef] [PubMed]
43. Morrison, A.J.; Highland, J.; Krogan, N.J.; Arbel-Eden, A.; Greenblatt, J.F.; Haber, J.E.; Shen, X. Ino80 and gamma-h2ax interaction links atp-dependent chromatin remodeling to DNA damage repair. *Cell* **2004**, *119*, 767–775. [CrossRef] [PubMed]
44. Van Attikum, H.; Fritsch, O.; Gasser, S.M. Distinct roles for swr1 and ino80 chromatin remodeling complexes at chromosomal double-strand breaks. *Embo J.* **2007**, *26*, 4113–4125. [CrossRef] [PubMed]
45. Zhang, C.; Cao, L.; Rong, L.; An, Z.; Zhou, W.; Ma, J.; Shen, W.H.; Zhu, Y.; Dong, A. The chromatin-remodeling factor atino80 plays crucial roles in genome stability maintenance and in plant development. *Plant J.* **2015**, *82*, 655–668. [CrossRef] [PubMed]
46. Zhou, W.; Gao, J.; Ma, J.; Cao, L.; Zhang, C.; Zhu, Y.; Dong, A.; Shen, W.H. Distinct roles of the histone chaperones nap1 and nrp and the chromatin-remodeling factor ino80 in somatic homologous recombination in arabidopsis thaliana. *Plant J.* **2016**, *88*, 397–410. [CrossRef] [PubMed]
47. Kang, H.; Ma, J.; Wu, D.; Shen, W.H.; Zhu, Y. Functional coordination of the chromatin-remodeling factor atino80 and the histone chaperones nrp1/2 in inflorescence meristem and root apical meristem. *Front. Plant Sci.* **2019**, *10*, 115. [CrossRef]
48. Muller, J.; Oma, Y.; Vallar, L.; Friederich, E.; Poch, O.; Winsor, B. Sequence and comparative genomic analysis of actin-related proteins. *Mol. Biol. Cell* **2005**, *16*, 5736–5748. [CrossRef] [PubMed]
49. Szerlong, H.; Hinata, K.; Viswanathan, R.; Erdjument-Bromage, H.; Tempst, P.; Cairns, B.R. The hsa domain binds nuclear actin-related proteins to regulate chromatin-remodeling atpases. *Nat. Struct. Mol. Biol.* **2008**, *15*, 469–476. [CrossRef] [PubMed]
50. Kandasamy, M.K.; McKinney, E.C.; Deal, R.B.; Smith, A.P.; Meagher, R.B. Arabidopsis actin-related protein arp5 in multicellular development and DNA repair. *Dev. Biol.* **2009**, *335*, 22–32. [CrossRef]

51. Kang, H.; Zhang, C.; An, Z.; Shen, W.H.; Zhu, Y. Atino80 and atarp5 physically interact and play common as well as distinct roles in regulating plant growth and development. *NEW Phytol.* **2019**, *223*, 336–353. [CrossRef] [PubMed]
52. Choi, K.; Kim, J.; Hwang, H.J.; Kim, S.; Park, C.; Kim, S.Y.; Lee, I. The frigida complex activates transcription of flc, a strong flowering repressor in arabidopsis, by recruiting chromatin modification factors. *Plant Cell* **2011**, *23*, 289–303. [CrossRef] [PubMed]
53. Lázaro, A.; Gómez-Zambrano, A.; López-González, L.; Piñeiro, M.; Jarillo, J.A. Mutations in the arabidopsis swc6 gene, encoding a component of the swr1 chromatin remodelling complex, accelerate flowering time and alter leaf and flower development. *J. Exp. Bot.* **2008**, *59*, 653–666. [CrossRef] [PubMed]
54. Choi, K.; Kim, J.; Muller, S.Y.; Oh, M.; Underwood, C.; Henderson, I.; Lee, I. Regulation of microrna-mediated developmental changes by the swr1 chromatin remodeling complex. *Plant Physiol.* **2016**, *171*, 1128–1143. [PubMed]
55. Xu, M.L.; Leichty, A.R.; Hu, T.Q.; Poethig, R.S. H2a.Z promotes the transcription of mir156a and mir156c in arabidopsis by facilitating the deposition of h3k4me3. *Development* **2018**, *145*. [CrossRef] [PubMed]
56. Bieluszewski, T.; Galganski, L.; Sura, W.; Bieluszewska, A.; Abram, M.; Ludwikow, A.; Ziolkowski, P.A.; Sadowski, J. Ateaf1 is a potential platform protein for arabidopsis nua4 acetyltransferase complex. *BMC Plant Biol.* **2015**, *15*. [CrossRef] [PubMed]
57. Berriri, S.; Gangappa, S.N.; Kumar, S.V. Swr1 chromatin-remodeling complex subunits and h2a.Z have non-overlapping functions in immunity and gene regulation in arabidopsis. *Mol. Plant* **2016**, *9*, 1051–1065. [CrossRef] [PubMed]
58. Holt, B.F.; Boyes, D.C.; Ellerstrom, M.; Siefers, N.; Wiig, A.; Kauffman, S.; Grant, M.R.; Dangl, J.L. An evolutionarily conserved mediator of plant disease resistance gene function is required for normal arabidopsis development. *Dev. Cell* **2002**, *2*, 807–817. [CrossRef]
59. Kandasamy, M.K.; Deal, R.B.; McKinney, E.C.; Meagher, R.B. Silencing the nuclear actin-related protein atarp4 in arabidopsis has multiple effects on plant development, including early flowering and delayed floral senescence. *Plant J.* **2005**, *41*, 845–858. [CrossRef]
60. March-Díaz, R.; García-Domínguez, M.; Florencio, F.J.; Reyes, J.C. Sef, a new protein required for flowering repression in arabidopsis, interacts with pie1 and arp6. *Plant Physiol.* **2007**, *143*, 893–901. [CrossRef]
61. Choi, K.; Park, C.; Lee, J.; Oh, M.; Noh, B.; Lee, I. Arabidopsis homologs of components of the swr1 complex regulate flowering and plant development. *Development* **2007**, *134*, 1931–1941. [CrossRef] [PubMed]
62. Deal, R.B.; Topp, C.N.; McKinney, E.C.; Meagher, R.B. Repression of flowering in arabidopsis requires activation of flowering locus c expression by the histone variant h2a.Z. *Plant Cell* **2007**, *19*, 74–83. [CrossRef] [PubMed]
63. March-Díaz, R.; García-Domínguez, M.; Lozano-Juste, J.; León, J.; Florencio, F.J.; Reyes, J.C. Histone h2a.Z and homologues of components of the swr1 complex are required to control immunity in arabidopsis. *Plant J.* **2008**, *53*, 475–487. [CrossRef] [PubMed]
64. Cai, H.; Zhang, M.; Chai, M.; He, Q.; Huang, X.; Zhao, L.; Qin, Y. Epigenetic regulation of anthocyanin biosynthesis by an antagonistic interaction between h2a.Z and h3k4me3. *New Phytol.* **2019**, *221*, 295–308. [CrossRef] [PubMed]
65. Carter, B.; Bishop, B.; Ho, K.K.; Huang, R.; Jia, W.; Zhang, H.; Pascuzzi, P.E.; Deal, R.B.; Ogas, J. The chromatin remodelers pkl and pie1 act in an epigenetic pathway that determines h3k27me3 homeostasis in arabidopsis. *Plant Cell* **2018**, *30*, 1337–1352. [CrossRef]
66. Choi, K.; Kim, S.; Kim, S.Y.; Kim, M.; Hyun, Y.; Lee, H.; Choe, S.; Kim, S.G.; Michaels, S.; Lee, I. Suppressor of frigida3 encodes a nuclear actin-related protein6 required for floral repression in arabidopsis. *Plant Cell* **2005**, *17*, 2647–2660. [CrossRef]
67. Martin-Trillo, M.; Lazaro, A.; Poethig, R.S.; Gomez-Mena, C.; Pineiro, M.A.; Martinez-Zapater, J.M.; Jarillo, J.A. Early in short days 1 (esd1) encodes actin-related protein 6 (atarp6), a putative component of chromatin remodelling complexes that positively regulates flc accumulation in arabidopsis. *Development* **2006**, *133*, 1241–1252. [CrossRef]
68. Rosa, M.; Von Harder, M.; Cigliano, R.A.; Schlogelhofer, P.; Mittelsten Scheid, O. The arabidopsis swr1 chromatin-remodeling complex is important for DNA repair, somatic recombination, and meiosis. *Plant Cell* **2013**, *25*, 1990–2001. [CrossRef]

69. Qin, Y.; Zhao, L.H.; Skaggs, M.I.; Andreuzza, S.; Tsukamoto, T.; Panoli, A.; Wallace, K.N.; Smith, S.; Siddiqi, I.; Yang, Z.B.; et al. Actin-related protein6 regulates female meiosis by modulating meiotic gene expression in arabidopsis. *Plant Cell* **2014**, *26*, 1612–1628. [CrossRef]
70. Zhao, L.; Cai, H.; Su, Z.; Wang, L.; Huang, X.; Zhang, M.; Chen, P.; Dai, X.; Zhao, H.; Palanivelu, R.; et al. Klu suppresses megasporocyte cell fate through swr1-mediated activation of wrky28 expression in arabidopsis. *Proc. Natl. Acad. Sci. USA* **2018**, *115*, E526–E535. [CrossRef]
71. Sura, W.; Kabza, M.; Karlowski, W.M.; Bieluszewski, T.; Kus-Slowinska, M.; Paweloszek, L.; Sadowski, J.; Ziolkowski, P.A. Dual role of the histone variant h2a.Z in transcriptional regulation of stress-response genes. *Plant Cell* **2017**, *29*, 791–807. [CrossRef] [PubMed]
72. Smith, A.P.; Jain, A.; Deal, R.B.; Nagarajan, V.K.; Poling, M.D.; Raghothama, K.G.; Meagher, R.B. Histone h2a.Z regulates the expression of several classes of phosphate starvation response genes but not as a transcriptional activator. *Plant Physiol.* **2010**, *152*, 217–225. [CrossRef] [PubMed]
73. Zacharaki, V.; Benhamed, M.; Poulios, S.; Latrasse, D.; Papoutsoglou, P.; Delarue, M.; Vlachonasios, K.E. The arabidopsis ortholog of the yeats domain containing protein yaf9a regulates flowering by controlling h4 acetylation levels at the flc locus. *Plant Sci.* **2012**, *196*, 44–52. [CrossRef] [PubMed]
74. Su, Y.H.; Wang, S.L.; Zhang, F.; Zheng, H.; Liu, Y.N.; Huang, T.T.; Ding, Y. Phosphorylation of histone h2a at serine 95: A plant-specific mark involved in flowering time regulation and h2a.Z deposition. *Plant Cell* **2017**, *29*, 2197–2213. [CrossRef] [PubMed]
75. Wils, C.R.; Kaufmann, K. Gene-regulatory networks controlling inflorescence and flower development in arabidopsis thaliana. *Biochim. Biophys. Acta Gene Regul. Mech.* **2017**, *1860*, 95–105. [CrossRef] [PubMed]
76. Lee, J.H.; Yoo, S.J.; Park, S.H.; Hwang, I.; Lee, J.S.; Ahn, J.H. Role of svp in the control of flowering time by ambient temperature in arabidopsis. *Genes Dev.* **2007**, *21*, 397–402. [CrossRef]
77. Li, D.; Liu, C.; Shen, L.; Wu, Y.; Chen, H.; Robertson, M.; Helliwell, C.A.; Ito, T.; Meyerowitz, E.; Yu, H. A repressor complex governs the integration of flowering signals in arabidopsis. *Dev. Cell* **2008**, *15*, 110–120. [CrossRef] [PubMed]
78. Putterill, J.; Laurie, R.; Macknight, R. It's time to flower: The genetic control of flowering time. *Bioessays* **2004**, *26*, 363–373. [CrossRef] [PubMed]
79. Kobor, M.S.; Venkatasubrahmanyam, S.; Meneghini, M.D.; Gin, J.W.; Jennings, J.L.; Link, A.J.; Madhani, H.D.; Rine, J. A protein complex containing the conserved swi2/snf2-related atpase swr1p deposits histone variant h2a.Z into euchromatin. *Plos Biol.* **2004**, *2*, 587–599. [CrossRef]
80. Cui, Z.; Tong, A.; Huo, Y.; Yan, Z.; Yang, W.; Yang, X.; Wang, X.X. Skip controls flowering time via the alternative splicing of sef pre-mrna in arabidopsis. *BMC Biol.* **2017**, *15*, 80. [CrossRef]
81. Xiao, J.; Zhang, H.; Xing, L.; Xu, S.; Liu, H.; Chong, K.; Xu, Y. Requirement of histone acetyltransferases ham1 and ham2 for epigenetic modification of flc in regulating flowering in arabidopsis. *J. Plant Physiol.* **2013**, *170*, 444–451. [CrossRef] [PubMed]
82. Le Masson, I.; Yu, D.Y.; Jensen, K.; Chevalier, A.; Courbeyrette, R.; Boulard, Y.; Smith, M.M.; Mann, C. Yaf9, a novel nua4 histone acetyltransferase subunit, is required for the cellular response to spindle stress in yeast. *Mol. Cell Biol.* **2003**, *23*, 6086–6102. [CrossRef] [PubMed]
83. Schulze, J.M.; Wang, A.Y.; Kobor, M.S. Yeats domain proteins: A diverse family with many links to chromatin modification and transcription. *Biochem. Cell Biol.* **2009**, *87*, 65–75. [CrossRef] [PubMed]
84. Klein, B.J.; Ahmad, S.; Vann, K.R.; Andrews, F.H.; Mayo, Z.A.; Bourriquen, G.; Bridgers, J.B.; Zhang, J.Y.; Strahl, B.D.; Cote, J.; et al. Yaf9 subunit of the nua4 and swr1 complexes targets histone h3k27ac through its yeats domain. *Nucleic Acids Res.* **2018**, *46*, 421–430. [CrossRef] [PubMed]
85. Zhang, H.Y.; Richardson, D.O.; Roberts, D.N.; Utley, R.; Erdjument-Bromage, H.; Tempst, P.; Cote, J.; Cairns, B.R. The yaf9 component of the swr1 and nua4 complexes is required for proper gene expression, histone h4 acetylation, and htz1 replacement near telomeres. *Mol. Cell Biol.* **2004**, *24*, 9424–9436. [CrossRef] [PubMed]
86. Lu, P.Y.T.; Levesque, N.; Kobor, M.S. Nua4 and swr1-c: Two chromatin-modifying complexes with overlapping functions and components. *Biochem Cell Biol.* **2009**, *87*, 799–815. [CrossRef] [PubMed]
87. Neuwald, A.F.; Aravind, L.; Spouge, J.L.; Koonin, E.V. Aaa+: A class of chaperone-like atpases associated with the assembly, operation, and disassembly of protein complexes. *Genome Res.* **1999**, *9*, 27–43. [PubMed]

88. Kanemaki, M.; Kurokawa, Y.; Matsu-ura, T.; Makino, Y.; Masani, A.; Okazaki, K.; Morishita, T.; Tamura, T. Tip49b, a new ruvb-like DNA helicase, is included in a complex together with another ruvb-like DNA helicase, tip49a. *J. Biol. Chem.* **1999**, *274*, 22437–22444. [CrossRef] [PubMed]
89. Luo, Y.; Guo, Z.; Li, L. Evolutionary conservation of microrna regulatory programs in plant flower development. *Dev. Biol.* **2013**, *380*, 133–144. [CrossRef] [PubMed]
90. Samad, A.F.A.; Sajad, M.; Nazaruddin, N.; Fauzi, I.A.; Murad, A.M.A.; Zainal, Z.; Ismail, I. Microrna and transcription factor: Key players in plant regulatory network. *Front. Plant Sci.* **2017**, *8*, 565. [CrossRef]
91. Sheng, W.; Chen, Y.; Gong, Y.; Dong, T.; Zhang, B.; Gao, W. Mir-148a inhibits self-renewal of thyroid cancer stem cells via repressing ino80 expression. *Oncol. Rep.* **2016**, *36*, 3387–3396. [CrossRef] [PubMed]
92. Dai, X.; Bai, Y.; Zhao, L.; Dou, X.; Liu, Y.; Wang, L.; Li, Y.; Li, W.; Hui, Y.; Huang, X.; et al. H2a.Z represses gene expression by modulating promoter nucleosome structure and enhancer histone modifications in arabidopsis. *Mol. Plant* **2017**, *10*, 1274–1292. [CrossRef] [PubMed]
93. Seo, E.; Park, C.; Choi, K.; Lee, D.; Seok, C.; Lee, I. Molecular evolution of actin related protein 6, a component of swr1 complex in arabidopsis. *J. Plant Biol.* **2016**, *59*, 467–477. [CrossRef]
94. Cheng, X.; Auger, A.; Altaf, M.; Drouin, S.; Paquet, E.; Utley, R.T.; Robert, F.; Cote, J. Eaf1 links the nua4 histone acetyltransferase complex to htz1 incorporation and regulation of purine biosynthesis. *Eukaryot Cell* **2015**, *14*, 535–544. [CrossRef] [PubMed]
95. Ladurner, A.G.; Inouye, C.; Jain, R.; Tjian, R. Bromodomains mediate an acetyl-histone encoded antisilencing function at heterochromatin boundaries. *Mol. Cell* **2003**, *11*, 365–376. [CrossRef]
96. Durant, M.; Pugh, B.F. Nua4-directed chromatin transactions throughout the saccharomyces cerevisiae genome. *Mol. Cell Biol.* **2007**, *27*, 5327–5335. [CrossRef] [PubMed]
97. Yang, X.J. Lysine acetylation and the bromodomain: A new partnership for signaling. *Bioessays* **2004**, *26*, 1076–1087. [CrossRef]

International Journal of
Molecular Sciences

MDPI

Article

Mutations in the Rice *OsCHR4* Gene, Encoding a CHD3 Family Chromatin Remodeler, Induce Narrow and Rolled Leaves with Increased Cuticular Wax

Tingting Guo [1,†], Daofeng Wang [2,†], Jingjing Fang [2], Jinfeng Zhao [2], Shoujiang Yuan [3], Langtao Xiao [1,*] and Xueyong Li [2,*]

1 Hunan Provincial Key Laboratory of Phytohormones, Hunan Provincial Key Laboratory for Crop Germplasm Innovation and Utilization, College of Bioscience and Biotechnology, Hunan Agricultural University, Changsha 410128, China; guoting0118@126.com
2 National Key Facility for Crop Gene Resources and Genetic Improvement, Institute of Crop Science, Chinese Academy of Agricultural Sciences, Beijing 100081, China; w2806047078@126.com (D.W.); fangjingjing@caas.cn (J.F.); zhaojinfeng@caas.cn (J.Z.)
3 Shandong Rice Research Institute, Jinan 250100, China; ysj868@sina.com
* Correspondence: langtaoxiao@163.com (L.X.); lixueyong@caas.cn (X.L.); Tel.: +86-731-8463-5260 (L.X.); +86-10-8210-7409 (X.L.)
† These authors contributed equally to this work.

Received: 15 May 2019; Accepted: 24 May 2019; Published: 25 May 2019

Abstract: Leaf blade width, curvature, and cuticular wax are important agronomic traits of rice. Here, we report the rice *Oschr4-5* mutant characterized by pleiotropic phenotypes, including narrow and rolled leaves, enhanced cuticular wax deposition and reduced plant height and tiller number. The reduced leaf width is caused by a reduced number of longitudinal veins and increased auxin content. The cuticular wax content was significantly higher in the *Oschr4-5* mutant, resulting in reduced water loss rate and enhanced drought tolerance. Molecular characterization reveals that a single-base deletion results in a frame-shift mutation from the second chromodomain of OsCHR4, a CHD3 (chromodomain helicase DNA-binding) family chromatin remodeler, in the *Oschr4-5* mutant. Expressions of seven wax biosynthesis genes (*GL1-4*, *WSL4*, *OsCER7*, *LACS2*, *LACS7*, *ROC4* and *BDG*) and four auxin biosynthesis genes (*YUC2*, *YUC3*, *YUC5* and *YUC6*) was up-regulated in the *Oschr4-5* mutant. Chromatin immunoprecipitation assays revealed that the transcriptionally active histone modification H3K4me3 was increased, whereas the repressive H3K27me3 was reduced in the upregulated genes in the *Oschr4-5* mutant. Therefore, *OsCHR4* regulates leaf morphogenesis and cuticle wax formation by epigenetic modulation of auxin and wax biosynthetic genes expression.

Keywords: auxin; chromatin remodeling factor; cuticular wax; drought tolerance; epigenetic regulation; leaf width; histone modification; narrow leaf; *OsCHR4*; rice

1. Introduction

In plants, leaves are the major organ used for photosynthesis and transpiration, and are considered to be the main source of dry matter accumulation in plants. Blade width and curvature are key factors of leaf morphology. As reported, blade width, particularly that of the first and second uppermost leaves, can significantly influence the rice grain yield, whereas appropriately rolled leaves can optimize canopy light transmission, increase the effective leaf area per unit of land and, consequently, the canopy photosynthesis efficiency [1].

To date, a number of narrow and/or rolled leaf genes have been reported in rice. The majority of narrow leaf genes are related to auxin signaling. For example, a mutant of *Nal1* (encoding a plant-specific protein with unknown biochemical function) exhibited a characteristic phenotype of narrow leaves

due to decreased number of longitudinal veins and polar auxin transport capacity [2,3]. Mutation in *TDD1* (encoding a protein homologous to anthranilate synthase beta-subunit involved in the upstream of Trp-dependent auxin biosynthesis) could induce obviously narrow leaves [4]. *NAL7* and its allelic gene *CONSTITUTIVELY WILTED1* encode an auxin biosynthesis enzyme OsYUCCA8 and their mutants exhibit narrow leaves [5,6]. Similar to the auxin-deficient mutant, the leaves of the *osarf11-1*, a loss-of-function mutant of the *auxin-response factor 11* (*OsARF11*), are also moderately narrowed [7]. Mutations in genes involved in other pathways could also produce narrow leaves such as *NAL9* (encoding an ATP-dependent Clp protease proteolytic subunit) and *NAL11* (encoding a heat shock DNAJ protein) [8,9]. For rolled leave, it could be divided into adaxialized and abaxialized curling. The mutant of *SLL1*/*RL9* (encoding a SHAQKYF class MYB family transcription factor) displayed completely adaxialized leaves [10]. This gene mainly functions in the modulation of sclerenchymatous cells formation on the abaxial side during leaf development [11]. The mutant of *ADL1* (a plant-specific calpain-like cysteine proteinase) exhibited abaxially rolled leaves due to abnormal bulliform-like cells distribution [12]. Meanwhile, overexpression of *ACL1* (encodes a protein with unknown functional domains) and its homolog *ACL2* caused abaxial leaf curling [13], while overexpression of *OsAGO7* was correlated with adaxial leaf curling [14]. *SRL1* encodes a putative glycosylphosphatidylinositol-anchored protein and modulates leaf adaxial rolling by regulating the formation of bulliform cells [15]. Interestingly, several genes were associated with both narrow and rolled leaves. The mutants of *NRL1* (encoding cellulose synthase-like protein D4), *NRL2* and *NRL3* (both encoding a novel protein with unknown biochemical function) could induce semi-rolled leaves with reduced blade width [16–19].

The surface of rice leaf is covered by cuticular wax which provides self-protection against potential external stresses, such as non-stomatal water loss, pathogen infection and ultraviolet (UV) radiation [20]. The main composition of cuticular wax is the very-long-chain fatty acids (VLCFAs) as well as their following derivatives: aldehydes, primary and secondary alcohols, alkanes, ketones and wax esters. Through years of study, many genes encoding enzymes and transcription factors involved in biosynthesis of cuticular wax in rice have been uncovered by bioinformatics and genetic approaches. The *Glossy1* (*GL1*) gene family, reported first in maize, encodes the fatty aldehyde decarbonylase required for the synthesis of cuticular wax. Through homologous sequence alignment, 11 *OsGL1* family genes were found in rice [21]. Subsequent studies validated that *OsGL1-1*/*WSL2*, *OsGL1-2*, *OsGL1-3*, *OsGL1-5*/*Wda1* and *OsGL1-6* affect wax synthesis on various parts of rice plant [21–25]. AP2/ERF family transcription factors OsWR1 and OsWR2, homologs of the *Arabidopsis WIN1*/*SHN1* gene, promote wax production via activating wax biosynthesis gene [26,27]. Homeodomain-leucine zipper class IV family transcription factor ROC4 positively regulates cuticular wax biosynthesis via directly binding to the conserved L1 box *cis*-element in the promoters of Os-*BDG*, which encodes an extracellular synthase responsible for the formation of cuticle [28]. DROUGHT HYPERSENSITIVE (DHS), a RING-type E3 ligase, interacts with ROC4 and promotes its degradation via the ubiquitin/26S proteasome [28]. After synthesized in the endoplasmic reticulum, wax is transferred to the plant surface via adenosine triphosphate binding cassette transporters as well as lipid transfer proteins [29].

Proper regulation of gene expression during development is dependent on the dynamic modifications of chromatin, during which the accessibility of specific DNA regions to the transcription machinery may be altered. The chromodomain helicase DNA-binding (CHD) proteins are one family of chromatin remodeling factors, which are defined by a plant homeodomain (PHD) finger, two chromodomains, one SNF2 (sucrose non-fermenting)-related ATPase/helicase domain, and one DNA binding motif [30,31]. CHD chromatin remodelers directly change the chromatin structures and are important regulators of gene expression. Mutations of CHD protein could always induce pleiotropic phenotypes in plants. PICKLE is a typical CHD protein in *Arabidopsis*. The *pickle* mutant was initially characterized by pickle roots with green tuber due to failed repression of seed-specific genes [32]. This protein was then found to function in repression of ectopic stipules and meristems in leaf tissue and inhibition of meristematic genes in carpel tissue [33,34]. In rice, the closest homolog with PICKLE

is OsCHR702, while both T-DNA insertion mutation and RNAi of *OsCHR702* did not produce any morphological phenotypes [35,36]. OsCHR4 is another CHD member characterized in rice. The *Oschr4* mutant shows defective chloroplasts in the adaxial mesophyll cells due to blocked proplastid growth and thylakoid membrane formation [37]. As an allelic gene of *OsCHR4*, *OsCHR729* was revealed to encode a bifunctional chromatin regulator associated with gene transcription regulation through modulation of histone H3K4 and H3K27 methylation during plant development [36]. Meanwhile, the Os*chr729* mutant induced by T-DNA insertion shows pleiotropic phenotypes, including small and rolled leaves, reduced stem elongation and chlorophyll contents, and absence of secondary panicle branches [36]. One study reported that *CHR729* regulates seedling development by affecting contents of gibberellin acid (GA) in rice, and the transcript level of GA biosynthesis genes was altered in the corresponding mutant line *t483* [38]. In addition, *CRL6*, an allelic gene of *CHR729*, was speculated to regulate crown root development via auxin signaling pathway due to decreased expression of most *OsIAA* genes in *crl6* compared with the wild type (WT) [39]. Recently, *rfs*, another allelic mutant of *OsCHR4*/*OsCHR729*, was characterized by the chlorotic and cell death phenotypes due to accumulation of reactive oxygen species (ROS). Both transcript and H3K4me3 levels of five ROS-related genes declined in the *rfs* mutant [40].

In this study, three additional allelic mutants of *OsCHR4* were reported, namely *Oschr4-5*, *Oschr4-6*, and *Oschr4-7*, which exhibited pleiotropic phenotypes such as narrow and rolled leaf, reduced plant height, tiller number and seed size at mature stage. Anatomical investigations revealed that the reduced leaf width was due to a decreased number of major and minor veins while the cell size remained unchanged. The auxin content was significantly higher in *Oschr4-5*, which may explain the altered venation pattern and leaf size at physiological level. Interestingly, more cuticular wax was deposited on the surface of the *Oschr4-5* leaves, which reduced the water-loss rate and enhanced the drought tolerance. Expression levels of several auxin and wax biosynthesis genes were up-regulated in the *Oschr4-5* mutant. Consistent with the role of CHD3 protein in chromatin remodeling, histone modifications H3K4me3 and H3K27me3 in the upregulated genes were increased and reduced in *Oschr4-5*, respectively. Our data reveal novel functions of *OsCHR4* in the epigenetic regulation of auxin and wax biosynthesis-related genes, leaf development and cuticle wax formation in rice.

2. Results

2.1. Pleiotropic Phenotype of the Oschr4-5 Mutant

A rice mutant characterized by narrow and rolled leaves was isolated from the gamma ray mutagenized *Indica* rice cultivar Indica 9, which was named as *Oschr4-5* based on the gene identity revealed in the following study. At the seedling stage, slight dwarfism and albino on the adaxial side of leaves were observed in *Oschr4-5* (Figure 1A,B). At the mature stage, the plant height and tiller number of *Oschr4-5* was significantly reduced by 45% and 76% when compared with that of WT ($p < 0.01$) (Figure 1C, Table S1). The length and width of the leaves in *Oschr4-5* was significantly reduced by 38% and 50% when compared with that of the WT ($p < 0.01$) (Figure 1D,F, Table S1). Meanwhile, smaller seeds were also observed in *Oschr4-5* (Figure 1G). Later on, two allelic mutants, namely *Oschr4-6* and*Oschr4-7*, were isolated from the Ethyl methane sulfonate (EMS) mutagenized *japonica* cultivar Nipponbare, which exhibited the same pleiotropic phenotypes, including narrow and rolled leaves with albino on the adaxial side, significantly reduced leaf length, plant height, tiller number and seed size (Figure S1, Table S1).

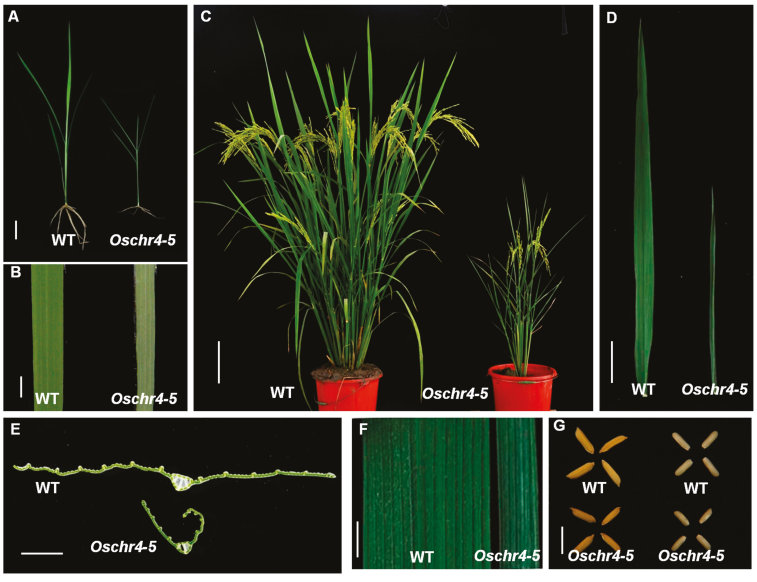

Figure 1. Phenotypic characterization of the *Oschr4-5* mutant. (**A**) Phenotypes of wild type (WT) and *Oschr4-5* mutant plants at seedling stage. Bar = 1 cm. (**B**) Adaxial side of leaf blade from wild type and *Oschr4-5* mutant at seedling stage. Bar = 0.5 cm. (**C**) Phenotypes of wild type and *Oschr4-5* mutant plants at mature stage. Bar = 15 cm. (**D**) Comparison of leaf length between wild type and *Oschr4-5* mutant at mature stage. Bar = 5 cm. (**E**) Cross sections through mature leaves from wild type and *Oschr4-5* mutant. Bar = 0.25 cm. (**F**) Comparison of leaf width between wild type and *Oschr4-5* mutant at mature stage. Bar = 0.5 cm. (**G**) Phenotypes of seeds from wild type and *Oschr4-5* mutant. Bar = 1 cm.

2.2. *Anatomical and Physiological Basis of Reduced Leaf Width*

To reveal the underlying cellular basis of narrow leaves in the *Oschr4-5* mutant, the venation pattern of leaf was first observed. The number of large veins and small veins of *Oschr4-5* was significantly reduced by 36% and 42%, respectively, of that of the WT ($p < 0.01$) (Figure 2A–D,G–H). Then the epidermal cell profile on the abaxial side of leaf blade was examined. Neither the number of cell column between the adjacent small vein nor the cell width at the horizontal orientation showed significant difference between *Oschr4-5* and WT (Figure 2E,F,I,J). These results indicate that the decreased leaf width in *Oschr4-5* may be caused by reduction in the number of veins. Since auxin is required for specification of the venation pattern in leaves [3,41] and auxin overproduction usually leads to narrow and epinastic leaves in *Arabidopsis* [42,43], the amount of free indole acetic acid (IAA), the major auxin, in *Oschr4-5* and WT was measured. As a result, the content of IAA in *Oschr4-5* was significantly higher than that of WT (86.39 ± 4.55 vs. 24.39 ± 0.76 ng/g, $p < 0.01$) (Figure 2L).

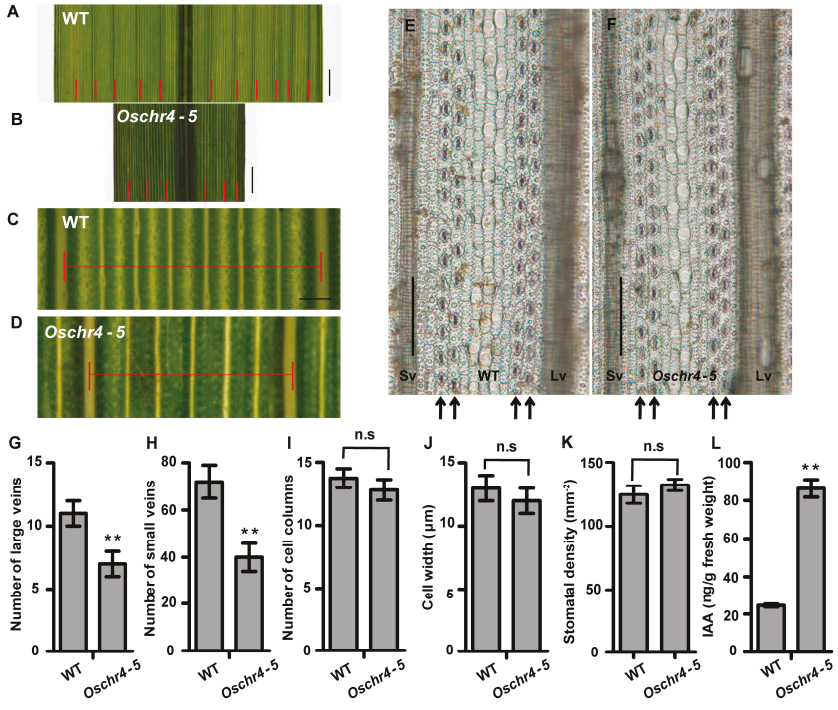

Figure 2. The *Oschr4-5* mutant affects leaf width. (**A**–**D**) The morphology of leaf veins from wild type and *Oschr4-5*mutant. Red bars represent large veins. Bar = 0.2 cm (**A**,**B**), 0.2 mm (**C**,**D**). (**E**,**F**) The abaxial epidermal cells of leaf blade from wild type and *Oschr4-5* mutant. Bar = 50 μm. The columns with stoma were indicated with black arrow. Sv: Small vein; Lv: Large vein. (**G**–**K**) Comparison of the large veins (**G**), small veins (**H**), cell columns (**I**), cell width (**J**) and stomatal density (**K**) on abaxial epidermis of leaf blade and indole acetic acid (IAA) contents between wild type and *Oschr4-5* mutant (**L**). Data are the means ± standard errors, $n = 15$ (**G**–**J**), 5 (**K**), 3 (**L**). Significance of data is tested by student's t test. ** $p < 0.01$.

2.3. Increased Cuticular Wax on the Surface of Leaves with Enhanced Drought Tolerance in Oschr4-5

Scanning electron microscopy was used to examine the surface of leaves. Interestingly, the platelet-like wax crystals deposited on the leaves' surface were larger and denser in *Oschr4-5* compared with WT (Figure 3A,B). Then the compositions and contents of cuticular wax were measured by gas chromatography-mass spectrometry (GC-MS). As shown in Figure 3C, the wax components of fatty acids, aldehydes, alcohols and alkanes were all significantly increased in *Oschr4-5* than WT ($p < 0.05$).

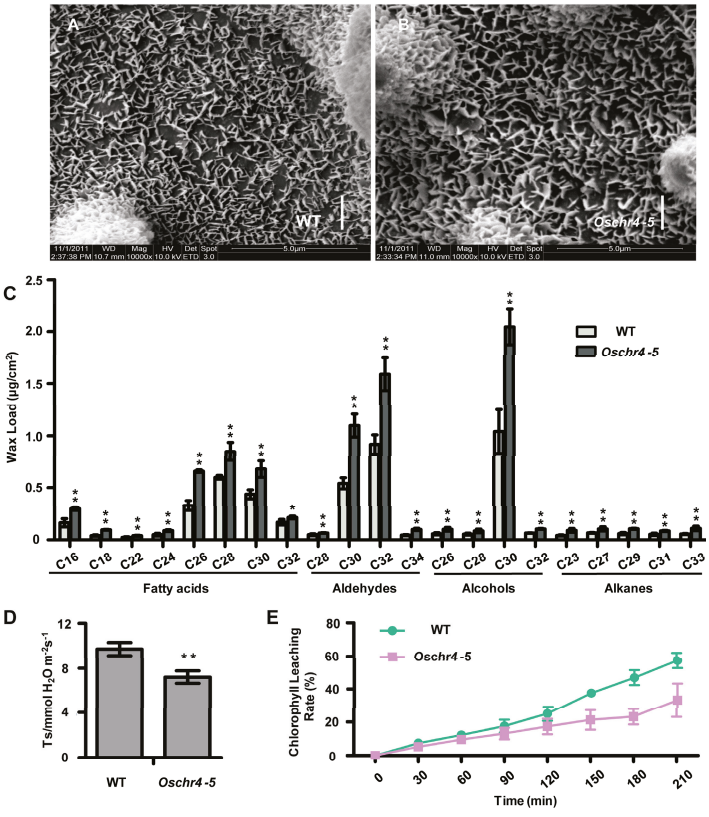

Figure 3. More cuticular wax deposited on leaves of the *Oschr4-5* mutant. (**A**–**C**) Scanning electron microscope (SEM) images of adaxially leaf surface (**A**,**B**) and cuticular wax composition and loads (**C**) from wild type and the *Oschr4-5* mutant. Bar = 2 μm. Data are the means ± standard errors (n = 3). Significance of data is tested by student's t test. * $p < 0.05$, ** $p < 0.01$. (**D**,**E**) The transpiration rate (**D**) and chlorophyll leaching rate (**E**) of leaf blades from wild type and *Oschr4-5* mutant. Data are the means ± standard errors (n = 3). Significance of data is tested by student's t test. ** $p < 0.01$.

As the content and structure of cuticular wax could strongly influence cuticle permeability, its effects on transpiration rate were first evaluated. Indeed, the transpiration rate of *Oschr4-5* was significantly lower than that of WT ($p < 0.01$) (Figure 3D). Secondly, measurement of cuticle membrane permeability as demonstrated by chlorophyll-leaching rate showed that chlorophyll leaches slower from *Oschr4-5* than WT at different time points (Figure 3E). Furthermore, a dehydration-rehydartion treatment revealed that drought tolerance of *Oschr4-5* was significantly enhanced. The *Oschr4-5* seedlings showed significantly higher recovery rate than WT (60% vs. 8%, $p < 0.01$) (Figure 4A–D). The water loss rate was also measured to evaluate the water retention capacity of detached leaves. The data showed that water loss rates of *Oschr4-5* were significantly slower than in WT (Figure 4E). The possible effects of stomatal density and leaf thickness on the differential water loss rate might be ruled out because no significant difference was detected in the stomatal density (Figure 2E,F,K) and leaf blade thickness (WT: 107.43 ± 7.51 μm; *Oschr4-5*: 108.17 ± 7.23 μm) between *Oschr4-5* and WT. These results prove that *Oschr4-5* exhibited lower cuticle permeability and water loss because of higher cuticular wax content on the surface of leaves compared to WT.

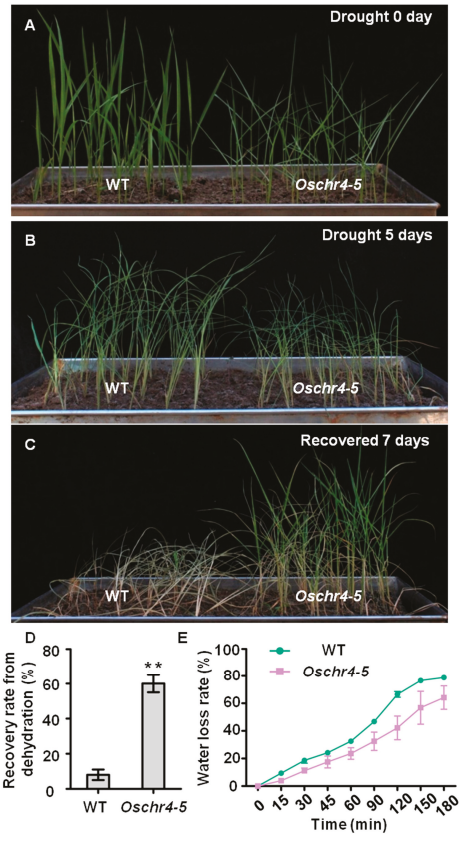

Figure 4. The drought stress responses of the *Oschr4-5* mutant. (**A**–**C**) Drought experiment with the 4 week-old plants for 0 day (**A**), 5 days (**B**), seedling recovered 7 days after rehydration (**C**). (**D**) Recovery rate from dehydration of wild type and *Oschr4-5* mutant in (**C**). Data are the means ± standard errors ($n = 3$). Significance of data is tested by student's t test, ** $p < 0.01$. (**E**) Water loss rate of detached leaf blades between wild type and the *Oschr4-5* mutant. Data are the means ± standard errors ($n = 3$).

2.4. Characterization of the Molecular Lesions in the Oschr4 Mutant

To find out the molecular lesion responsible for the pleiotropic phenotypes of the *Oschr4-5* mutant, three F_2 populations were generated (*Oschr4-5* × 9311; *Oschr4-5* × Nipponbare; *Oschr4-5* × 02428). Within these F_2 populations, a mendelian segregation ratio of 3:1 ($\chi^2_{0.05} < 3.84$) was calculated, which indicated the mutant phenotype was controlled by a single recessive gene. Then a large F_2 population generated by *Oschr4-5* × 02428 was used to map the causative locus. In primary mapping, 116 F_2 mutant individuals located this gene between two Indel markers ha1 and ha10 on the long arm of chromosome 7. Fine mapping using 7 new Indel markers and 2000 F_2 recessive individuals further localized this gene within 50 kb region delimited by Indel markers ha5 and ha6 (Figure 5A).

According to the MSU (Michigan State University) Rice Genome Annotation Release 7 (http://rice.plantbiology.msu.edu), a total of 5 predicted open reading frames (ORFs) were revealed within the 50 kb fine mapping interval, including 3 ORFs with known biochemical functions (ORF 2: phosphate-induced protein 1; ORF 4: OsCHR4/CHR729; ORF 5: peptide-Nasparagine amidase), 1 ORF encoding expressed hypothetical protein (ORF 3) and 1 transposon (ORF 1) (Figure 5B). Then genomic DNA of all these five ORFs in the *Oschr4-5* mutant was sequenced and compared with that of WT.

A single-base deletion at position 3688 was found in the ORF4 in *Oschr4-5* (created through gamma ray radiation), whereas no mutation was found in other four ORFs. Sequence analysis of other two allelic mutants *Oschr4-6* and *Oschr4-7* created through EMS mutagenesis revealed a C4382T and G5190A substitution in ORF4, respectively (Figure 5C). Therefore, ORF4 encoding OsCHR4/CHR729 was found to be the target gene, which is quite large with 11 exons and 10 introns.

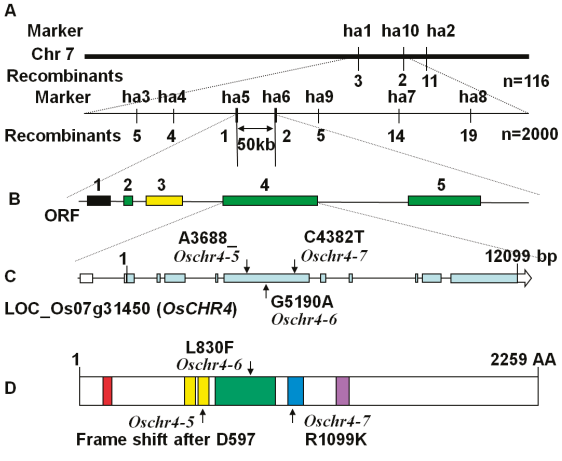

Figure 5. Molecular characterization of mutation sites in the *OsCHR4* gene. (**A**) Fine mapping of the gene on chromosome 7. The mutated gene was localized within 50 kb region delimited by two indel marker ha5 and ha6. (**B**) Predicted open reading frames (ORFs) within the fine mapping interval. Green, ORFs with known biochemical functions; Yellow, ORFs encoding expressed hypothetical proteins; Black, ORFs encoding transposons. (**C**) Gene structure of *OsCHR4*. The mutation sites in the*Oschr4-5*, *Oschr4-6* and *Oschr4-7* mutant were indicated as black arrows. Blue boxes, exons; white boxes, UTR; black line, introns. (**D**) Protein structure of OsCHR4. Each domain is represented in different color box. Red, PHD domain; yellow, Chromo domains; green, SNF2 related helicase/ATPase domain; blue, Helicase C domain; purple, DNA-binding domain.

2.5. Alignment and Phylogenetic Analysis

OsCHR4 encodes a member of the CHD3 subfamily of chromatin remodeling factors [36,37]. OsCHR4 has 2259 amino acids in length with several putative domains, including one PHD domain, two chromodomains, one SNF2 related helicase/ATPase domain, one Helicase C and one DNA-binding domain from amino terminus to carboxyl terminus (Figure 5D). In the *Oschr4-5* mutant, the single-base deletion results in a frame-shift mutation from the second chromodomain. In *Oschr4-6*, the amino acid substitution L830F (CTC to TTC) occurred within the SNF2 related helicase/ATPase domain. In *Oschr4-7*, the amino acid substitution R1099K (AGA to AAA) occurred within the Helicase C domain (Figure 5D).

Multiple sequence alignment of the OsCHR4 homologous proteins in eight species was performed. As shown in Figure S2A, the substitution mutation sites in *Oschr4-6* and *Oschr4-7* were highly conserved in these species, which highlights the important role of these residuals in CHR4. Then the evolutionary relationship among CHD families in rice and *Arabidopsis* was evaluated. As a result, CHR705 was revealed to belong to the member of subfamily I (CHD1), and the other CHR proteins belonged to subfamily II (CHD3). There were no subfamily III members found in rice or *Arabidopsis*. Meanwhile, PICKLE in *Arabidopsis* was found to be close to CHR702 in rice, and the closest gene with *OsCHR4* in *Arabidopsis* was CHR4 (PKR1) (Figure S2B).

2.6. Expression of Several Wax and Auxin Biosynthesis Related Genes Were Upregulated in Oschr4-5

As a chromatin remodeling factor, the loss of OsCHR4 function was identified to influence the rice plant growth and development in various ways [36–40], but the underlying molecular mechanisms need to be further analyzed. To understand why the content of cuticular wax increased in the *Oschr4-5* mutant, we examined the expression levels of 16 genes encoding enzymes involved in wax biosynthesis and three genes (*ROC4*, *WR1*, *WR2*) encoding transcription factors that activate the expression of wax biosynthetic genes [26–28,44,45]. Quantitative real-time polymerase chain reaction (RT-PCR) using RNA samples prepared from leaves of 30-day-old plants revealed that transcript levels of six wax biosynthetic genes (*GL1-4*, *WSL4*, *OsCER7*, *LACS2*, *LACS7*, *BDG)* and one transcription factor gene (*ROC4*) [26–28,44,45] were significantly upregulated in *Oschr4-5*, compared with WT (Figure 6A). This result suggests that loss of function of CHR4 affects the expression of important genes involved in the wax biosynthesis.

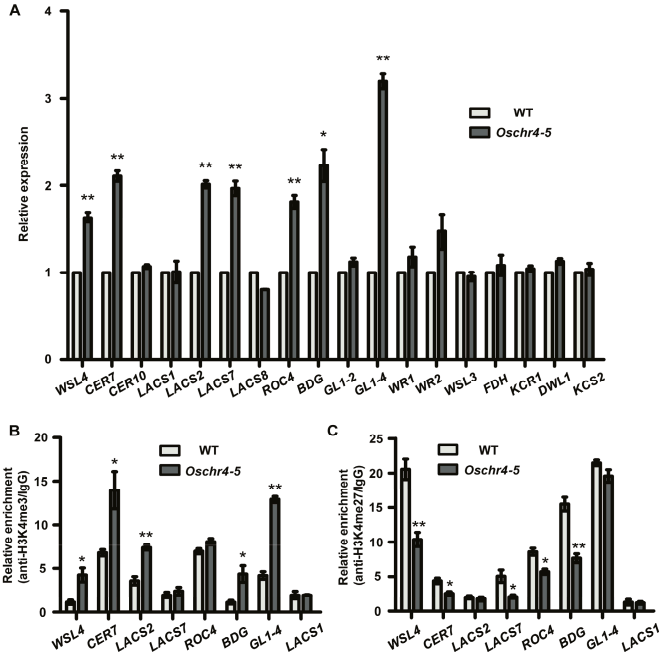

Figure 6. *OsCHR4* regulates expression of genes related to wax biosynthesis. (**A**) Quantitative real-time polymerase chain reaction (qRT-PCR) analysis of 19 wax genes in 30-day-old plants of WT and *Oschr4-5*. Data are the means ± standard errors (n = 3). Significance of data is tested by student's t test. * $p < 0.05$, ** $p < 0.01$. (**B**,**C**) ChIP-qPCR analysis for H3K4me3 (**B**) and H3K27me3 (**C**) levels on 7 up-regulated wax genes in *Oschr4-5* relative to the WT. Data are the means ± standard errors (n = 3). Significance of data is tested by student's t test. * $p < 0.05$, ** $p < 0.01$.

The *YUCCA* gene, which encodes a flavin monooxygenase-like enzyme, is known to be involved in Trp-dependent auxin biosynthesis [46]. The *TAA/TAR* genes, which encode putative Trp aminotransferases, have been proposed to act in the same pathway with *YUCCA* genes [47]. To explain the increased IAA level in the *Oschr4-5* mutant, we measured the expression levels of 13 genes from the *YUCCA* and *TAA/TAR* family between three-day-old seedlings of WT and *Oschr4-5*. The transcript levels of four *YUCCA* related genes including *YUC2*, *YUC3*, *YUC5* and *YUC6* were upregulated significantly in the *Oschr4-5* mutants (Figure 7A). However, the other 9 genes showed no significant alteration in the *Oschr4-5* mutants. These results suggested that *OsCHR4* may influence the expression

of several wax-related and IAA-related genes, and the increased gene expressions in the *Oschr4-5* mutants conduces to higher wax and IAA content in *Oschr4-5* than WT.

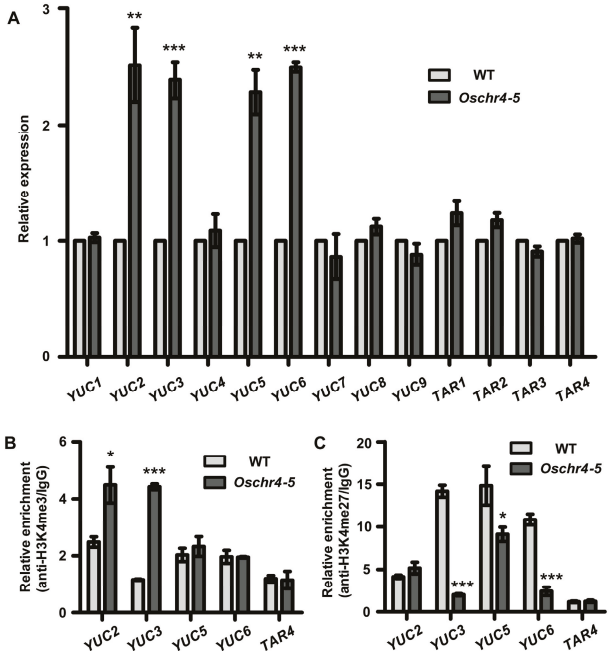

Figure 7. Expression and histone modification of genes involved in IAA biosynthesis in WT and *Oschr4-5*. (**A**) qRT-PCR analysis showed 4 of 13 tested IAA biosynthesis genes were up-regulated in 3-day-old seedlings of *Oschr4-5* relative to the WT. Data are the means ± standard errors ($n = 3$). Significance of data is tested by student's *t* test. ** $p < 0.01$, *** $p < 0.001$. (**B**,**C**) ChIP-qPCR analysis showed variations of H3K4me3 (**B**) and H3K27me3 (**C**) levels on 4 up-regulated IAA genes in *Oschr4-5* compared to WT. Data are the means ± standard errors ($n = 3$). Significance of data is tested by student's *t* test. * $p < 0.05$,*** $p < 0.001$.

2.7. Histone Modifications of the Wax and Auxin Biosynthesis-Related Genes Were Affected in Oschr4-5

Histone modification is recognized as an important mechanism in the epigenetic regulation of gene expression. For example, trimethylation of histone H3 lysine 4 (H3K4me3) is generally correlated with gene activation, whereas trimethylation of histone H3 lysine 27 (H3K27me3) is generally correlated with gene repression [48,49]. As reported, the rice CHD3 protein OsCHR4/CHR729 is a chromatin remodeler and can modulate H3K4me3 and H3K27me3 level to regulate the genes expression [35]. In order to test whether increased expression of wax and auxin biosynthesis related genes in *Oschr4-5* could be attributed to altered histone modification, a ChIP analysis with antibody recognizing H3K4me3 and H3K27me3 was performed. Of the seven wax biosynthetic genes, three genes (*WSL4*, *CER7*, *BDG*) showed increased H3K4me3 and decreased H3K27me3 simultaneously, four genes showed either increased H3K4me3 (*GL1-4*, *LACS2*) or decreased H3K27me3 (*LACS7*, *ROC4*) (Figure 6B,C). Similarly, of the four auxin biosynthetic genes, one gene (*YUC3*) showed increased H3K4me3 and decreased H3K27me3 simultaneously, three genes showed either increased H3K4me3 (*YUC2*) or decreased H3K27me3 (*YUC5*, *YUC6*) (Figure 7B,C). *LACS1* and *TAR4*, two control genes which were not differentially expressed between *Oschr4-5* and WT, did not show significant changes in level of H3K4me3 and H3K27me3 (Figure 6; Figure 7). Taken together, *OsCHR4* affects modifications

of histone protein associated with wax and auxin biosynthesis related genes and regulates their expression epigenetically.

3. Discussion

In rice, a total of six CHD-related (CHR) genes were found in its genome (http://www.chromdb.org), including *CHR705* (*Os07g46590*), *CHR702* (*PKL*, *Os06g08480*), *CHR703* (*Os01g65850*), *CHR4*/*CHR729* (*PKR1*, *Os07g31450*), *CHR723* (*Os06g01320*) and *CHR744* (*Os02g02050*). Among these CHR proteins, CHR729 was a typical chromatin remodeling factor which belonged to subfamily II (CHD3) [38]. It has been reported that three additional allelic mutants of *CHR4* displayed pleiotropic phenotypes [37,38,50]. In this study, three more allelic mutants of *CHR4* (*Oschr4-5, -6, -7*) were isolated, which exhibited similar pleiotropic phenotypes, including slight dwarfism, narrow and rolled leaves, and reduced chlorophyll contents in adaxial cells. More importantly, we found some novel phenotypes such as reduced number of longitudinal veins, increased IAA content, enhanced cuticular wax disposition and enhanced drought tolerance in *Oschr4-5*, which further illustrated the multiple functions of *OsCHR4* in plant development.

The closest homolog gene with *OsCHR4* in *Arabidopsis* is considered to be *AtCHR4 (PICKLE RELATED1, PKR1*) (Figure S2B), while their functions in plants seem to be different. Homozygous mutants of neither *PICKLE* homologs *PKR1* nor *PKR2* exhibited significant phenotypic differences to WT plants under standard growth conditions [51]. However, *OsCHR4* was revealed to be closely related with the development of rice leaves in this study. It is noteworthy that the function of *OsCHR4* is more similar to CHD3-related *PICKLE*. *PICKLE* was initially isolated from the *Arabidopsis pickle* mutant characterized by green tuberous root phenotype [52]. It has been reported that *PICKLE* functions in repression of ectopic stipules and meristems in leaf tissue and represses meristematic genes in carpel tissue [51,53]. *PICKLE* is not only involved in organ or cell polarity, but also plays an important role in cell differentiation [52]. Loss-of-function mutations in *PICKLE* could always influence cell transition from embryonic to vegetative development, thereby inducing pleiotropic phenotypes in the root, leaves and even the whole plants [54,55]. These phenotypes were just consistent with those of *Oschr4-5* isolated in this study and indicated a similar function between *OsCHR4* and *PICKLE.* However, T-DNA insertion mutation and RNAi of the closest homolog gene with *PICKLE* in rice (Os*CHR702*) did not produce any morphological phenotype [36]. Therefore, we suspect that the function of CHR proteins may be diversified between *Arabidopsis* and rice due to specific species difference.

Cuticular waxes are complex mixtures of very-long-chain fatty acids (VLCFAs) and their derivatives and provide effective protection for plants to confront various environmental stresses [28]. In this study, we discovered that *OsCHR4* negatively regulates the wax biosynthesis and more cuticle wax accumulated on the adaxial side of leaves in *Oschr4-5* mutant compared to the WT. Previous reports demonstrate that excessive deposition of cuticular wax can decrease nonstomatal water loss in plants [24,56]. We also proved that increased wax content in *Oschr4-5* results in reduced water loss and improved drought tolerance. As a result of increased wax deposition in *Oschr4-5*, the mutant *Oschr4-5* exhibits less chlorophyll leaching rate compared with WT. Furthermore, increased transcript levels of genes involved in wax biosynthesis in *Oschr4-5* were also in support of the regulation of *OsCHR4* in wax synthesis. Among the seven up-regulated genes in *Oschr4-5* (Figure 6A), *WSL4* and its homolog gene *OsCER7* encode β-Ketoacyl-coenzyme A synthase (KCS) which is the key enzyme in the first step of VLCFA elongation [45,57]. *OsGL1-4* encodes the fatty aldehyde decarbonylase, which has been identified to positively regulate various steps of wax biosynthesis [21–25]. *LACS2* and *LACS7* encode long-chain acyl-CoA synthase that preferentially modifies VLCFAs for wax biosynthesis [58]. *BDG* (*BODYGUARD*) encodes an α/β-hydrolase fold protein important for cuticle development [28]. *ROC4* encodes a HD-ZIP IV transcription factor which positively regulates wax deposition in rice by activating wax biosynthetic gene such as *BDG* [28]. This result suggests multiple steps of wax biosynthesis pathway are affected by the loss of function of CHR4 and is consistent with the quantification data that many wax components were significantly increased in *Oschr4-5* (Figure 3C).

It has been demonstrated in previous research that *OsCHR4* is essential for various aspects of plant development via influencing the gibberellin pathway and ROS homeostasis [38,40]. In this study, we found that the content of IAA in *Oschr4-5* was significantly higher than that of WT. As reported, many narrow leaves genes were interrelated with IAA. Auxin overproduction is well known to lead to narrow and epinastic leaves. Ectopic overexpression of either *YUCCA* genes (encoding flavin monooxygenases) in *Arabidopsis* [46] or the Agrobacterium auxin biosynthetic gene *iaaM* (encoding tryptophan monooxygenase) and petunia *FLOOZY* gene (ortholog of *YUCCA*) in petunia resulted in narrow and rolled leaves with high levels of IAA [42,43]. In *Arabidopsis*, narrow and rolled leaves were also caused by elevated IAA levels by overexpressing cytochrome P450 *CYP79B2* which converts tryptophan (Trp) to indole-3-acetaldoxime [59]. A similar case was reported in rice, where *OsYUCCA8/NAL7* also affects leaf width via altered IAA content [6]. In this study, increased IAA content was also detected in the narrow leaf mutant *Oschr4-5*. Auxin is principally converted from tryptophan via the TAA family of aminotransfrases and the YUCCA (YUC) family of flavin-containing monooxygenases [60,61]. For further verification of the altered IAA concentration in *Oschr4-5*, we detected the expression of *TAA* and *YUC* family genes and found that expression levels of four *YUC* genes increased in *Oschr4-5* mutants compared with WT. The finding is consistent with increased IAA concentration in *Oschr4-5*, which strengthens the evidence that *OsCHR4* might regulate auxin biosynthetic process in rice. Interestingly, 31 *OsAux/IAA* genes involved in the auxin signaling pathway was significantly downregulated in *crl6*, an allelic mutant of *Oschr4-5* [39]. The decreased transcript level of *OsIAA* genes might be due to higher IAA content as revealed in this study. As early-response genes and negative regulators of auxin signaling, *Aux/IAA* transcripts tend to be rapidly induced and then repressed by elevated IAA content [62].

Histone modification was an important mechanism in regulation of DNA transcription and other activities. As reported, trimethylated histone H3 lysine 27 (H3K27me3) was associated with gene silencing and repression during plant development, while trimethylated histone H3 lysine 4 (H3K4me3) is generally correlated with gene activation [63,64]. In the *chr729* mutant, 56% and 23% of marked genes lost H3K27me3 and H3K4me3, while 754 and 724 genes gained ectopic H3K27me3 and H3K4me3 [36]. Meanwhile, *PICKLE* was revealed to be able to reduce the level of H3K27me3 on root stem cells, thereby promoting the expression of meristem marker genes [65]. To evaluate the histone modification states in the *Oschr4-5* mutant, ChIP was performed on several differently expressed genes involved in wax and auxin biosynthesis in this study. As a result, the increased level of H3K4me3 and/or reduced level of H3K27me3 in the *Oschr4-5* mutant were significantly correlated with increased expression of genes related to wax or IAA biosynthesis. Consistent with the genome-wide ChIP-Seq analysis showing that 724 genes were detected to have gained ectopic H3K4me3 in the *chr729* mutant [36], H3K4me3 was also increased in several auxin and wax biosynthesis genes in the *Oschr4-5* mutant in our study. The underlying mechanism for the increased H3K4me3 at some specific loci still remains elusive [36]. As a bifunctional chromatin regulator that recognizes and modulates both H3K4 and H3K27 methylation, the function of OsCHR4 might be determined by sequence-specific transcription factors that associates with their targets and/or by the recruitment of different histone modification enzymes that catalyze methylation or demethylation.

In conclusion, our results suggest that *OsCHR4* not only regulates the accumulation of cuticle wax on leaf surface, but also plays an essential role in the modulation of IAA biosynthesis. Expression levels of several genes involved in the two pathways were increased accompanied with up-regulated H3K4me3 or down-regulated H3K27me3. Epigenetic regulation by *OsCHR4* is required for multiple aspects of plant development.

4. Materials and Methods

4.1. Plant Materials and Growth Condition

The rice mutant *Oschr4-5* (requested from Dale Bumpers National Rice Research Center, Stuttgart, AR, USA) was isolated from the *indica* cultivar Indica 9 treated by gamma ray radiation. The other two allelic mutants *Oschr4-6* and *Oschr4-7* were isolated from the *japonica* cultivar Nipponbare treated with EMS in the Institute of Crop Science, Chinese Academy of Agricultural Sciences, Beijing, China. All rice plants were cultivated in the experimental field of Shandong Rice Research Institute (Jining, China) under natural growing conditions, and the climatic conditions during the rice growing season were listed in Table S2. The mutant phenotype inherited stably after continuous cultivation. Field data of the mutant and WT plants, including plant height, tiller number, leaf width and leaf length were measured at the heading stage. The transpiration rate of plants was detected in field using LI-6400XT Portable Photosynthesis System.

4.2. Microscopic Observation

At the heading stage, the top first leaf of the mutant and WT were cut into pieces (2 cm) in the widest part and divided into three groups. One group of samples were used for microscopic observation of leaf vein and transverse cross section. Another group of samples were air-pumped in 2% cellulase R-10 solution for 30 min and digested for at least 2 days. After washing with water, mesophyll cells were peeled and the abaxial epidermis was observed under microscope. The cell width was measured using the Image J software (https://imagej.nih.gov/ij/). Stomatal density (mm^{-2}) was counted between two lateral veins in the center region of five individual leaves. Finally, the last group of samples were fixed in fixative solution (75% ethanol, 5% acetic acid, 5% glycerol, 5% formaldehyde and 10% deionized water) for at least one day, and then critical point dried, sputter-coated with gold and observed with a scanning electron microscope (UANTA 200).

4.3. Measurement of Chlorophyll and Indole Acetic Acid (IAA)

The top first leaf of plants at heading stage was used for chlorophyll measurement. Briefly, 0.05 g leaf samples were cut into small pieces and incubated in 80% acetone overnight in dark. Then the chlorophyll contents were measured and calculated by absorption spectrophotometry. For the measurement of IAA, 0.2 g freeze dried sample of the whole shoots of 3-day-old seedlings was harvested for each replicate. Free IAA extraction and measurement was performed as described previously [66].

4.4. Measurement of Cuticular Waxes

The content of cuticular waxes in the leaf of mutant and WT was measured as described previously [24]. Briefly, cuticular wax samples were first extracted from the top first leaf of plants at the heading stage by immersion in chloroform (60 °C, 30 s). A total of 20 μg n-tetracosane (C24, SUPELCO, Sigma, Saint Louis, USA) was added to these samples as an internal standard. Then the solutions were soaked with 100 mm^3 bis-N,N-(trimethylsilyl) trifluoroacetamide (BSTFA, SUPELCO, Sigma) and 100 mm^3 pyridine for 1 h at 70 °C. After evaporation and filtration (WHATMAN, PTFE, 13 mm × 0.22 μm), the compositions of cuticular waxes were analyzed using a capillary gas chromatograph equipped with an HP-1MS column (30 m length, inner diameter 0.32 mm, film thickness 0.25 μm) attached to a mass spectrometer (GCMS-QP2010, Kyoto, Japan). The GC-MS protocol included injection at 250, 50 °C for 2 min, ramped to 200 at 20 °C min^{-1}, 2 min at 200 °C, ramped to 320 at 2 °C min^{-1}, 14 min at 320 °C with supplied at 1.2 cm^3 min^{-1} as the carrier gas. A flame ionization detector was used for quantitative analyses, and the quantification of each component was calculated by the equivalent ratio of mass to peak area between the component and internal standard.

4.5. Water Loss and Chlorophyll-Leaching Assays

Leaf water loss rate was measured using detached leaves of the same parts from 6 week-old seedlings cultured in climate chambers. Each leaf was kept in a box without lid, and weighed every 15 min [28]. The water loss rate was calculated by dividing the lost weight of leaf at different time points by the initial weight. In the assay of chlorophyll leaching, the leaves (0.25 g) were cut into 2 cm lengths and immersed in 25 cm^3 80% ethanol. 1 cm^3 chlorophyll leaching solution was taken for spectrophotometry at wave lengths of 664 and 647 nm every 30 min. 1 cm^3 80% ethanol was used as control. The solution should be collected and poured back in the same tube after each measurement. The chlorophyll concentration was calculated by the formula of 7.939 A664 × 19.539 A647 [24]. The chlorophyll-leaching rate was given by dividing the concentration monitored at different time points by the chlorophyll concentration measured after 24 h of immersion. The experiment comprised three replicates.

4.6. Mapping and Sequencing

An F_2 segregating population generated from a cross between *Oschr4-5* and 02428 (a polymorphic *japonica* cultivar) was used for mapping and cloning of the target gene. For the primary mapping, a DNA pool composed of DNA from 10 individual mutant plants was used for bulked segregation analysis (BSA) [67]. Approximately 200 polymorphic indel markers distributed evenly throughout the rice genome were used for the BSA analysis. For fine mapping, new indel markers were designed by utilizing genomic sequence information from *Indica* and *Japonica* (http://rgp.dna.affrc.go.jp/) (specific primers were shown in Table S3). DNA was extracted from fresh leaves of each plant. PCR program included 5 min at 95 °C followed by 35 cycles of 30 s at 94 °C, 30 s at 55 °C, 30 s at 72 °C, and a final extension of 10 min at 72 °C. PCR products were analyzed on a polyacrylamide gel stained with silver nitrate. The genomic region of the candidate gene was divided into several overlapping 1.5-kb fragments, and amplified using high-fidelity PrimeSTAR DNA polymerase (TaKaRa Bio, DaLian, China). The PCR program included 3 min at 94 °C followed by 40 cycles at 98 °C for 30 s, 55 °C for 5 s, 72 °C for 1.5 min, and a final extension at 72 °C for 10 min. PCR products were sequenced directly.

4.7. Real-Time Polymerase Chain Reaction (RT-PCR)

Total RNA was first extracted from rice plants with Trizol method, and then first-strand cDNA was synthesized using a Superscript III Reverse Transcription Kit (Invitrogen, Carlsbad, CA, USA). Semiquantitative PCR was performed using LA Taq DNA polymerase (TaKaRa) with the rice *ACTIN1* gene serving as an internal control. The PCR program included 1 min at 94 °C followed by 30 cycles at 94 °C for 30 s, 60 °C for 30 s, 72 °C for 30 s, and a final extension at 72 °C for 10 min. Quantitative PCR was performed using a SYBR Premix Ex Taq2 kit (TaKaRa) on ABI PRISM 7900HT under the following conditions: 10 s denaturing at 95 °C, 30 s annealing at 60 °C, 40 cycles. The mRNA amount relative to *ACTIN1* was finally calculated. Specific primers were shown in Table S4.

4.8. Sequence and Phylogenetic Analyses

Gene prediction was performed using online search software (http://rice.plantbiology.msu.edu/cgi-bin/gbrowse/rice). Exon/intron structures were identified by alignment of coding sequences (CDS) and genomic DNA sequences. Multiple sequence alignments were conducted using CLUSTALX software, and a phylogenetic tree was built using MEGA 4 software [68].

4.9. Chromatin Immunoprecipitation (*ChIP*) *Analysis*

The ChIP experiment was performed based on a previously published protocol [69]. Simply, 0.5 g of 3-day-old or four-leaf-old seedlings of *Oschr4-5* and WT were first harvested and crosslinked in 1% formaldehyde under vacuum for 15 min or 30 min, respectively. Then the isolated chromatin complex was fragmented to 200–500 bp by sonication, and 1% of the fragmented chromatin from each tube

was kept as input DNA. The chromatin modification states of several target genes were analyzed using antibodies recognizing H3K4me3 (ab8580, Abcam, Cambridge, UK) and H3K27me3 (ab6002, Abcam) and the pre-immune serum (02-6502, Invitrogen) as a negative control. Then the immune complexes were collected with Protein A Agarose beads (P3476, Sigma). After reversing the crosslink, the precipitated and input DNAs were detected by real-time PCR, and the enrichment of H3K4me3 and H3K27me3 of each genes was quantified by normalizing the threshold cycle (*C*t) of the ChIP sample with that of the input with $2^{(\text{Ct of input} - \text{Ct of sample ChIP})}$. Specific primers used in ChIP-PCR are shown in Table S4.

4.10. Accession Number

Sequence data from this article can be found in the GenBank databases under the following accession numbers: *OsCHR4* genomic DNA, MK765112; *OsCHR4* cDNA, MK765113.

Supplementary Materials: Supplementary materials can be found at http://www.mdpi.com/1422-0067/20/10/2567/s1.

Author Contributions: Conceptualization, X.L.; methodology, T.G., D.W.; validation, J.F., and J.Z.; resources, S.Y.; writing—original draft preparation, T.G. and D.W.; writing—review and editing, X.L.; supervision, X.L. and L.X.; funding acquisition, X.L.

Funding: This research was funded by National Natural Science Foundation of China, grant number 31870271; National Major Project for Developing New GM Crops, grant number 2016ZX08009-003; and the Agricultural Science and Technology Innovation Program of Chinese Academy of Agricultural Sciences. The APC was funded by National Natural Science Foundation of China.

Acknowledgments: We thank Dale Bumpers National Rice Research Center (Stuttgart, AR, USA) for providing the rice seeds of *Oschr4-5* (*GSOR22*) and Indica 9; Tianfu Han (Institute of Crop Science, Chinese Academy of Agricultural Sciences) for assistance in measurement of photosynthetic and transpiration rate.

Conflicts of Interest: The authors declare no conflict of interest.

Abbreviations

CHD3	Chromodomain Helicase DNA-binding (CHD) protein 3
ChIP	Chromatin immunoprecipitation
CHR4	CHD-related protein 4
NAL1	Narrow leaf 1

References

1. Lang, Y.; Zhang, Z.; Gu, X.; Yang, J.; Zhu, Q. Physiological and ecological effect of crimpy leaf character in rice (Oryza sativa L.). II. Photosynthetic character, dry mass production and yield forming. *Acta Agron. Sin.* **2004**, *30*, 883–887.
2. Jiang, D.; Fang, J.; Lou, L.; Zhao, J.; Yuan, S.; Yin, L.; Sun, W.; Peng, L.; Guo, B.; Li, X. Characterization of a null allelic mutant of the rice *NAL1* gene reveals its role in regulating cell division. *PLoS ONE* **2015**, *10*, e0118169. [CrossRef] [PubMed]
3. Qi, J.; Qian, Q.; Bu, Q.; Li, S.; Chen, Q.; Sun, J.; Liang, W.; Zhou, Y.; Chu, C.; Li, X.; et al. Mutation of the rice *Narrow leaf1* gene, which encodes a novel protein, affects vein patterning and polar auxin transport. *Plant Physiol.* **2008**, *147*, 1947–1959. [CrossRef] [PubMed]
4. Takashi, S.; Noriko, K.; Takeshi, N.; Kozue, O.; Yutaka, S.; Kohei, I.; Yasuo, N.; Tomokazu, K.; Yoshiaki, N.; Motoyuki, A. A rice tryptophan deficient dwarf mutant, *tdd1*, contains a reduced level of indole acetic acid and develops abnormal flowers and organless embryos. *Plant J.* **2009**, *60*, 227–241.
5. Woo, Y.M.; Park, H.J.; Su'udi, M.; Yang, J.I.; Park, J.J.; Back, K.; Park, Y.M.; An, G. *Constitutively wilted 1*, a member of the rice YUCCA gene family, is required for maintaining water homeostasis and an appropriate root to shoot ratio. *Plant Mol. Biol.* **2007**, *65*, 125–136. [CrossRef] [PubMed]
6. Fujino, K.; Matsuda, Y.; Ozawa, K.; Nishimura, T.; Koshiba, T.; Fraaije, M.W.; Sekiguchi, H. *NARROW LEAF 7* controls leaf shape mediated by auxin in rice. *Mol. Genet. Genom.* **2008**, *279*, 499–507. [CrossRef] [PubMed]

7. Sakamoto, T.; Morinaka, Y.; Inukai, Y.; Kitano, H.; Fujioka, S. Auxin signal transcription factor regulates expression of the brassinosteroid receptor gene in rice. *Plant J.* **2013**, *73*, 676–688. [CrossRef] [PubMed]
8. Li, W.; Wu, C.; Hu, G.; Xing, L.; Qian, W.; Si, H.; Sun, Z.; Wang, X.; Fu, Y. Characterization and Fine Mapping of a Novel Rice Narrow Leaf Mutant *nal9*. *J. Integr. Plant Biol.* **2013**, *55*, 1016–1025. [CrossRef] [PubMed]
9. Wu, Y.; Luo, L.; Chen, L.; Tao, X.; Huang, M.; Wang, H.; Chen, Z.; Xiao, W. Chromosome mapping, molecular cloning and expression analysis of a novel gene response for leaf width in rice. *Biochem. Biophys. Res. Commun.* **2016**, *480*, 394–401. [CrossRef] [PubMed]
10. Song, Y.; Yan, C.; Zeng, X.; Yang, Y.; Fang, Y.; Tian, C.; Sun, Y.; Cheng, Z.; Gu, M. *ROLLED LEAF 9*, encoding a GARP protein, regulates the leaf abaxial cell fate in rice. *Plant Mol. Biol.* **2008**, *68*, 239–250.
11. Zhang, G.; Xu, Q.; Zhu, X.; Qian, Q.; Xue, H. SHALLOT-LIKE1 Is a KANADI Transcription Factor That Modulates Rice Leaf Rolling by Regulating Leaf Abaxial Cell Development. *Plant Cell* **2009**, *21*, 719–735. [CrossRef]
12. Ken-Ichiro, H.; Mari, O.; Emi, H.; Masashi, A.; Tsutomu, I.; Hikaru, S.; Jun-Ichi, I.; Yasuo, N. The *ADAXIALIZED LEAF1* gene functions in leaf and embryonic pattern formation in rice. *Dev. Biol.* **2009**, *334*, 345–354.
13. Li, L.; Shi, Z.; Li, L.; Shen, G.; Wang, X.; An, L.; Zhang, J. Overexpression of *ACL 1* (*abaxially curled leaf 1*) Increased Bulliform Cells and Induced Abaxial Curling of Leaf Blades in Rice. *Mol. Plant.* **2010**, *3*, 807–817. [CrossRef]
14. Shi, Z.; Wang, J.; Wan, X.; Shen, G.; Wang, X.; Zhang, J. Over-expression of rice *OsAGO7* gene induces upward curling of the leaf blade that enhanced erect-leaf habit. *Planta* **2007**, *226*, 99–108. [CrossRef] [PubMed]
15. Xiang, J.; Zhang, G.; Qian, Q.; Xue, H. *Semi-rolled leaf1* encodes a putative glycosylphosphatidylinositol-anchored protein and modulates rice leaf rolling by regulating the formation of bulliform cells. *Plant Physiol.* **2012**, *159*, 1488–1500. [CrossRef]
16. Wu, C.; Fu, Y.; Hu, G.; Si, H.; Cheng, S.; Liu, W. Isolation and characterization of a rice mutant with narrow and rolled leaves. *Planta* **2010**, *232*, 313–324. [CrossRef]
17. Hu, J.; Zhu, L.; Zeng, D.; Gao, Z.; Guo, L.; Fang, Y.; Zhang, G.; Dong, G.; Yan, M.; Liu, J. Identification and characterization of *NARROW ANDROLLED LEAF 1*, a novel gene regulating leaf morphology and plant architecture in rice. *Plant Mol. Biol.* **2010**, *73*, 283–292. [CrossRef]
18. Zhao, S.; Zhao, L.; Liu, F.; Wu, Y.; Zhu, Z.; Sun, C.; Tan, L. *NARROW AND ROLLED LEAF 2* regulates leaf shape, male fertility, and seed size in rice. *J. Integr. Plant Biol.* **2016**, *58*, 983–996. [CrossRef]
19. Chen, W.; Sheng, Z.; Cai, Y.; Li, Q.; Wei, X.; Xie, L.; Jiao, G.; Shao, G.; Tang, S.; Wang, J.; et al. Rice Morphogenesis and chlorophyll accumulation is regulated by the protein encoded by *NRL3* and its interaction with NAL9. *Front. Plant Sci.* **2019**, *10*, 1–13. [CrossRef]
20. Xia, Y.; Nikolau, B.J.; Schnable, P.S. Cloning and characterization of *CER2*, an Arabidopsis gene that affects cuticular wax accumulation. *Plant Cell* **1996**, *8*, 1291–1304. [CrossRef]
21. Islam, M.A.; Hao, D.; Jing, N.; Ye, H.; Xiong, L. Characterization of *Glossy1*-homologous genes in rice involved in leaf wax accumulation and drought resistance. *Plant Mol. Biol.* **2009**, *70*, 443–456. [CrossRef] [PubMed]
22. Qin, B.; Tang, D.; Huang, J.; Li, M.; Wu, X.; Lu, L.; Wang, J.; Yu, X.; Chen, J.; Gu, M. Rice *OsGL 1-1* is involved in leaf cuticular wax and cuticle membrane. *Mol. Plant.* **2011**, *4*, 985–995. [CrossRef]
23. Zhou, L.; Ni, E.; Yang, J.; Zhou, H.; Liang, H.; Li, J.; Jiang, D.; Wang, Z.; Liu, Z.; Zhuang, C. Rice *OsGL1-6* is involved in leaf cuticular wax accumulation and drought resistance. *PLoS ONE* **2013**, *8*, e65139. [CrossRef]
24. Mao, B.; Cheng, Z.; Lei, C.; Xu, F.; Gao, S.; Ren, Y.; Wang, J.; Zhang, X.; Wang, J.; Wu, F. *Wax crystal-sparse leaf2*, a rice homologue of WAX2/GL1, is involved in synthesis of leaf cuticular wax. *Planta* **2012**, *235*, 39–52. [CrossRef]
25. Jung, K.; Han, M.; Lee, D.; Lee, Y.; Lukas, S.; Rochus, F.; Andrea, F.; Alexander, Y.; Heinz, S.; Kim, Y.; et al. *Wax-deficient anther1* is involved in cuticle and wax production in rice anther walls and is required for pollen development. *Plant Cell* **2006**, *18*, 3015–3032. [CrossRef] [PubMed]
26. Wang, Y.; Wan, L.; Zhang, L.; Zhang, Z.; Zhang, H.; Quan, R.; Zhou, S.; Huang, R. An ethylene response factor *OsWR1* responsive to drought stress transcriptionally activates wax synthesis related genes and increases wax production in rice. *Plant Mol. Biol.* **2012**, *78*, 275–288. [CrossRef] [PubMed]
27. Zhou, X.; Jenks, M.A.; Liu, J.; Liu, A.; Zhang, X.; Xiang, J.; Zou, J.; Peng, Y.; Chen, X. Overexpression of Transcription Factor *OsWR2* Regulates Wax and Cutin Biosynthesis in Rice and Enhances its Tolerance to Water Deficit. *Plant Mol. Biol. Rep.* **2014**, *32*, 719–731. [CrossRef]

28. Wang, Z.; Tian, X.; Zhao, Q.; Liu, Z.; Li, X.; Ren, Y.; Tang, J.; Fang, J.; Xu, Q.; Bu, Q. The E3 Ligase DROUGHT HYPERSENSITIVE Negatively Regulates Cuticular Wax Biosynthesis by Promoting the Degradation of Transcription Factor ROC4 in Rice. *Plant Cell* **2018**, *30*, 228–244. [CrossRef]
29. Bernard, A.; Joubès, J. Arabidopsis cuticular waxes: Advances in synthesis, export and regulation. *Prog. Lipid Res.* **2013**, *52*, 110–129. [CrossRef] [PubMed]
30. Clapier, C.R.; Cairns, B.R. The biology of chromatin remodeling complexes. *Annu. Rev. Biochem.* **2009**, *78*, 273–304. [CrossRef]
31. Hall, J.A.; Georgel, P.T. CHD proteins: A diverse family with strong ties. *Biochem. Cell Biol.* **2007**, *85*, 463–476. [CrossRef]
32. Stanley, D.R.; Henderson, J.T.; Jerome, R.E.; Edenberg, H.J.; Jeanne, R.S.; Joe, O. Coordinate repression of regulators of embryonic identity by PICKLE during germination in Arabidopsis. *Plant J.* **2010**, *35*, 33–43.
33. Hay, A.; Kaur, H.; Phillips, A.; Hedden, P.; Hake, S.; Tsiantis, M. The Gibberellin Pathway Mediates KNOTTED1-Type Homeobox Function in Plants with Different Body Plans. *Curr. Biol.* **2002**, *12*, 1557–1565. [CrossRef]
34. Franziska, T.; Francois, R.; Sara, F.; Marie-Laure, M.M.; Elodie, G.; Nicolas, B.; Séverine, G.; Martienssen, R.A.; George, C.; Vincent, C. Arabidopsis TFL2/LHP1 specifically associates with genes marked by trimethylation of histone H3 lysine 27. *PLoS Genet.* **2007**, *3*, 855–866.
35. Hu, Y.; Lai, Y.; Zhu, D. Transcription regulation by CHD proteins to control plant development. *Front. Plant Sci.* **2014**, *5*, 223. [CrossRef]
36. Hu, Y.; Liu, D.; Zhong, X.; Zhang, C.; Zhang, Q.; Zhou, D. CHD3 protein recognizes and regulates methylated histone H3 lysines 4 and 27 over a subset of targets in the rice genome. *Proc. Natl. Acad. Sci. USA* **2012**, *109*, 5773–5778. [CrossRef]
37. Zhao, C.; Xu, J.; Chen, Y.; Mao, C.; Zhang, S.; Bai, Y.; Jiang, D.; Wu, P. Molecular cloning and characterization of *OsCHR4*, a rice chromatin-remodeling factor required for early chloroplast development in adaxial mesophyll. *Planta* **2012**, *236*, 1165–1176. [CrossRef]
38. Ma, X.; Ma, J.; Zhai, H.; Xin, P.; Chu, J.; Qiao, Y.; Han, L. CHR729 Is a CHD3 Protein That Controls Seedling Development in Rice. *PLoS ONE* **2015**, *10*, e0138934. [CrossRef]
39. Wang, Y.; Wang, D.; Gan, T.; Liu, L.; Long, W.; Wang, Y.; Niu, M.; Li, X.; Zheng, M.; Jiang, L.; et al. CRL6, a member of the CHD protein family, is required for crown root development in rice. *Plant Physiol. Biochem.* **2016**, *105*, 185–194. [CrossRef]
40. Cho, S.; Lee, C.; Gi, E.; Yim, Y.; Koh, H.; Kang, K.; Paek, N. The Rice Rolled Fine Striped (RFS) CHD3/Mi-2 Chromatin Remodeling Factor Epigenetically Regulates Genes Involved in Oxidative Stress Responses During Leaf Development. *Front. Plant Sci.* **2018**, *9*, 364. [CrossRef]
41. Enrico, S.; Michalis, B.; Miltos, T. Control of leaf and vein development by auxin. *Cold Spring Harbor Perspect. Biol.* **2010**, *2*, a001511.
42. Klee, H.J.; Horsch, R.B.; Hinchee, M.A.; Hein, M.B.; Hoffmann, N.L. The effects of overproduction of two Agrobacterium tumefaciens T-DNA auxin biosynthetic gene products in transgenic petunia plants. *Gene Dev.* **1987**, *1*, 86–96. [CrossRef]
43. Rafael, T.S.; Mattijs, B.; Karin, L.; GöRan, S.; Mol, J.N.M.; Erik, S.; Ronald, K. FLOOZY of petunia is a flavin mono-oxygenase-like protein required for the specification of leaf and flower architecture. *Genes Dev.* **2002**, *16*, 753.
44. Zhu, X.; Xiong, L. Putative megaenzyme DWA1 plays essential roles in drought resistance by regulating stress-induced wax deposition in rice. *Proc. Natl. Acad. Sci. USA* **2013**, *110*, 17790–17795. [CrossRef]
45. Wang, X.; Guan, Y.; Zhang, D.; Dong, X.; Tian, L.; Qu, L. A β-ketoacyl-CoA synthase is Involved in Rice Leaf Cuticular Wax Synthesis and requires a CER2-LIKE Protein as a Cofactor. *Plant Physiol.* **2017**, *173*, 944–955. [CrossRef] [PubMed]
46. Zhao, Y.; Christensen, S.K.; Fankhauser, C.; Cashman, J.R.; Cohen, J.D.; Weigel, D.; Chory, J. A role for flavin monooxygenase-like enzymes in auxin biosynthesis. *Science* **2001**, *291*, 306–309. [CrossRef]
47. Abu-Zaitoon, Y.M.; Bennett, K.; Normanly, J.; Nonhebel, H.M. A large increase in IAA during development of rice grains correlates with the expression of tryptophan aminotransferase OsTAR1 and a grain-specific YUCCA. *Physiol. Plant.* **2012**, *146*, 487–499. [CrossRef] [PubMed]

48. Li, X.; Wang, X.; He, K.; Ma, Y.; Su, N.; He, H.; Stolc, V.; Tongprasit, W.; Jin, W.; Jiang, J.; et al. High-resolution mapping of epigenetic modifications of the rice genome uncovers interplay between DNA methylation, histone methylation, and gene expression. *Plant Cell* **2008**, *20*, 259–276. [CrossRef]
49. Wang, X.; Elling, A.; Li, X.; Li, N.; Peng, Z.; He, G.; Sun, H.; Qi, Y.; Liu, X.; Deng, X. Genome-wide and organ-specific landscapes of epigenetic modifications and their relationships to mRNA and small RNA transcriptomes in maize. *Plant Cell* **2009**, *21*, 1053–1069. [CrossRef]
50. Wang, F.; Tang, Y.; Miao, R.; Xu, F.; Lin, T.; He, G.; Sang, X. Identification and gene mapping of a narrow and upper-albino leaf mutant in rice (*Oryza sativa* L.). *Chin. Sci. Bull.* **2012**, *57*, 3798–3803. [CrossRef]
51. Ernst, A.; Villar, C.B.R.; Sara, F.; Reyes, J.C.; Lars, H.; Claudia, K.H. CHD3 proteins and polycomb group proteins antagonistically determine cell identity in Arabidopsis. *PLoS Genet.* **2009**, *5*, e1000605.
52. Ogas, J.; Cheng, J.; Sung, Z.; Somerville, C. Cellular differentiation regulated by gibberellin in the Arabidopsis thaliana *pickle* mutant. *Science* **1997**, *277*, 91–94. [CrossRef] [PubMed]
53. Henderson, J.T.; Li, H.-C.; Rider, S.D.; Mordhorst, A.P.; Romero-Severson, J.; Cheng, J.-C.; Robey, J.; Sung, Z.R.; de Vries, S.C.; Ogas, J. *PICKLE* acts throughout the plant to repress expression of embryonic traits and may play a role in gibberellin-dependent responses. *Plant Physiol.* **2004**, *134*, 995–1005. [CrossRef] [PubMed]
54. Li, H.; King, C.; Henderson, J.T.; Stanley Dean, R.; Yinglin, B.; Heng, Z.; Matthew, F.; Jacob, G.; Joe, O. PICKLE acts during germination to repress expression of embryonic traits. *Plant J.* **2005**, *44*, 1010–1022. [CrossRef] [PubMed]
55. Ogas, J.; Kaufmann, S.; Henderson, J.; Somerville, C. PICKLE is a CHD3 chromatin-remodeling factor that regulates the transition from embryonic to vegetative development in Arabidopsis. *Proc. Natl. Acad. Sci. USA* **1999**, *96*, 13839–13844. [CrossRef] [PubMed]
56. Zhou, X.; Li, L.; Xiang, J.; Gao, G.; Xu, F.; Liu, A.; Zhang, X.; Peng, Y.; Chen, X.; Wan, X. *OsGL1-3* is involved in cuticular wax biosynthesis and tolerance to water deficit in rice. *PLoS ONE* **2015**, *10*, e116676. [CrossRef] [PubMed]
57. Gan, L.; Zhu, S.; Zhao, Z.; Liu, L.; Wang, X.; Zhang, Z.; Zhang, X.; Wang, J.; Wang, J.; Guo, X.; et al. *Wax Crystal-Sparse Leaf 4*, encoding a b-ketoacyl-coenzyme A synthase 6, is involved in rice cuticular wax accumulation. *Plant Cell Rep.* **2017**, *36*, 1655–1666. [CrossRef]
58. Lco, S.; Song, T.; Kosma, D.K.; Parsons, E.P.; Rowland, O.; Jenks, M.A. Arabidopsis *CER8* encodes LONG-CHAIN ACYL-COA SYNTHETASE 1 (LACS1) that has overlapping functions with LACS2 in plant wax and cutin synthesis. *Plant J.* **2010**, *59*, 553–564.
59. Zhao, Y.; Hull, A.K.; Gupta, N.R.; Goss, K.A.; José, A.; Ecker, J.R.; Jennifer, N.; Joanne, C.; Celenza, J.L. Trp-dependent auxin biosynthesis in Arabidopsis: Involvement of cytochrome P450s CYP79B2 and CYP79B3. *Genes Dev.* **2002**, *16*, 3100–3112. [CrossRef]
60. Kakei, Y.; Nakamura, A.; Yamamoto, M.; Ishida, Y.; Yamazaki, C.; Sato, A.; Narukawa-Nara, M.; Soeno, K.; Shimada, Y. Biochemical and chemical biology study of rice *OsTAR1* revealed that tryptophan aminotransferase is involved in auxin biosynthesis; identification of a potent OsTAR1 inhibitor, pyruvamine2031. *Plant Cell Physiol.* **2017**, *58*, 598–606. [CrossRef] [PubMed]
61. Dai, X.; Kiyoshi, M.; Chen, Q.; Hiroyuki, K.; Yuji, K.; Sunil, O.; Jennifer, D.B.; David, B.; Zhao, Y. The biochemical mechanism of auxin biosynthesis by an Arabidopsis YUCCA flavin-containing monooxygenase. *J. Biol. Chem.* **2013**, *288*, 1448–1457. [CrossRef]
62. Chapman, E.J.; Estelle, M. Mechanism of Auxin-Regulated Gene Expression in Plants. *Annu. Rev. Genet.* **2009**, *43*, 265–285. [CrossRef]
63. Bannister, A.J.; Kouzarides, T. Regulation of chromatin by histone modifications. *Cell Res.* **2011**, *21*, 381–395. [CrossRef] [PubMed]
64. Jörg, F.; Dmitri, D.; Andreas, H.; Ingo, S. Chromosomal histone modification patterns—From conservation to diversity. *Trends Plant Sci.* **2006**, *11*, 199–208.
65. Ernst, A.; Villar, C.B.R.; Riccardo, D.M.; Sabrina, S.; Claudia, K. The CHD3 chromatin remodeler PICKLE and polycomb group proteins antagonistically regulate meristem activity in the Arabidopsis root. *Plant Cell* **2011**, *23*, 1047–1060.
66. Gou, J.; Strauss, S.H.; Tsai, C.J.; Fang, K.; Chen, Y.; Jiang, X.; Busov, V.B. Gibberellins regulate lateral root formation in Populus through interactions with auxin and other hormones. *Plant Cell* **2010**, *22*, 623–639. [CrossRef] [PubMed]

67. Michelmore, R.W.; Paran, I.; Kesseli, R.V. Identification of markers linked to disease-resistance genes by bulked segregant analysis: A rapid method to detect markers in specific genomic regions by using segregating populations. *Proc. Natl. Acad. Sci. USA* **1991**, *88*, 9828–9832. [CrossRef]
68. Tamura, K.; Dudley, J.; Nei, M.; Kumar, S. MEGA4: Molecular Evolutionary Genetics Analysis (MEGA) software version 4.0. *Mol. Biol. Evol.* **2007**, *24*, 1596–1599. [CrossRef]
69. Gendrel, A.V.; Lippman, Z.; Martienssen, R.; Colot, V. Profiling histone modification patterns in plants using genomic tiling microarrays. *Nat. Methods* **2005**, *2*, 213–218. [CrossRef]

International Journal of
Molecular Sciences

MDPI

Article

Identification and Characterization of Tomato SWI3-Like Proteins: Overexpression of *SlSWIC* Increases the Leaf Size in Transgenic *Arabidopsis*

Zhongyi Zhao [1,2,3,†], Tao Li [4,†], Xiuling Peng [2,5], Keqiang Wu [6,*] and Songguang Yang [2,*]

1 Ministry of Education Key Laboratory for Bio-Resource and Eco-Environment, College of Life Science, Sichuan University, Chengdu 610064, China; zzycwnu@163.com
2 Key Laboratory of South China Agricultural Plant Molecular Analysis and Genetic Improvement, Guangdong Provincial Key Laboratory of Applied Botany, South China Botanical Garden, Chinese Academy of Sciences, Guangzhou 510650, China; m13203206354_2@163.com
3 College of Life Sciences, China West Normal University, Nanchong 637002, China
4 Vegetable Research Institute, Guangdong Academy of Agricultural Sciences, Guangzhou 510650, China; tianxing84@163.com
5 University of Chinese Academy of Sciences, Chinese Academy of Sciences, Beijing 100049, China
6 Institute of Plant Biology, National Taiwan University, Taipei 106, Taiwan
* Correspondence: yangsongguang@scbg.ac.cn (S.Y.); kewu@ntu.edu.tw (K.W.)
† These authors contributed equally to this work.

Received: 12 September 2019; Accepted: 10 October 2019; Published: 16 October 2019

Abstract: As the subunits of the SWI/SNF (mating-type switching (SWI) and sucrose nonfermenting (SNF)) chromatin-remodeling complexes (CRCs), Swi3-like proteins are crucial to chromatin remodeling in yeast and human. Growing evidence indicate that AtSWI3s are also essential for development and response to hormones in *Arabidopsis*. Nevertheless, the biological functions of Swi3-like proteins in tomato (*Solanum lycopersicum*) have not been investigated. Here we identified four Swi3-like proteins from tomato, namely SlSWI3A, SlSWI3B, SlSWI3C, and SlSWI3D. Subcellular localization analysis revealed that all SlSWI3s are localized in the nucleus. The expression patterns showed that all *SlSWI3s* are ubiquitously expressed in all tissues and organs, and *SlSWI3A* and *SlSWI3B* can be induced by cold treatment. In addition, we found that SlSWI3B can form homodimers with itself and heterodimers with SlSWI3A and SlSWI3C. SlSWI3B can also interact with SlRIN and SlCHR8, two proteins involved in tomato reproductive development. Overexpression of *SlSWI3C* increased the leaf size in transgenic *Arabidopsis* with increased expression of *GROWTH REGULATING FACTORs*, such as *GRF3*, *GRF5*, and *GRF6*. Taken together, our results indicate that SlSWI3s may play important roles in tomato growth and development.

Keywords: Swi3-like proteins; gene expression; protein interaction; leaf development; tomato

1. Introduction

The fundamental unit of chromatin is the nucleosome, which is composed of two turns of DNA wrapped around a histone octamer (two H2A-H2B dimers and one H3-H4 tetramer) [1]. To readout genomic information, a dynamic chromatin environment is needed during the cellular processes such as transcription, DNA replication and recombination. The modification of chromatin can occur through multiple mechanisms, including nucleosome composition and positioning by ATP-dependent chromatin-remodeling complexes (CRCs) and enzyme complexes that modify DNA or chromatin proteins [2,3]. CRCs use energy from ATP hydrolysis [4] and change local chromatin structure, thus enriching accessibility of transcription factors and availability of genomic information [5].

The first CRC, SWI/SNF CRC, was identified in two independent screens for mutants affecting mating-type switching (SWI) and growth on sucrose (sucrose nonfermenting, SNF) in yeast [6,7]. Biochemical analysis indicated that yeast SWI/SNF CRC is composed of 12 subunits [8], and the core complex including SWI2/SNF2-type ATPase, one SNF5, and two copies of SWI3 subunits, is sufficient for execution of nucleosome remodeling in vitro [9]. Moreover, several accessory subunits associating with the core complex act as an interface for interactions with other auxiliary proteins that affect chromatin remodeling activity [10].

As part of SWI/SNF CRC, yeast Swi3p is essential for the assembly of this complex, ATP-dependent H2A-H2B displacement and recruitment to target genes [11,12]. Further genome analysis indicated that Swi3-like proteins are found in virtually all eukaryotes, such as *Drosophila*, mammals and *Arabidopsis*. Intriguingly, studies in both yeast and mammalian cells showed that Swi3p and its mammalian homologs BAF155 and BAF170 can target many genes and genomic locations in the absence of Swi2 and other components of the SWI/SNF CRC complex [13,14], suggesting that they may have unique functions in gene regulation. Generally, all Swi3-like proteins contain two typical domains, the SWIRM and SANT domains. The SWIRM domain (Swi3p, Rsc8p, and Moira) consists of 85 amino acid residues and forms a compact helix-turn-helix (HTH)-related structure [15], while the SANT (SWI3, ADA2, N-CoR and TFIIIB) domain is structurally related to the homeodomain and the Myb DNA-binding domain [16]. Furthermore, in addition to Swi3-like proteins, the SWIRM domain is also found in LSD1 (Lysine-specific demethylase 1), Ada2 (Adenosine deaminase isoenzymes 2), and in a JAB domain-containing protein involved in protein degradation through the ubiquitin pathway [15]. Functional analysis demonstrated that SANT domains tether to both DNA and proteins and are essential for histone acetyltransferase activity [16,17].

In *Arabidopsis*, four Swi3-like proteins, namely CHB1 (AtSWI3A), CHB2 (AtSWI3B), CHB3 (AtSWI3C) and CHB4 (AtSWI3D), have been identified [18,19]. Current data show that they operate as modifiers of transcriptional or epigenetic regulation in plant growth and development. For example, mutations of *AtSWI3A* and *AtSWI3B* result in disruption of embryo development at the globular stage, while mutations in *AtSWI3C* and *AtSWI3D* display severe dwarfism, abnormal vegetative development, and reduced fertility [20]. Moreover, yeast-two-hybrid assays demonstrated that AtSWI3A and AtSWI3B can form homodimers and heterodimers, and also interact with BSH/SNF5, AtSWI3C, and the flowering regulator FCA, while AtSWI3D can only bind AtSWI3B [18,20]. Interestingly, when expressed in *Saccharomyces cerevisiae*, AtSWI3B can partially complement the *swi3* mutant phenotype [18]. In addition to interacting with other SWI3 subunits, AtSWI3B also interacts with HYPERSENSITIVE TO ABA1 (HAB1), a negative regulator of ABA signaling, indicating that SWI3B is involved in the ABA signaling [21]. Subsequent research found that AtSWI3B physically interacts with IDN2, a lncRNA-binding protein, and contributes to lncRNA-mediated transcriptional silencing [22]. Recent data demonstrated that AtSWI3B (as well as AtSWI3C and AtSWI3D) interacts with MORC6 (MICRORCHIDIA 6) and a SET domain-containing histone methyltransferase SUVH9 (SU(VAR)3-9 homolog) to mediate transcriptional silencing [23].

In leaf development, the expression of *IAMT1* (*IAA Carboxyl Methyltransferase 1*) is regulated by AtSWI3B-mediated chromatin remodeling [24]. In addition to auxin and ABA, the *Arabidopsis* Swi3-like proteins are also involved in other hormone signaling. For instance, the *AtSWI3C* mutation down-regulates the expression of *GID1* GA receptor genes, affecting the GA perception in leaves [25]. Meanwhile, AtSWI3C physically interacts with several DELLA proteins, indicating that chromatin remodeling mediated by AtSWI3C may be required for the DELLA-mediated effects, such as activation of *GID1* [25]. Moreover, the AtSWI3C (as well as AtSWI3D)-containing SWI/SNF chromatin remodeling complex is recruited by the transcriptional coactivator AN3 (ANGUSTIFOLIA3) to the promoters of leaf development related genes [26]. Consistently, modification of the *AtSWI3C* expression increases leaf size by increasing cell number but not cell size [26]. Moreover, recent data indicated that *ZmCHB101*, one of three maize *SWI3D* genes, plays essential roles in maize growth and development at both

vegetative and reproductive stages [27], since the *ZmCHB101* RNA interference plant lines displayed abaxially curling leaf and impaired tassel and cob development phenotypes.

Compared to *Arabidopsis*, the functions of Swi3-like proteins are largely unknown in other plant species. Nevertheless, phylogenetic analysis indicated that the Swi3-like proteins are widely present in the genomes of other plant species such as rice (*Oryza sativa*), *Medicago truncatula* and *Zea mays* [28]. In this study, we identified and characterized four Swi3-like proteins, namely SlSWI3A, SlSWI3B, SlSWI3C, and SlSWI3D, in tomato (*Solanum lycopersicum*). The expression profiles and subcellular localization of tomato Swi3-like proteins were investigated. In addition, the interaction of Swi3-like proteins with RIN and SlCHR8, two proteins involved in reproductive development, was also explored. Furthermore, ectopic expression of *SlSWI3C* in *Arabidopsis* resulted in the increased leaf size. Taken together, our results shed light on the potential functions of Swi3-like proteins during tomato development.

2. Results

2.1. Identification and Phylogenetic Analysis of Tomato Swi3-Like Proteins

The Swi3-like proteins sequences of *Arabidopsis*, rice, yeast and human were used as queries to search against the SGN annotation database with the BLAST program. All sequences with an E-value below 10^{-2} were selected for further analysis. Pfam and SMART databases were used to confirm each candidate protein sequence. Like *Arabidopsis*, four Swi3-like proteins (namely SlSWI3A, SlSWI3B, SlSWI3C, and SlSWI3D) were identified in the tomato genome (Table 1). The open reading frames (ORFs) of *SlSWI3s* ranged from 1470 to 2838 bp, and the length of SlSWI3 proteins varied from 490 to 946 amino acids. Further bioinformatics analysis indicated that SlSWI3 proteins were potentially localized in different organelles including the nucleus, cytoplasm, chloroplast and mitochondria (Table 1).

To further investigate the evolutionary relationships of SlSWI3, we carried out phylogenetic analyses using Swi3-like proteins of different species. The phylogenetic tree indicated that the plant Swi3-like proteins can be clearly divided into four groups: SWI3A, SWI3B, SWI3C, and SWI3D, while the SWI3A/SWI3B pairs are more related to the branches of yeast and animal Swi3 sequences (Figure 1A). The conserved domain analyses showed that all Swi3-like proteins contain two characteristic domains: SWIRM and SANT domains (Figure 1B). Moreover, the SWIRM-assoc_1 (SWIRM-associated region 1) domain (Interpro: IPR032451), which was previously identified as the leucine zipper domain [20], was found in all members of Swi3-like proteins except for SlSWI3B (Figure 1B). Like the AtSWI3D and OsSWI3Ds, a ZnF_ZZ domain (Interpro: IPR000433), which was named because of the ability to bind two zinc ions [29], was also found in the N-terminus of SlSWI3D. In general, ZZ-type zinc finger domains contained 4–6 Cys residues that participate in zinc binding as well as protein-protein interaction [30].

Table 1. The SWI3-like proteins in Tomato, *Arabidopsis* and rice.

SWI3 Gene Family	Gene Name	Gene Code	Accession Number [a]	ORF Length [b]	Protein Length	Localization [c]	Number of Exons	Nuclear Localization Signal [d]
SWI3A	*SlSWI3A*	Solyc03g097450	XP_004235292	1772	574	nucl, cyto	7	Yes
	AtSWI3A	AT2G47620	NP_850476	1539	513	nucl, cyto	7	Yes
	OsSWI3A	LOC_Os04g40420	BAF15014	1683	561	nucl, cyto, plas	7	Yes
SWI3B	*SlSWI3B*	Solyc04g082760	XP_004238459	1470	490	nucl, cyto	6	Yes
	AtSWI3B	AT2G33610	NP_180919	1410	469	nucl, cyto	6	Yes
	OsSWI3B	LOC_Os02g10060	XP_015625317	1536	512	nucl	6	Yes
SWI3C	*SlSWI3C*	Solyc06g060120	XP_004242041	2376	792	nucl, chlo, mito	8	Yes
	AtSWI3C	AT1G21700	NP_173589	2424	807	nucl, chlo, plas	9	Yes
	OsSWI3C1	LOC_Os12g07730	ABA96607	2520	840	nucl, chlo, mito	9	Yes
	OsSWI3C2	LOC_Os11g08080	XP_015617508	2355	785	nucl, chlo, mito	9	Yes
SWI3D	*SlSWI3D*	Solyc01g109510	XP_004230866	2838	946	nucl	6	Yes
	AtSWI3D	AT4G34430	NP_974682	2961	986	nucl	7	Yes
	OsSWI3D1	LOC_Os03g51220	XP_015632283	2745	915	nucl, cyto	8	Yes
	OsSWI3D2	LOC_Os04g01970	XP_015633469	2661	887	nucl, chlo, mito	7	Yes

[a] Accession numbers of full-length protein sequence available at NCBI (https://www.ncbi.nlm.nih.gov/). [b] Length of open reading frame (number of basepair). [c] Localization of tomato SWI3-like proteins supported by WoLFPSORT (http://www.genscript.com/psort/wolf_psort.html), Plant-mPLoc (http://www.csbio.sjtu.edu.cn/bioinf/plant-multi/#) and Euk-mPLoc 2.0 (http://www.csbio.sjtu.edu.cn/bioinf/euk-multi-2/). All SWI3-like proteins of plants was localized in the nucleus using Plant-mPLoc and Euk-mPLoc 2.0 programs. cyto, cytoplasm; nucl, nucleus; Plas, plasmamembrane; mito, mitochondrion; chlo, chloroplast. [d] Nuclear localization signal prediction based on frequent pattern mining and linear motif scoring using SeqNLS (http://mleg.cse.sc.edu/seqNLS/) and NucPred (https://nucpred.bioinfo.se/cgi-bin/single.cgi) programs.

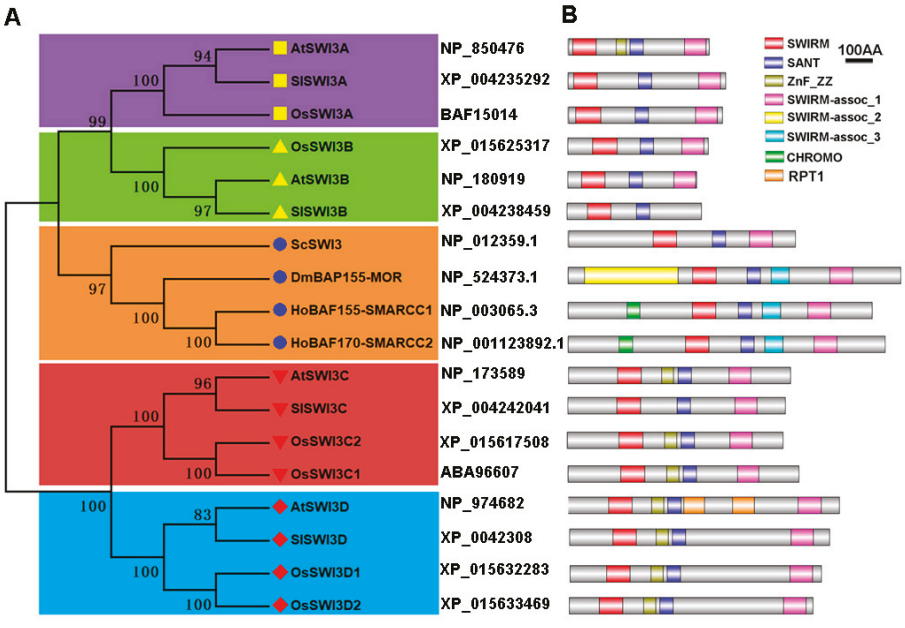

Figure 1. Phylogenetic tree and domain architecture of SlSWI3s in tomato. (**A**) Phylogenetic tree of Swi3-like proteins in plants and animal. Neighbor-joining (NJ) phylogenetic tree for SWI3s in *S. cerevisiae* (Sc), *D. melanogaster* (Dm), *H. sapiens* (Ho), *A. thaliana* (At), and *S. lycopersicum* (Sl). The groups of homologous genes identified, bootstrap values and accession numbers are shown. The reliability of branching was assessed by the bootstrap resampling method using 1000 bootstrap replicates. (**B**) Domain architecture of the Swi3-like proteins was drawn by DOG2.0. according to analysis by SMART and PFAM searches. The location of domains is shown by different color as indicated. The scale represents the length of the protein and all proteins are displayed in proportion. The proteins belonging to each family are grouped together.

2.2. Subcellular Localization of Tomato Swi3-Like Proteins

Bioinformatics analysis showed that SlSWI3 proteins exhibit various patterns of subcellular localization (Table 1). Nevertheless, a previous study demonstrated that *Arabidopsis* AtSWI3B localizes at the nucleus [21]. To determine the subcellular localization of tomato Swi3-like proteins, we performed in vivo targeting experiments in tobacco (*N. benthamiana*). To this end, *SlSWI3A*, *SlSWI3B SlSWI3C* and *SlSWI3D* were subcloned into the pEAQ-GFP vector to generate *35S*: *SlSWI3A-GFP*, *35S*: *SlSWI3B-GFP*, *35S*: *SlSWI3C-GFP* and 35S: *SlSWI3D-GFP* constructs, respectively. The constructs were introduced into leaf cells of tobacco by *A. tumefaciens* infiltration [31]. The fluorescence was visualized through a laser-scanning confocal microscope, and DAPI staining was used to visualize nuclei localization. We found that the *N. benthamiana* epidermal cells exhibited strong fluorescence in the nuclei (Figure 2, Figure S1), suggesting that the tomato SlSWI3-like proteins are nuclear proteins.

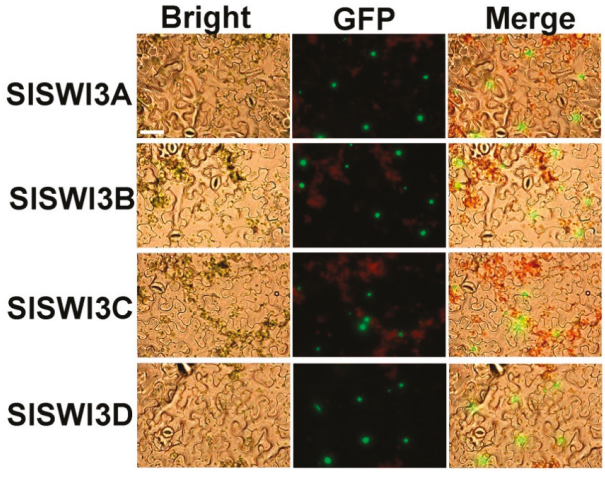

Figure 2. Subcellular localization of SlSWI3s. *A. tumefaciens* strain GV3103 harboring *SlSWI3s-GFP* constructs were infiltrated into young but fully expanded leaves of tobacco. After growth at 23 °C for 48 h, the epidermis of tobacco leaves were used to determine the distribution of the fusion protein using a confocal fluorescence microscope. The MADS-box transcriptional factor SlRIN was used as a positive control for localization of a nuclear protein. Bars = 50 μm. Similar results were obtained in three independent experiments, and one representative result was shown.

2.3. The Expression Patterns of Tomato Swi3-Like Genes

In order to explore the possible roles of *SlSWI3s*, we first analyzed their tissue and organ specific expression profiles from publicly available RNA-seq datasets [32]. As shown in Figure 3A, the transcripts of all *SlSWI3s* were ubiquitously expressed in all tissues and organs. *SlSWI3C* and *SlSWI3D* had similar expression profiles and were expressed mainly in roots (R) and fruits from 1 cm to 10-day post breaker (B + 10) stages (Figure 3A), suggesting that these genes may play redundant roles in root and fruit development. *SlSWI3B* showed a high expression in buds (B), flowers (F), roots (R) and B + 10 fruits, but its expression was low in other tissues. Compare with other *SlSWI3s*, the expression level of *SlSWI3A* was low in all tissues, especially in leaves (L) and B + 10 fruits (Figure 3A). Indeed, all *SlSWI3s* displayed low expression patterns in L compared with other tissues (Figure 3A).

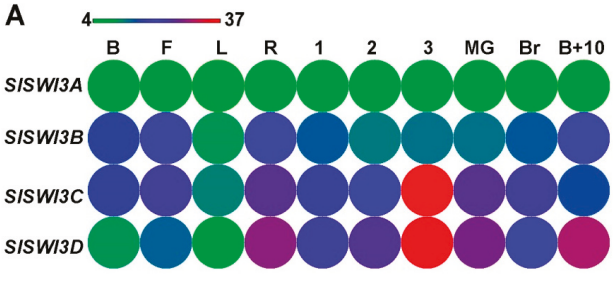

Figure 3. *Cont.*

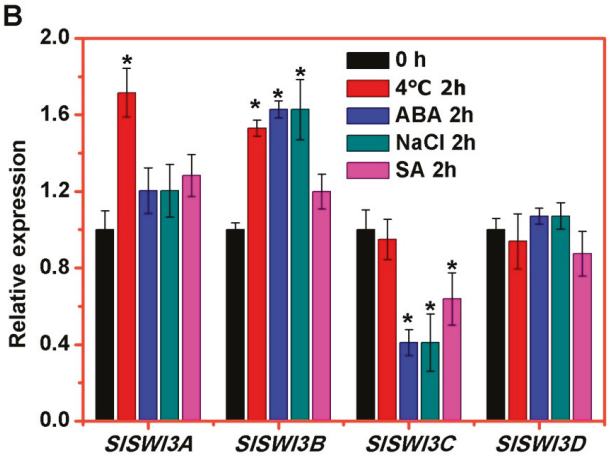

Figure 3. The expression patterns *SlSWI3s*. (**A**) Tissue-specific expression patterns of *SlSWI3s*. Heat map of RNA-seq expression data from bud (B), flower (F), leaf (L), root (R), 1 cm_fruit (1), 2cm_fruit (2), 3cm_fruit (3), mature green fruit (MG), berry at breaker stage (Br), and berry ten days after breaking (B + 10). The expression values are measured as reads per kilobase of the exon model per million mapped reads (RPKM). (**B**) Expression profiles of *SlSWI3s* under responding to hormones, salt, and cold tested by qRT-PCR. Seedlings of two-week-old plate-cultured plants were treated with SA (2 mM), ABA (100 μM), NaCl (200 mM), and cold (4 °C) for 2 h and collected for total RNA isolation. qRT-PCR was amplified using gene-specific primers. The tomato *ACTIN* (*Solyc03g078400*) was used as an internal control. Error bars indicate the SE. Asterisks indicate significant difference from wild-type plants ($p < 0.05$, Student's *t* test). The data are representative from three independent experiments.

Next, we investigated the expression pattern of *SlSWI3s* in response to environmental stimuli including hormones, salt, and cold by qRT-PCR. *SlSWI3A* and *SlSWI3B* were clearly induced by cold treatment, and *SlSWI3B* was also induced by ABA and salt treatments (Figure 3B). The transcript of *SlSWI3C* was strongly repressed by ABA, salt and SA treatment. Unlike *SlSWI3C*, the expression of *SlSWI3A* and *SlSWI3B* was not changed under SA treatment (Figure 3B). Interestingly, the transcript of *SlSWI3D* showed no difference under all treatments compared to control (Figure 3B). These results revealed that *SlSWI3A*, *SlSWI3B*, and *SlSWIC* may be involved in response to different environmental stimuli in tomato.

2.4. Members of SlSWI3s Interact with Other Proteins

In *Arabidopsis*, yeast-two-hybrid screens showed that AtSWI3A and AtSWI3B interact with the MADS-box transcriptional factors AGL18 (AGAMOUS-LIKE 18) and AGL73 [33]. In addition, AtSWI3A and AtSWI3B form homodimers and heterodimers and interact with BSH/SNF5 [20], while AtSWI3B and AtSWI3C form heterodimers and interact with the Snf2-like protein BRM (the ATPase of the SWI/SNF chromatin-remodeling complex) [18,34]. Thus, to explore whether SlSWI3s showed the similar interaction pattern, yeast-two-hybrid assays were performed. Like AtSWI3A and AtSWI3B, SlSWI3A, and SlSWI3B can also form heterodimers and homodimers (Figure 4A, Figure S2). In addition, SlSWI3B also interacted with SlSWI3C in yeast cells (Figure 4A). The interactions of SlSWI3s with the SlRIN and the Snf2-like protein SlCHR8 were also analyzed. Indeed, SlRIN is encoded by a member of the *SEPALLATA4* (*SEP4*) clade of MADS-box genes [35], which function as a master regulator of the ripening process in tomato. SlCHR8 displays high sequence homology with BRM in *Arabidopsis* [36], and overexpression of *SlCHR8* in tomato resulted in considerably compacter growth including significantly shorter roots and hypocotyls as well as reduced cotyledon and fruit size [37]. The yeast-two-hybrid assay showed that SlRIN interacted with SlSWI3A, SlSWI3B, and SlSWI3C,

while SlCHR8 only interacted with SlSWI3B (Figure 4A, Figure S2). Intriguingly, the yeast-two-hybrid assay also indicated that SlSWI3C can interacte with *Arabidopsis* SWI3A, SWI3B, and SWI3D, respectively (Figure S3). Taken together, these results suggested that the function of SWI3s may be conserved in tomato and *Arabidopsis*.

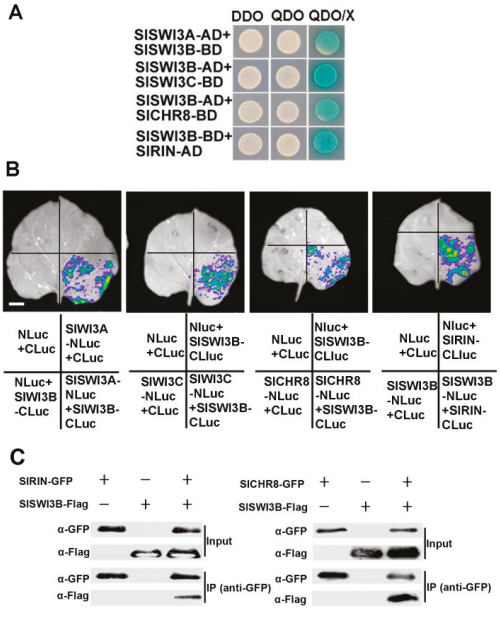

Figure 4. SlSWI3s interacted with SlSWI3A, SlSWI3C SlRIN, and SlCHR8 proteins. (**A**) SlSWI3B interacted with SlSWI3A, SlSWI3C SlRIN and SlCHR8 in yeast-two-hybrid assays. *SlSWI3B* was either cloned into pGBKT7 or pGADT7 vectors, whereas *SlSWI3A*, *SlSWI3C* and *SlCHR8* were cloned into pGBKT7 vector, and *SlRIN* was cloned into pGADT7 vectors, respectively. Different constructs were cotransformed into the yeast strain AH109. The transformants were grown on the selective minimal medium without Leu and Trp (DDO). The transformants were also plated on QDO or QDO/X to test for possible interaction. QDO, SD/-Leu/-Trp/-His/-Ade. X, x-a-gal. The same results were obtained in three independent experiments, and one representative result was shown. (**B**) SlSWI3B interacted with SlSWI3A, SlSWI3C SlRIN and SlCHR8 by LCI assay. The *A. tumefaciens* carrying the indicated construct pairs were injected into tobacco leaves, and the luciferase activities were measured 2 d after injection. Similar results were obtained in three independent experiments, and one representative result was shown. Bars = 0.5 cm. (**C**) SlSWI3B interacted with SlRIN and SlCHR8 by Co-IP assay.The *SlSWI3B* and *SlRIN* (or *SlCHR8*) were subcloned into the pHB (Flag tag) and pEAQ-GFP (GFP tag) vector, respectively.These constructs were co-transformed into tobacco cells by Agrobacterium mediated infiltration. Transiently expressed SlSWI3B-Flag and SlRIN-GFP (or SlCHR8-GFP) were immunoprecipitated with an anti-GFP antibody, and then detected by western-blotting assay with an anti-Flag antibody.

To confirm their interaction in plant cells, SlSWI3A, SlSWI3B, SlSWI3C, SlRIN and SlCHR8 were fused with Nluc or Cluc and coexpressed in tobacco leaves and subjected for firefly luciferase complementation imaging assays. Consistent with the yeast-two-hybrid results, strong LUC activity was observed when Cluc-SlSWI3B and SlSWI3A-Nluc/or SlSWI3C-Nluc/or SlCHR8-Nluc were coexpressed (Figure 4B). Similar results were also observed when SlSWI3B-Nluc and CLuc-SlRIN were coexpressed in tobacco leaves (Figure 4B). Next, the interaction of SlSWI3B with SlRIN and SlCHR8 was examined by co-immunoprecipitation (Co-IP) assays. We transiently expressed SlSWI3B, SlRIN and SlCHR8

proteins in tobacco. The SlSWI3B fused with three FLAG tags (pHB-SlSWI3B) and SlRIN (or SlCHR8) fused with a GFP tag (pEAQ-SlRIN) constructs were co-transformed into tobacco epidermal cells by *Agrobacterium*-mediated infiltration assays. The anti-GFP antibody (GFP-Trap®_A beads) was used for immunoprecipitation, and the immunoprecipitated protein was then analyzed by western-blotting assays using an anti-Flag antibody. We showed that SlSWI3B-FLAG protein was co-immunoprecipitated by SlRIN-GFP or SlCHR8-GFP (Figure 4C). Collectively, these data supported that SlSWI3B interacts with SlSWI3A, SlSWI3C, SlCHR8, and SlRIN both in vivo and in vitro.

2.5. Ectopic Overexpression of SlSWI3C Enhances Leaf Growth

In *Arabidopsis*, overexpression of *SWI3C* frequently leads to an increase in rosette area [26]. To further analyze their functions, *SlSWI3A*, *SlSWI3B*, *SlSWI3C,* and *SlSWI3D* were ectopically expressed in *Arabidopsis* plants driven by the 35S promoter. The independent hygromycin-resistant T_1 transformants were transferred into soil and grown in a greenhouse and self-pollinated to obtain segregated T_2 progeny for genetic analysis. All overexpression lines showed a 3:1 segregation pattern for hygromycin resistance, and three homozygous lines were selected for further analysis. As for *SlSWI3C*, all these selected lines showed increased expression of *SlSWI3C* (Figure S4). Phenotypic analysis showed that the 21-day-old soil-grown seedlings of *35S:SlSWI3C 1*, *35S:SlSWI3C 2* and *35S:SlSWI3C 3* were much larger than Col-0 (Figure 5A). Consistent with this observation, *35S:SlSWI3C 1*, *35S:SlSWI3C 2* and *35S:SlSWI3C 3* plants had significantly larger rosette leaves (Figure 5B). In addition, the surface area of the 5th rosette leaf of *35S:SlSWI3C 1*, *35S:SlSWI3C 2* and *35S:SlSWI3C 3* is 38.2, 46.04, and 46.08 mm^2, respectively, which were significantly larger than that of Col-0 (Figure 5C). Consistent with the larger leaves, the fresh weights (FW) of up-ground parts of all *SlSWI3C* overexpressing plants was increased when compared with Col-0 plants (Figure S5). In contrast, transgenic *Arabidopsis* plants overexpression of *SlSWI3A, SlSWI3B,* and *SlSWI3D* showed no visible phenotypes including the rosette sizes compared with Col-0 (Figure S4, Figure S6).

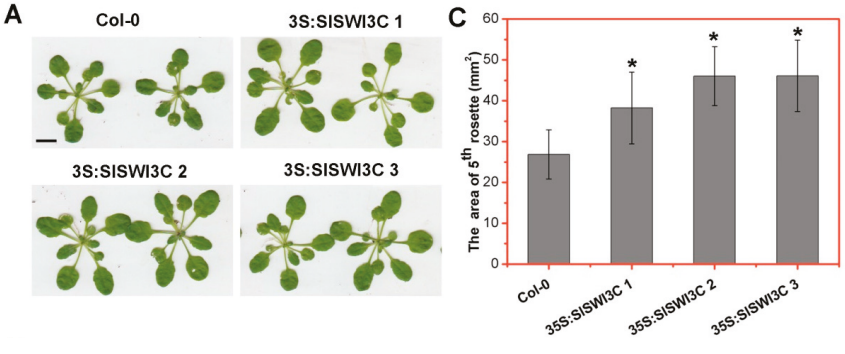

Figure 5. *Cont.*

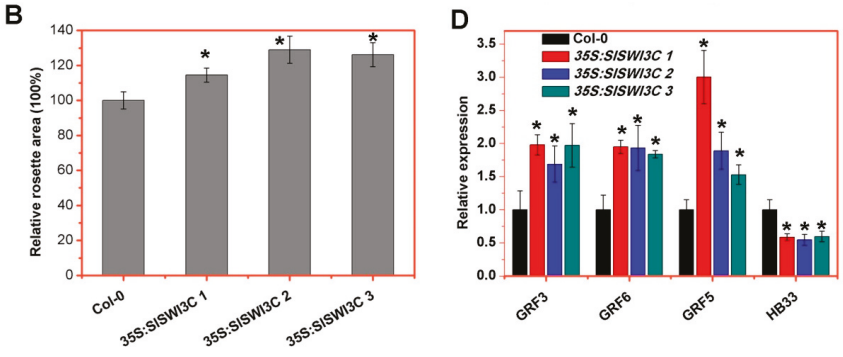

Figure 5. Overexpression of SlSWI3C enhances leaf growth. (**A**) Rosettes of 21-d-old Col-0 and 35S:SlSWI3C lines showing enhanced leaf growth. Three experiments were repeated with similar results, and one representative result was shown. Bar = 0.5 cm. (**B**, **C**) Total (**B**) and 5th rosette (**C**) area calculated using ImageJ (http://rsb.info.nih.gov/ij/) software. The individual leaf from 21-d-old Col-0 and *35S:SlSWI3Cs* plants was photographed and calculated using ImageJ. Error bars are SE (n = 15). Asterisks indicate significant difference from the Col-0 ($p < 0.05$, Student's t test). The data are representative from three independent experiments. (**D**) *SlSWI3C* promotes the expression of *GRFs* in *Arabidopsis*. Expression levels determined by qRT-PCR in 21-d-old Col-0 and *35S:SlSWI3Cs* rosettes grown in long-day (16 h light/8 h dark) conditions. qRT-PCR was amplified using gene-specific primers. The *ACTIN2* (*AT3G18780*) was used as an internal control. Error bars are SE. Asterisks indicate significant difference from wild-type plants ($p < 0.05$, Student's t test). The data are representative from three independent experiments.

Next, we determined the role of *SlSWI3C* in the expression of the genes related to leaf development. As shown in Figure 5D, the expression levels of *GROWTH REGULATING FACTOR 3* (*GRF3)*, *GRF5*, and *GRF6* were significantly increased in 21-day-old *35S:SlSWI3Cs* shoots grown in long-day conditions compared with Col-0 (Figure 5D). GRFs are comprised of nine members (GRF1 to GRF9) [38] and stimulate leaf cell proliferation, since overexpression of *GRF1*, *GRF2*, and *GRF5* enhances leaf growth and cell division [39,40]. Thus, the increased expression of *GRFs* in *35S:SlSWI3Cs* may be responsible for the larger leaf size. Intriguingly, *HB33*, a gene that is upregulated in *brm* mutants [26], was significantly downregulated in *35S:SlSWI3Cs* plants (Figure 5D).

3. Discussion

As one of the subunit of CRCs, SWI3 plays key roles in different cellular process in eukaryotic cells. In yeast, the SWI–SNF assembly and ATP-dependent H2A–H2B displacement are controlled by Swi3p [11,12]. Human BAF170 (SMARCC2) and BAF155 (SMARCC1), the homologs of Swi3p, are involved in cancers since BAF170 and BAF155 mutations were found in gastric and colorectal cancers and small cell lung cancers, respectively [41,42]. In *Arabidopsis*, both *AtSWI3A* and *AtSWI3B* are essential for early embryonic development, whereas *AtSWI3C* and *AtSWI3D* affect different phases of vegetative and reproductive development [20]. In this study, we identified four SWI3-like proteins in tomato: SWI3A, SWI3B, SWI3C, and SWI3D (Table 1, Figure 1A). Intriguingly, there are 6 SWI3-like proteins in rice (Table 1, Figure 1A) and 7 SWI3-like proteins in maize [27], indicating more SWI3-like proteins present in monocot. The fact that more SWI3 homologs exist in monocot may suggest the functional diversification of SWI3 paralogs in monocot.

All SlSWI3s contain the typical SWIRM and SANT domains (Figure 1B). The SWIRM domain forms a compact helix-turn-helix (HTH)-related structure and mediates specific protein-protein interactions [15], while the SANT domain, which is characterized by its homology to the DNA binding domain of c-myb, functions as a histone tail binding module [17,43]. In addition to SWIRM and SANT domains, a SWIRM-assoc_1 domain was found in the C-terminus of SlSWI3s (Figure 1B). A leucine

zipper domain located on the C-terminus of SWI3s [20] is involved in the interaction between SWI3s, since human BAF155 and BAF170 form heterodimers (BAF155/BAF170) or homodimers (BAF155/155 or BAF170/170) through the leucine zipper domain [44]. The sequences of the SWIRM-assoc_1 domain are larger than that of leucine zipper domain and the function of the SWIRM-assoc_1 domain is still unclear. Similar to the *Arabidopsis* AtSWI3B [21], all SlSWI3s are also localized in the nucleus (Figure 2), which is consistent with their roles as the subunits of CRCs.

The tissue-specific and stress-responsive expression patterns may be a useful way to explore gene functions. The expression profiles of *SlSWI3s* suggested that some *SlSWI3s* may play a similar role with their homologs in *Arabidopsis*. For instance, *SlSWI3C* is mainly expressed in roots and reproductive organs (Figure 3A), indicating that it functions in root and reproductive development [20]. Furthermore, functional divergence was also observed between *SlSWI3B* and its homolog *AtSWI3B*, since *SlSWI3B* is only poorly expressed in leaves (Figure 3A), whereas *AtSWI3B* is highly expressed in this organ [45], and knock-down of *AtSWI3B* results in an upward-curling leaf phenotype [24]. In addition, we found that the expression of *SlSWI3A* and *SlSWI3B* is induced by cold treatment, while *SlSWI3C* is strongly repressed by ABA, salt and SA treatment (Figure 3B). These data indicate that some SlCHRs may also respond to environmental stimuli.

In *Arabidopsis*, AtSWI3A and AtSWI3B can form homodimers and heterodimers, AtSWI3C can form heterodimers with both AtSWI3A and AtSWI3B, whereas AtSWI3D can form heterodimers only with AtSWI3B [18,20], suggesting their functional together in a complicated controlling network. In addition, AtSWI3B interacts with BSH/SNF5 and BRM, two core subunits of the SWI/SNF chromatin-remodeling complex [20,34]. Consistent with these data, our results also showed that SlSWI3A and SlSWI3B can form heterodimers and homodimers, whereas SlSWI3B and SlSWI3C can form heterodimers (Figure 4, Figure S2). Moreover, SlSWI3C can also form heterodimers with AtSWI3s (Figure S3), and interacts with SlCHR8, the *Arabidopsis* homolog of BRM. Collectively, these data suggested that CRCs in *Arabidopsis* and tomato may have similar functions. Nevertheless, the interaction between SlSWI3s (SlSWI3A, SlSWI3B, and SlSWI3C) with the MADS-box protein SlRIN (Figure 4, Figure S2) indicated that SlSWI3s may be involved in fruit ripening in tomato.

Previous studies showed that *AtSWI3B* is essential for early embryonic development and ABA signaling [20,21], while *AtSWI3C* and *AtSWI3D* play important roles in vegetative and reproductive development [20] as well as GA signaling [25]. Mutations of *AtSWI3C* cause leaf curling and reduced fertility, while mutations of *AtSWI3D* lead to leaf curling, severe dwarfism, and alteration in the number and development of flower organs with complete male and female sterility [20]. Moreover, over-expression of*AtSWI3C* increases the leaf size due to increased cell numbers [26]. *AtSWI3B* is also involved in leaf development via regulating *IAMT1*, which encodes a carboxyl methyltransferase in the auxin metabolism [24]. Intriguingly, the maize *SWI3D*-like gene *ZmCHB101* knock-down lines also show curling leaves and impaired development in reproductive tissues, such as significant reduction of spikelet numbers and smaller and lighter ears compared to WT [27]. Collectively, these observations indicated that the physiological functions of SWI3s may be evolutionarily conserved in different plant species.

Like *AtSWI3C*, over-expression of *SlSWI3C* also resulted in the increased leaf size in transgenic *Arabidopsis* (Figure 5A–C). The expression of *GRF3*, *GRF5*, and *GRF6* was significantly increased in *SlSWI3C* overexpressing seedlings (Figure 5D). These data suggested that the bigger leaf size of over-expression *SlSWI3C* transgenic *Arabidopsis* may be caused by the increased expression of *GRFs*, since overexpression of *GRF1*, *GRF2*, and *GRF5* enhances leaf growth and cell division [39,40]. Nevertheless, transgenic *Arabidopsis* seedlings overexpression of *SlSWI3A*, *SlSWI3B*, and *SlSWI3D* showed no difference in the rosette sizes compared with Col-0 (Figure S5), suggesting that SlSWI3C may function differently from other SlSWI3 proteins. Taken together, our results indicated that the functions of SWI3C may, at least in some developmental processes, be conserved in tomato and *Arabidospis*. Further in-depth analysis using transgenic tomato is required to investigate the functions of SlSWI3s in tomato development.

4. Materials and Methods

4.1. Plant Materials and Growth Conditions

Solanum lycopersicum cultivar "Heinz 1706" was used in this study. Surface-sterilized tomato seeds were grown in the Murashige and Skoog (MS) medium with 1.5% sucrose and 0.8% agar for 14 days in a controlled environment greenhouse with a long photoperiod (16 h light/8 h dark) at 23 ± 1 °C.

For hormone and stress treatments, 14-day-old "Heinz 1706" seedlings grown in the MS medium were transferred to the liquid MS medium containing SA (5 mM), ABA (100 μM), and NaCl (200 mM) for 2 h, respectively. For cold stress test, the plates were transferred to a 4 °C growth cabinet for 2 h. After treatment, the seedlings were harvested and immediately frozen in liquid nitrogen for further gene expression. The seedlings without treatment (seedlings grown in the MS medium) were used as control. For each treatment, about 10 seedlings were used for RNA extraction.

4.2. Identification of Tomato Swi3-Like Genes and Phylogenetic Tree Construction

The AtSWI3A, AtSWI3B, AtSWI3C and AtSWI3D sequences of *Arabidopsis thaliana* and yeast ScSWI3 were used to perform a search in the *Solamum lycopersicum* genome using the BLASTP program in the SGN (http://solgenomics.net/). Then, the candidates of Swi3-like proteins were confirmed using the HMMER-based SMART (http://smart.embl-heidelberg.de/) and Pfam (http://pfam.xfam.org/) programs. The domain architecture was drawn using DOG2.0 software [46].

The Swi3-like protein sequences from tomato, *Arabidopsis*, rice (*O. sativa*), yeast (*S. cerevisiae*), fruit fly (*D. melanogaster*) and human (*H. sapiens*) were aligned with ClustalW, and the alignment was imported in MEGA5.2 for phylogenetic generation using Neighbor-Joining method [47].

4.3. Subcellular Localization Assays

The subcellular localizations of SlSWI3s were first predicted using the WoLFPSORT (http://www.genscript.com/psort/wolf_psort.html), Plant-mPLoc (http://www.csbio.sjtu.edu.cn/bioinf/plant-multi/#) and Euk-mPLoc 2.0 (http://www.csbio.sjtu.edu.cn/bioinf/euk-multi-2/) programs, and confirmed by GFP-tagged transient expression assays in tobacco (*Nicotiana benthamiana*) leaves [31]. The full length CDS of *SlSWI3s* were subcloned into the pEAQ-GFP vector (the C-terminus of SlSWI3s was fused with GFP) [48], and all the constructs were subsequently transformed into *Agrobacterium tumefaciens* strain GV3103. After grown in LB medium at 28 °C overnight, bacterial suspensions were infiltrated into young but fully expanded leaves of tobacco using a needleless syringe. After infiltration, plants were immediately covered with plastic bags and placed at 23 °C for 48 h before bag removal. The distribution of the fusion protein was determined using a confocal fluorescence microscope. To locate the fluorescent proteins in nuclei, the tobacco leaves were infiltrated with PBS containing 4′, 6-diamidino-2-phenylindole (DAPI, 1μg/mL). Three independent experiments were repeated to confirm results.

4.4. Yeast-Two-Hybrid Assay

Yeast-two-hybrid assays were performed according to the manufacturer's instructions for the Matchmaker GAL4-based two-hybrid system 3 (Clontech, Takara, Dalian, China). *SlSWI3s*, *SlCHR8* and *SlRIN* were cloned into the pGBKT7 or pGADT7 vectors. Protein interactions were tested by stringent (SD/-Leu/-Trp/-His/-Ade) selection supplied with β-galactosidase activity measurement (Clontech, Takara, Dalian, China). Three independent experiments were repeated to confirm results.

4.5. LCI Assay

Luciferase complementation imaging (LCI) assays were performed as described previously [49]. The CDS of *SlSWI3A*, *SlSWI3B*, *SlSWI3C*, *SlCHR8,* and *SlRIN* was cloned into either pCAMBIA-Nluc or pCAMBIA-Cluc. All the constructs were transformed into *A. tumefaciens* strain GV3103. An equal

volume of *A. tumefaciens* harboring pCAMBIA-NLuc and pCAMBIA-CLuc (or their derivative constructs) was mixed to a final concentration of OD_{600} = 1.0. Four different combinations of *A. tumefaciens* were infiltrated into four different positions at the same leaves of tobacco. Plants were placed in 23 °C and allowed to recover for 60 h. A low-light cooled CCD imaging apparatus (NightOWL II LB983 with indiGO software) was used to capture the LUC image. Three independent experiments were repeated to confirm results.

4.6. Co-Immunoprecipitation (Co-IP) Assays

Co-IP assays were performed as described previously [50]. Two days after infiltration, tobacco leaves were harvested and ground to a fine powder in liquid nitrogen. Proteins were extracted in an extraction buffer (50 mM Tris-HCl, pH 7.4, 150 mM NaCl, 2 mM $MgCl_2$, 1 mM DTT, 20% glycerol, and 1% NP-40) containing protease inhibitor cocktail (Roche, Shanghai, China). Cell debris was pelleted by centrifugation at 14,000× *g* for 20 min. The supernatant was incubated with 30 µL of GFP-Trap®_A beads (Chromo Tek, Martinsried, Germany) at 4 °C for 4 h, then the beads were centrifuged and washed six times with a washing buffer (50 mM Tris-HCl, pH 7.4, 150 mM NaCl, 2 mM $MgCl_2$, 1mM DTT, 10% glycerol, and 1% NP-40). Proteins were eluted with 40 µL of 2× loading buffer and analyzed by western blotting using anti-GFP (Roche, Shanghai, China) and anti-Flag antibodies (LifeTein, Beijing, China).

4.7. RNA Extraction and Expression Analyses

Total RNA was isolated using Trizol Reagent (Invitrogen, Shanghai, China) according to the manufacturer's protocol. cDNAs were synthesized from 2 µg of total RNA using the TransScript™ One-Step gDNA Removal and cDNA Synthesis Supermix kit (TransGenBiotech, Guangzhou, China). Real-Time PCR was performed with iTaq™ Universal SYBR® Green Supermix (BIO-RAD, Shanghai, China) using ABI7500 Fast Real-Time PCR system. The gene-specific primers for real-time PCR were designed by PrimerQuest Tool (https://sg.idtdna.com/Primerquest/Home/Index) and listed in Table S1. The *Arabidopsis ACTIN2* (*AT3G18780*) and tomato *ACTIN* (Solyc03g078400) were used as a reference gene. Three independent sets of biological replicates were conducted with two technical replicates to confirm results.

For tissue and organ specific expression profiles, the expression data of tomato *SlSWI3s* were extracted from publicly available RNA-seq datasets from the Tomato Genome Consortium [32] and visualized with Matrix2PNG (https://matrix2png.msl.ubc.ca/bin/matrix2png.cgi) [51]. The publicly available RNA-seq data were obtained from transcriptome sequencing using three-week-old sand-grown seedlings, roots, leaves, buds (unopened flower buds), and flowers (fully open flowers) as well as fruits (at 1 cm, 2 cm, and 3 cm), MG (mature green), breaker (Br, early ripening), and 10-day post-breaker (B + 10, red ripe) stages of tomato "Heinz 1706" [32]. The expression data of *SlSWI3s* were normalized to have mean zero and variance one before producing the heat maps.

4.8. Generation of Transgenic Plants

To construct the *SlSWI3C* and *SlSWI3D* overexpression vectors, the CDS without a stop codon of *SlSWI3C* and *SlSWI3D* were cloned into the plasmid pHB-flag containing the 35S promoter [52]. The constructed plasmids were separately transformed into the *A. tumefaciens strain* GV3103 by the heat shock method. The bacteria carrying different constructs were used to transform WT (Col-0) plants via floral dip transformation.

Leaf areas were measured with ImageJ (http://rsb.info.nih.gov/ij/) using three-week-old seedlings grown in soil (the same stage seedlings were also for RNA isolation) after dissection of individual leaves. Rosette areas were calculated as the sum of the individual leaf areas. Three independent sets of biological replicates were conducted to confirm results.

5. Conclusions

In this study, four Swi3-like proteins, SlSWI3A, SlSWI3B, SlSWI3C, and SlSWI3D, were identified from tomato. All SlSWI3s contain two characteristic domains: SWIRM and SANT domains, and are localized in the nucleus. All *SlSWI3s* are ubiquitously expressed in all tissues and organs, and *SlSWI3A* and *SlSWI3B* can be induced by cold treatment. In addition, SlSWI3B forms homodimers with itself and heterodimers with SlSWI3A and SlSWI3C. SlSWI3B also interacts with SlRIN and SlCHR8, two proteins associated with tomato reproductive development, indicating that SlSWI3B may be involved in gene regulation in reproductive development. Furthermore, over-expression of *SlSWI3C* increases the leaf size in transgenic *Arabidopsis* with increased expression of *GRF3*, *GRF5* and *GRF6*.

Supplementary Materials: Supplementary materials can be found at http://www.mdpi.com/1422-0067/20/20/5121/s1. Figure S1. The subcellular localization of tomato SWI3-like proteins. Figure S2. Self-activation (**A**) and the interactions of SlSWI3s with each other (**B**) were examined in yeast cells. Figure S3. The interactions of SlSWI3s with AtSWI3s were examined in yeast cells. Figure S4. The transcripts of *SlSWI3s* in 21-day-old transgenic *Arabidopsis* seedlings. Figure S5. The fresh weights (FW) of up-ground parts of Col-0 and *SlSWI3C* overexpressing plants grown in soil for two weeks. Figure S6. The phenotype of overexpression of *SlSWI3A*, *SlSWI3B*, and *SlSWI3D* transgenic *Arabidopsis* seedlings.

Author Contributions: Z.Z., T.L., and X.P. performed the research, Z.Z., T.L., and S.Y. analyzed data. S.Y. and K.W. conceived the idea and revised and organized the manuscript.

Funding: This work was supported by the Guangdong Natural Science Funds for Distinguished Young Scholars (2016A030306047); Pearl River S&T Nova Program of Guangzhou (201610010138); the Youth Innovation Promotion Association, CAS (2017398); the Science and Technology Program of Guangzhou (201607010270) and the National Natural Science Foundation of China (No. 31672161). Modern Agricultural Innovation Team Project of Guangdong Province (2018LM2150, 2019KJ106); Guangdong Academy of Agricultural Sciences Foundation (201630TD).

Acknowledgments: We are grateful to Yawen Lei (SUN YAT-SEN UNIVERSITY) and Lomonossoff (Department of Biological Chemistry, John Innes Centre, Norwich, UK) for providing the pHB and pEAQ-GFP plasmids.

Conflicts of Interest: The authors declare no conflict of interest.

References

1. Luger, K.; Mader, A.W.; Richmond, R.K.; Sargent, D.F.; Richmond, T.J. Crystal structure of the nucleosome core particle at 2.8 A resolution. *Nature* **1997**, *389*, 251–260. [CrossRef] [PubMed]
2. Henikoff, S.; Shilatifard, A. Histone modification: Cause or cog? *Trends in Genet.* **2011**, *27*, 389–396. [CrossRef] [PubMed]
3. Jerzmanowski, A. SWI/SNF chromatin remodeling and linker histones in plants. *Biochim. Biophys. Acta* **2007**, *1769*, 330–345. [CrossRef] [PubMed]
4. Imbalzano, A.N. Energy-dependent chromatin remodelers: Complex complexes and their components. *Crit. Rev. Eukaryot. Gene Expr.* **1998**, *8*, 225–255. [CrossRef]
5. Clapier, C.R.; Cairns, B.R. The Biology of Chromatin Remodeling Complexes. *Annu. Rev. Biochem.* **2009**, *78*, 273–304. [CrossRef]
6. Neigeborn, L.; Carlson, M. Genes Affecting the Regulation of Suc2 Gene-Expression by Glucose Repression in Saccharomyces-Cerevisiae. *Genetics* **1984**, *108*, 845–858.
7. Peterson, C.L.; Herskowitz, I. Characterization of the Yeast Swi1, Swi2, and Swi3 Genes, Which Encode a Global Activator of Transcription. *Cell* **1992**, *68*, 573–583. [CrossRef]
8. Cairns, B.R.; Kim, Y.J.; Sayre, M.H.; Laurent, B.C.; Kornberg, R.D. A Multisubunit Complex Containing the Swi1/Adr6, Swi2/Snf2, Swi3, Snf5, and Snf6 Gene-Products Isolated from Yeast. *Proc. Natl Acad. Sci. USA* **1994**, *91*, 1950–1954. [CrossRef]
9. Phelan, M.L.; Sif, S.; Narlikar, G.J.; Kingston, R.E. Reconstitution of a core chromatin remodeling complex from SWI/SNF subunits. *Mol. Cell* **1999**, *3*, 247–253. [CrossRef]
10. Johnson, C.N.; Adkins, N.L.; Georgel, P. Chromatin remodeling complexes: ATP-dependent machines in action. *Biochem. Cell Biol.* **2005**, *83*, 405–417. [CrossRef]
11. Yang, X.F.; Zaurin, R.; Beato, M.; Peterson, C.L. Swi3p controls SWI/SNF assembly and ATP-dependent H2A-H2B displacement. *Nat. Struct. Mol. Biol.* **2007**, *14*, 540–547. [CrossRef] [PubMed]

12. Dechassa, M.L.; Zhang, B.; Horowitz-Scherer, R.; Persinger, J.; Woodcock, C.L.; Peterson, C.L.; Bartholomew, B. Architecture of the SWI/SNF-nucleosome complex. *Mol. Cell Biol.* **2008**, *28*, 6010–6021. [CrossRef] [PubMed]
13. Hu, Z.Z.; Killion, P.J.; Iyer, V.R. Genetic reconstruction of a functional transcriptional regulatory network. *Nat. Genet.* **2007**, *39*, 683–687. [CrossRef] [PubMed]
14. Euskirchen, G.M.; Auerbach, R.K.; Davidov, E.; Gianoulis, T.A.; Zhong, G.N.; Rozowsky, J.; Bhardwaj, N.; Gerstein, M.B.; Snyder, M. Diverse Roles and Interactions of the SWI/SNF Chromatin Remodeling Complex Revealed Using Global Approaches. *Plos Genet.* **2011**, *7*, e1002008. [CrossRef]
15. Aravind, L.; Iyer, L.M. The SWIRM domain: A conserved module found in chromosomal proteins points to novel chromatin-modifying activities. *Genome Bio.* **2002**, *3*. [CrossRef]
16. Aasland, R.; Stewart, A.F.; Gibson, T. The SANT domain: A putative DNA-binding domain in the SWI-SNF and ADA complexes, the transcriptional corepressor N-CoR and TFIIIB. *Trends Biochem. Sci.* **1996**, *21*, 87–88. [CrossRef]
17. Boyer, L.A.; Langer, M.R.; Crowley, K.A.; Tan, S.; Denu, J.M.; Peterson, C.L. Essential role for the SANT domain in the functioning of multiple chromatin remodeling enzymes. *Mol. Cell* **2002**, *10*, 935–942. [CrossRef]
18. Sarnowski, T.J.; Swiezewski, S.; Pawlikowska, K.; Kaczanowski, S.; Jerzmanowski, A. AtSWI3B, an Arabidopsis homolog of SWI3, a core subunit of yeast Swi/Snf chromatin remodeling complex, interacts with FCA, a regulator of flowering time. *Nucleic Acids Res.* **2002**, *30*, 3412–3421. [CrossRef]
19. Zhou, C.H.; Miki, B.; Wu, K.Q. CHB2, a member of the SWI3 gene family, is a global regulator in Arabidopsis. *Plant Mol. Biol.* **2003**, *52*, 1125–1134. [CrossRef]
20. Sarnowski, T.J.; Rios, G.; Jasik, J.; Swiezewski, S.; Kaczanowski, S.; Li, Y.; Kwiatkowska, A.; Pawlikowska, K.; Kozbial, M.; Kozbial, P.; et al. SWI3 subunits of putative SWI/SNF chromatin-remodeling complexes play distinct roles during Arabidopsis development. *Plant Cell* **2005**, *17*, 2454–2472. [CrossRef]
21. Saez, A.; Rodrigues, A.; Santiago, J.; Rubio, S.; Rodriguez, P.L. HAB1-SWI3B Interaction Reveals a Link between Abscisic Acid Signaling and Putative SWI/SNF Chromatin-Remodeling Complexes in Arabidopsis. *Plant Cell* **2008**, *20*, 2972–2988. [CrossRef] [PubMed]
22. Zhu, Y.Y.; Rowley, M.J.; Bohmdorfer, G.; Wierzbicki, A.T. A SWI/SNF Chromatin-Remodeling Complex Acts in Noncoding RNA-Mediated Transcriptional Silencing. *Mol. Cell* **2013**, *49*, 298–309. [CrossRef] [PubMed]
23. Liu, Z.W.; Zhou, J.X.; Huang, H.W.; Li, Y.Q.; Shao, C.R.; Li, L.; Cai, T.; Chen, S.; He, X.J. Two Components of the RNA-Directed DNA Methylation Pathway Associate with MORC6 and Silence Loci Targeted by MORC6 in Arabidopsis. *Plos Genet.* **2016**, *12*, e1006026. [CrossRef] [PubMed]
24. Han, W.X.; Han, D.L.; He, Z.P.; Hu, H.; Wu, Q.; Zhang, J.J.; Jiang, J.M.; Qin, G.J.; Cui, Y.H.; Lai, J.B.; et al. The SWI/SNF subunit SWI3B regulates IAMT1 expression via chromatin remodeling in Arabidopsis leaf development. *Plant Sci.* **2018**, *271*, 127–132. [CrossRef] [PubMed]
25. Sarnowska, E.A.; Rolicka, A.T.; Bucior, E.; Cwiek, P.; Tohge, T.; Fernie, A.R.; Jikumaru, Y.; Kamiya, Y.; Franzen, R.; Schmelzer, E.; et al. DELLA-Interacting SWI3C Core Subunit of Switch/Sucrose Nonfermenting Chromatin Remodeling Complex Modulates Gibberellin Responses and Hormonal Cross Talk in Arabidopsis. *Plant Physiol.* **2013**, *163*, 305–317. [CrossRef] [PubMed]
26. Vercruyssen, L.; Verkest, A.; Gonzalez, N.; Heyndrickx, K.S.; Eeckhout, D.; Han, S.K.; Jegu, T.; Archacki, R.; Van Leene, J.; Andriankaja, M.; et al. ANGUSTIFOLIA3 Binds to SWI/SNF Chromatin Remodeling Complexes to Regulate Transcription during Arabidopsis Leaf Development. *Plant Cell* **2014**, *26*, 210–229. [CrossRef] [PubMed]
27. Yu, X.; Jiang, L.; Wu, R.; Meng, X.; Zhang, A.; Li, N.; Xia, Q.; Qi, X.; Pang, J.; Xu, Z.Y.; et al. The Core Subunit of a Chromatin-Remodeling Complex, ZmCHB101, Plays Essential Roles in Maize Growth and Development. *Sci. Rep.* **2016**, *6*, 38504. [CrossRef]
28. Gao, Y.; Yang, S.G.; Yuan, L.Y.; Cui, Y.H.; Wu, K.Q. Comparative Analysis of SWIRM Domain-Containing Proteins in Plants. *Comp. Funct. Genom.* **2012**, *2012*, 310402. [CrossRef]
29. Ponting, C.P.; Blake, D.J.; Davies, K.E.; KendrickJones, J.; Winder, S.J. ZZ and TAZ: New putative zinc fingers in dystrophin and other proteins. *Trends Biochem. Sci.* **1996**, *21*, 11–13. [CrossRef]
30. Legge, G.B.; Martinez-Yamout, M.A.; Hambly, D.M.; Trinh, T.; Lee, B.M.; Dyson, H.J.; Wright, P.E. ZZ domain of CBP: An unusual zinc finger fold in a protein interaction module. *J. Mol. Biol.* **2004**, *343*, 1081–1093. [CrossRef]

31. Sparkes, I.A.; Runions, J.; Kearns, A.; Hawes, C. Rapid, transient expression of fluorescent fusion proteins in tobacco plants and generation of stably transformed plants. *Nat. Protoc.* **2006**, *1*, 2019–2025. [CrossRef] [PubMed]
32. Sato, S.; Tabata, S.; Hirakawa, H.; Asamizu, E.; Shirasawa, K.; Isobe, S.; Kaneko, T.; Nakamura, Y.; Shibata, D.; Aoki, K.; et al. The tomato genome sequence provides insights into fleshy fruit evolution. *Nature* **2012**, *485*, 635–641.
33. Efroni, I.; Han, S.K.; Kim, H.J.; Wu, M.F.; Steiner, E.; Birnbaum, K.D.; Hong, J.C.; Eshed, Y.; Wagner, D. Regulation of Leaf Maturation by Chromatin-Mediated Modulation of Cytokinin Responses. *Dev. Cell* **2013**, *24*, 438–445. [CrossRef] [PubMed]
34. Hurtado, L.; Farrona, S.; Reyes, J.C. The putative SWI/SNF complex subunit BRAHMA activates flower homeotic genes in Arabidopsis thaliana. *Plant. Mol. Biol.* **2006**, *62*, 291–304. [CrossRef] [PubMed]
35. Vrebalov, J.; Ruezinsky, D.; Padmanabhan, V.; White, R.; Medrano, D.; Drake, R.; Schuch, W.; Giovannoni, J.A. MADS-box gene necessary for fruit ripening at the tomato ripening-inhibitor (Rin) locus. *Science* **2002**, *296*, 343–346. [CrossRef]
36. Zhang, D.D.; Gao, S.J.; Yang, P.; Yang, J.; Yang, S.G.; Wu, K.Q. Identification and Expression Analysis of Snf2 Family Proteins in Tomato (Solanum lycopersicum). *Int. J. Genom.* **2019**. [CrossRef]
37. Folta, A.; Bargsten, J.W.; Bisseling, T.; Nap, J.P.; Mlynarova, L. Compact tomato seedlings and plants upon overexpression of a tomato chromatin remodelling ATPase gene. *Plant. Biotechnol. J.* **2016**, *14*, 581–591. [CrossRef]
38. Kim, J.H.; Choi, D.S.; Kende, H. The AtGRF family of putative transcription factors is involved in leaf and cotyledon growth in Arabidopsis. *Plant. J.* **2003**, *36*, 94–104. [CrossRef]
39. Horiguchi, G.; Kim, G.T.; Tsukaya, H. The transcription factor AtGRF5 and the transcription coactivator AN3 regulate cell proliferation in leaf primordia of Arabidopsis thaliana. *Plant. J.* **2005**, *43*, 68–78. [CrossRef]
40. Kim, J.H.; Lee, B.H. GROWTH-REGULATING FACTOR4 of Arabidopsis thaliana is required for development of leaves, cotyledons, and shoot apical meristem. *J. Plant. Biol.* **2006**, *49*, 463–468. [CrossRef]
41. Kim, S.S.; Kim, M.S.; Yoo, N.J.; Lee, S.H. Frameshift mutations of a chromatin-remodeling gene SMARCC2 in gastric and colorectal cancers with microsatellite instability. *Apmis* **2013**, *121*, 168–169. [CrossRef] [PubMed]
42. Kadoch, C.; Hargreaves, D.C.; Hodges, C.; Elias, L.; Ho, L.; Ranish, J.; Crabtree, G.R. Proteomic and bioinformatic analysis of mammalian SWI/SNF complexes identifies extensive roles in human malignancy. *Nat. Genet.* **2013**, *45*, 592–601. [CrossRef] [PubMed]
43. Boyer, L.A.; Latek, R.R.; Peterson, C.L. The SANT domain: A unique histone-tail-binding module? *Nat. Rev. Mol. Cell Biol.* **2004**, *5*, 158–163. [CrossRef] [PubMed]
44. Wang, W.D.; Xue, Y.T.; Zhou, S.; Kuo, A.; Cairns, B.R.; Crabtree, G.R. Diversity and specialization of mammalian SWI/SNF complexes. *Gene Dev.* **1996**, *10*, 2117–2130. [CrossRef]
45. Winter, D.; Vinegar, B.; Nahal, H.; Ammar, R.; Wilson, G.V.; Provart, N.J. An "Electronic Fluorescent Pictograph" Browser for Exploring and Analyzing Large-Scale Biological Data Sets. *PLoS ONE* **2007**, *2*, e718. [CrossRef]
46. Ren, J.; Wen, L.P.; Gao, X.J.; Jin, C.J.; Xue, Y.; Yao, X.B. DOG 1.0: Illustrator of protein domain structures. *Cell Res.* **2009**, *19*, 271–273. [CrossRef]
47. Tamura, K.; Peterson, D.; Peterson, N.; Stecher, G.; Nei, M.; Kumar, S. MEGA5: Molecular Evolutionary Genetics Analysis Using Maximum Likelihood, Evolutionary Distance, and Maximum Parsimony Methods. *Mol. Biol. Evol.* **2011**, *28*, 2731–2739. [CrossRef]
48. Peyret, H.; Lomonossoff, G.P. The pEAQ vector series: The easy and quick way to produce recombinant proteins in plants. *Plant. Mol. Biol.* **2013**, *83*, 51–58. [CrossRef]
49. Chen, H.M.; Zou, Y.; Shang, Y.L.; Lin, H.Q.; Wang, Y.J.; Cai, R.; Tang, X.Y.; Zhou, J.M. Firefly luciferase complementation imaging assay for protein-protein interactions in plants. *Plant. Physiol.* **2008**, *146*, 368–376. [CrossRef]
50. Zhao, M.; Yang, S.; Chen, C.Y.; Li, C.; Shan, W.; Lu, W.; Cui, Y.; Liu, X.; Wu, K. Arabidopsis BREVIPEDICELLUS interacts with the SWI2/SNF2 chromatin remodeling ATPase BRAHMA to regulate KNAT2 and KNAT6 expression in control of inflorescence architecture. *Plos Genet.* **2015**, *11*, e1005125. [CrossRef]
51. Pavlidis, P.; Noble, W.S. Matrix2png: A utility for visualizing matrix data. *Bioinformatics* **2003**, *19*, 295–296. [CrossRef] [PubMed]

52. Mao, J.; Zhang, Y.C.; Sang, Y.; Li, Q.H.; Yang, H.Q. From The Cover: A role for Arabidopsis cryptochromes and COP1 in the regulation of stomatal opening. *Proc. Natl. Acad. Sci. USA* **2005**, *102*, 12270–12275. [CrossRef] [PubMed]

International Journal of
Molecular Sciences

MDPI

Article

The SWI/SNF ATP-Dependent Chromatin Remodeling Complex in Arabidopsis Responds to Environmental Changes in Temperature-Dependent Manner

Dominika M. Gratkowska-Zmuda [1,†], Szymon Kubala [1,†], Elzbieta Sarnowska [2], Pawel Cwiek [1], Paulina Oksinska [1], Jaroslaw Steciuk [1], Anna T. Rolicka [1,3], Magdalena Zaborowska [1], Ernest Bucior [1,3], Anna Maassen [1], Rainer Franzen [4], Csaba Koncz [4,5] and Tomasz J. Sarnowski [1,†,*]

1 Institute of Biochemistry and Biophysics, Polish Academy of Sciences, 02-106 Warsaw, Poland; gratkowskad@gmail.com (D.M.G.-Z.); szymonglobus@gmail.com (S.K.); p.cwiek23@gmail.com (P.C.); p.oksinska@ibb.waw.pl (P.O.); keraj3000@gmail.com (J.S.); arolicka@gmail.com (A.T.R.); magdalena.zaborowska@ibb.waw.pl (M.Z.); ebucior@gmail.com (E.B.); maassen.anna@gmail.com (A.M.)
2 Maria Sklodowska-Curie Cancer Center Institute of Oncology, 02-781 Warsaw, Poland; elasarn@coi.waw.pl
3 Faculty of Biology, University of Warsaw, 02-106 Warsaw, Poland
4 Max-Planck Institut für Pflanzenzüchtungsforschung, Köln 50829, Germany; franzen@mpipz.mpg.de (R.F.); koncz@mpipz.mpg.de (C.K.)
5 Institute of Plant Biology, Biological Research Center of Hungarian Academy, 6726 Szeged, Hungary
* Correspondence: tsarn@ibb.waw.pl
† These authors contributed equally to this work.

Received: 10 November 2019; Accepted: 22 January 2020; Published: 23 January 2020

Abstract: SWI/SNF ATP-dependent chromatin remodeling complexes (CRCs) play important roles in the regulation of transcription, cell cycle, DNA replication, repair, and hormone signaling in eukaryotes. The core of SWI/SNF CRCs composed of a SWI2/SNF2 type ATPase, a SNF5 and two of SWI3 subunits is sufficient for execution of nucleosome remodeling in vitro. The Arabidopsis genome encodes four SWI2/SNF2 ATPases, four SWI3, a single SNF5 and two SWP73 subunits. Genes of the core SWI/SNF components have critical but not fully overlapping roles during plant growth, embryogenesis, and sporophyte development. Here we show that the Arabidopsis *swi3c* mutant exhibits a phenotypic reversion when grown at lower temperature resulting in partial restoration of its embryo, root development and fertility defects. Our data indicates that the *swi3c* mutation alters the expression of several genes engaged in low temperature responses. The location of SWI3C-containing SWI/SNF CRCs on the *ICE1*, *MYB15* and *CBF1* target genes depends on the temperature conditions, and the *swi3c* mutation thus also influences the transcription of several cold-responsive (COR) genes. These findings, together with genetic analysis of *swi3c/ice1* double mutant and enhanced freezing tolerance of *swi3c* plants illustrate that SWI/SNF CRCs contribute to fine-tuning of plant growth responses to different temperature regimes.

Keywords: SWI3C; SWI/SNF; cold response; ATP-dependent chromatin remodeling; transcriptional control of gene expression

1. Introduction

The SWI/SNF class of ATP-dependent chromatin remodeling complexes (CRCs), a prototype of which was first described in yeast, are conserved from fungi to plants and mammals. SWI/SNF CRCs control basic regulatory processes, such as transcription, cell cycle, replication, carcinogenesis,

hormone-dependent gene expression, stress response etc. (for review see: [1]). For their full basic remodeling activity in vitro, the SWI/SNF complexes require a catalytic subunit, the Snf2-type ATPase, as well as a single SNF5 and two SWI3-type subunits, which together compose the core chromatin remodeling complex [2]. Beside core subunits, SWI/SNF CRCs carry several accessory subunits [1]. The Arabidopsis genome encodes four SWI2/SNF2-type ATPases (BRM, SYD, CHR12/MINU1, and CHR23/MINU2; [3–6]), a single SNF5-type (BSH; [7]) and four SWI3 subunits (SWI3A, B, C, D; [8]). As in mammals, the Arabidopsis core SWI/SNF subunits play important roles in the control of developmental and signaling processes [1].

SWI/SNF complexes assembled by distinct combinations of core and accessory subunits are implicated in the regulation of different cellular processes [1,8–11]. *SWI3A* and *SWI3B* are essential genes, their inactivation leads to embryo arrest at the globular stage of embryogenesis. *SWI3B* also plays an important role during gametophyte development. By contrast, *SWI3C* and *SWI3D* appear to be dispensable for embryogenesis. The *swi3c* and *swi3d* mutants are viable, although they exhibit strong developmental aberrations. The *swi3d* mutation causes a complete sterility, whereas *swi3c* mutant plants are characterized by dramatic root shortening and branching, semi-dwarfism, altered leaf and flower development, and reduced fertility [8]. However, these developmental defects are less severe when *swi3c* plants are grown at 14–16 °C compared to 20–24 °C [12]. Intriguingly, inactivation of SWP73 SWI/SNF subunit in yeast is similarly reported to cause sensitivity to elevated temperature [13]. In Arabidopsis, BRM-containing SWI/SNF CRC interacts with the histone deacetylase HD2C, which is implicated in the repression of a battery of heat-activated genes [14]. These findings suggest that the SWI/SNF CRCs are involved in temperature-dependent control of transcription but so far, the underlying molecular mechanisms are largely unclear.

Here, we show that developmental defects of the Arabidopsis *swi3c* mutant, including embryo arrest at early stages and defective root elongation, are partially reverted when plants are grown at 14 °C. Our data indicate that SWI3C-containing SWI/SNF CRCs modulate the expression of several genes involved in low temperature signaling including *ICE1*, *CBF1-3*, *MYB15*, *RAP2.6*, *ZAT10*, and *ZAT12*. SWI3C-containing SWI/SNF CRCs were found to bind to the *ICE1*, *MYB15* and *CBF1* loci and their locations on these target genes is changed by the temperature conditions. Characterization of the *swi3c/ice1* double mutant suggests a genetic interaction between *SWI3C* and *ICE1*. The *swi3c* mutation also influences the expression of downstream-acting cold-responsive (COR) genes and confers enhanced freezing tolerance. In conclusion, our data illustrate that the SWI3C-containing SWI/SNF CRCs are implicated in temperature-dependent regulation of plant growth and developmental responses.

2. Results

2.1. Lower Temperature Alleviates Phenotypic Defects Caused by Mutations of the SWI3C Core Subunit Gene of Arabidopsis SWI/SNF CRC

Inactivation of genes encoding the SWI3-type subunits of SWI/SNF CRCs results in distinct effects on Arabidopsis development. The *swi3a* and *swi3b* mutations cause lethality at the early (globular) stage of embryo development. By contrast, the *swi3c* and *swi3d* mutants are viable but exhibit severe developmental defects including reduced fertility of *swi3c* and complete sterility of *swi3d* plants grown under optimal conditions [8]. We previously observed that reducing the ambient temperature to 14–16 °C substantially improved the fertility of the *swi3c* mutant, which displayed an enhanced elongation of siliques containing viable seeds [12]. This observation has prompted us to examine how lower growth temperature affects the phenotypic traits conferred by mutations of all four Arabidopsis *SWI3* genes. When grown at 14 °C, the number of white translucent seeds carrying aborted embryos was reduced from 24.8% to 6.8% and 14.8% to 0.8% in siliques of *swi3a*/+ and *swi3b*/+ plants, respectively. Gametophyte lethality of *swi3b*/+ line decreased from 34.5% to 11.95% as a result of decreasing the growth temperature (Table 1). Further analysis of mature seeds by PCR-based genotyping of isolated embryos confirmed that the reduction of growth temperature partially suppressed the defect of embryo development at the globular stage. In the progeny of *swi3a*/+

plants, we identified mature *swi3a* embryos, although their cotyledons appeared to be underdeveloped and degenerated. Similar inspection of *swi3b*/+ offspring identified *swi3b* embryos that displayed a torpedo-stage-like developmental status. Nonetheless, germination of seeds collected from *swi3a*/+ or *swi3b*/+ plants grown at 14 °C did not result in viable homozygous *swi3a* or *swi3b* progeny. This indicated that reduction of the growth temperature permitted the *swi3a* and *swi3b* embryos to reach later stages of development but did not completely suppress the block of embryo development by the *swi3a* or *swi3b* mutations (Figure 1A).

Table 1. The effect of decreased growth temperature on *swi3a* and *swi3b* embryo development.

		Number of Analyzed Seeds	Embryo Lethality [%]	Gametophyte Lethality [%]
14 °C	WT	265	0	0
	swi3a/+	350	6.29	0
	swi3b/+	502	0.80	11.95
22 °C	WT	263	0	0
	swi3a/+	310	24.84	0
	swi3b/+	244	14.75	34.43

Decreasing the growth temperature resulted in notable alleviation of the block of root elongation (Figure 1B) and enhanced root branching [12] of the *swi3c* mutant. At 14 °C, the length of siliques and the yield of viable seeds increased considerably from 24 to 66% and 5 to 31% compared to wild type [12], respectively, although no gross changes in overall differentiation and development of flower organs and growth of *swi3c* plants were detected with the exception of slightly reduced leaf curling (Figure 1C,D, Supporting Information Figure S1). In comparison, lower growth temperature resulted in remarkable growth retardation (Figure 1E) and did not restore the fertility of *swi3d* mutant. Nonetheless, we found a nearly two-fold extension of *swi3d* silique length in plants growing at 14 °C (Supporting Information Figure S2A,B). Despite the extension of silique length, the *swi3d* mutant displayed complete sterility under both low and normal temperature conditions.

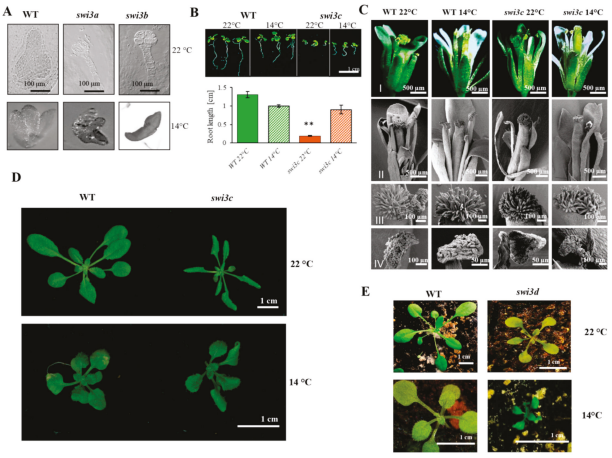

Figure 1. Phenotypic Characterization of Arabidopsis *swi3* Mutants Grown at 14 °C. (**A**) Nomarski image of WT, *swi3a* and *swi3b* embryos at 22°C (upper panel) and at 14°C (lower panel). (**B**) Root phenotype of 14-days-old *swi3c* line grown at 22°C and 14°C. Root length measurement showed that the *swi3c* mutant plants exhibited partial reversion of root elongation defect at 14°C. (**): Significantly different at $p < 0.01$ according to t-test, three biological replicates were used, at least ten plants from each genotype were measured. (**C**) Appearance of mature flowers (I) and analysis of their organs (II) including stigma (III) and anther (IV) by scanning microscopy in WT and *swi3c* plants grown at 22°C and 14°C. (**D**) The rosette of WT and *swi3c* plants grown at 22°C and 14°C. Scale bar 1 cm. (**E**) Comparison of 14-days-old WT and *swi3d* plants grown at 22°C and 14°C.

In summary, except for *swi3d* where only siliques became longer, characteristic developmental defects caused by mutations of *SWI3* core subunit genes of SWI/SNF CRCs were partially suppressed at lower temperature. As only the *swi3c* mutant produced viable homozygous progeny, further analysis of the mechanisms underlying temperature sensitivity of *swi3* mutants addressed the question how inactivation of *SWI3C* gene influences the expression of genes implicated in cold temperature signaling and downstream responses.

2.2. Genes Involved in Low Temperature Responses Show Altered Expression in the Swi3c Mutant

Transcription responses to cold temperature are controlled by the ICE1 (Inducer of CBF Expression 1) Myc transcription factor (TF), which stimulates the expression of three C-Repeat Binding Factors (CBFs) of APETALA2/ETHYLENE RESPONSE FACTOR TF family. The function of ICE1 master regulator of CBFs is regulated post-translationally [15–17]. The HOS1 ubiquitin ligase targets ICE1 for proteasomal degradation, which is counteracted by SIZ1-mediated sumoylation of ICE1 [18]. CBFs are central activators of cold-responsive (COR) genes, which are either positively or negatively regulated by the CBF-controlled TFs RAP2.1, RAP2.6 and RAP2.7 [19]. CBF expression is repressed by MYB15, which is inactivated by ICE1 under cold stress, as well as by the C2H2 zinc finger TF ZAT12 [20,21]. Another zinc finger TF ZAT10 appears to be activated by CBF3 and acts as a repressor of a set of *COR* genes [22]. Quantitative real-time PCR measurement indicated that the *ICE1* transcript levels were comparable in wild type and *swi3c* mutant plants at 14 °C, although *ICE1* mRNA levels were 2-fold lower at 22 °C in the *swi3c* mutant (Figure 2A). Similarly, *HOS1* and *SIZ1* mRNA levels were similar in wild type and *swi3c* plants under both temperature conditions. Although *MYB15* showed 4.5-fold higher expression in *swi3c* plants under normal growth condition, its mRNA level did not differ from wild type at 14°C. In comparison, expression levels of *RAP2.6*, *ZAT10* and *ZAT12* were elevated (respectively 2, 4 and 4.5-fold) at 22 °C but showed a notable down-regulation (50, 3 and 6.5-fold, respectively) at 14 °C in *swi3c* compared to wild type plants. Transcript levels of *CBF2* and

CBF3 did not differ at normal temperature, but *CBF1* expression was somewhat (2-fold) higher in *swi3c* plants as in wild type. However, at 14 °C all three *CBF* genes showed higher (2.5, 1.5 and 4.0-fold, respectively) induction in the *swi3c* mutant compared to wild type. In conclusion, this data indicated that the *swi3c* mutation elevates the steady-state levels of *CBF* mRNAs, while decreases in parallel the transcript levels of ZAT12 CBF repressor and downstream-acting ZAT10 and RAP2.6 negative regulators of subsets of *COR* genes at 14 °C. In addition, differential up-regulation of *MYB15*, *RAP2.6*, *ZAT10* and *ZAT12* expression levels at 22 °C in the *swi3c* mutant suggested that SWI3C-containing SWI/SNF CRCs could play a role in temperature-dependent modulation of transcription responses.

2.3. Temperature-Dependent Shift of Localization of SWI3C-Containing SWI/SNF CRCs in the 5′-UTR Regions of ICE1, MYB15 and CBF1 Genes

To map chromatin localization of SWI3C-containing SWI/SNF CRCs on genes involved in cold signaling, the *swi3c* mutant was complemented by a SWI3C-YFP-HA gene construct carried by the Agrobacterium binary vector pEarley101 [23]. Constitutive expression of SWI3C-YFP-HA restored at both 22 °C and 14 °C the phenotypic defects, such as leaf curling (Supporting Information Figure S3A), block of root elongation and sterility of the *swi3c* mutant to wild type and resulted in the production of intact SWI3C-YFP-HA protein of 115 kDa detected by western blotting with anti-GFP antibody (Supporting Informationn Figure S3B). Chromatin immunoprecipitation followed by quantitative PCR (ChIP-qPCR) was performed with nuclear extracts prepared from formaldehyde cross-linked *swi3c*/SWI3C-YFP-HA and control wild type plants using primers for amplification of 120–160 bp segments of 5′-UTRs located between positions +450 and −1200 relative to the transcription start site (TSS). In the promoter region of *ICE1* gene, SWI3C-YFP-HA was localized between positions +449 and +571 at 22 °C (Figure 2B). The peak value of SWI3C-YFP-HA increased approximately 3-fold and its localization was shifted to position −104 at 14 °C (Figure 2C). In the 5′-UTR of *MYB15*, SWI3C-YFP-HA was localized around position of +458 at 22°C (Figure 2D) but at 14 °C the level of SWI3C-YFP-HA decreased approximately 2-fold and its localization was shifted to position −817 (Figure 2E). A similar change in positioning of SWI3C-YFP-HA was detected in the 5′-UTR region of the *CBF1* gene, in which the peak of ChIP-signal was detected around position +343 at 22 °C (Figure 2F), while at 14 °C the localization was shifted to position −695 in parallel with approximately 2.5 fold increase of signal intensity (Figure 2G). The ChIP-PCR data thus indicated that in the case of *ICE1*, lowering the temperature resulted in a shift toward proximal position of TSS, whereas in the 5′-UTR of *MYB15* the localization of SWI3C-YFP-HA was changed to a more distant upstream position. On the other hand, the localization of SWI3C-YFP-HA both downstream and upstream of TSS of the *CBF1* gene suggested that SWI3C-containing SWI/SNF CRCs might act as negative regulators because *CBF1* transcript levels were 2 and 2.5-fold higher in the *swi3c* mutant compared to wild type. Finally, localization of SWI3C-YFP-HA closer to TSS did not seem to affect *ICE1* transcription, which is comparable between wild type and the *swi3c* mutant at 14 °C. Nevertheless, more upstream localization of SWI3C correlated with a 2-fold reduction of *ICE1* mRNA levels at 22 °C. In summary, these data indicated that the localization of SWI3C-SWI/SNF CRCs is dynamically changed in the promoter regions of examined genes in a temperature-dependent manner.

Analysis of predicted transcription factor binding sites in the SWI3C-binding region using the MEME software [25] identified several potential *cis*-regulatory elements in the SWI3C-targeted regions of *MYB15*, *ICE1* and *CBF1* genes (Supporting Information Table S2). However, subsequent GOMo analysis did not confirm potential biological roles of motives derived from the MEME analyses (Supporting Information Table S2). Additional predictions obtained by using the AGRIS server (AGRIS; http://arabidopsis.med.ohio-state.edu/) suggested potential conservation of a MYB4 binding site (ACCTAAC, [26] at mapped positions of SWI3C binding to *CBF1* locus at 22 °C. In addition, a SWI3C-binding domain mapped around position −695 relative to the TSS of *CBF1* at 14 °C was predicted to carry RAV1-A (CAACA), SORLIP2 (GGGCC) and LFY (LEAFY) binding (CCAGTG) motives. The RAV1-A binding site is recognized by the ABI3/VP1 transcription factors family [27],

the SORLIP2 motif is involved in the control of light-regulated gene expression [28], whereas the LFY consensus is recognized by the LEAFY transcription factor, which is reported to mediate the recruitment of SWI/SNF CRCs to their target site on e.g., *AP3* (*APETALA 3*) promoter [29]. The 5′-UTRs of *ICE1* and *MYB15* genes however lacked these motives. The only known predicted TF-binding site in these 5′-UTRs was a BELLRINGER motif (AAATTAAA), which was identified in the SWI3C-binding region in *MYB15* (position −817) at 14 °C. This motif is used by homeobox/MYB transcription factors of regulatory networks controlling development, metabolism and responses to biotic and abiotic stresses in Arabidopsis [30] (Supporting Information Table S2).

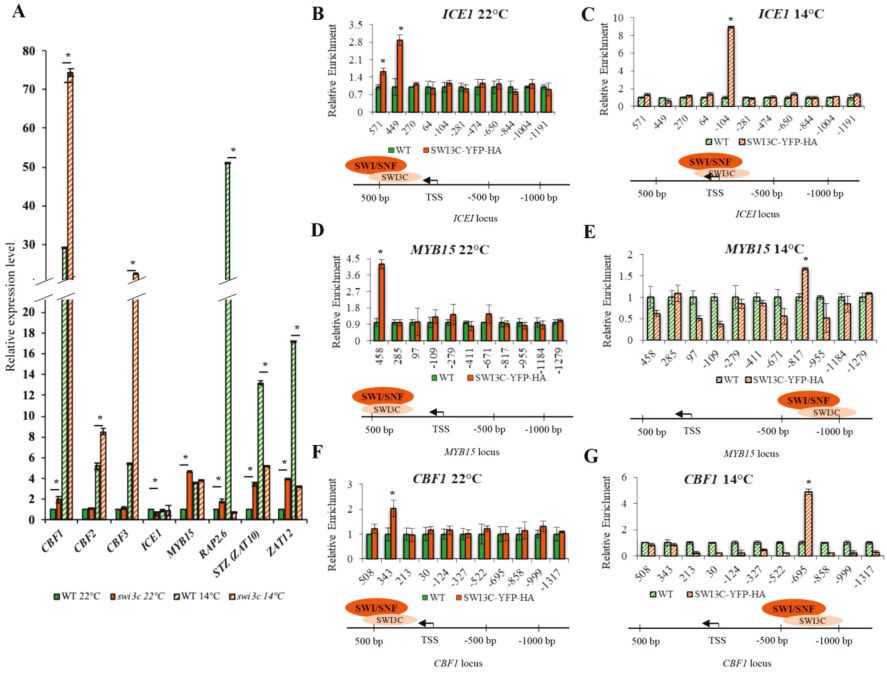

Figure 2. Altered Transcription of Genes Involved in Cold Signaling in the *swi3c* Mutant. (**A**) Relative expression levels of genes of cold signaling pathway in wild type and *swi3c* plants grown at 22°C and 14° C. Plants were in a developmental stage with 12 rosette leaves > 1mm length according to Boyes et al. (2001) [24]. Asterisks indicate significant difference (*): $p < 0.05$ according to t-test. (**B**) SWI3C binding to 5′-UTR region of ICE1 at 22°C and (**C**) at 14°C. (**D**) SWI3C binding to the promoter region of MYB15 at 22 °C and (**E**) at 14°C. (**F**) Peak position of SWI3C in the CBF1 promoter at 22°C and (**G**) at 14 °C. The TA3 transposon served as reference gene. Three biological and three technical replicates were used. Plants were in the principal stage with 12 rosette leaves > 1mm length according to Boyes et al. (2001) [24]. Asterisks indicate significant difference from wild type (*): $p < 0.05$ according to t-test. Bars refer to SD.

2.4. The Swi3c Mutation Changes Nucleosome Positioning on the ICE1, MYB15 and CBF1 Loci

To correlate the SWI3C chromatin localization data with alterations of nucleosome positioning in the *swi3c* mutant, micrococcal nuclease protection qPCR (MNase-qPCR) assays were performed using a set of primers positioned between +600 and −1100 relatively to TSSs of the *ICE1*, *MYB15* and *CBF1* genes. In wild type plants grown at 22 °C five nucleosomes protected from MNase digestion were mapped to positions −200 (−1 nucleosome), −360 (−2 nucleosome), +225 bp (+1), + 360 bp (+2) and +530 (+3) relative to the TSS of *ICE1*. In the *swi3c* mutant the TSS proximal nucleosome exhibited a

slight shift to position −140 and fuzziness, as well as increased occupancy, correlating with lower than wild type transcript levels at 22°C. In addition, the *swi3c* mutation resulted in enhanced positioning of nucleosome +2 and fuzziness of nucleosome +3, both located close to mapped position of SWI3C at normal temperature (Figure 3A). By contrast, wild type and *swi3c* plants grown under decreased temperature did not show a change in nucleosome occupancy correlating with no difference in *ICE1* transcription between wild type and *swi3c* plants under this condition (Figure 3B).

In case of the *MYB15* locus four nucleosomes protected from MNase digestion were mapped in wild type plants grown at 22 °C. Two of these were located in the distal promoter region centered to positions −816 (−1 nucleosome) and −1130 (−2 nucleosome), whereas the other two nucleosomes were mapped into the gene body around positions + 394 bp (+1) and +574 (+2). In correlation with a 4.5-fold increase of *MYB15* transcript levels at 22°C, in the *swi3c* mutant we found a complete loss of nucleosomes −1 and −2, as well as decreased occupancy of nucleosome +1 located in the vicinity of mapped SWI3C-binding region at position +458 (Figure 3C). At 14 °C, the positioning of nucleosomes was slightly shifted to positions −726 bp (−1) 1000 (−2), +244 (+1) and 544 (+2). Compared to wild type, in the *swi3c* mutant the positioning of nucleosomes was fuzzier, and nucleosomes +1 and −2 were slightly shifted (Figure 3D). However, no striking difference was found in positioning of nucleosomes correlating with no difference in *MYB15* mRNA levels between wild type and *swi3c* plants at 14 °C.

In both wild type and *swi3c* plants grown under normal temperature four nucleosomes were protected from MNase in the *CBF1* locus. Two nucleosomes were located in the distal promoter region centered to positions −815 (−1) and −990 (−2), while others were situated at positions the +120 (+1) and + 325 (+2) in the gene body. In correlation with a 2-fold increase of *CBF1* mRNA levels compared to wild type at 22 °C, the −1 nucleosome exhibited a slight fuzziness, and nucleosomes +1 and +2 in the vicinity of identified SWI3C binding site at position +343 (Figure 3E) showed decreased occupancy in the *swi3c* mutant (Figure 3F). At 14°C, the positions of nucleosomes were shifted to positions −680 (−1), −855 bp (−2) −1000 (−3) and +270. In contrast to normal temperature, at 14 °C the positioning of nucleosome +1 did not change. However, a complete loss of nucleosome −2 was detected close to the location of mapped SWI3C target region at position −695. This observation, together with a 2.5-fold increase of *CBF1* mRNA levels in *swi3c* plants indicated that lack of SWI3C caused two different, temperature-dependent changes to generate more open chromatin structure in the promoter region of *CBF1*gene (Figure 3F).

As this analysis did not show a clear correlation between nucleosome positioning, SWI3C occupancy and *ICE1, MYB15* and *CBF1* gene expression, we reanalyzed the data and compared nucleosome positioning and transcript level detected in the WT 22 °C *vs* WT 14°C and *swi3c* 22 °C *vs swi3c* 14 °C datasets (Supporting Information Figure S4A,B). This indicated that both WT and *swi3c* mutant plants responded to decreased temperature in a similar way concerning *ICE1* and *CBF1* genes (Supporting Information Figure S4B), although some nucleosome positioning changed in temperature-dependent manner (Supporting Information Figure S4A). The nucleosome positions differed between WT and *swi3c* mutant at 22°C and *CBF1* expression in the mutant plants was much higher than in WT in both temperature conditions (Figure 2A). Interestingly, the highest changes in transcription for *swi3c* mutant *vs* WT at 22 °C were observed for *MYB15* gene (Figure 2A). In the *swi3c* mutant, the *MYB15* gene responded to decreased growth temperature in different way than in WT, where *MYB15* expression was elevated at 14°C, whereas *swi3c* plants exhibited similar levels of *MYB15* mRNA regardless of temperature conditions (Supporting Information Figure S4B). Moreover, we found that the nucleosomes −1 and −2 at 22 °C on *MYB15* in the in *swi3c* mutant were missing from promoter region close to TSS, which could explain the almost 5-fold highest expression at 22°C compared to WT. At lower temperature, the positioning of nucleosomes in this region is observed and the activation of transcription and proper response (elevated expression) occurred in WT plants. By contrast, the *MYB15* expression level in the *swi3c* mutant exposed to lower temperature resembled WT under the same conditions. Thus, although in the *MYB15* promoter region two nucleosomes were located in cold, the *swi3c* mutation did not seem to alter *MYB15* transcription in response to low temperature.

In conclusion, the MNase nucleosome mapping data only partially supported the results of transcript measurements and SWI3C ChIP-qRT-PCR assays revealing that the lack of SWI3C subunit of SWI/SNF CRCs results in distinct temperature-dependent changes in the chromatin structure of genes involved in cold signaling. This suggests that likely other remodelers (i.e., other classes of SWI/SNF complexes) are also involved in transcriptional control of genes in the cold response pathway in response to decreased temperature. However, replacement of the missing SWI3C-SWI/SNF complex by alternative CRCs remains to be confirmed by further studies.

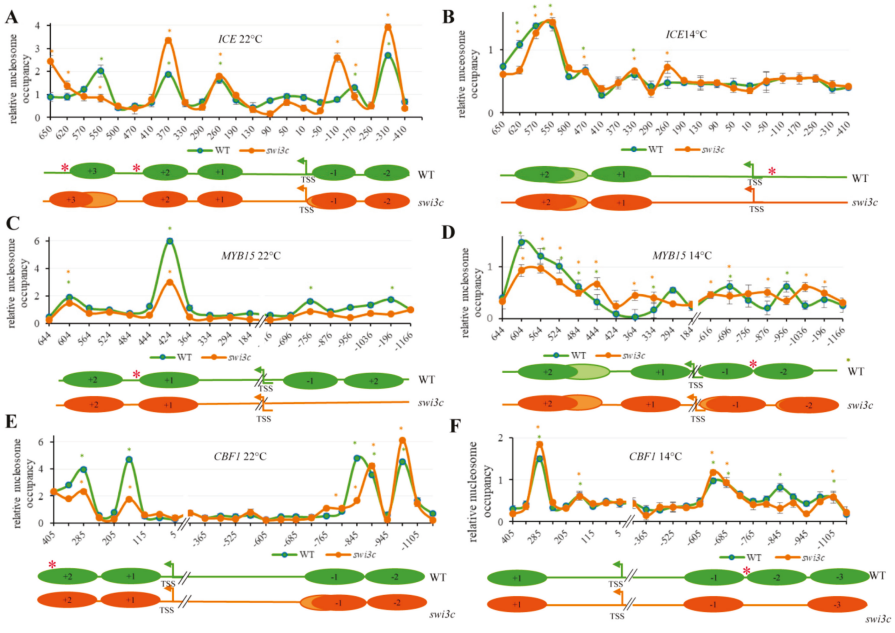

Figure 3. The Effect of SWI3C Inactivation on Nucleosomal Structures of *ICE1*, *MYB15* and *CBF1* Genes. (**A**) Relative nucleosomes occupancy on the *ICE1* locus in WT and *swi3c* plants grown at 22°C and (**B**) 14°C. (**C**) Relative nucleosome occupancy on *MYB15* in WT and *swi3c* plants at 22°C and (**D**) 14°C. (**E**) Relative nucleosome occupancy on *CBF1* in WT and *swi3c* plants at 22°C and (**F**) 14°C. Plants were in the principal stage with 12 rosette leaves > 1mm length according to Boyes et al. (2001) [24]. Three biological and three technical replicates were used. The fraction of undigested genomic DNA amplified for each amplicon was normalized to that of the −73 position of GYPSY-LIKE retrotransposon (At4g07700) as control. Lower panels in each figure section show schematic illustration of nucleosome positioning and dynamics. Red asterisks indicate the localization of SWI3C protein determined by ChIP-qPCR analysis. Dark-color circles indicate positioned nucleosomes, and light colors mark non-positioned nucleosomes. Green and orange asterisks (*) indicate significant ($p < 0.05$) protection of DNA from MNase digestion in WT or *swi3c*, respectively.

2.5. Genetic Interactions Between SWI3C and ICE1

ICE1 is a key positive regulator of the cold signaling pathway. To test how inactivation of *ICE1* affect the cold temperature-dependent suppression of *swi3c* developmental and fertility defects, the *swi3c-1* mutation [8] was introduced by crossing into the *ice1* (SALK_068119) T-DNA insertion mutant. In the SALK_068119 mutant a T-DNA insertion in exon 4 of *ICE1* resulted in a C-terminal truncation of the coding domain, which showed still active transcription 5′ upstream of the insertion site (Supporting Information Figure S5A,B). Nonetheless, the mutation appeared to cause at least a partial loss of ICE1 function because in the F2 offspring of *swi3c/+ice1/+* hybrid we failed to identify homozygous *swi3c ice1*

double mutants. In the siliques of *swi3c/+ice1* F2 progeny we did not observe embryo lethality, which suggested that *swi3 ice1* homozygous seeds were either not viable or incapable of germinating in soil under normal conditions. When germinating 216 F2 seed of a *swi3c/+ice1* plant on 0.5 MS medium only 8 (3.7%) *swi3 ice1* seedlings were identified by PCR-based genotyping indicating a significant deviation from the expected 3:1 ratio. Upon transfer into soil, the double mutant plants displayed an enhanced severity of *swi3c* developmental defects, including enhanced dwarfism and reduction of leaf blade size (Supporting Information Figure S6A) and complete sterility. Comparative microscopic analysis of developmental status of embryos using Nomarski optics indicated retarded development of embryos in both *swi3c* and *ice1* mutants compared to wild type plants. However, both *swi3c* and *ice1* single mutants could produce viable progeny, whereas in the double *swi3c ice1* mutant pollen tubes could not germinate into the embryo sac and fertilization did not occur resulting in a failure of embryo formation (Supporting Information Figure S6B).

2.6. Inactivation of SWI3C Alters the Expression of Cold-Responsive (COR) Genes

The expression of cold-responsive maker genes *ADH1* (Alcohol Dehydrogenase 1), *COR15A* (Cold-Regulated 15A), *COR47* (Cold-Regulated 47), *KIN1* (Kinase 1), *KIN2* (Kinase 2), *RD22* (Responsive to Desiccation 22), and *RD29A* (Responsive to Desiccation 29A) [19,31,32] in the *swi3c* mutant was compared to wild type by quantitative real-time (qRT-PCR). Under normal conditions (22 °C), 4.5-fold elevated expression of *MYB15* (Figure 2A) correlated with 2 to 4-fold reduced expression of *COR15A*, *COR47* and *RD29A* genes in the *swi3c* mutants compared to wild type plants (Supporting Information Figure S6C). By contrast in *swi3c* plants growing at 14 °C we detected 2.0-fold and 1.5-fold lower expression of *ADH1* and *COR15A* genes compared to WT.. We also found a discrete up-regulation of *COR47* and 2.0-fold elevated expression of *RD22* and *RD29A* genes in the *swi3c* mutant compared to WT plants grown at 14 °C. In summary, these results indicated an involvement of SWI3C in transcriptional regulation of *COR* genes under both normal and low temperature conditions.

2.7. Swi3c Mutant Exhibits Enhanced Freezing Tolerance

Overexpression of CBFs in cooperation with other cold-regulated first-wave transcription factors was demonstrated to increase freezing tolerance [33]. Therefore, we examined the freezing tolerance trait of *swi3c* mutant by performing a freezing-survival assays. Wild type and *swi3c* plants were moved to 4 °C, and then within 30 min the temperature decreased to 0 °C. Subsequently, the temperature decreased by 1°C every hour until it reached −8 °C. Next, the plants were moved to a growth chamber with long day and 22 °C conditions. After 7 days recovery period, the number of surviving plants was determined. We found that the survival rate for wild type plants was approximately 20% while for *swi3c* it reached up to −90% (Figure 4A,B) indicating enhanced freezing tolerance. We also found that the constitutive expression of SWI3C-YFP-HA restored, upon freezing, the phenotypic defects exhibited by the *swi3c* plants (Supporting Information Figure S7). To further confirm enhanced freezing tolerance of *swi3c* mutant, we performed electrolyte leakage assays [34] (and determined the EL50 value (the temperature at which 50% of cellular electrolytes was released due to freezing tolerance). For wild type plants, the EL50 value was ~ −6 °C, whereas the *swi3c* mutant exhibited only ~ 30% of cellular electrolyte release at the same temperature (Figure 4C). Collectively, these results demonstrated that the *swi3c* mutant exhibited increased freezing tolerance.

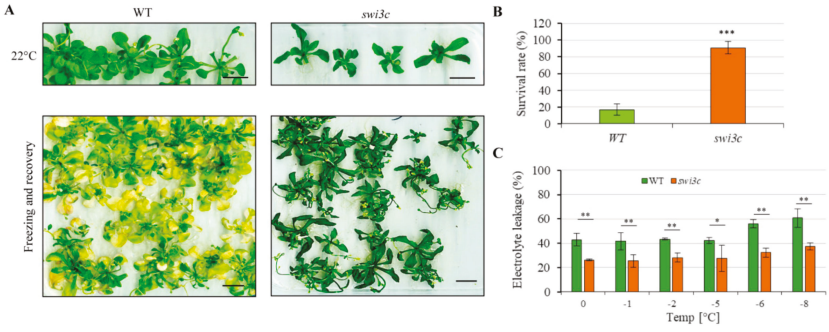

Figure 4. The *swi3c* Mutant Exhibits Enhanced Freezing Tolerance. (**A**) *swi3c* plants are more tolerant to freezing than wild type control. Upper panel: 3-weeks old WT and *swi3c* plants grown on plates under long day conditions. Lower panel: WT and *swi3c* plants exposed to freezing and subsequently recovered for seven days under long day conditions at 22°C. (**B**) The survival rate of wild type and *swi3c* plants subjected to freezing tolerance assay indicate enhanced freezing tolerance of *swi3c* plants. (**C**) *swi3c* plants exhibit lower electrolyte leakage after freezing damage than WT plants further confirming their enhanced freezing tolerance. Asterisks indicate significant difference from wild type (*): $p < 0.05$; (**): $p < 0.01$ (***): $p < 0.001$ according to t-test. Error bars refer to SD.

3. Discussion

Plants, as sessile organisms, are constantly exposed to various abiotic and biotic stresses. To be able to survive in a changing environment, plants evolved numerous defense mechanisms allowing them to survive under stress conditions. The phenotypic plasticity plays a crucial role in adaptation to changing environmental conditions, thanks to which plants developed adaptive defense reactions to response to unfavorable conditions. Epigenetic changes occurring at the chromatin level play a pivotal role in the genotype-environment interaction [35].

Exposure to low temperature stimulates signaling pathways that control the expression of genes conferring plant tolerance to cold stress [36]. *ICE1* (*Inducer of CBF Expression 1*), also called SCREAM1 [37], is a key positive regulator of the cold-responsive pathway, which is activated by sumoylation. ICE1 is critical for induction of the *CBF* (*C-Repeat Binding Factor*) regulon and inhibition of the *CBF* repressor MYB15 [20]. ICE1 is negatively regulated through ubiquitination by the HOS1 (High Expression of Osmotically Responsive Genes 1) RING finger-type ubiquitin E3 ligase, which stimulates its proteasomal degradation [18]. CBFs cross-regulate their own transcription [22] and bind to *cis*-elements in the promoters of *COR* genes and activate their transcription [38]. The ICE1-MYB15-CBF signaling module plays a major role in adaptation and acclimation of plants to cold stress [39].

Adaptation to abiotic stresses is accompanied by either activation or inactivation of a large number of genes, implying changes in their chromatin structures. Alterations in the chromatin structure are induced by DNA methylation, modification of core histone tails, exchange of histone variants, and altered positioning of nucleosomes [40,41]. Histone deacetylase HD2C was reported recently to play an important role in plant adaptation to temperature changes by modulating the transcription of cold-responsive genes *COR15A* and *COR47* [42]. HD2C is known to co-operate with SWI/SNF chromatin remodeling complexes in response to high temperature in Arabidopsis [14]; however, it is yet unknown whether HD2C interaction with SWI/SNF CRCs plays also a role in plant responses to cold temperature, which is suggested by the observation that reduced fertility of plants carrying mutations of the SWI3C core subunit of SWI/SNF CRCs is largely alleviated by decreasing the growth temperature to 14°C [12].

In this report, we investigated cold temperature sensitivity of developmental defects caused by mutations of SWI3 core subunit genes of Arabidopsis SWI/SNF CRCs. We showed that decreasing the growth temperature to 14°C permitted the *swi3a* and *swi3b* mutant embryos to develop close to

final maturation, although their development was arrested at the globular stage at 22 °C. Similarly, the *SWI3B*-dependent female gametophytic defect is partially restored by lowering the growth temperature to 14 °C. In case of the *swi3c* mutant, in addition to improved fertility, lowering the temperature partially suppressed the block of root elongation and enhanced root branching, and leaf curling. As exception, developmental defects of the *swi3d* mutant were not restored by decreased growth temperature. The plants growing at decreased temperature exhibited even more retarded growth but displayed a slight extension of siliques compared to *swi3d* plants grown at 22 °C. In contrast to the *swi3c* mutant, *swi3d* plants did not improve their fertility at 14°C and remained fully sterile. The differential behavior of *swi3c* and *swi3d* mutants further supports our previous findings that SWI3C and SWI3D are present in different classes of SWI/SNF CRCs [8] and suggests that SWI3D-containing SWI/SNF CRCs class acts distinctly from temperature signaling pathways.

Inactivation of SWI3C was found to alter transcriptional regulation of several genes acting in the cold signaling pathway, including *CBF1-3*, *ICE1*, *MYB15*, *RAP2.6*, *ZAT10* and *ZAT12*. Interestingly, the transcription of these genes was differentially deregulated in the *swi3c* mutant at 22 and 14 °C. This suggested that the function of SWI3C-containing SWI/SNF CRCs is differently regulated depending on the ambient temperature. The *swi3c* mutation was found to enhance transcription of the *CBF1-3* genes at 14°C, which normally correlates with enhanced cold tolerance [43]. Subsequent chromatin immunoprecipitation study indicated direct targeting of SWI3C to the *ICE1*, *MYB15* and *CBF1* loci, and in all three cases SWI3C was localized at 22°C 3′ downstream of TSS in these genes. Although unexpected, this observation is in line with recent mapping studies of human [44] and Arabidopsis [45] SWI/SNF CRCs, which were located in various gene regions. Similarly, SWI/SNF CRCs in Drosophila were observed to bind gene body regions affecting transcription elongation [46] and RNA polymerase II pausing [47]. The location of SWI3C on the *ICE1*, *CBF1* and *MYB15* loci has remarkably changed in a temperature-dependent manner and was shifted 5′-upstream of TSSs in the promoter regions of *ICE1*, *MYB15* and *CBF1* genes.

In the case of the *CBF1* gene, SWI3C-binding under control conditions occurred in close proximity to a MYB4-binding motif, which is targeted by various MYB transcription factors including MYB15 [20], another regulatory target of SWI3C-SWI/SNF CRCs. By contrast, under decreased temperature SWI3C shifted from this site in the gene body to the putative RAV1-A, SORLIP2 and LFY (LEAFY) consensus binding sites in the distal *CBF1* promoter region. While the LEAFY transcription factor is a known binding partner of SWI/SNF CRCs, there is so far no report on the regulatory interdependence of RAV1 and SWI/SNF. The SORLIP2 motif was identified in the promoter regions of phytochrome A-regulated genes [28] and the BRM ATPase subunit of SWI/SNF CRCs is reported to interact directly with PIF1 (PHYTOCHROME-INTERACTING-PARTNER 1) [48]. Nonetheless, so far, no regulatory link was identified between SORLIP2 and SWI/SNF. A different localization of SWI3C on the *CBF1* gene indicated two different temperature-dependent modes of transcriptional regulation by SWI/SNF-mediated chromatin remodeling at 22 and 14°C. By contrast, different localization of SWI3C-SWI/SNF CRCs on the *ICE1* locus, which is not coupled to altered transcription at 14°C, might reflect altered chromatin loop formation, transcription factor binding, histone modifications, etc. [47].

On the *CBF1*, *ICE1*, and *MYB15* loci the chromatin nucleosome structure varies in and between wild type and *swi3c* mutant plants depending on the growth temperature. Lower transcription of *ICE1* in the *swi3c* mutant at 22°C correlates with altered (enhanced) positioning and shift of nucleosomes. An opposite effect is found on the *MYB15* locus, where we observed an absence (promoter region) and decreased positioning (gene body) of particular nucleosomes. Decreased positioning of nucleosomes in the gene body and slight fuzziness of nucleosomes in the promoter region correlate with enhanced transcription of *CBF1* and *MYB15* genes under normal growth condition in the *swi3c* mutant. These findings are in line with the results showing that the presence of SWI/SNF CRCs in the gene body plays an important role in the control of nucleosome density during transcriptional elongation in Drosophila [46]. The contrasting situation was observed under a lower growth temperature where the chromatin structure on *ICE1* did not differ from the wild type, whereas only some fuzziness of

nucleosomes was detected on *MYB15*, while the expression of these genes was not altered in the *swi3c* mutant compared to wild type. These results suggest that inactivation of SWI3C has no effect on the *MYB15* gene expression at decreased temperature. However, the comparative analysis of *MYB15* expression levels in WT and *swi3c* plants growing at 22°C vs. 14°C indicated that indeed WT and *swi3c* exhibit substantially different activation modes of the *MYB15* gene. In WT plants growing at decreased temperature, *MYB15* activation occurs but the *swi3c* plants are unable to elevate *MYB15* expression under these conditions. By contrast, the *swi3c* mutant was still able to elevate *CBF1* expression under decreased temperature condition compared to *swi3c* plants grown at 22°C, although under both temperature conditions the expression of *MYB15* was higher in *swi3c* than in WT plants. Interestingly, on the *CBF1* gene, a loss of nucleosome-2 was observed at 14°C, corresponding to the position of potential *cis*-regulatory sequences and enhanced transcription of *CBF1* in the *swi3c* mutant. Collectively, these findings indicate that SWI/SNF CRCs are likely implicated in chromatin remodeling of *ICE1*, *MYB15* and *CBF1* transcription units under changing ambient temperature.

The analysis of *swi3c/ice1* double mutant shows that simultaneous inactivation of *ICE1* and *SWI3C* has a dramatic effect on Arabidopsis development, i.e., the plants were severely dwarfed and completely sterile, while both *swi3c* and *ice1* single mutants produced some seeds [8,49]. Consistently, further investigation of expression of cold-responsive genes indicated their temperature-dependent deregulation in the *swi3c* mutant plants. These results suggest that *SWI3C* is involved in fine-tuning of cold responses in Arabidopsis (Figure 5A–C), in addition to its previously documented roles in modulation of leaf and flower development and hormone signaling pathways [1,11,12]. This conclusion is supported by the fact that *swi3c* plants exhibit an enhanced freezing tolerance, which was demonstrated by their increased survival rate and decreased electrolyte leakage at −8°C. It was recently shown that overexpression of CBFs increases freezing tolerance in Arabidopsis [33]. Thus, enhanced freezing tolerance of the *swi3c* mutant is consistent with observed overexpression of *CBF1-3* genes under decreased temperature.

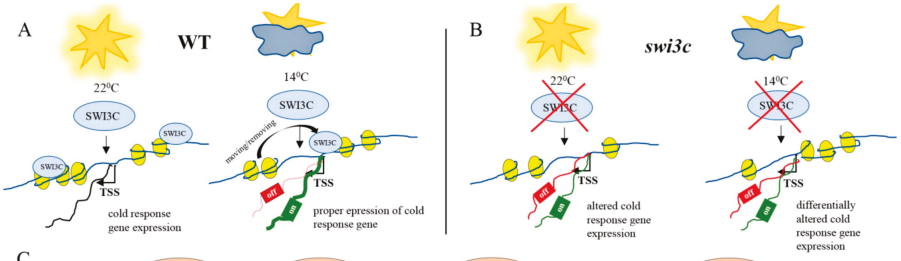

gene	WT 22°C	swi3c 22°C vs WT 22°C	WT 14°C vs WT 22°C	swi3c 14°C vs WT 14°C	swi3c 14°C vs swi3c 22°C
ICE1	-	↓	-	-	-
MYB15	-	↑	↑	-	↓
CBF1	-	↑	↑	↑	↑
CBF2	-	-	↑	↑	↑
CBF3	-	-	↑	↑	↑
ZAT10	-	↑	↑	↓	↑
ZAT12	-	↑	↑	↓	↓
RAP2.6	-	↑	↑	↓	↓
ADH1	-	-	-	↓	↓
COR15	-	↓	↑	↓	↑
COR47	-	↓	↑	↑	↑
KIN1	-	↑	↑	-	↑
KIN2	-	-	↑	-	↑
RD22	-	-	↓	↑	-
RD29A	-	↓	↑	↑	↑

Figure 5. The Action of SWI3C-containing SWI/SNF CRCs in the Transcriptional Control of Genes in the Cold-Responsive Pathway Depends on the Growth Temperature. (**A**) Schematic model illustrating the role of intact SWI3C-containing SWI/SNF CRCs in the transcriptional control of *ICE1*, *CBF1* and *MYB15* genes in WT plants. The SWI3C-containing SWI/SNF complex modulates the expression of cold-responsive genes in wild type plants at 22°C in different manner than during growth at 14°C. The position of SWI3C-SWI/SNF CRC localization differs depending on the temperature. Blue circles indicate SWI3C protein and yellow ellipses represent nucleosomes. (**B**) Schematic model illustrating the impact of SWI3C inactivation on transcription of *ICE1*, *CBF1* and *MYB15* genes in *swi3c* plants. Blue circles symbolize the SWI3C protein and yellow ellipses represent nucleosomes.(**C**) The overview of transcriptional changes of cold-responsive genes in wild type and *swi3c* mutant plants. Green arrows mark elevated expression, red arrows indicate decreased expression.

4. Materials and Methods

4.1. Plant Lines and Growth Conditions

Wild type and mutant lines were of the *Arabidopsis thaliana L. Heynh.* Columbia-0 (Col-0 further referred as WT) ecotype (Lehleseeds, Round Rock, TX, USA). The *swi3a-1*, *swi3b-1*, *swi3c-1* and *swi3d-1* mutant alleles (referred further as *swi3a*, *swi3b*, *swi3c* and *swi3d*, respectively) were characterized previously [8]. The *ice1* (SALK_068119) T-DNA insertion mutant was obtained from the Nottingham Arabidopsis Stock Centre [50]. PCR primers used for genotyping are listed in Supporting Information Table S1.

Seeds were sown on soil or plated on half-strength MS medium (Sigma-Aldrich) containing 0.5% sucrose and 0.8% agar (pH 5.8). Plants were grown under long day (LD) conditions (16h light/8h dark) at 22°C or 14°C, 70% humidity and 140 mM m^{-2} s^{-1} light intensity. For qRT-PCR, ChIP-qPCR and MNase-qPCR analyses plant material was collected six hours after the onset of the light period from the aerial part of plants in principal stage growth with 12 rosette leaves > 1mm length according to

Boyes et al. (2001) [24]. For each experiment, three biological and three technical replicates were used. For the assessment of phenotypic alterations three biological replicates were used.

4.2. Construction of Genetically Complemented Plants by Expression of YFP-HA Tagged SWI3C Protein

The *SWI3C* cDNA was cloned into pDONR207, sequenced, and moved into pEarley101 [23] using the Gateway procedure. Transgenic lines were generated by floral dip transformation of *swi3c-1*/+ plants using the Agrobacterium GV3101 (pMP90) strain [51,52]. Primary transformants were selected based on their BASTA (100μM) resistance. Homozygous *swi3c* plants complemented with the SWI3C-YFP-HA construct were identified by PCR-based genotyping and subjected to subsequent analysis of their phenotypic traits. The expression of SWI3C-YFP-HA protein in *swi3c*/SWI3C-YFP-HA plants was confirmed by Western blotting using a rat anti-GFP antibody (Chromotek).

4.3. RNA Extraction and qRT-PCR Analysis

RNA was extracted using RNeasy plant kit (Qiagen). Traces of genomic DNA were removed using a TURBO DNA-free kit (Ambion). 2.5 μg of total RNA was reverse-transcribed using a first-strand cDNA synthesis kit (Roche). qRT-PCR assays were performed with SYBR Green Master mix (BioRad) and specific primers for PCR amplification. qRT-PCR data were recorded and analyzed using iQ-PCR (BioRad) or LightCycler480 (Roche) equipment and software according to manufacturers' recommendations. *PP2A* and *UBQ5* (AT1G13320 and AT3G62250, respectively) mRNAs were used as reference. The relative transcript level of each gene was determined by the $2^{-\Delta\Delta Ct}$ method [53]. For each primer pair, the primer efficiency was measured and melting curve analyzed. For each experiment, three biological and three technical replicates were used. Primers used for qRT-PCR study are listed in Supporting Information Table S1.

4.4. Chromatin Immunoprecipitation (ChIP)

Chromatin was isolated from 2g samples of WT and *swi3c*/SWI3C-YFP-HA seedlings in the principal growth stage 1.12 [24] grown at 22ºC or 14ºC, respectively, and sonicated according to [54] with the exception that instead of pepstatin A and aprotinin, 1% PIC (Sigma), 1mM PMSF and 5mM β-me were included in the extraction buffer. Cross-linked SWI3C-YFP-HA samples were subjected to immunoprecipitation using 25μL of GFP-TRAP beads (Chromotek) according to the manufacturer's protocol. The percentage of input was calculated using $2^{-\Delta\Delta Ct}$ method [53]. To facilitate the comparison of different samples, the calculated percent input of wild type was set to 1. The relative enrichment represents the fold change compared to the wild type. The exon region of *TA3* was used as negative control [55]. For each experiment three biological and three technical replicates were used.

4.5. Mapping of Nucleosome Locations Using MNase Protection Assay

For the mapping of nucleosome positions, 2g samples of WT and *swi3c* seedlings in the principal growth stage 1.12 [56] grown at 22ºC or 14ºC, respectively, were proceeded according to Saleh et al., (2008) [54] and Zhu et al., (2013) [57] with minor modifications (i.e., the buffer contained 1% proteinase inhibitor cocktail (Sigma) instead of pepstatin A and aprotinin). 200 Kunitz units of Micrococcal Nuclease (NEB) was used for digestion of each sample. DNA was purified with phenol: chloroform extraction, ethanol precipitation and subsequently separated on 2% agarose gels. Bands corresponding to ~150 bp were gel isolated, purified, and used for qPCR measurements. Relative nucleosome occupancy was represented as fraction of undigested chromatin DNA and plotted against the *ICE1*, *MYB15* and *CBF1* genes position with respect to the TSS (transcription start site) for each primer pair where the position denotes the center of each 70–110 bp amplicon. For each experiment three biological and three technical replicates were used.

4.6. Microscopic Analyses

Immature seeds were cleared in Hoyer's solution (30 mL of water, 100 g of chloral hydrate, 7.5 g of Arabic gum, and 5 mL of glycerin) on a glass slide and examined with a compound microscope equipped with Nomarski optics. For scanning electron microscopy (SEM) the plant material was dried in liquid carbon dioxide and mounted on stubs using double sided adhesive and conductive tabs. Next, plant material was coated with gold and platin before imaging with a Zeiss Supra 40VP SEM (Carl Zeiss NTS, Oberkochen, Germany). For each experiment at least three biological replicates were used.

4.7. Freezing Tolerance Assay

To determine the freezing tolerance of *swi3c* plants, the electrolyte leakage and survival rate measurements were used. Electrolyte leakage assay was performed according to the methods described by Guo et al., (2002) [58] and Zhao et al., (2016) [34]. Briefly, rosette leaves from 3 weeks old plants grown on 0.5 Murashige and Skoog medium (Sigma Aldrich) containing 0.5% sucrose and 0.8% agar under long day condition (LD) (16h day/8h night) were excised and placed in Eppendorf tubes containing 100 µl deionized water. To each tube a similar ice cube was added and immediately transferred to a freezing bath cooled to 0°C. When all the tubes were placed in freezing bath the program started according to conditions 1°C decrements every 30 min until reached −8°C. The tubes were removed from freezing bath when samples reached desired temperature. Solutions with leaves were then transferred to a falcon tube containing 20 mL of deionized water. Then tubes were incubated overnight and electroconductivity was measured. After measurements, the tubes were incubated in −80°C overnight and the next day electroconductivity was measured again. The electrolyte leakage was calculated as a percentage ratio of conductivity before and after −80°C incubation. Three biological and technical replicates were used.

The survival freezing assay was performed by incubation of 3 weeks old plant grown on MS medium in freezing incubator by applying following temperature program: start temperature was set at 4°C and then dropped to 0°C by 30 min and then temperature decreased by 1°C every 1 h until reached −8°C. After treatment plants were recovered at control condition for 7 days when survival rate was counted. Three biological and technical replicates were done.

4.8. Bioinformatic Analysis of Cis-Regulatory Elements

Bioinformatic analysis of *cis*-regulatory elements was performed using the Multiple EM for Motif Elicitation (MEME) [25] and followed by Gene Ontology for Motifs (GOMo) [59]. MEME analysis was performed with default settings using minw = 4 and maxw = 50 parameters. GOMo analysis was done with default settings.

To get the more comprehensive picture of *cis*-regulatory elements the additional bioinformatic analysis of *cis*-regulatory elements was performed using the Arabidopsis Gene Regulatory Information Server (AGRIS; http://arabidopsis.med.ohio-state.edu/) [60–62].

4.9. Statistical Analyses

The method used in this paper for statistical analyses was unpaired Student's T-test.

Supplementary Materials: Supplementary materials can be found at http://www.mdpi.com/1422-0067/21/3/762/s1.

Author Contributions: D.MG.-Z. performed research and wrote parts of the paper; S.K., P.C., P.O., E.S., J.S., R.F., A.T.R., M.Z., E.B., A.M., performed research; ES analyzed the data; S.K. and C.K. analyzed the data and wrote the paper; T.J.S. designed the research, analyzed data, and wrote the paper. All authors have read and agreed to the published version of the manuscript.

Funding: This work was supported by: the Diamond grant No DI 2011 0269 41 Ministry of Science and Higher Education Republic of Poland (MNiSW) to DMGZ and No. 466/STYP/11/2016 to SK and National Science Centre, Poland grants: UMO-2011/01/N/NZ1/01525 to ATR., UMO-2011/01/N/NZ1/01530 to EB, UMO-2014/13/B/NZ2/01187 to TJS and UMO-2017/01/X/NZ2/00282 to AM.

Acknowledgments: We thank Sabine Schäfer and Ingrid Reinsch for their technical help, Malgorzata Garnczarska and Lukasz Wojtyla for technical support in the electrolyte leakage assay.

Conflicts of Interest: The authors declare no conflict of interest. The funders had no role in the design of the study; in the collection, analyses, or interpretation of data; in the writing of the manuscript, or in the decision to publish the results.

References

1. Sarnowska, E.; Gratkowska, D.M.; Sacharowski, S.P.; Cwiek, P.; Tohge, T.; Fernie, A.R.; Siedlecki, J.A.; Koncz, C.; Sarnowski, T.J. The Role of SWI/SNF Chromatin Remodeling Complexes in Hormone Crosstalk. *Trends Plant. Sci.* **2016**, *21*, 594–608. [CrossRef] [PubMed]
2. Phelan, M.L.; Sif, S.; Narlikar, G.J.; Kingston, R.E. Reconstitution of a core chromatin remodeling complex from SWI/SNF subunits. *Mol. Cell* **1999**, *3*, 247–253. [CrossRef]
3. Farrona, S. The Arabidopsis thaliana SNF2 homolog AtBRM controls shoot development and flowering. *Development* **2004**, *131*, 4965–4975. [CrossRef] [PubMed]
4. Mlynárová, L.; Nap, J.P.; Bisseling, T. The SWI/SNF chromatin-remodeling gene AtCHR12 mediates temporary growth arrest in Arabidopsis thaliana upon perceiving environmental stress. *Plant. J.* **2007**, *51*, 874–885. [CrossRef] [PubMed]
5. Sang, Y.; Silva-Ortega, C.O.; Wu, S.; Yamaguchi, N.; Wu, M.F.; Pfluger, J.; Gillmor, C.S.; Gallagher, K.L.; Wagner, D. Mutations in two non-canonical Arabidopsis SWI2/SNF2 chromatin remodeling ATPases cause embryogenesis and stem cell maintenance defects. *Plant. J.* **2012**, *72*, 1000–1014. [CrossRef] [PubMed]
6. Wagner, D.; Meyerowitz, E.M. SPLAYED, a novel SWI/SNF ATPase homolog, controls reproductive development in Arabidopsis. *Curr. Biol.* **2002**, *12*, 85–94. [CrossRef]
7. Brzeski, J.; Podstolski, W.; Olczak, K.; Jerzmanowski, A. Identification and analysis of the Arabidopsis thaliana BSH gene, a member of the SNF5 gene family. *Nucleic Acids Res.* **1999**, *27*, 2393–2399. [CrossRef]
8. Sarnowski, T.J.; Ríos, G.; Jásik, J.; Swiezewski, S.; Kaczanowski, S.; Li, Y.; Kwiatkowska, A.; Pawlikowska, K.; Koźbiał, M.; Koźbiał, P.; et al. SWI3 subunits of putative SWI/SNF chromatin-remodeling complexes play distinct roles during Arabidopsis development. *Plant. Cell* **2005**, *17*, 2454–2472. [CrossRef]
9. Bezhani, S.; Winter, C.; Hershman, S.; Wagner, J.D.; Kennedy, J.F.; Kwon, C.S.; Pfluger, J.; Su, Y.; Wagner, D. Unique, Shared, and Redundant Roles for the Arabidopsis SWI/SNF Chromatin Remodeling ATPases BRAHMA and SPLAYED. *Plant. Cell* **2007**, *19*, 403–416. [CrossRef]
10. Vercruyssen, L.; Verkest, A.; Gonzalez, N.; Heyndrickx, K.S.; Eeckhout, D.; Han, S.-K.; Jegu, T.; Archacki, R.; Van Leene, J.; Andriankaja, M.; et al. ANGUSTIFOLIA3 Binds to SWI/SNF Chromatin Remodeling Complexes to Regulate Transcription during Arabidopsis Leaf Development. *Plant. Cell* **2014**, *26*, 210–229. [CrossRef]
11. Sacharowski, S.P.; Gratkowska, D.M.; Sarnowska, E.A.; Kondrak, P.; Jancewicz, I.; Porri, A.; Bucior, E.; Rolicka, A.T.; Franzen, R.; Kowalczyk, J.; et al. SWP73 subunits of arabidopsis SWI/SNF chromatin remodeling complexes play distinct roles in leaf and flower development. *Plant. Cell* **2015**, *27*, 1889–1906. [CrossRef] [PubMed]
12. Sarnowska, E.A.; Rolicka, A.T.; Bucior, E.; Cwiek, P.; Tohge, T.; Fernie, A.R.; Jikumaru, Y.; Kamiya, Y.; Franzen, R.; Schmelzer, E.; et al. DELLA-Interacting SWI3C Core Subunit of Switch/Sucrose Nonfermenting Chromatin Remodeling Complex Modulates Gibberellin Responses and Hormonal Cross Talk in Arabidopsis. *Plant. Physiol.* **2013**, *163*, 305–317. [CrossRef] [PubMed]
13. Cairns, B.R.; Levinson, R.S.; Yamamoto, K.R.; Kornberg, R.D. Essential role of Swp73p in the function of yeast SWI/SNF complex. *Genes Dev.* **1996**, *10*, 2131–2144. [CrossRef] [PubMed]
14. Buszewicz, D.; Archacki, R.; Palusiński, A.; Kotliński, M.; Fogtman, A.; Iwanicka-Nowicka, R.; Sosnowska, K.; Kuciński, J.; Pupel, P.; Olędzki, J.; et al. HD2C histone deacetylase and a SWI/SNF chromatin remodelling complex interact and both are involved in mediating the heat stress response in Arabidopsis. *Plant. Cell Environ.* **2016**, *39*, 2108–2122. [CrossRef]
15. Chinnusamy, V.; Ohta, M.; Kanrar, S.; Lee, B.H.; Hong, X.; Agarwal, M.; Zhu, J.K. ICE1: A regulator of cold-induced transcriptome and freezing tolerance in arabidopsis. *Genes Dev.* **2003**, *17*, 1043–1054. [CrossRef]

16. Stockinger, E.J.; Gilmour, S.J.; Thomashow, M.F. Arabidopsis thaliana CBF1 encodes an AP2 domain-containing transcriptional activator that binds to the C-repeat/DRE, a cis-acting DNA regulatory element that stimulates transcription in response to low temperature and water deficit. *Proc. Natl. Acad. Sci. USA* **1997**, *94*, 1035–1040. [CrossRef]
17. Liu, Q.; Kasuga, M.; Sakuma, Y.; Abe, H.; Miura, S.; Yamaguchi-Shinozaki, K.; Shinozaki, K. Two transcription factors, DREB1 and DREB2, with an EREBP/AP2 DNA binding domain separate two cellular signal transduction pathways in drought- and low-temperature-responsive gene expression, respectively, in Arabidopsis. *Plant. Cell* **1998**, *10*, 1391–1406. [CrossRef]
18. Dong, C.-H.; Agarwal, M.; Zhang, Y.; Xie, Q.; Zhu, J.-K. The negative regulator of plant cold responses, HOS1, is a RING E3 ligase that mediates the ubiquitination and degradation of ICE1. *Proc. Natl. Acad. Sci. USA* **2006**, *103*, 8281–8286. [CrossRef]
19. Fowler, S.; Thomashow, M.F. Arabidopsis Transcriptome Profiling Indicates That Multiple Regulatory Pathways Are Activated during Cold Acclimation in Addition to the CBF Cold Response Pathway. *Plant. Cell* **2002**, *14*, 1675–1690. [CrossRef]
20. Agarwal, M.; Hao, Y.; Kapoor, A.; Dong, C.H.; Fujii, H.; Zheng, X.; Zhu, J.K. A R2R3 type MYB transcription factor is involved in the cold regulation of CBF genes and in acquired freezing tolerance. *J. Biol. Chem.* **2006**, *281*, 37636–37645. [CrossRef]
21. Fowler, S.G.; Cook, D.; Thomashow, M.F. Low temperature induction of Arabidopsis CBF1, 2, and 3 is gated by the circadian clock. *Plant. Physiol.* **2005**, *137*, 961–968. [CrossRef] [PubMed]
22. Chinnusamy, V.; Zhu, J.; Zhu, J.K. Cold stress regulation of gene expression in plants. *Trends Plant. Sci.* **2007**, *12*, 444–451. [CrossRef] [PubMed]
23. Earley, K.W.; Haag, J.R.; Pontes, O.; Opper, K.; Juehne, T.; Song, K.; Pikaard, C.S. Gateway-compatible vectors for plant functional genomics and proteomics. *Plant. J.* **2006**, *45*, 616–629. [CrossRef] [PubMed]
24. Boyes, D.C.; Zayed, A.M.; Ascenzi, R.; McCaskill, A.J.; Hoffman, N.E.; Davis, K.R.; Görlach, J. Growth Stage–Based Phenotypic Analysis of Arabidopsis. *Plant. Cell* **2001**, *13*, 1499–1510. [CrossRef]
25. Bailey, T.L.; Elkan, C. Fitting a mixture model by expectation maximization to discover motifs in biopolymers. *Proc. Int. Conf. Intell. Syst. Mol. Biol.* **1994**, *2*, 28–36.
26. Stracke, R.; Werber, M.; Weisshaar, B. The R2R3-MYB gene family in Arabidopsis thaliana. *Curr. Opin. Plant. Biol.* **2001**, *4*, 447–456. [CrossRef]
27. Riechmann, J.L.; Heard, J.; Martin, G.; Reuber, L.; Jiang, C.Z.; Keddie, J.; Adam, L.; Pineda, O.; Ratcliffe, O.J.; Samaha, R.R.; et al. Arabidopsis transcription factors: Genome-wide comparative analysis among eukaryotes. *Science* **2000**, *290*, 2105–2110. [CrossRef]
28. Hudson, M.E. Identification of Promoter Motifs Involved in the Network of Phytochrome A-Regulated Gene Expression by Combined Analysis of Genomic Sequence and Microarray Data. *Plant. Physiol.* **2003**, *133*, 1605–1616. [CrossRef]
29. Wu, M.-F.; Sang, Y.; Bezhani, S.; Yamaguchi, N.; Han, S.-K.; Li, Z.; Su, Y.; Slewinski, T.L.; Wagner, D. SWI2/SNF2 chromatin remodeling ATPases overcome polycomb repression and control floral organ identity with the LEAFY and SEPALLATA3 transcription factors. *Proc. Natl. Acad. Sci. USA* **2012**, *109*, 3576–3581. [CrossRef]
30. Dubos, C.; Stracke, R.; Grotewold, E.; Weisshaar, B.; Martin, C.; Lepiniec, L. MYB transcription factors in Arabidopsis. *Trends Plant. Sci.* **2010**, *15*, 573–581. [CrossRef]
31. Thomashow, M.F. PLANT COLD ACCLIMATION: Freezing Tolerance Genes and Regulatory Mechanisms. *Annu. Rev. Plant. Physiol. Plant. Mol. Biol.* **1999**, *50*, 571–599. [CrossRef] [PubMed]
32. Jia, Y.; Ding, Y.; Shi, Y.; Zhang, X.; Gong, Z.; Yang, S. The cbfs triple mutants reveal the essential functions of CBFs in cold acclimation and allow the definition of CBF regulons in Arabidopsis. *New Phytol.* **2016**, *212*, 345–353. [CrossRef] [PubMed]
33. Park, S.; Lee, C.M.; Doherty, C.J.; Gilmour, S.J.; Kim, Y.; Thomashow, M.F. Regulation of the Arabidopsis CBF regulon by a complex low-temperature regulatory network. *Plant. J.* **2015**, *82*, 193–207. [CrossRef] [PubMed]
34. Zhao, C.; Zhang, Z.; Xie, S.; Si, T.; Li, Y.; Zhu, J.-K. Mutational Evidence for the Critical Role of CBF Genes in Cold Acclimation in Arabidopsis. *Plant. Physiol.* **2016**, *171*, 2744–2759. [CrossRef] [PubMed]
35. Schlichting, C.D.; Wund, M.A. Phenotypic plasticity and epigenetic marking: An assessment of evidence for genetic accommodation. *Evolution (N. Y).* **2014**, *68*, 656–672. [CrossRef]

36. Chinnusamy, V.; Zhu, J.K.; Sunkar, R. Gene regulation during cold stress acclimation in plants. *Methods Mol. Biol.* **2010**, *639*, 39–55.
37. Siddiqua, M.; Nassuth, A. Vitis CBF1 and Vitis CBF4 differ in their effect on Arabidopsis abiotic stress tolerance, development and gene expression. *Plant. Cell Environ.* **2011**, *34*, 1345–1359. [CrossRef]
38. Zhang, X.; Fowler, S.G.; Cheng, H.; Lou, Y.; Rhee, S.Y.; Stockinger, E.J.; Thomashow, M.F. Freezing-sensitive tomato has a functional CBF cold response pathway, but a CBF regulon that differs from that of freezing-tolerant Arabidopsis. *Plant J.* **2004**, *39*, 905–919. [CrossRef]
39. Hannah, M.A. Natural Genetic Variation of Freezing Tolerance in Arabidopsis. *Plant Physiol.* **2006**, *142*, 98–112. [CrossRef]
40. Jaskiewicz, M.; Conrath, U.; Peterhälnsel, C. Chromatin modification acts as a memory for systemic acquired resistance in the plant stress response. *EMBO Rep.* **2011**, *12*, 50–55. [CrossRef]
41. Kumar, S.V.; Wigge, P.A. H2A.Z-Containing Nucleosomes Mediate the Thermosensory Response in Arabidopsis. *Cell* **2010**, *140*, 136–147. [CrossRef]
42. Park, J.; Lim, C.J.; Shen, M.; Park, H.J.; Cha, J.-Y.; Iniesto, E.; Rubio, V.; Mengiste, T.; Zhu, J.-K.; Bressan, R.A.; et al. Epigenetic switch from repressive to permissive chromatin in response to cold stress. *Proc. Natl. Acad. Sci. USA* **2018**, *115*, E5400–E5409. [CrossRef] [PubMed]
43. Gilmour, S.J.; Zarka, D.G.; Stockinger, E.J.; Salazar, M.P.; Houghton, J.M.; Thomashow, M.F. Low temperature regulation of the Arabidopsis CBF family of AP2 transcriptional activators as an early step in cold-induced COR gene expression. *Plant J.* **1998**, *16*, 433–442. [CrossRef] [PubMed]
44. Euskirchen, G.M.; Auerbach, R.K.; Davidov, E.; Gianoulis, T.A.; Zhong, G.; Rozowsky, J.; Bhardwaj, N.; Gerstein, M.B.; Snyder, M. Diverse roles and interactions of the SWI/SNF chromatin remodeling complex revealed using global approaches. *PLoS Genet.* **2011**, *7*. [CrossRef]
45. Archacki, R.; Yatusevich, R.; Buszewicz, D.; Krzyczmonik, K.; Patryn, J.; Iwanicka-Nowicka, R.; Biecek, P.; Wilczynski, B.; Koblowska, M.; Jerzmanowski, A.; et al. Arabidopsis SWI/SNF chromatin remodeling complex binds both promoters and terminators to regulate gene expression. *Nucleic Acids Res.* **2016**, *45*, 3116–3129. [CrossRef] [PubMed]
46. Jordán-Pla, A.; Yu, S.; Waldholm, J.; Källman, T.; Östlund Farrants, A.K.; Visa, N. SWI/SNF regulates half of its targets without the need for ATP-driven nucleosome remodeling by Brahma. *BMC Genomics* **2018**, *19*, 367. [CrossRef]
47. Lake, R.J.; Boetefuer, E.L.; Tsai, P.F.; Jeong, J.; Choi, I.; Won, K.J.; Fan, H.Y. The Sequence-Specific Transcription Factor c-Jun Targets Cockayne Syndrome Protein B to Regulate Transcription and Chromatin Structure. *PLoS Genet.* **2014**, *10*, e1004284. [CrossRef]
48. Zhang, D.; Li, Y.; Zhang, X.; Zha, P.; Lin, R. The SWI2/SNF2 Chromatin-Remodeling ATPase BRAHMA Regulates Chlorophyll Biosynthesis in Arabidopsis. *Mol. Plant.* **2017**, *10*, 155–167. [CrossRef]
49. Wei, D.; Liu, M.; Chen, H.; Zheng, Y.; Liu, Y.; Wang, X.; Yang, S.; Zhou, M.; Lin, J. INDUCER OF CBF EXPRESSION 1 is a male fertility regulator impacting anther dehydration in Arabidopsis. *PLOS Genet.* **2018**, *14*, 1–32. [CrossRef]
50. Alonso, J.M.; Stepanova, A.N.; Leisse, T.J.; Kim, C.J.; Chen, H.; Shinn, P.; Stevenson, D.K.; Zimmerman, J.; Barajas, P.; Cheuk, R.; et al. Genome-wide insertional mutagenesis of Arabidopsis thaliana. *Science (80-.)* **2003**, *301*, 653–657. [CrossRef]
51. Koncz, C.; Schell, J. The promoter of TL-DNA gene 5 controls the tissue-specific expression of chimaeric genes carried by a novel type of Agrobacterium binary vector. *Mol. Gen. Genet. MGG* **1986**, *204*, 383–396. [CrossRef]
52. Davis, A.M.; Hall, A.; Millar, A.J.; Darrah, C.; Davis, S.J. Protocol: Streamlined sub-protocols for floral-dip transformation and selection of transformants in Arabidopsis thaliana. *Plant. Methods* **2009**, *5*, 3. [CrossRef] [PubMed]
53. Schmittgen, T.D.; Livak, K.J. Analyzing real-time PCR data by the comparative CT method. *Nat. Protoc.* **2008**, *3*, 1101–1108. [CrossRef] [PubMed]
54. Saleh, A.; Alvarez-Venegas, R.; Avramova, Z. An efficient chromatin immunoprecipitation (ChIP) protocol for studying histone modifications in Arabidopsis plants. *Nat. Protoc.* **2008**, *3*, 1018–1025. [CrossRef] [PubMed]
55. Pastore, J.J.; Limpuangthip, A.; Yamaguchi, N.; Wu, M.F.; Sang, Y.; Han, S.K.; Malaspina, L.; Chavdaroff, N.; Yamaguchi, A.; Wagner, D. LATE MERISTEM IDENTITY2 acts together with LEAFY to activate APETALA1. *Development* **2011**, *138*, 3189–3198. [CrossRef] [PubMed]

56. Boyes, D.C. Growth Stage-Based Phenotypic Analysis of Arabidopsis: A Model for High Throughput Functional Genomics in Plants. *Plant. Cell* **2001**, *13*, 1499–1510. [CrossRef] [PubMed]
57. Zhu, Y.; Rowley, M.J.; Böhmdorfer, G.; Wierzbicki, A.T. A SWI/SNF Chromatin-Remodeling Complex Acts in Noncoding RNA-Mediated Transcriptional Silencing. *Mol. Cell* **2013**, *49*, 298–309. [CrossRef]
58. Guo, Y.; Xiong, L.; Ishitani, M.; Zhu, J.-K. An Arabidopsis mutation in translation elongation factor 2 causes superinduction of CBF/DREB1 transcription factor genes but blocks the induction of their downstream targets under low temperatures. *Proc. Natl. Acad. Sci. USA* **2002**, *99*, 7786–7791. [CrossRef]
59. Buske, F.A.; Bodén, M.; Bauer, D.C.; Bailey, T.L. Assigning roles to DNA regulatory motifs using comparative genomics. *Bioinformatics* **2010**, *26*, 860–866. [CrossRef]
60. Palaniswamy, S.K.; James, S.; Sun, H.; Lamb, R.S.; Davuluri, R.V.; Grotewold, E. AGRIS and AtRegNet. A Platform to Link cis-Regulatory Elements and Transcription Factors into Regulatory Networks. *PLANT Physiol.* **2006**, *140*, 818–829. [CrossRef]
61. Davuluri, R.V.; Sun, H.; Palaniswamy, S.K.; Matthews, N.; Molina, C.; Kurtz, M.; Grotewold, E. AGRIS: Arabidopsis Gene Regulatory Information Server, an information resource of Arabidopsis cis-regulatory elements and transcription factors. *BMC Bioinformatics* **2003**, *4*, 25. [CrossRef] [PubMed]
62. Yilmaz, A.; Mejia-Guerra, M.K.; Kurz, K.; Liang, X.; Welch, L.; Grotewold, E. AGRIS: The arabidopsis gene regulatory information server, an update. *Nucleic Acids Res.* **2011**, *39*, 1118–1122. [CrossRef] [PubMed]

International Journal of
Molecular Sciences

MDPI

Article

The Position and Complex Genomic Architecture of Plant T-DNA Insertions Revealed by 4SEE

Ronen Krispil [1,†], Miriam Tannenbaum [1,†], Avital Sarusi-Portuguez [1], Olga Loza [1], Olga Raskina [2] and Ofir Hakim [1,*]

[1] The Mina and Everard Goodman Faculty of Life Sciences, Bar-Ilan University, Ramat-Gan 5290002, Israel; ronen.krispil@biu.ac.il (R.K.); miriam.tannenbaum@biu.ac.il (M.T.); avital1005@gmail.com (A.S.-P.); olgaloza28@gmail.com (O.L.)

[2] Institute of Evolution, University of Haifa, Haifa 3498838, Israel; olga@evo.haifa.ac.il

* Correspondence: Ofir.Hakim@biu.ac.il; Tel.: +972-3-738-4295; Fax: 972-3-738-4296

† These authors contribute equally to this work.

Received: 8 February 2020; Accepted: 26 March 2020; Published: 30 March 2020

Abstract: The integration of T-DNA in plant genomes is widely used for basic research and agriculture. The high heterogeneity in the number of integration events per genome, their configuration, and their impact on genome integrity highlight the critical need to detect the genomic locations of T-DNA insertions and their associated chromosomal rearrangements, and the great challenge in doing so. Here, we present 4SEE, a circular chromosome conformation capture (4C)-based method for robust, rapid, and cost-efficient detection of the entire scope of T-DNA locations. Moreover, by measuring the chromosomal architecture of the plant genome flanking the T-DNA insertions, 4SEE outlines their associated complex chromosomal aberrations. Applying 4SEE to a collection of confirmed T-DNA lines revealed previously unmapped T-DNA insertions and chromosomal rearrangements such as inversions and translocations. Uncovering such events in a feasible, robust, and cost-effective manner by 4SEE in any plant of interest has implications for accurate annotation and phenotypic characterization of T-DNA insertion mutants and transgene expression in basic science applications as well as for plant biotechnology.

Keywords: circular chromosome conformation capture; genome architecture; T-DNA; transgenic; chromosomal rearrangements; synthetic biology

1. Introduction

The development of efficient methods for introducing foreign DNA into plant genomes by *Agrobacterium tumefaciens* mediated transformation prompted its widespread application in biotechnology and basic science [1]. Ongoing efforts to improve the transformation technology continuously expand its use to multiple crop species and genotypes including corn, soybeans, cotton, canola, potatoes, rice, sugarcane, wheat, and tomatoes. However, the random nature of genomic integration, which is a major drawback for agricultural biotechnology, has been utilized to generate powerful resources for genetic studies by large-scale T-DNA-based mutagenesis in the model plant *Arabidopsis thaliana* [2–4]. The use of Agrobacterium mediated transformation is expected to increase with the developing capability of targeting T-DNA to specific genomic locations by contemporary genome editing technologies such as CRISPR/Cas9 or the use of Agrobacterium to deliver genome editing reagents to the plant cells [1,5].

Despite its critical significance, mapping the precise T-DNA insertion point remains a challenge due to the variable number of genomic insertion events that are frequently associated with a plethora of chromosomal rearrangements such as translocations, inversions, insertions, and deletions [6–9]. The widespread use of T-DNA-based mutagenesis and genomic engineering

prompted the development of methods to map its integration sites and their associated chromosomal abnormalities. Advanced mapping technologies, from Southern blotting, cytology, and genetic mapping [10] to genomic and molecular approaches, have increased the resolution and throughput of detection capability.

PCR-based methods to detect T-DNA insertion sites, such as inverse PCR [11], thermal asymmetric interlaced (TAIL)-PCR [12], restriction PCR [13], and the biotinylated primer approach [14], use the sequence of the left and right borders of the integrated T-DNA to uncover its fusion point with the plant genome. However, given that T-DNA insertion often compromises the integrity of both plant and T-DNA sequences [9] and that the insertions include the binary vector backbone [15], the integration site may not be detected by these methods [16,17]. For example, high-resolution analysis detected small (more than 1 bp) insertions or deletions in 80% of the T-DNA borders in *Arabidopsis thaliana* [9] and small deletions of the T-DNA border were reported in ~30% of transgenic sorghum and barley plants, suggesting that the frequency of these events is high in multiple plant species [18,19]. T-DNA insertions are also associated with more complex rearrangements, such as translocations or inversions [20]. Given that T-DNA tends to integrate into several genomic loci and that in many cases only one end of the T-DNA insert is mapped, these events are more challenging to annotate. Unbiased whole-genome sequencing methods can detect both ends of the T-DNA insert in most cases despite possible sequence variations at the integration sites [21]. However, given that the size of one T-DNA insert is in the range of a few kb and that commonly the insertion consists of several T-DNA copies, uncovering chromosomal translocations by capturing the sequence continuity of the entire T-DNA insert by sequencing very long reads [15] is challenging and costly for large-scale applications.

Chromosome conformation capture (3C)-based methods detect spatial proximity between genomic loci by measuring the relative frequency of their proximity-ligated DNA. The polymer properties of the genome dictate high contact frequency between linearly adjacent sequences. Circular 3C (4C), which profiles genomic loci in spatial proximity to a point of interest (viewpoint) [22], was applied in this study to map T-DNA insertions based on the enrichment of genomic sequences in their linear proximity. The resulting 4SEE method detects the genomic position of T-DNA inserts by capturing the local enrichment of spatial chromosomal associations in their genomic proximity without prior knowledge of their genomic locations. Moreover, deviations in this pattern were used to identify chromosomal rearrangements associated with T-DNA insertions. We analyzed several *Arabidopsis thaliana* transgenic lines and validated the location of their T-DNA insertions. Additionally, we uncovered previously unmapped T-DNA insertions and complex chromosomal rearrangements in these plants, highlighting the need for a robust and cost-efficient high-throughput method for mapping and characterizing the structure of T-DNA insertions. 4SEE is independent of the number of T-DNA copies and the genome size and thus can be readily applied to any plant with a sequenced genome.

2. Results

2.1. 4C Signal as a Pointer for Genomic Location

Chromosome conformation capture (3C) methods [23] measure long-range chromosomal associations by enzymatic cleavage and ligation of chemically fixed nuclei. Since the resolution of 4C relies also on the frequency of sites in the genome that are recognized by the restriction enzyme (RE), chromatin was cleaved with Csp6I, a RE with a 4-bp recognition sequence (first RE in Figure 1A). In circular 3C (4C), the proximity–ligation DNA (3C) products are further processed to form DNA circles by a second digestion (DpnII; second RE in Figure 1A). This allows the selective amplification of ligation junctions with a point of interest (viewpoint) by inverse PCR (Figure 1A). The inverse PCR primers are positioned adjacent to the ligation junction so that short (>60 bp) reads include the viewpoint and the associating region. This allows for multiplexing of tens of experiments on a single sequencing lane. Following the mapping of sequences of the associating region to the reference genome, their local enrichment reflects long-range chromosomal association with the viewpoint.

Due to the polymer nature of the chromatin fiber, the chromosomal association frequency is the highest in proximity to the viewpoint and exponentially declines as the distance increases on the linear chromosome template [24]. This feature, which is common to data derived from 3C techniques, can be applied for analysis of the linear DNA scaffold [25–28].

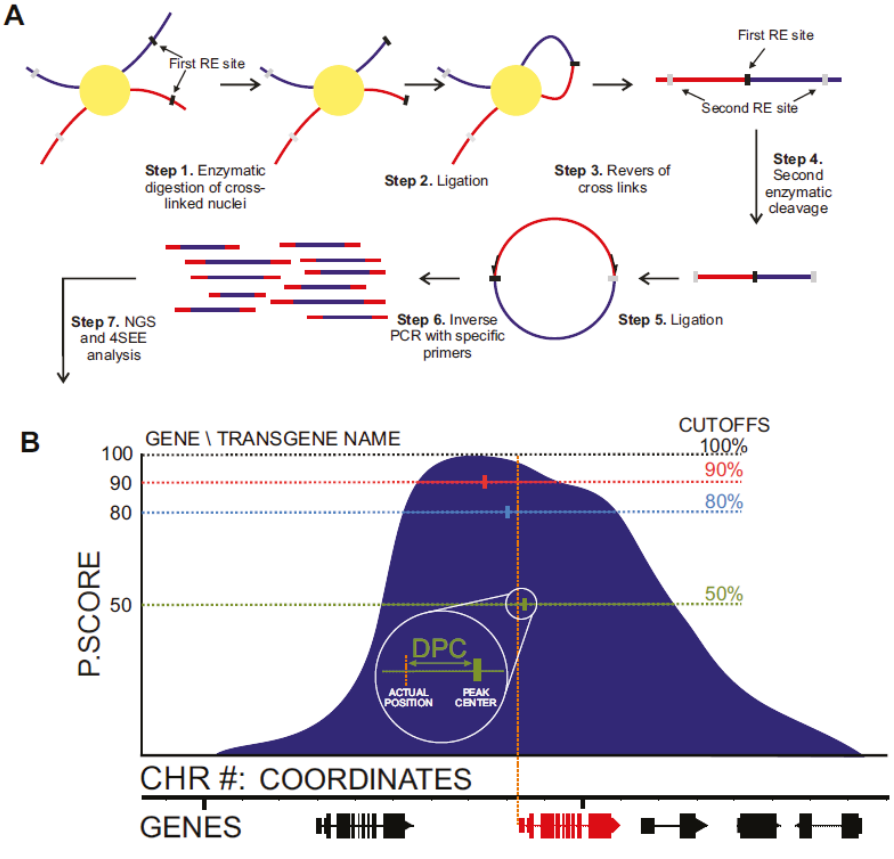

Figure 1. Principles of 4SEE procedure. (**A**) In circular chromosome conformation capture (4C), enzymatic cleavage and ligation of crosslinked chromatin give rise to chimeric DNA molecules between spatially proximal loci. Following reversal of the crosslinks, the DNA is cleaved with a second restriction enzyme (RE) followed by a second ligation, giving rise to circular DNA. The loci (blue) associated with the viewpoint (red) are amplified by inverse PCR and sequenced. (**B**) In 4SEE analysis, enrichment of proximity ligation products is reflected in a peak at the viewpoint position (marked by vertical red line). In this study, the distance between the viewpoint position and the center of the peak base at various cutoffs relative to the maximal p-score value (100%) of a given peak, called distance from peak center (DPC), was calculated.

To establish both experimental and bioinformatics approaches for mapping genomic loci, we generated 4C libraries using endogenous genes as viewpoints: *ACTIN DEPOLYMERIZING FACTOR 8* (*ADF8*; At4G00680), *SBT4.12* (At5G59090), *PIF4* (At2G43010), and *MBP1* (At1G52040). Following alignment of the sequenced proximity–ligation DNA to the *Arabidopsis thaliana* TAIR10 genome, enrichment analysis was performed by assigning to the genomic RE recognition sequences a p-score reflecting the relative enrichment of signal in the surrounding 50 kb (see Methods).

As expected, the highest density of RE sites with reads was at the viewpoint proximal region, allowing a simple annotation of the viewpoint position (Figure 2A, Supplemental Figure S1).

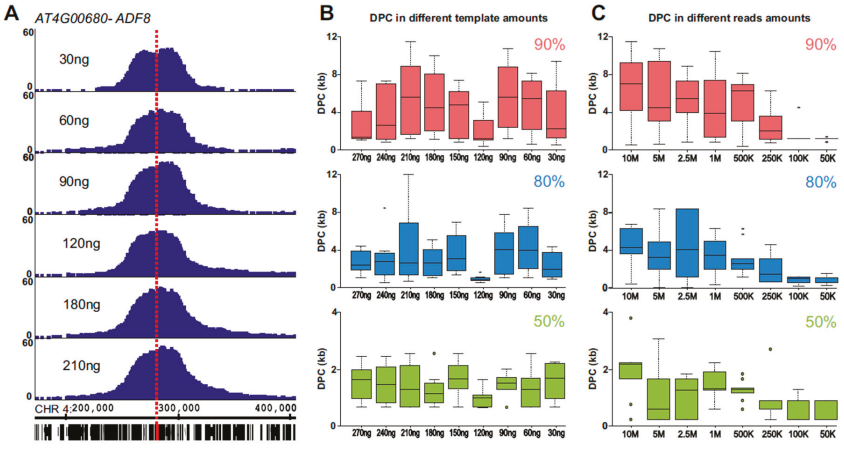

Figure 2. 4SEE points to genomic locations of viewpoints in a wide range of input DNA and sequencing depths. (**A**) 4C peaks of *ACTIN DEPOLYMERIZING FACTOR 8* (*ADF8*) viewpoint in different amounts of 4C template. Genomic coordinates (bp) and genes are at the bottom (TAIR10). *ADF8* gene viewpoint is marked with dashed red vertical line. The *y*-axis indicates p-score. (**B**) Distance from peak center (DPC) for different amounts of input DNA. Boxplots include sequencing depths for each template amount. (**C**) DPC calculated for gradients of sequencing depths in three cutoffs. Boxplots include template amounts for particular sequencing depths.

Aiming to apply 4SEE to annotate the genomic location of a viewpoint based on the position of its 4C peak, we assessed how the position of the peak center of the *ADF8* promoter is aligned with its genomic position in a wide range of 4C DNA template amounts and sequencing depths. The ligation junctions were amplified by PCR from 4C templates ranging from 30 ng to 270 ng. To vary the sequencing depth, reads containing the viewpoint sequence were subsampled from each experiment. The resulting 4C profiles demarcate a robust peak at the *ADF8* genomic position in various input amounts (Figure 2A). To assess the capability of 4C to retrieve the genomic location of the viewpoint in high resolution, we calculated the genomic coordinates of the peak base at 90%, 80%, or 50% of the maximal p-score signal. Then, for each cutoff, the distance between the center of the peak base and the genomic position of the viewpoint was calculated. A smaller distance from peak center (DPC) value indicates a smaller deviation from the viewpoint position (Figure 1B). The peak center was overall closer to the viewpoint (smaller DPC) when calculated from the base at half of the peak's height (50% cutoff) relative to the 90% or 80% cutoff, independent of the template amounts we tested. In the 50% cutoff, the DPC maintained a robust range from ~200 bp to 4,000 bp (Figure 2B, Supplemental Tables S1 and S2). As noted for the various template amounts, the center of the peak was closer to the viewpoint when calculated from the 50% cutoff relative to the 80% or 90% cutoff for the entire range of sequencing depths we tested (Figure 2C, Supplemental Table S2). In addition, the range of DPC values was much narrower in the 50% cutoff (166.5 bp to 2407 bp, median 915.5 bp) relative to the 90% or 80% cutoff (385–11,511 bp, median 3949.5 bp, and 32.5–12,114 bp, median 2,011 bp, respectively) for all sequencing depths and template amounts. Notably, the DPC calculated for *ADF8* in the 50% cutoff was lower than 2 kb for a wide range of tested template amounts and sequencing depths and lower than 1 kb in sequencing depths of 250 k reads or less in 60 out of 70 experiments (Figure 2, Supplemental Table S2).

Overall, these results suggest that 4SEE is a robust tool for annotating the genomic position of a point of interest at high resolution and cost-efficiently using a wide range of starting templates.

2.2. Using 4SEE as a Pointer for T-DNA Insertion Sites

Having demonstrated the use of 4SEE to determine the genomic location of a locus of choice in hundreds of base pair resolutions, we sought to test its capability to map the genomic locations of T-DNA insertions in transgenic *Arabidopsis* plants. We focused on plants with single T-DNA insertions that were mapped in a base pair resolution by PCR [2]. 4C libraries were prepared from SALK_011436, SALK_009469, SALK_041474, SALK_064627, SALK_005512, and SALK_063720 homozygote plants. To capture insertions in which the left or right border of the T-DNA may have been trimmed, the 4C viewpoint we used was located in the middle of the T-DNA, ~4 kb from each border. Consequently, a large proportion of the proximity–ligation 4C signal was expected to be derived from the sequence of T-DNA insert flanking the viewpoint, thus would not provide useful positional information. Therefore, we examined whether the amount of template used to map the endogenous genes had sufficient complexity to capture the genomic fragments flanking the T-DNA insertion. To this end, we analyzed a 4C template ranging from 30 ng to 210 ng at a sequencing depth lower than 500,000 reads (Supplemental Table S3). These amounts of DNA were sufficient to capture ligation junctions at the genome flanking the T-DNA insert. The DPC calculated for these experiments did not show a clear trend related to the amount of input DNA (Figure 3, Supplemental Table S3). A median DPC of 1132 bp calculated for the different plant lines and conditions all together reflects the accuracy of 4SEE in determining the integration position. The mean DPC for these experiments was ~ 3 kb, SD = 3.8 kb, reflecting the effect of outliers. These outliers do not seem to be related to a particular condition, such as the amount of input DNA, and may be inevitable given the genomic distribution of recognition sequences of the endonuclease used in 4C.

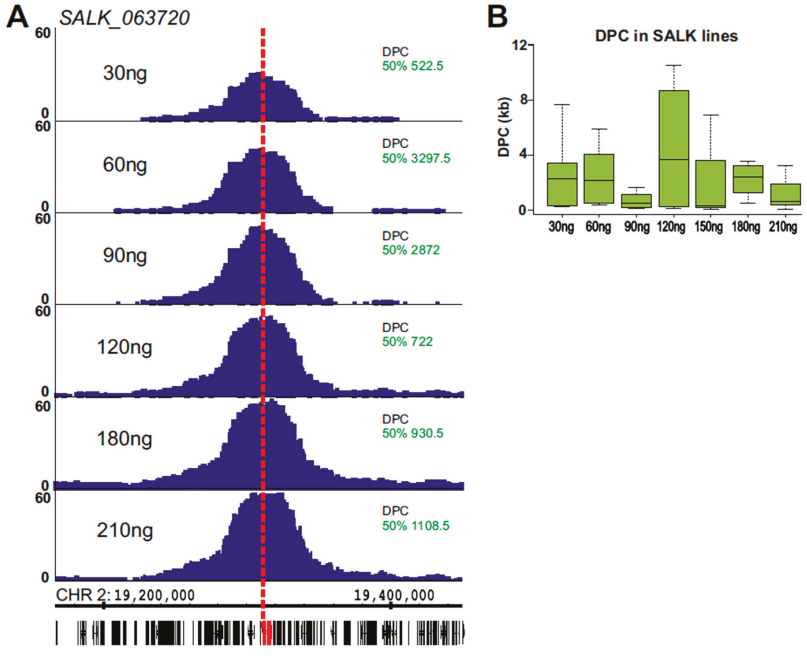

Figure 3. Annotation of T-DNA locations in transgenic plants by 4SEE. (**A**) 4C peaks from a gradient of 4C template amounts used for inverse PCR. Genomic coordinates and gene positions are at the bottom (TAIR10). T-DNA insertion site is marked in red, and viewpoint in vertical dashed line. DPC for the 50% cutoff is indicated. The *y*-axis indicates p-score. (**B**) DPC distribution for a gradient of template amounts in SALK lines 063720, 064627, 005512 (50% cutoff).

While all the T-DNA insertions were uncovered by 4SEE at the expected positions, a robust 4C peak was detected in SALK_064627 on chromosome 1 in addition to the annotated insertion on chromosome 3, likely representing an independent T-DNA integration event that escaped previous analysis (Figure 4D,E). Overall, 4SEE demonstrates the capability to annotate the positions of all six known T-DNA insertions in these lines in kb resolution (Figures 3A and 4A–D,F).

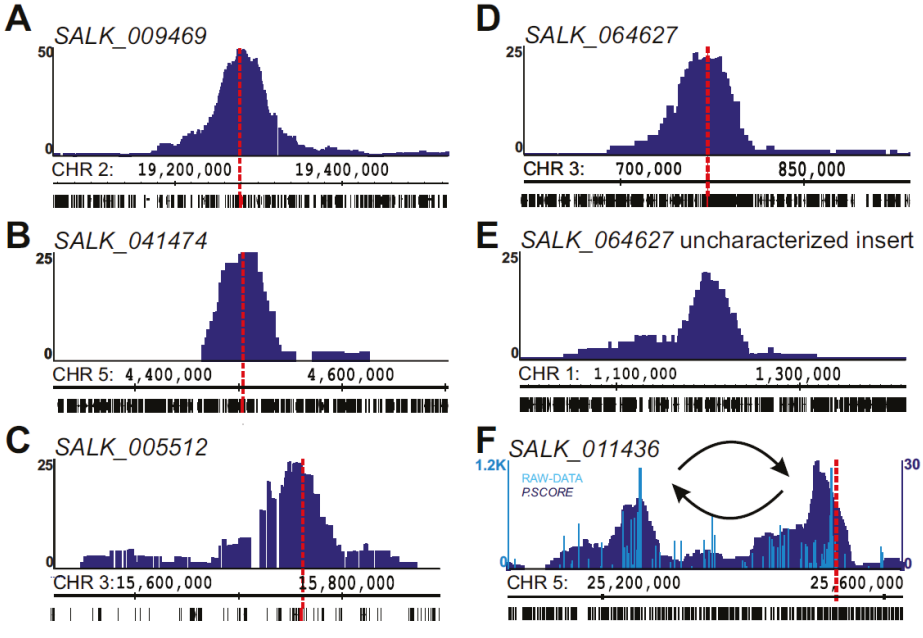

Figure 4. Annotating T-DNA insertions. (**A**–**D**) 4C profiles at T-DNA insertion sites (marked with vertical dashed line) in SALK lines. (**E**) Novel T-DNA insertion in SALK_064627 depicted by 4SEE. (**F**) Two 4C peaks indicate chromosomal inversion in SALK_011436. Raw data are presented in light blue bars. The *y*-axis indicates p-score. Chromosomal coordinates of *Arabidopsis thaliana* TAIR10 genome build are indicated.

2.3. Chromosomal Rearrangements Uncovered by 4SEE

Interestingly, an additional peak in SALK_011436 was positioned ~400 kb from the known insertion site (Figure 4F). Notably, the two peaks show an asymmetric profile as the signal drops sharply at one side of the peak. This drop in the smoothed profile is clearly visualized as a sharp transition from dense to sparse 4C reads in the raw data, indicating discontinuity in the DNA that is presented on the genome browser. Such profiles indicate chromosomal rearrangements [15,29]. Given that these are the only viewpoint peaks across the SALK_011436 genome, strongly suggests that the insertion of T-DNA was associated with chromosomal inversion at this locus.

2.4. INTACT ADF8p:NTF/ACT2p:BirA Transgene Position and Chromatin Composition

Unlike T-DNA insertions used for genetic perturbation of endogenous genes, less attention is paid to mapping their exact positions when they are used for transgene expression. Therefore, as a test case, we aimed to annotate by 4SEE the T-DNA insertions in a widely used transgene bearing the INTACT system for affinity purification of nuclei (see [30–35]). This plant was generated by introducing a T-DNA expressing the nuclear targeting fusion (NTF) synthetic protein under the control of the *ACTIN DEPOLYMERIZING FACTOR 8* (*ADF8*) promoter (ADF8p:NTF) into a transgenic line expressing

the *E. coli* biotin ligase BirA from the constitutive ACTIN2 (ACT2) promoter (ACT2p:BirA). By carrying the two types of T-DNA, NTF is biotinylated in *ADF8*-active cell types in the ADF8p:NTF/ACT2p:BirA line (CS68932).

The integration of the ADF8p:NTF construct was uncovered by using the endogenous ADF8 promoter fragment as a viewpoint. In addition to the expected prominent peak at the ADF8 genomic position (Figure 2), four distinct 4SEE signals, representing T-DNA insertions, were found across the ADF8p:NTF/ACT2p:BirA genome (Figure 5). To validate these insertion sites, we took advantage of available deeply sequenced datasets of paired-end reads from ATAC-seq (GSE101482, 69,166,811 pairs) and DHS-seq (GSE53324, 21,138,263 pairs). We searched for reads in which one end was mapped to the T-DNA sequence and the other to the *Arabidopsis* genome as an indication of the insertion position. Strikingly, this approach revealed mate mapping to all four loci shown in Figure 5 (Supplemental Figure S2). An additional T-DNA insertion site (Chr4:18,149,544) was also uncovered in the Gl2p:NTF/ACT2p:BirA line that was generated from the same parental line carrying the ACT2p:BirA insert [32], suggesting that it demarcates the ACT2p:BirA insertion. The four ADF8 insertion loci were also retrieved, but only from the ATAC-seq dataset (GSE101482), by TDNAScan software, which maps paired-end reads to the T-DNA sequence and the genome (Supplemental Figure S2) [36].

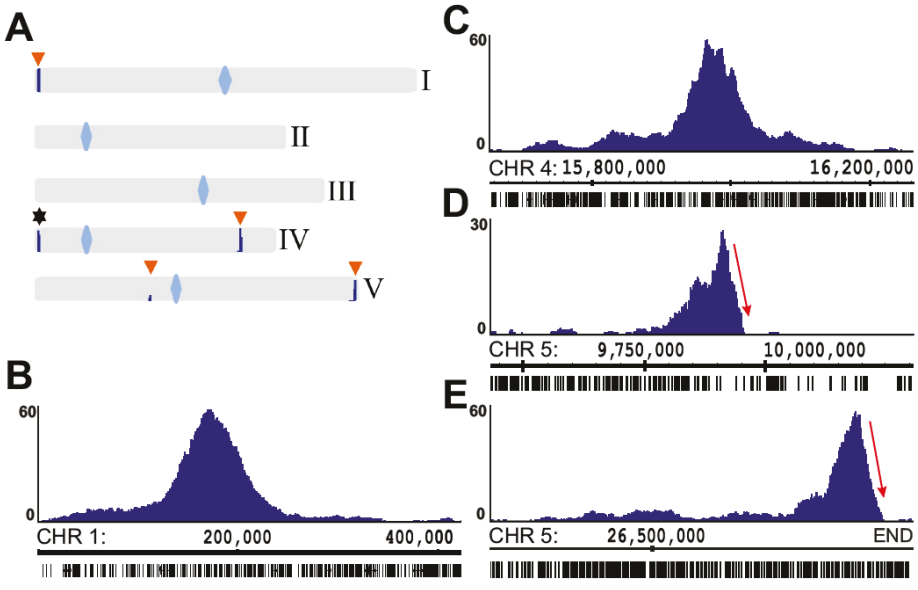

Figure 5. Map of endogenous and transgenic ADF8 loci. (**A**) Genome-wide map of 4SEE analysis indicating endogenous *ADF8* position (star) and four additional T-DNA insertion loci (orange arrowheads). Centromeres are marked as blue rhombuses. (**B–E**) Close-ups of T-DNA integration loci reveal asymmetric drop in signal intensity on chromosome 5 (D and E). The *y*-axis indicates p-score. Chromosomal coordinates of *Arabidopsis thaliana* TAIR10 genome build are indicated.

Interestingly, in two of these loci, the 4C signal drops sharply at one side of the 4C peak (Figure 5D–E), suggesting an abnormality in the chromosome integrity in those loci potentially due to chromosomal rearrangements. Nevertheless, symmetric 4SEE peaks could reflect chromosomal abnormalities if the two ends of the rearranged loci contain the T-DNA sequence. To further understand the chromosomal structure of these loci by 4C, we analyzed genomic loci distant from the integration sites. *C2H2C* (At5G27880, Chr5: 9,885,872) is located ~53 kb from the expected chromosomal break point, as predicted by the *ADF8* 4SEE (labeled by dashed red line, Figure 6A, dark blue track). The 4C signal

of *C2H2C* on chromosome 5 drops sharply at the rearrangement point in the transgenic plants, while it continues homogeneously along the chromosome in the wild-type (WT) plants (Figure 6A, light blue tracks). In addition, a high *cis*-like signal emerges in the transgenic plants on chromosome 1 at the point of a T-DNA insertion (Figure 6A, light blue tracks). The *COX11* (At1G02410, Chr1: 480,859) location is more distant relative to *C2H2C* from the T-DNA insertion (~300 kb), thus the chromosomal breakpoint is expected to deviate from the main 4C peak. Nevertheless, based on the principle that sequences located on the same chromosome in *cis* interact more frequently than sequences in *trans*, in agreement with *C2H2C* analysis, the *COX11* 4C signal drops sharply at the translocation point on chromosome 1 and continues on chromosome 5 only in the transgenic line (Figure 6A, purple tracks). Reconstruction of the fusion between chromosomes 1 and 5 at the breakpoints that were retrieved from this analysis shows a continuous and complementary 4C signal, further supporting the annotation of chromosomal translocation at this point (Figure 6B). Further support for this chromosomal rearrangement is provided by DNA fluorescence in situ hybridization (FISH) using 10-O-11 (red) and F1H21 (green) probes, positioned approximately 300 kb and 200 kb from the breakpoint on chromosomes 1 and 5, respectively. While the relative positions of the two loci are random overall in nuclei from WT plants, they constantly cluster together in nuclei from ADF8p:NTF/ACT2p:BirA plants (100 nuclei were analyzed for each plant type), indicating that they are physically linked (Figure 6C, Supplemental Figure S3).

To complete the analysis of the chromosomal structure of the ADF8p:NTF/ACT2p:BirA line, we analyzed six additional viewpoints flanking the remaining three putative break sites. This revealed a complex exchange of three sub-telomeric regions between chromosomes 1 and 5 (Figure 6D, Supplemental Figure S4). Notably, according to the 4C analysis, the fusions 5.2:5.4 and 5.1:5.3 did not contain T-DNA. In the absence of T-DNA sequence, the chromosomal fusion is expected to be retrieved from the dataset of paired sequences from this plant (GSE101482, GSE53324). Indeed, six nonredundant paired-end reads from ADF8p:NTF/ACT2p:BirA ATAC-seq were aligned to each chimeric DNA template that was merged at the postulated fusion points based on the 4C signal, indicating the continuity of DNA in these regions. No reads were aligned to these loci from Gl2p:NTF/ACT2p:BirA ATAC-seq data from the same lab and in similar sequencing depth, serving as a negative control (Supplemental Figure S5). Overall, the ADF8p:NTF/ACT2p:BirA plant carries four inter- and intra-chromosomal rearrangements between chromosomes 1 and 5 but only two of the rearranged loci contain T-DNA.

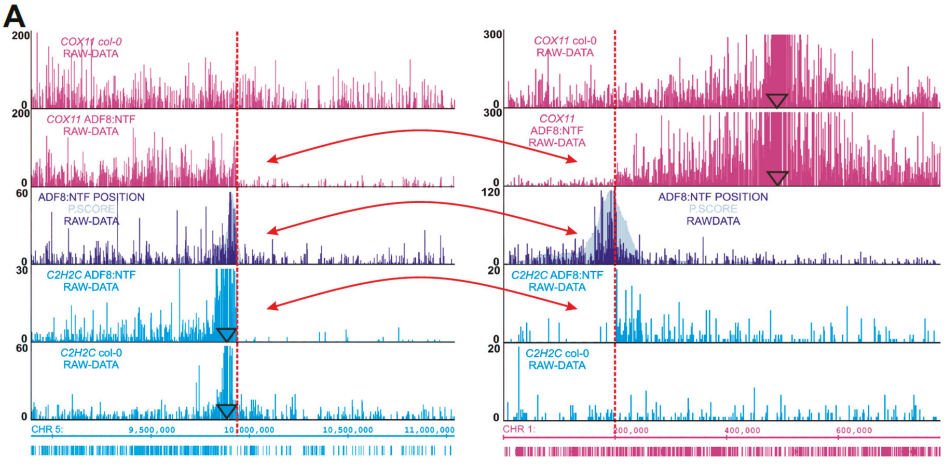

Figure 6. *Cont.*

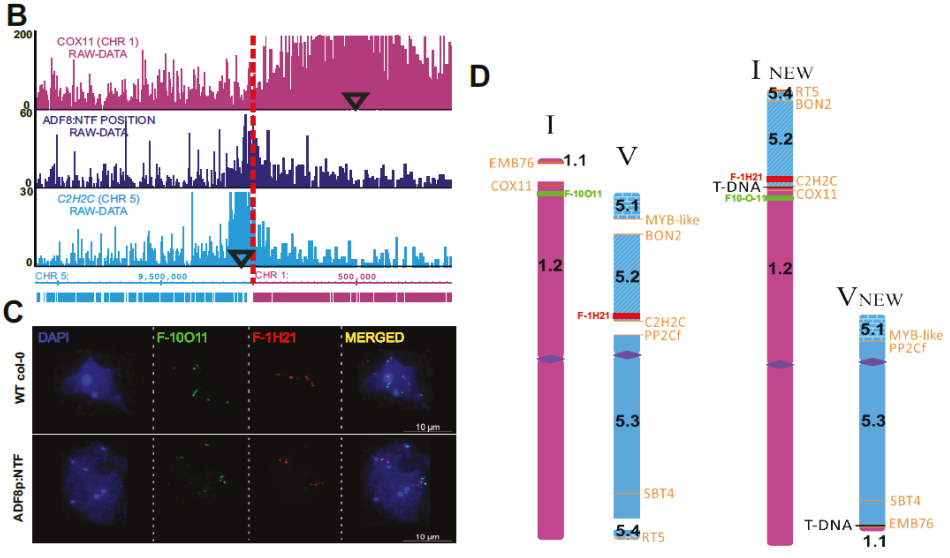

Figure 6. Chromosomal translocations map in INTACT ADF8p:NTF/ACT2p:BirA line revealed by 4SEE. (**A**) Translocation between left arms of chromosome 5 (fragment 5.2, left) and chromosome 1 (fragment 1.2, right). 4C signal of *COX11* on chromosome 1 continues monotonically in wild-type (WT) plants (top track), but drops sharply in transgenic plants (second track, transition from 1.2 to 1.1). This high "*cis*-like" signal appears on chromosome 5 (fragment 5.2) only in the ADF8p:NTF/ACT2p:BirA line. Transitions in 4C signal intensity occur at the T-DNA insertion position, demarcated by ADF8p:NTF/ACT2p:BirA 4C (third, dark blue track.). Similar transitions in signal intensity in transgenic plants occur for the *C2H2* viewpoint located on chromosome 5 (fourth, light blue track, fragment 5.2). The red arrows mark fusion points between the two chromosomes. (**B**) Continuous 4C profile of the three viewpoints on the reconstructed hybrid chromosome (fragments 5.2 and 1.2). (**C**) DNA fluorescence in situ hybridization (FISH) of somatic nuclei from *Arabidopsis thaliana* WT (left) and ADF8p:NTF/ACT2p:BirA transgenic plants (right). F1H21 probe on chromosome 5 labeled in green, 10-O-11 probe on chromosome 1 labeled in red, DNA counterstaining with DAPI in blue. Chromosomes at anaphase and prometaphase stages are shown for WT and ADF8p:NTF/ACT2p:BirA plants, respectively (FISH foci are indicated with arrows). Enlarged translocated chromosome is shown in the small box (**D**) Schematic diagram (in scale) summarizing chromosomal rearrangements in INTACT ADF8p:NTF/ACT2p:BirA line. Genes used as viewpoints to characterize chromosomal breakpoints and fusions are indicated alongside the chromosomes (their 4C profiles are shown in Supplemental Figure S4). T-DNA inserts are noted in black. Locations of probes for DNA FISH are indicated in green and red.

3. Discussion

In this study, we present 4SEE, which combines the application of 4C-seq in plants with a computational approach and guidelines to detect the genomic positions of T-DNA insertions together with their associated chromosomal rearrangements at high genomic resolution.

Based on the polymer properties of the chromatin, in the close *cis* range, the spatial association frequency between chromosomal loci decays as a function of their linear genomic distance. This is reflected as a peak of high density of proximity ligation junctions at the viewpoint in the 4C-seq measurements. This peak at the viewpoint position is consistently higher than peaks from possible intra- and inter-chromosomal associations.

To increase the genomic resolution, 4C-seq was performed using 4 bp endonuclease. However, the center of the 4C peak did not align perfectly with the viewpoint due to biases

introduced by the amplification of the ligation junctions by PCR and the non-uniform distribution of the recognition sequence of the endonuclease used for 4C. To minimize these biases, we calculated the local enrichment of restriction-enzyme loci having ligation junction sequences in a 50 kb sliding window. Depicting the local enrichment of positive ligation junctions rather than the number of reads was intended to reduce biases arising from PCR amplification and sequencing. The window size was aimed at averaging local asymmetry in the distribution of positive ligation junctions in proximity to the viewpoint. This local asymmetry of the 4C peak relative to the viewpoint is more pronounced at the top of the peak. Thus, the center of the peak base at 50% of the peak height was closer to the position of the viewpoint relative to the upper and narrower bases.

In many cases, the T-DNA integration process affects both the plant and T-DNA sequences [9]. Often, the T-DNA border is truncated or includes repeats, insertions, or deletions [36]. These events may hamper detection of the T-DNA insert by using primers complementary to these sequences [16,17]. The capability to capture multiple proximity ligation junctions far from the viewpoint and use them for accurate positional mapping allows 4SEE to map T-DNAs in which the sequences at the left or right border are absent as well as inserts with multiple T-DNA copies. Thus, 4SEE uncovered additional T-DNA insertions in previously characterized SALK lines (Figure 4D,E).

Remarkably, the accuracy of positional mapping by 4SEE was not hampered using amounts as low as 30 ng of 4C template. Ideally, the viewpoint fragment provides one ligation junction per genome, including the T-DNA insert. Here, 30 ng of 4C template, reflecting approximately 100,000 *Arabidopsis* genomes, provided sufficient complexity to capture the genomic loci flanking the T-DNA insert. Nevertheless, increasing the library complexity by increasing the amount of DNA template strengthen the 4C signal at the T-DNA insertion locus (Supplemental Figure S6). In addition to the amount of genomic DNA, the genomic coverage also depends on the efficiency of the molecular steps along the 4C procedure, such as enzymatic cleavage and ligation. To account for less optimal 4C experiments, the amount of DNA template should not be reduced if possible. Reducing the number of ligation junctions by sub-sampling the number of reads that contain the viewpoint sequence to 50,000 per experiment was sufficient to map the T-DNA insertion. Taking into account that only half of the single-end reads contain the proximity ligation junction, a range of 100,000 reads per plant should suffice for annotating the T-DNA position.

4SEE resolution can reach a few hundred bp and diverge to a few kb in different measurements for the same T-DNA locus. Therefore, to annotate the T-DNA insertion site in a bp resolution, it is possible to sequence the fusion point after amplification with PCR primers for genomic loci around the 4SEE peak center. 4SEE positions for different amounts of input DNA were distributed up- and downstream to the T-DNA position. While overall approximately half of the peak centers fell less than 1 kb from the T-DNA, two measurements were more than 10 kb away (Supplemental Table S3 and Supplemental Figure S7). Thus, if data from multiple experiments are available, averaging their genomic positions while discarding outliers or calculating their median will likely increase the resolution of the T-DNA annotation to a few kb.

Along with annotating T-DNA insertions, 4SEE uncovered chromosomal inversion in SALK_011436 and chromosomal translocations associated with T-DNA insertions in the ADF8p:NTF/ACT2p:BirA line. This line is widely used to isolate specific cell-types [30–35]. Structural analysis genomic loci flanking these insertions by 4C-seq validated these rearrangements and unraveled their complexity. Interestingly, only two of the four chromosomal fusions, involved with chromosomes 1 and 5, harbor T-DNA. Such heterogeneous T-DNA integration had been found recently in *Arabidopsis* and birch by high-throughput sequencing approaches [20,37] and may be more pronounced than previously noted.

Chromatin interactions have been used for genome assembly [25–28], and 4C was used to detect chromosomal translocations [29]. 4SEE does not require any species-specific reagent and can be applied to map T-DNA or transposon insertions [38,39] in any plant of interest by adjusting the amount of input DNA to the genome size of the analyzed plant. Annotating chromosomal rearrangements using

viewpoints that are more distant from the fusion point by imbalanced distribution of ligation junctions may require deeper sequencing and higher complexity of the 4C template.

In conclusion, we present how, in a single experiment, 4SEE is capable of detecting not only integration sites, but also structural rearrangements, such as inversions and translocations, from a small amount of NGS reads.

4. Materials and Methods

4.1. Plant Materials and Growth Conditions

Arabidopsis thaliana Columbia ecotype (Col-0), SALK_011436; SALK_009469; SALK_041474; SALK_064627; and SALK_005512 from the SALK stock; and CS68932 from the Arabidopsis Biological Resource Center (ABRC) were used in this study. All plants were grown in a growth room under cool white LED light at ~100 LUX for 16 h/day at 22 °C. Surface-sterilized seeds were sown on agar-coated floats on 1/8 Murashige and Skoog (MS) media; and 14-day-old seedlings were harvested into liquid nitrogen

4.2. Circular Chromosome Conformation Capture (4C)

4.2.1. Nucleus Isolation and Fixation

Frozen tissue was ground in liquid nitrogen using mortar and pestle, and transferred into nuclear isolation buffer 1 (10 mM HEPES, pH = 7.5, 0.4 M sucrose, 5 mM KCl, 5 mM $MgCl_2$, 5 mM EDTA, supplemented with 0.2 mM spermine, 0.5 mM spermidine, and 0.6% Triton X-100) and incubated on a rotator at 4 °C for 30 min. The sample was then passed through 40 μm mesh and centrifuged (2500× *g* at 4 °C). The pellet was resuspended with nuclear isolation buffer 2 (10 mM HEPES, pH = 7.5, 0.25 M sucrose, 5 mM KCl, 5 mM $MgCl_2$, and 5 mM EDTA). The debris was further reduced by 2 rounds of gentle centrifugation at 300× *g* at 4 °C for 15 sec and the supernatant was collected. The supernatant was further centrifuged for 10 min at 2000× *g* at 4 °C and the resulting nucleus pellet was resuspended with NIB2. For crosslinking, the sample was incubated with 1% formaldehyde for 10 min at room temperature and neutralized with 125 mM glycine for 5 min at room temperature (RT).

4.2.2. Enzymatic Digestion, Reverse Crosslinking, and Ligation

A total of 10^6 crosslinked nuclei were washed twice with Csp6I RE buffer (Thermo Scientific, Waltham, MA, USA, #ER0211) and resuspended in Csp6I RE buffer. SDS was added for a final concentration of 0.3% (*v/v*). After 30 min of incubation at 65 °C, Triton X-100 was added for a final concentration of 1.8% and the sample was incubated for 1 h at 37 °C. Then, 150 units of restriction enzyme Csp6I (Thermo Scientific, Waltham, MA, USA, #ER0211) were added and the sample was incubated overnight at 37 °C. The inactivation of Csp6I was achieved by incubating the samples at 65 °C for 25 min. Ligation reaction was then done in 1.5 mL of 1X ligase buffer with 25 units of T4 ligase (Roche, Rotkreuz, Switzerland, #EL0011) and incubated overnight at 4 °C, followed by 30 min of incubation at RT. To reverse the crosslinks, the sample was supplemented with 50 μg of proteinase K (Invitrogen, Waltham, MA, USA, #25530049) and incubated overnight at 65 °C, followed by incubation with 150 μg of RNAse (Thermo Scientific, Waltham, MA, USA, #EN0551) for 45 min at 37 °C. The resulting proximity-ligated DNA was extracted by phenol–chloroform followed by ethanol precipitation and dissolved in 20 μl of TE buffer. To generate DNA circles, DNA was then digested overnight with DpnII (NEB, Ipswich, MA, USA, #R0543T) at 37 °C.

4.2.3. 4C Template Purification and Amplification

DNA was purified using an Expin CleanUp kit (GeneAll, Seoul, South Korea, #112-102) and DNA concentration was determined by NanoDrop 2000 (Thermo Scientific, Waltham, MA, USA). Ligation junctions were amplified by inverse PCR with viewpoint primers and Phusion hot-start

high-fidelity Taq (Thermo Scientific, Waltham, MA, USA, #F-549) and the following thermal cycle conditions: 30 sec at 98 °C; 25 cycles of 98 °C for 10 sec, 60 °C for 30 sec and 72 °C for 2 min; 72 °C for 5min. PCR products were purified on Expin columns, and 30, 120, and twice 60 ng (4 amplified libraries in total) DNA templates from SALK and ADF8p:NTF/ACT2p:BirA lines were amplified separately with primer-specific barcodes. The primers were designed to hybridize as close as possible to the Csp6I and DpnII recognition sites, on the known bait sequence (genomic or T-DNA sequence). To achieve the maximum length of the capture molecule sequence (blue molecule in Figure 1A), it is recommended that the primers fit the edges of the bait sequence (red molecule in Figure 1A). To further vary the template amounts, the sequenced tags from these libraries were combined. Libraries for Illumina sequencing were prepared using NEBNext Ultra II system (NEB, Ipswich, MA, USA, #E7645, #E7103) and sequenced on a NextSeq platform (Illumina, San Diego, CA, USA). To multiplex several samples on the same sequencing lane, 4-letter barcodes were added to the primers used for inverse PCR. The list of primers is provided in Supplemental Table S4. The data are available under accession number GSE147542.

4.3. 4SEE Analysis of 4C-seq Data

Reads were sorted into different fastq files for each viewpoint according to the viewpoint and index sequences and aligned to the TAIR10 *Arabidopsis* genome using Bowtie [40] with the parameters –m 1 –trim primer length. To avoid possible quantitative PCR or sequencing bias, the data were transformed to represent unique coverage (>1 reads per RE site was set to 1). To identify genomic loci with higher sequence capture frequency than expected, a p score (= $-\log_{10}$(*p*-value)) was calculated for each restriction enzyme (RE) site using a one-tailed binomial test with 50 kb running window centered at the RE site and the entire chromosome as background. Computational procedures are available at https://github.com/HakimLab/4SEE.

4.4. Mapping T-DNA Insertion Sites and Chromosomal Translocations from Chromatin Accessibility Data

To map the T-DNA insertion sites from ATAC-seq and DHS-seq datasets (GSE101482, GSE53324), paired-end (PE) reads were mapped to the T-DNA plasmid sequence used to generate the ADF8p:NTF/ACT2p:BirA plant and to TAIR10 *Arabidopsis thaliana* genome using bowtie2 [41]. Reads in which one mate was mapped to the plasmid and the additional mate was mapped to the genome were extracted from the SAM file. TDNAScan [36] was used with default parameters. To find PE reads crossing chromosomal translocation junctions, reads were mapped by bowtie2 [41] to chimeric chromosomes that were generated by fusing both ends of the predicted chromosomal segments. The mapped reads were visualized using IGV software [42].

4.5. DNA Fluorescence In Situ Hybridization (FISH)

For nucleus isolation and slide preparation, we followed [43,44] with modifications. Young seedlings, 9–14 days post-germination, were fixed in 3:1 (*v/v*) 100% ethanol:acetic acid and washed (3 × 5 min) in water. Then tissue was incubated in an enzyme buffer (10 mM citrate buffer at pH 4.6) and partially digested for 20 min at 37 °C in 6% pectinase plus 0.5% cellulase (NBC Biomedicals, UK) plus 5% cellulase "Onozuka" R-10 (Yakult Honsha Co., Ltd.) followed by washes in enzyme buffer (3 × 5 min) and distilled water (3 × 5 min). The leaves of 2 to 3 seedlings, in a small drop of water, were transferred onto a grease-free microscope slide, and the cells were spread with a stainless metal needle in a small drop of 60% acetic acid at room temperature and allowed to partially air-dry with slide rotation, then fixed in 3:1 (*v/v*) 100% ethanol:acetic acid, then immersed in absolute ethanol for 3–5 s and air-dried. For DNA probes, ABRC BAC clones (F1H21; Chr5:9635,755-9730,934, F10O11; Chr1: 491,600-603,132) were labelled by nick translation with Cy3 and Alexa Flour 488 (Cy3 and AF488 NT Labeling Kits, respectively, Jena Bioscience, Germany). FISH was conducted as previously described [43,45] with modifications. Specifically, cells were treated with 1 µg/mL of DNase-free RNase A in 2 × SSC (0.3 M NaCl plus 30 mM trisodium citrate) for 60 min at 37 °C followed by

3 × 3 min washes with 2 × SSC at 37 °C. The preparations were then dehydrated in an ethanol series (70, 90, and 100%, 3 min each) at room temperature, washed 2 × 2 min with 2 × SSC, then allowed to air-dry. The hybridization mixture (20 µL per slide under the glass coverslip 18 mm × 18 mm) contained 10% dextran sulfate, 2 × SSC, and 700 to 800 ng each of DNA probe. DNA probes and nuclei spreads were simultaneously denatured at 93 °C for 3 min and hybridized using ThermoBrite StatSpin System (Abbott, USA). Hybridization was carried out at 63 °C for 50 min. After removal of the coverslips in 2 × SSC at 63 °C, the slides were washed for 2 × 5 min in 2 × SSC at 63 °C, once in 0.1 × SSC for 5 min at 63 °C to increase stringency, then cooled to 37 °C and washed for 2 × 5 min in 0.1 × SSC, cooled to room temperature, washed in distilled water for 1 min, allowed to air-dry for 10 min, counterstained with 2.5 µg/mL DAPI for 10 min, and mounted in VECTASHIELD antifade mounting medium (Vector Laboratories). The slides were examined on a Leica DMi8 fluorescent inverted microscope using Leica Application Suite X (LAS X) software.

Supplementary Materials: The following are available online at http://www.mdpi.com/1422-0067/21/7/2373/s1. Figure S1: Endogenous 4C cis signal. Figure S2: T-DNA insertion validated by deep sequencing of PE reads from ADF8p:NTF/ACT2p:BirA transgene. Figure S3: Fluorescent in situ hybridization (FISH) on somatic nuclei from Arabidopsis thaliana WT (A-C) and ADF8p:NTF/ACT2p:BirA transgenic plants (D-F). Supplemental Figure S4: Mapping chromosomal rearrangements in ADF8p:NTF/ACT2p:BirA line. Figure S5: Chromosomal translocations on chromosome 5 validated by PE sequencing ATAC-seq data. Figure S6: Genomic coverage of 4C-seq for SALK_063720 and SALK_064627 in different template amounts. Figure S7: Genomic distribution of peak centers at 50% cutoff in SALK lines. Table S1: 4SEE analysis of MBP1, CytC ans SBT4. Table S2: 4SEE of the endogenous ADF8 gene. Table S3: 4SEE of SALK lines. Table S4: Primer sequences used for 4C.

Author Contributions: Conceptualization, M.T., R.K. and O.H.; 4C-seq R.K.; computational analysis, M.T., R.K. and A.S.-P. DNA-FISH, O.R.; technical assistance, O.L.; data curation, M.T., R.K. and O.H.; writing M.T., R.K. and O.H.; supervision, O.H. All authors have read and agreed to the published version of the manuscript.

Funding: This work was supported by the Israel Science Foundation (grant 748/14) and I-CORE Program of the Planning and Budgeting Committee and the Israel Science Foundation, grant no. 41/11. R.K. and M.T. were supported by the Mordecai and Monique Katz Graduate Fellowship Program.

Acknowledgments: We thank Orly Yaron and Sarit Lampert of the BIU sequencing facility for helping with Illumina sequencing.

Conflicts of Interest: The authors declare no conflict of interest.

Abbreviations

4C	Circular chromosome confirmation capture
bp	Base pair
DPC	Distance from peak center
NGS	Next-generation sequencing
RE	Restriction enzyme
WT	Wild type

References

1. Sardesai, N.; Subramanyam, S. Agrobacterium: A Genome-Editing Tool-Delivery System. *Curr. Top. Microbiol. Immunol.* **2018**, *418*, 463–488.
2. Alonso, J.M.; Stepanova, A.N.; Leisse, T.J.; Kim, C.J.; Chen, H.; Shinn, P.; Stevenson, D.K.; Zimmerman, J.; Barajas, P.; Cheuk, R.; et al. Genome-wide insertional mutagenesis of Arabidopsis thaliana. *Science* **2003**, *301*, 653–657. [CrossRef] [PubMed]
3. Rosso, M.G.; Li, Y.; Strizhov, N.; Reiss, B.; Dekker, K.; Weisshaar, B. An Arabidopsis thaliana T-DNA mutagenized population (GABI-Kat) for flanking sequence tag-based reverse genetics. *Plant Mol. Biol.* **2003**, *53*, 247–259. [CrossRef] [PubMed]
4. Berardini, T.Z.; Reiser, L.; Li, D.; Mezheritsky, Y.; Muller, R.; Strait, E.; Huala, E. The Arabidopsis information resource: Making and mining the "gold standard" annotated reference plant genome. *Genesis* **2015**, *53*, 474–485. [CrossRef] [PubMed]
5. Lee, K.; Eggenberger, A.L.; Banakar, R.; McCaw, M.E.; Zhu, H.; Main, M.; Kang, M.; Gelvin, S.B.; Wang, K. CRISPR/Cas9-mediated targeted T-DNA integration in rice. *Plant Mol. Biol.* **2019**, *99*, 317–328. [CrossRef]

6. Nacry, P.; Camilleri, C.; Courtial, B.; Caboche, M.; Bouchez, D. Major chromosomal rearrangements induced by T-DNA transformation in Arabidopsis. *Genetics* **1998**, *149*, 641–650.
7. Forsbach, A.; Schubert, D.; Lechtenberg, B.; Gils, M.; Schmidt, R. A comprehensive characterization of single-copy T-DNA insertions in the Arabidopsis thaliana genome. *Plant Mol. Biol.* **2003**, *52*, 161–176. [CrossRef]
8. Clark, K.A.; Krysan, P.J. Chromosomal translocations are a common phenomenon in Arabidopsis thaliana T-DNA insertion lines. *Plant J.* **2010**, *64*, 990–1001. [CrossRef]
9. Kleinboelting, N.; Huep, G.; Appelhagen, I.; Viehoever, P.; Li, Y.; Weisshaar, B. The Structural Features of Thousands of T-DNA Insertion Sites Are Consistent with a Double-Strand Break Repair-Based Insertion Mechanism. *Mol. Plant* **2015**, *8*, 1651–1664. [CrossRef]
10. Cockram, J.; Mackay, I. Genetic Mapping Populations for Conducting High-Resolution Trait Mapping in Plants. *Adv. Biochem. Eng. Biotechnol.* **2018**, *164*, 109–138.
11. Ochman, H.; Gerber, A.S.; Hartl, D.L. Genetic applications of an inverse polymerase chain reaction. *Genetics* **1988**, *120*, 621–623. [PubMed]
12. Liu, Y.G.; Mitsukawa, N.; Oosumi, T.; Whittier, R.F. Efficient isolation and mapping of Arabidopsis thaliana T-DNA insert junctions by thermal asymmetric interlaced PCR. *Plant J.* **1995**, *8*, 457–463. [CrossRef] [PubMed]
13. Ji, J.; Braam, J. Restriction Site Extension PCR: A Novel Method for High-Throughput Characterization of Tagged DNA Fragments and Genome Walking. *PLoS ONE* **2010**, *5*, e10577. [CrossRef] [PubMed]
14. Lepage, É.; Zampini, É.; Boyle, B.; Brisson, N. Time- and Cost-Efficient Identification of T-DNA Insertion Sites through Targeted Genomic Sequencing. *PLoS ONE* **2013**, *8*, e70912. [CrossRef]
15. Jupe, F.; Rivkin, A.C.; Michael, T.P.; Zander, M.; Motley, S.T.; Sandoval, J.P.; Slotkin, R.K.; Chen, H.; Castanon, R.; Nery, J.R.; et al. The complex architecture and epigenomic impact of plant T-DNA insertions. *PLoS Genet.* **2019**, *15*, e1007819. [CrossRef]
16. Wu, L.; Di, D.-W.; Zhang, D.; Song, B.; Luo, P.; Guo, G.-Q. Frequent problems and their resolutions by using thermal asymmetric interlaced PCR (TAIL-PCR) to clone genes in Arabidopsis T-DNA tagged mutants. *Biotechnol. Biotechnol. Equip.* **2015**, *29*, 260–267. [CrossRef]
17. Krysan, P.J.; Young, J.C.; Sussman, M.R. T-DNA as an Insertional Mutagen in Arabidopsis. *Plant Cell* **1999**, *11*, 2283–2290. [CrossRef]
18. Wu, E.; Lenderts, B.; Glassman, K.; Berezowska-Kaniewska, M.; Christensen, H.; Asmus, T.; Zhen, S.; Chu, U.; Cho, M.-J.; Zhao, Z.-Y. Optimized Agrobacterium-mediated sorghum transformation protocol and molecular data of transgenic sorghum plants. *Vitr. Cell. Dev. Biol. Plant* **2014**, *50*, 9–18. [CrossRef]
19. Bartlett, J.; Smedley, M.; Harwood, W. Analysis of T-DNA/Host-Plant DNA Junction Sequences in Single-Copy Transgenic Barley Lines. *Biology* **2014**, *3*, 39–55. [CrossRef]
20. Hu, Y.; Chen, Z.; Zhuang, C.; Huang, J. Cascade of chromosomal rearrangements caused by a heterogeneous T-DNA integration supports the double-stranded break repair model for T-DNA integration. *Plant J.* **2017**, *90*, 954–965. [CrossRef]
21. Inagaki, S.; Henry, I.M.; Lieberman, M.C.; Comai, L. High-Throughput Analysis of T-DNA Location and Structure Using Sequence Capture. *PLoS ONE* **2015**, *10*, e0139672. [CrossRef] [PubMed]
22. De Vree, P.J.P.; de Wit, E.; Yilmaz, M.; van de Heijning, M.; Klous, P.; Verstegen, M.J.A.M.; Wan, Y.; Teunissen, H.; Krijger, P.H.L.; Geeven, G.; et al. Targeted sequencing by proximity ligation for comprehensive variant detection and local haplotyping. *Nat. Biotechnol.* **2014**, *32*, 1019–1025. [CrossRef] [PubMed]
23. Hakim, O.; Misteli, T. SnapShot: Chromosome Conformation Capture. *Cell* **2012**, *148*, 1068.e1–2. [CrossRef] [PubMed]
24. Belton, J.-M.; McCord, R.P.; Gibcus, J.H.; Naumova, N.; Zhan, Y.; Dekker, J. Hi–C: A comprehensive technique to capture the conformation of genomes. *Methods* **2012**, *58*, 268–276. [CrossRef] [PubMed]
25. Burton, J.N.; Adey, A.; Patwardhan, R.P.; Qiu, R.; Kitzman, J.O.; Shendure, J. Chromosome-scale scaffolding of de novo genome assemblies based on chromatin interactions. *Nat. Biotechnol.* **2013**, *31*, 1119–1125. [CrossRef] [PubMed]
26. Kaplan, N.; Dekker, J. High-throughput genome scaffolding from in vivo DNA interaction frequency. *Nat. Biotechnol.* **2013**, *31*, 1143–1147. [CrossRef]
27. Jiao, W.-B.; Accinelli, G.G.; Hartwig, B.; Kiefer, C.; Baker, D.; Severing, E.; Willing, E.-M.; Piednoel, M.; Woetzel, S.; Madrid-Herrero, E.; et al. Improving and correcting the contiguity of long-read genome

assemblies of three plant species using optical mapping and chromosome conformation capture data. *Genome Res.* **2017**, *27*, 778–786. [CrossRef]
28. Moll, K.M.; Zhou, P.; Ramaraj, T.; Fajardo, D.; Devitt, N.P.; Sadowsky, M.J.; Stupar, R.M.; Tiffin, P.; Miller, J.R.; Young, N.D.; et al. Strategies for optimizing BioNano and Dovetail explored through a second reference quality assembly for the legume model, Medicago truncatula. *BMC Genom.* **2017**, *18*, 578. [CrossRef]
29. Grob, S.; Grossniklaus, U. Invasive DNA elements modify the nuclear architecture of their insertion site by KNOT-linked silencing in Arabidopsis thaliana. *Genome Biol.* **2019**, *20*, 120. [CrossRef]
30. Cao, J.; Ye, C.; Hao, G.; Dabney-Smith, C.; Hunt, A.G.; Li, Q.Q. Root Hair Single Cell Type Specific Profiles of Gene Expression and Alternative Polyadenylation Under Cadmium Stress. *Front. Plant Sci.* **2019**, *10*, 589. [CrossRef]
31. Deal, R.B.; Henikoff, S. The INTACT method for cell type-specific gene expression and chromatin profiling in Arabidopsis thaliana. *Nat. Protoc.* **2011**, *6*, 56–68. [CrossRef] [PubMed]
32. Deal, R.B.; Henikoff, S. A simple method for gene expression and chromatin profiling of individual cell types within a tissue. *Dev. Cell* **2010**, *18*, 1030–1040. [CrossRef] [PubMed]
33. Maher, K.A.; Bajic, M.; Kajala, K.; Reynoso, M.; Pauluzzi, G.; West, D.A.; Zumstein, K.; Woodhouse, M.; Bubb, K.; Dorrity, M.W.; et al. Profiling of Accessible Chromatin Regions across Multiple Plant Species and Cell Types Reveals Common Gene Regulatory Principles and New Control Modules. *Plant Cell* **2018**, *30*, 15–36. [CrossRef] [PubMed]
34. Foley, S.W.; Gosai, S.J.; Wang, D.; Selamoglu, N.; Sollitti, A.C.; Köster, T.; Steffen, A.; Lyons, E.; Daldal, F.; Garcia, B.A.; et al. A Global View of RNA-Protein Interactions Identifies Post-transcriptional Regulators of Root Hair Cell Fate. *Dev. Cell* **2017**, *41*, 204–220.e5. [CrossRef] [PubMed]
35. Sullivan, A.M.; Arsovski, A.A.; Lempe, J.; Bubb, K.L.; Weirauch, M.T.; Sabo, P.J.; Sandstrom, R.; Thurman, R.E.; Neph, S.; Reynolds, A.P.; et al. Mapping and dynamics of regulatory DNA and transcription factor networks in A. thaliana. *Cell Rep.* **2014**, *8*, 2015–2030. [CrossRef]
36. Sun, L.; Ge, Y.; Sparks, J.A.; Robinson, Z.T.; Cheng, X.; Wen, J.; Blancaflor, E.B. TDNAscan: A Software to Identify Complete and Truncated T-DNA Insertions. *Front. Genet.* **2019**, *10*, 685. [CrossRef]
37. Gang, H.; Liu, G.; Zhang, M.; Zhao, Y.; Jiang, J.; Chen, S. Comprehensive characterization of T-DNA integration induced chromosomal rearrangement in a birch T-DNA mutant. *BMC Genom.* **2019**, *20*, 311. [CrossRef]
38. McCarty, D.R.; Mark Settles, A.; Suzuki, M.; Tan, B.C.; Latshaw, S.; Porch, T.; Robin, K.; Baier, J.; Avigne, W.; Lai, J.; et al. Steady-state transposon mutagenesis in inbred maize. *Plant J.* **2005**, *44*, 52–61. [CrossRef]
39. Saito, T.; Ariizumi, T.; Okabe, Y.; Asamizu, E.; Hiwasa-Tanase, K.; Fukuda, N.; Mizoguchi, T.; Yamazaki, Y.; Aoki, K.; Ezura, H. TOMATOMA: A Novel Tomato Mutant Database Distributing Micro-Tom Mutant Collections. *Plant Cell Physiol.* **2011**, *52*, 283–296. [CrossRef]
40. Langmead, B.; Trapnell, C.; Pop, M.; Salzberg, S.L. Ultrafast and memory-efficient alignment of short DNA sequences to the human genome. *Genome Biol.* **2009**, *10*, R25. [CrossRef]
41. Langmead, B.; Salzberg, S.L. Fast gapped-read alignment with Bowtie 2. *Nat. Methods* **2012**, *9*, 357–359. [CrossRef] [PubMed]
42. Robinson, J.T.; Thorvaldsdóttir, H.; Winckler, W.; Guttman, M.; Lander, E.S.; Getz, G.; Mesirov, J.P. Integrative genomics viewer. *Nat. Biotechnol.* **2011**, *29*, 24–26. [CrossRef] [PubMed]
43. Raskina, O.; Belyayev, A.; Nevo, E. Activity of the En/Spm-like transposons in meiosis as a base for chromosome repatterning in a small, isolated, peripheral population of Aegilops speltoides Tausch. *Chromosom. Res.* **2004**, *12*, 153–161. [CrossRef] [PubMed]
44. Lysak, M.; Fransz, P.; Schubert, I. Cytogenetic analyses of Arabidopsis. *Methods Mol. Biol.* **2006**, *323*, 173–186. [PubMed]
45. Celeda, D.; Aldinger, K.; Haar, F.-M.; Hausmann, M.; Durm, M.; Ludwig, H.; Cremer, C. Rapid fluorescence in situ hybridization with repetitive DNA probes: Quantification by digital image analysis. *Cytometry* **1994**, *17*, 13–25. [CrossRef] [PubMed]

International Journal of
Molecular Sciences

MDPI

Article

Different Modes of Action of Genetic and Chemical Downregulation of Histone Deacetylases with Respect to Plant Development and Histone Modifications

Gabriela Lochmanová [1], Ivana Ihnatová [2], Hana Kuchaříková [1,3], Sylva Brabencová [1,3], Dagmar Zachová [1], Jiří Fajkus [1,3], Zbyněk Zdráhal [1,3,*] and Miloslava Fojtová [1,3,*]

1 Mendel Centre for Plant Genomics and Proteomics, Central European Institute of Technology, Masaryk University, 62500 Brno, Czech Republic; gabriela.lochmanova@ceitec.muni.cz (G.L.); hana.kucharikova@ceitec.muni.cz (H.K.); 258751@mail.muni.cz (S.B.); dagmar.zachova@ceitec.muni.cz (D.Z.); fajkus@sci.muni.cz (J.F.)
2 RECETOX, Faculty of Science, Masaryk University, 62500 Brno, Czech Republic; ivana.ihnatova@recetox.muni.cz
3 Laboratory of Functional Genomics and Proteomics, National Centre for Biomolecular Research, Faculty of Science, Masaryk University, 62500 Brno, Czech Republic
* Correspondence: zdrahal@sci.muni.cz (Z.Z.); fojtova@sci.muni.cz (M.F.); Tel.: +420-549-498-258 (Z.Z.); Tel.: +420-549-498-063 (M.F.)

Received: 3 September 2019; Accepted: 10 October 2019; Published: 14 October 2019

Abstract: A high degree of developmental plasticity enables plants to adapt to continuous, often unfavorable and unpredictable changes in their environment. At the molecular level, adaptive advantages for plants are primarily provided by epigenetic machinery including DNA methylation, histone modifications, and the activity of noncoding RNA molecules. Using a mass spectrometry-based proteomic approach, we examined the levels of acetylated histone peptide forms in Arabidopsis plants with a loss of function of histone deacetylase 6 (HDA6), and in plants germinated in the presence of HDA inhibitors trichostatin A (TSA) and sodium butyrate (NaB). Our analyses revealed particular lysine sites at histone sequences targeted by the HDA6 enzyme, and by TSA- and NaB-sensitive HDAs. Compared with plants exposed to drugs, more dramatic changes in the overall profiles of histone post-translational modifications were identified in *hda6* mutants. However, loss of HDA6 was not sufficient by itself to induce hyperacetylation to the maximum degree, implying complementary activities of other HDAs. In contrast to *hda6* mutants that did not exhibit any obvious phenotypic defects, the phenotypes of seedlings exposed to HDA inhibitors were markedly affected, showing that the effect of these drugs on early plant development is not limited to the modulation of histone acetylation levels.

Keywords: *Arabidopsis thaliana*; epigenetics; histone; mass spectrometry; post-translational modifications; sodium butyrate; trichostatin A

1. Introduction

The dynamics of chromatin structure, reflecting changes related to specific developmental stages and various environmental conditions, is crucial for the maintenance of essential functions of each cell in a multicellular organism. Nucleosomes, the basic chromatin units, consisting of DNA wrapped around histone octamers, are sophisticatedly arranged in a higher-order supramolecular structure that is expected to allow for all processes in which DNA is involved, such as DNA replication, transcription and repair. Reversible modifications of protruding histone N-termini are important for modulating the

strength of association between histones and DNA, and for recruitment of chromatin-associated proteins. Modification of positively charged amino acids lysine (K) and arginine (R), which are frequently located at the N-termini of H3 and H4 histones, by addition of acetyl group results in neutralization of their positive charge, thus weakening electrostatic bonds between histones and phosphates in DNA and resulting in a more relaxed chromatin structure. Acetylated regions of chromatin are thus generally associated with transcriptionally active euchromatin [1,2], while histone hypoacetylation leads to the formation of more condensed heterochromatin [2–4]. Enzymes catalyzing loading on and removal of acetyl group from histones, histone acetyltransferases (HATs) and histone deacetylases (HDAs), respectively, play important roles in crucial processes in plant development, e.g., embryogenesis, timing of flowering and senescence, stress response and adaptation [5–8].

Two basic approaches are commonly utilized for functional studies of histone acetylation in the model plant *Arabidopsis thaliana*; analysis of mutants with a T-DNA insertion in genes encoding HATs or HDAs, or treatment of plants with chemical compounds that can modulate the activities of these enzymes. Regarding *HDAs*, 18 paralogs grouped into three types were identified; 12 RPD3 (reduced potassium deficiency 3)-like genes, 2 SIR2 (silent information regulator 2) genes, and four plant-specific genes so-called HD-tuins [9,10]. *HDA6* is a member of the RPD3-like superfamily. Two *HDA6* mutant alleles were described and analyzed; *hda6-6* obtained by EMS mutagenesis [11], and *hda6-7* with the T-DNA insertion [12]. Involvement of HDA6 in the maintenance of transcriptional gene silencing and nucleolar dominance [13–15], in the response to stress conditions [16,17], and in flowering-related processes [18] was described. As *hda6* mutants exhibited no crucial developmental abnormalities, other HDA members are assumed to act redundantly and compensate for HDA6 loss of function. Correspondingly, in *hda6/hda19* double mutants (with HDA19 being another prominent member of the RPD-3 superfamily), strong growth arrest during germination and formation of embryo-like structures were reported [6], and this phenotype was more severe compared to *hda19* single mutants [7]. In this respect, studies of plants exposed to HDA inhibitors, drugs that are able to influence the activity of several HDAs due to common structural domains of these enzymes, seem promising. Trichostatin A (TSA) and sodium butyrate (NaB) are the most commonly used inhibitors of RPD3-like HDAs. Using crystallographic studies, it was shown that TSA was able to insert its aliphatic chain into the hydrophobic cleft located in the catalytically active domain of HDAs [19]. A similar mode of action was proposed for NaB, because two NaB molecules could occupy the hydrophobic cleft in a similar way as demonstrated for TSA. Nevertheless, NaB is a non-competitive inhibitor of HDAs, thus does not associate with the substrate-binding region [20]. Details of NaB inhibition activity remain still enigmatic. As consequences of TSA exposure, de-repression of silenced rRNA genes [3], growth arrest and elevated transcription of embryogenesis-related genes [6] were reported in *A. thaliana*, and growth of primary roots was inhibited in poplar [21]. Interestingly, although inhibition of HDAs and increased levels of histone acetylation are supposed to lead to transcriptional up-regulation, significantly more genes were down-regulated than up-regulated in the latter study, suggesting that acetylation of histones may influence gene expression either positively or negatively [21]. Similarly to TSA, NaB activated silenced rRNA genes [3,22], and induced defects in seed germination and seedling growth were correlated with elevated transcription of base-excision repair genes in alfalfa [23].

For analyses of histone modifications, many methods are used, with mass spectrometry (MS) being widely recognized in the last years as an important tool for these studies. MS enables both qualitative and quantitative analysis of the distribution of histone post-translational modifications (PTMs). Although standard MS approaches are generally applicable for analysis of histones isolated from both mammalian and plant tissues, extraction of plant histones is complicated due to the presence of many secondary metabolites and other compounds contaminating histone extracts. Problems associated with histone solubility are also common. These difficulties are reflected in markedly more limited utilization of MS for analyses of PTMs of plant histones compared to mammals. To overcome these

obstacles, we presented a straightforward approach for preparation of plant histone samples for MS analysis based on filter-aided sample preparation coupled with histone propionylation [24].

Here, we monitored phenotype and compared the level of acetylated and non-acetylated histone peptide forms in *A. thaliana* plants with loss of function of the gene encoding HDA6, and plants germinated in the presence of HDA inhibitors TSA or NaB. Our results suggest that the strong and dose-dependent effects of TSA and NaB on early plant development are complex and are not restricted to the ability of these drugs to influence the levels of histone acetylation via inhibition of activity of RPD3-like HDA enzymes.

2. Results

2.1. Strong Phenotype of Seedlings Germinated in the Presence of HDA Inhibitors Is Recovered during Cultivation of Plants in the Soil

Morphological changes of *A. thaliana* plants associated with genetic (plants with loss of function of HDA6) or chemical (germination in the presence of HDA inhibitors, NaB or TSA) modulation of histone acetylation levels were examined. No clearly consistent alterations of phenotype were observed compared with wild-type Col-0 plants in both *hda6* lines germinated for 7 days followed by 7 weeks of cultivation in the soil, except for a slightly delayed flowering, in accordance with previously published observations [25]. However, when *A. thaliana* Col-0 seedlings were cultivated on MS medium supplemented with HDA inhibitors, a dose-dependent inhibition of early seedling development was observed (Figure 1a). One of the most distinctive symptoms was inhibition of root elongation, which was significantly more pronounced in seedlings germinated in the presence of NaB. The lengths of primary roots of 30 representatives per line were measured using the ImageJ software. The differences in their lengths compared to controls were significant in all HDA inhibitor-treated seedlings ($p < 0.001$; Figure 1b). NaB-exposed seedlings exhibited signs of agravitropism and chlorosis, and TSA exposure increased root hair length and density (Figure 1c). In spite of substantial developmental defects in seedlings germinated in the presence of HDA inhibitors, following 7 weeks of cultivation in soil without inhibitors, plants were morphologically indistinguishable from untreated controls, indicating recovery of plant phenotype (Figure 1d).

2.2. Distinct Alterations in Histone PTMs Are Hidden under a Mild Phenotype and Vice Versa

To examine changes in histone marks levels due to genetic or chemical inhibition of HDAs, the abundance of selected post-translationally modified histone peptides was evaluated from mass spectrometric analysis (experimental design is shown in Figure 2; see Materials and Methods for detailed description). As expected, peptide sequences corresponding to the N-termini of histones H3 and H4 exhibited high levels of PTMs. In particular, peptides of histone H3 included ten forms of K9STGGKAPR17 (H3K9–R17), three of K18QLATKAAR26 (H3K18–R26) and five of K27SAPATGGVKKPHR40 (H3K27–R40); peptides of histone H4 included eight forms of G4KGGKGLGKGGAKR17 (H4G4–R17). All these peptides possessed considerable levels of global acetylation, except for H3K27–R40 sequence. K27me2K36ac, with a relative abundance of <0.2%, represented the only acetylated form of H3K27–R40, whereas predominant forms of this peptide were dimethylated or monomethylated at K27 without any acetylation. Thus, the relative representation of acetylated forms of histone-peptides in HDA-deficient and control samples was evaluated for all above mentioned peptides except for H3K27–R40. The acetylation patterns of histone-peptides were statistically evaluated at three different levels: (1) comparison of overall acetylation status between HDA-deficient plants/seedlings and respective controls (i.e., the proportion of total abundance of all peptide forms containing acetyl group(s) relative to the total abundance of peptides without acetylation), (2) comparison of abundance of particular modified peptide forms between HDA-deficient plants/seedlings and respective controls (i.e., the proportional abundance of

a particular peptide form containing acetyl group(s) relative to the abundance of all other peptides), and (3) comparison of the ratio of each pair of peptide forms in experimental and control groups.

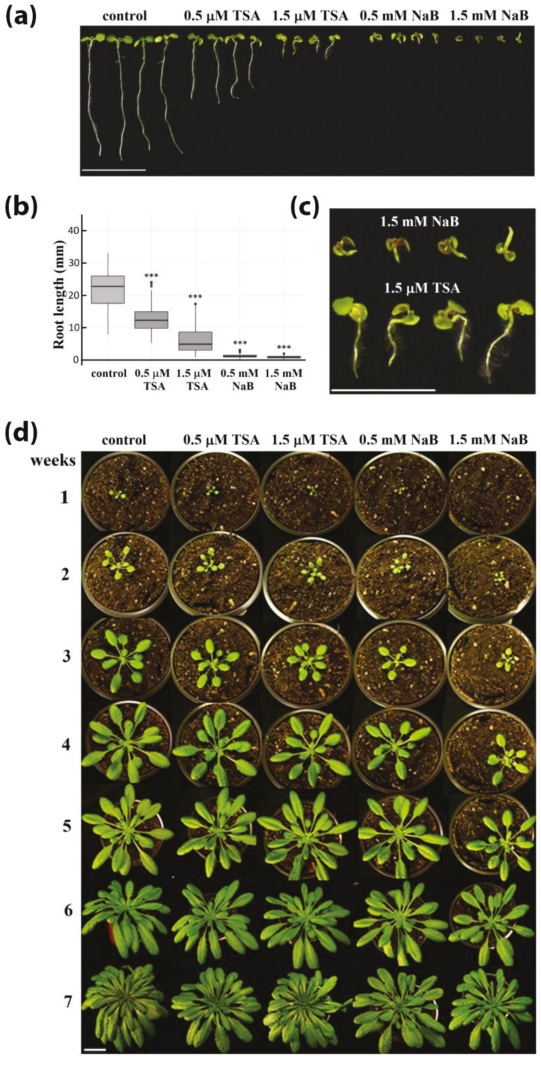

Figure 1. Effect of histone deacetylase (HDA) inhibitors on Arabidopsis growth and development. (**a**) Morphology of 7-day-old seedlings germinated in the presence of different concentrations of HDA inhibitors. Bar = 1 cm. (**b**) Lengths of primary roots in control and HDA inhibitor-treated seedlings. The box-plots show extremes, interquartile ranges and medians (n = 30). Statistically significant differences corresponding to $p < 0.001$ are marked by asterisks. (**c**) Detail of morphology of 7-day-old seedlings germinated in the presence of 1.5 mM NaB or 1.5 µM TSA. Bar = 0.5 cm. (**d**) Phenotype recovery of plants germinated in the presence of HDA inhibitors during the cultivation in the soil. Bar = 2 cm.

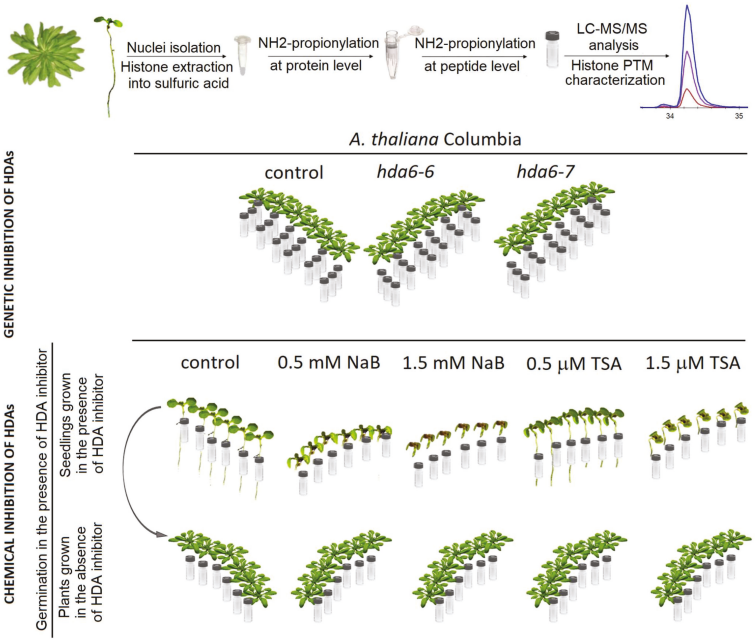

Figure 2. Experimental design. To quantify histone marks levels, histone proteins were extracted from seedlings germinated on different Petri dishes (6 replicates) or leaves of six independently cultivated plants. Samples were prepared for analysis by filter-aided sample preparation coupled with histone propionylation, digested with trypsin, and analyzed by LC-MS/MS. Leaves collected from 7-week-old *hda6* mutants and respective wild type plants were analyzed in a random order in three technical batches. Part of 7-day-old seedlings germinated in the presence of HDA inhibitors was harvested for proteomic analysis and part was transferred to the soil without HDA inhibitors and plants were grown for 7 weeks. These samples were analyzed in a random order in a single technical batch.

Compared to controls, significantly changed overall histone-peptide acetylation was observed in the leaves of both *hda6* lines (Figure 3a) corresponding to an increase by 9–11% in H3K9–R17 and H3K18–R26 acetylated peptide forms, and by 7–8% in H4G4–R17 acetylated peptide forms (Figure 3a and Table S1). Detailed investigation of modified peptide forms revealed significantly changed profiles in comparison to wild type controls, with a similar trend in both *hda6* lines.

Acetylation as the sole modification was detected as the prevailing form of H3K9–R17 modified peptides in control samples. In *hda6* lines, significantly increased levels of peptides with K14ac, including those containing me1 (methyl group), me2 or me3 at K9, were detected. On the other hand, the abundance of di-acetylated K9acK14ac peptide did not differ between *hda6* and control lines. Further, mono- and di-acetylated forms of H3K18–R26 peptide were elevated. In histone H4, mainly mono- and di-acetylated forms carrying acetylation in positions K8 and K16 were responsible for the hyperacetylation state in both *hda6-6* and *hda6-7* lines, while the abundance of peptides carrying three or four acetyl groups was comparable with control samples (Figure 3b). As expected, these changes were accompanied by significantly reduced levels of corresponding non-modified histone peptide sequences (Figure 3a; Tables S1 and S2). A disrupted balance of combinatorial patterns of histone modifications in *hda6* lines was also evident from the statistical evaluation of abundance of pairs of differentially modified histone peptide forms (Table S3). These results further indicate that HDA6 primarily affects acetylation at positions H3K14 and H4K16.

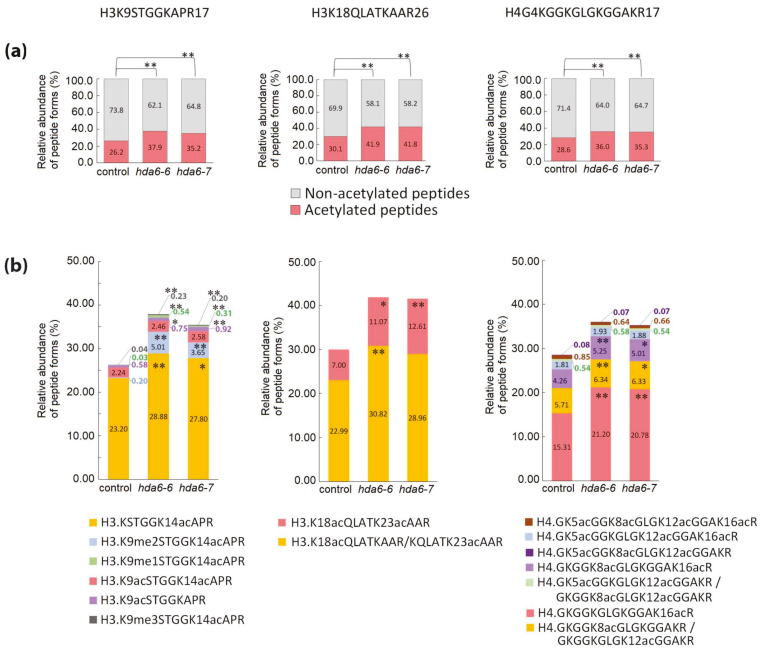

Figure 3. Relative abundance of peptide forms of histones H3 and H4 in leaves of wild type Arabidopsis plant (control) and *hda6* mutant lines (*hda6-6*, *hda6-7*). (**a**) The relative abundance of all peptide forms containing acetyl group(s) compared with that of peptides without acetylation. (**b**) The relative abundance of particular peptide forms containing acetyl group(s) compared with that of all other forms of respective peptide sequences. The levels of peptide forms were determined from the extracted ion chromatograms (XIC) peak areas. The significance of between-sample differences was assessed using t-tests, setting the significance threshold at ** $p < 0.01$ and * $p < 0.05$.

Increase in the levels of acetylated forms of histone-peptides in HDA inhibitor-treated seedlings was induced to a higher extent in histone H4 than in histone H3 (Figures 4 and 5). Significant changes in histone mark levels were observed only in seedlings treated with higher doses of HDA inhibitors (Table S1). Treatment with 1.5 mM NaB and 1.5 µM TSA caused 12% and 23% increases in overall acetylations of H4G4–R17 peptide, respectively (Figure 5a). Both HDA inhibitors increased the number of forms carrying 2–4 acetyl groups. In the case of 1.5 µM TSA treatment, a higher abundance was also observed for K16-monoacetylated peptide (Figure 5b). Hyperacetylation of H4G4–R17 induced by both inhibitors was accompanied by a significant decrease in the levels of the non-modified form of this peptide ($p < 0.05$ and $p < 0.001$ for NaB and TSA, respectively). Regarding H3 histone, overall acetylation in H3K9-R17 peptide, corresponding to ~9% increase, was observed in seedlings exposed to 1.5 µM TSA (Figure 4a). Detailed evaluation of particular modified forms revealed significant changes in K14-mono- and di-acetylated H3K9–R17 peptides and di-acetylated H3K18–R26 peptide forms (Figure 4b,d). Interestingly, an increased level of the di-acetylated H3K18–R26 peptide, together with an increase in K9me2K14ac-containing peptide were detected in seedlings treated with 1.5 mM NaB (Figure 4b,d), although this was not reflected in the total levels of non-modified and acetylated forms of these peptides (Figure 4a,c). As supported by peptide pair statistics, NaB treatment caused moderate effects on histone epigenetic marks, as manifested by some increase in H3K9me2K14ac and di- and tetra-acetylated forms of H4G4-R17. On the contrary, TSA induced a comprehensive imbalance of solely acetylated epigenetic marks on histones H4 and H3 (Tables S2 and S3).

Seven weeks of growth in soil, thus in the absence of HDA inhibitors, allowed the plants to readjust all imbalanced modifications of histone peptides observed in seedlings to levels comparable to control plants (Figures 4 and 5; Tables S1–S3).

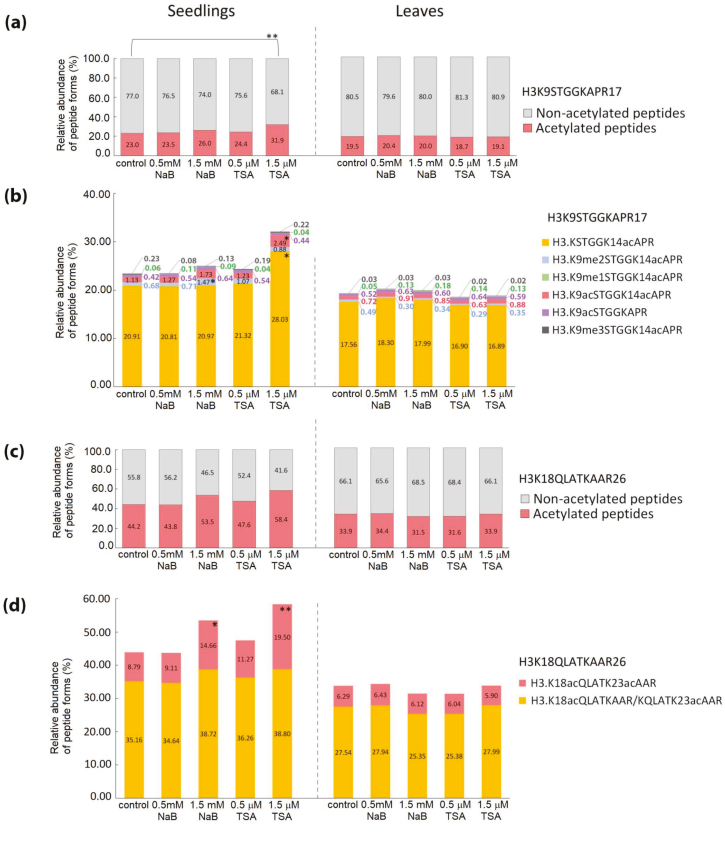

Figure 4. Relative abundance of peptide forms of histone H3 in seedlings germinated in the presence of HDA inhibitors, leaves of plants cultivated from these seedlings, and respective control samples. (**a**,**c**) The relative abundance of all peptide forms containing acetyl group(s) compared with that of peptides without acetylation. (**b**,**d**) The relative abundance of particular peptide forms containing acetyl group(s) compared with that of all other forms of respective peptide sequences. The levels of peptide forms were determined from the extracted ion chromatograms (XIC) peak areas. The significance of between-sample differences was assessed using t-tests, setting the significance threshold at ** $p < 0.01$ and * $p < 0.05$.

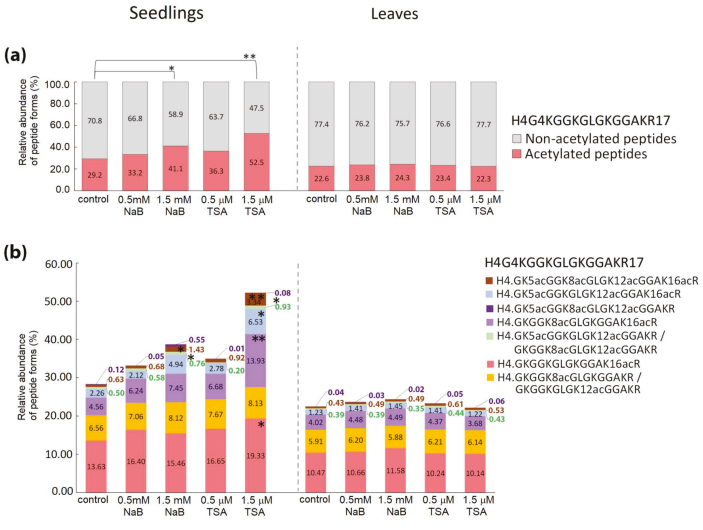

Figure 5. Relative abundance of peptide forms of histone H4 in seedlings germinated in the presence of HDA inhibitors, leaves of plants cultivated from these seedlings, and respective control samples. (**a**) The relative abundance of all peptide forms containing acetyl group(s) compared with that of peptides without acetylation. (**b**) The relative abundance of particular peptide forms containing acetyl group(s) compared with that of all other forms of respective peptide sequences. The levels of peptide forms were determined from the XIC peak areas. The significance of between-sample differences was assessed using t-tests, setting the significance threshold at ** $p < 0.01$ and * $p < 0.05$.

3. Discussion

The growth of plants is modulated by regulatory pathways influencing vegetative development and response to environmental conditions. Members of the HDA family represent important epigenetic regulators involved in these comprehensive networks. Considering functional diversity of HDAs, which is determined by their subcellular localizations and different expression profiles, together with the fact that activity of these enzymes can be further affected by the interactions with other proteins, the response mechanisms appear to be highly complex [26].

A wide range of biochemical and molecular biological approaches have been contributed to deciphering the machinery of epigenetic regulations. The scope of knowledge in the field of histone epigenetic modifications is determined by the feasibility of respective analyses, which are challenging due to the complex pattern of histone PTMs and the presence of histone variants.

In agreement with previously published data [11,12,25], mutations in the *HDA6* gene did not affect the phenotype of plants during early stages of growth. On the other hand, delayed flowering and the onset of leaf senescence in *hda6-6* and *HDA6-RNAi* plants have been reported, indicating that HDA6 affected rather later periods of plant development [25]. In these plants, except for an increase in the global level of H3 acetylation, H3 hyperacetylation was detected in the *FLC* gene locus, with *FLC* encoding a transcription factor that controls the transition from vegetative to reproductive developmental stages. Based on these data, we focused on analysis of 7-week-old *hda6* plants. Our MS-based approach allowed us to distinguish and quantify a number of post-translationally modified histone peptide forms. Although *hda6* plants exhibited no obvious morphological changes, significant alterations were found at the level of histone modifications (Figure 3). Based on circumstantial analyses, Earley et al. deduced H3K14, H4K5 and H4K12 as target sites for HDA6 deacetylase activity [13]. We confirmed the position K14 of histone H3 as a dominant HDA6 target, and demonstrated that K14 deacetylation is not dependent on PTMs present at K9. In addition, the lack of HDA6 also led to hyperacetylation at

positions H3K18 and H3K23 (Figure 3b). Instead of H4K5 and H4K12, as reported by Earley and coworkers [13], acetylation at H4K8 and primarily at H4K16 were found to be affected in *hda6* lines. Importantly, levels of tri- and tetra-acetylated forms of histone H4 peptides were not elevated, indicating that plant cells tend to minimize hyperacetylation due to an *HDA6* gene mutation using redundant activities of other HDAs to ensure plant survival and prevent growth and developmental defects.

As a parallel approach for modulating the activity of HDAs, we germinated Arabidopsis seeds in the presence of TSA or NaB. According to Ueda's classification [27], NaB is a selective inhibitor of class I HDAs (HDA6, HDA7, HDA9, HDA19) and class II (HDA5, HDA14, HDA15, HDA18) while TSA, as a pan-inhibitor, inhibits HDAs of classes I and II and also class IV (HDA2) and some unclassified HDAs (HDA8, HDA10, HDA17). Higher variability of histone PTMs in the biological replicates of TSA-treated *A. thaliana* leaves was previously observed in a proteomic study, and accordingly, a relatively low number of specific sites with modulated acetylation state were identified [28]. Analysis of six biological replicates (seedlings cultivated on six Petri dishes) revealed significantly changed levels of histone PTMs in samples treated with higher doses of inhibitors (Figures 4 and 5). Apparently, variability in the data of NaB- and TSA-exposed samples was higher compared to results of analyses of *hda6* mutants (Tables S1–S3), which obviously reflected the heterogeneous phenotype of seedlings germinated in the presence of HDA inhibitors (Figure 1a). In this context, it is necessary to stress the strong phenotypic defects of 7-day-old seedlings germinated in the presence of HDA inhibitors (Figure 1a,b).

However, and rather surprisingly, the extent of changes in histone acetylation did not correlate with morphological changes (Figures 4 and 5). Specifically, NaB-exposed seedlings had severely disturbed germination but changes in histone acetylation were remarkably lower than in seedlings treated with TSA, exhibiting a milder phenotype. The modest increase in histone acetylation levels in NaB-treated seedlings correlated with the lower number of HDAs that were inhibited by this drug, compared to TSA. The strong effect of NaB on the processes of early plant development is thus probably related to the modes of action of this drug other than HDA inhibition. The phenotype comparable with wild type plants, together with highly impaired histone acetylation status in *hda6* mutants, i.e., plants with loss of function of a single HDA, further supports this scenario. Indeed, the effect of HDA inhibitors on protein partners that are independent of HDA activity has previously been reported in several studies in mammalian cells [29–32]. Another possibility is that due to reduced HDA activity caused by HDA inhibitors, metabolic pathways that involve acetylated target proteins other than histones might be influenced. Acetylated lysines were found in a number of proteins localized in diverse subcellular compartments in both plants and mammals. Potential non-histone targets of RPD3-like enzymes in Arabidopsis were investigated in a recently published comprehensive proteomic study [28].

Detailed analysis revealed increased length and density of root hairs as striking features of TSA-treated seedlings (Figure 1c). Rapidly and reversibly altered patterns of root hair development after TSA treatment were previously reported and associated with histone hyperacetylation-related expression of *CPC*, *GL2*, and *WER* developmental patterning genes [33]. According to this study, HDA18 is a key component involved in the regulation of root hair formation. As activity of this class II HDA is supposed to be influenced by both TSA and NaB inhibitors, a broader inhibitory capacity of TSA may somehow augment the final effect. On the other hand, the process of germination was retarded by NaB to the extent of making the proper phenotypic analysis of roots impossible. Importantly, the effect of HDA inhibitors on the phenotype as well as on histone acetylation status was transient, since subsequent cultivation of plants in the soil conferred features comparable with control plants (Figures 1d, 4 and 5).

The regulatory role of HDAs in crucial developmental processes has been convincingly demonstrated using various plant species (reviewed in [34]). Here, we performed comprehensive proteomic characterization of histone PTMs to obtain new information on the relationship between phenotypic features and the pattern of histone modifications in *A. thaliana* plants with abolished HDA activities. Our data demonstrate the complexity not only of HDA action but also of effects of

HDA inhibitors, as the ability of these drugs to influence plant growth and development does not seem to be limited to modulation of histone acetylation.

4. Materials and Methods

4.1. Cultivation of Plants, Monitoring of Phenotype

Arabidopsis thaliana ecotype Col-0 (Nottingham Arabidopsis Stock Centre, Nottingham, UK) seeds collected from a set of parent plants were ethanol sterilized and placed on Petri dishes containing half-strength Murashige-Skoog medium (Duchefa Biochemicals, Haarlem, The netherlands) supplemented with 0.8% plant agar. The medium was then supplemented with inhibitors of HDAs, 0.5 mM NaB (Sigma-Aldrich, St Lous, MO, USA), 1.5 mM NaB, 0.5 μM TSA (Sigma-Aldrich), and 1.5 μM TSA. Seeds were vernalized for 3 days at 4 °C and germinated for 7 days in phytotrons under short day conditions (8 h light, 21 °C, illumination 100 μmol m^{-2} s^{-1}; 16 h dark, 19 °C). The lengths of roots of at least 30 seedlings cultivated on control medium or exposed to HDA inhibitors were measured using ImageJ software (Fiji; [35]), and results were statistically evaluated by the Mann–Whitney U test. A proportion of the seedlings was then harvested and a proportion was transferred to the soil. Plants were grown for seven weeks in the phytotrons under short day conditions; growth progress was monitored weekly.

Seeds of the *hda6-7* mutant line were germinated and plants were cultivated as described above. Plants were genotyped using a primer pair distinguishing a 37-bp deletion in the mutant as described in [12]. Seeds of *hda6-6* were germinated on half-strength Murashige-Skoog medium supplemented with 25 mg·mL^{-1} hygromycin, plants were then cultivated in soil as described above. Seeds of both *hda6* mutants were kindly provided by Frederic Pontvianne (CNRS and Universite' de Perpignan Via Domitia, Perpignan, France).

For LC-MS/MS analysis, histones extracted from seedlings germinated on six Petri dishes and leaves of six independently cultivated plants were taken. The samples isolated from leaves of 7-week old *hda6* mutant lines and wild type Col-0 plants were measured in random order in three technical batches. Seven-day-old seedlings germinated in the presence of HDA inhibitors and 7-week-old plants grown in the soil from these seedlings, as well as corresponding control samples, were analyzed in random order in a single technical batch. Experimental design is schematically illustrated in Figure 2.

4.2. Histone Isolation and Preparation of Samples for Mass Spectrometry

The procedures used for extraction and chemical derivatization of plant histones have been previously described [24]. Nuclei isolated from ~500 mg of plant tissues were resuspended in the nuclei lysis buffer (50 mM Tris-HCl pH 8.0, 100 mM NaCl, 3 mM EDTA, 1% CHAPS, 0.1 μM PMSF, 45 mM NaB, and 10 μL/mL of P9599 protease inhibitor cocktail from Sigma-Aldrich), incubated for 1 h on ice, and centrifuged (8 min, 10,000× *g*, 4 °C). The pellets were resuspended in 200–400 μL of ice-cold 0.2 M H_2SO_4 and incubated overnight with shaking at 4 °C. Samples were centrifuged (8 min, 16,100× *g*, 4 °C) and supernatants containing histone proteins were collected. Sixteen μg of plant histone extract in sulfuric acid was subjected to a double round of propionic anhydride derivatization. After pH adjustment to 8–9 with NH_4OH, 10 μL of propionylation reagent (1:3 mixture of propionic anhydride and acetonitrile (MeCN); both from Sigma-Aldrich) were added to the samples and incubated in a thermomixer (37 °C, 700 rpm, 20 min). The sample volumes were reduced in a Savant SPD121P concentrator (SpeedVac; Thermo Fisher Scientific, Waltham, MA, USA) to 5 μL. For the second round of propionylation, samples were diluted with 50% (*v*/*v*) MeCN to 20 μL and propionylation was carried out using the same protocol. Samples were diluted with 300 μL of 8 M urea (pH 8.5), placed in a YM-10 Microcon filter unit (Merck Millipore, Burlington, MA, USA), centrifuged (45 min, 14,000× *g*, 25 °C), washed two times with 200 μL of 8 M urea and three times with 100 μL of 100 mM ammonium bicarbonate (ABC; 45 min, 14,000× *g*, 25 °C). Trypsin (Promega, Madison, WI, USA) diluted in 50 μL of 100 mM ABC was added in a 1:40 (enzyme:protein) ratio. Digestion was carried out overnight at 37 °C.

The digest was collected by centrifugation (10 min, 14,000× *g*, 25 °C), subjected to two additional washes with 50 µL of 100 mM ABC and concentrated using the SpeedVac to a volume of ~20 µL. One µL of NH_4OH and 5 µL of the propionylation reagent prepared by mixing propionic anhydride with MeCN in a 1:3 ratio were added. The pH was adjusted to 8–9 with NH_4OH, samples were incubated in thermomixer at 37 °C at 700 rpm for 20 min, then the volume was reduced in the SpeedVac to 5 µL. For the second round of propionylation, samples were diluted with 50% (*v*/*v*) MeCN to a volume of 20 µL and the process was carried out using the same protocol. The samples were diluted with 0.1% formic acid to a volume of 100 µL. Labeled histones were desalted using a Hypersep SpinTip C-18 column (Thermo Fisher Scientific).

4.3. Mass Spectrometric Analysis, Database Searches and Quantification of Histone Peptide Forms

Mass spectrometric analysis of histone peptides and following data processing was done as described previously [24]. Propionylated peptides were measured using LC-MS/MS. The LC-MS/MS equipment consisted of an RSLCnano system, equipped with an X-Bridge BEH 130 C18 trap column (3.5 µm particles, 100 µm × 30 mm; Waters), and an Acclaim Pepmap100 C18 analytical column (3 µm particles, 75 µm × 500 mm; Thermo Fisher Scientific), coupled to an Orbitrap Elite hybrid spectrometer (Thermo Fisher Scientific) equipped with a Digital PicoView 550 ion source (New Objective, Woburn, MA, USA) using a PicoTip SilicaTip emitter (FS360-20-15-N-20-C12), and an Active Background Ion Reduction Device. Prior to LC separation, tryptic digests were online concentrated on a trap column. The mobile phase consisted of 0.1% formic acid in water (A) and 0.1% formic acid in 80% acetonitrile (B), with the following proportions of B: 1% for 3 min at 500 nL/min, then with a switch to 300 nL/min for the next 2 min, increasing linearly from 1% to 70% over 85 min, 70–85% over 20 min and followed by isocratic washing at 85% B for 10 min. Equilibration of the trapping and separation columns was carried out using 99:1 (mobile phase A:B; flow rate 500 nL/min) prior to sample injection to the sample loop. The analytical column outlet was directly connected to the ion source of the MS. MS data were acquired using a data-dependent strategy selecting up to the top 10 precursors based on precursor abundance in a survey scan (350–2000 m/z). The resolution of the survey scan was 60,000 (400 m/z) with a target value of 1×10^6, one microscan and maximum injection time of 1000 ms. HCD MS/MS spectra were acquired with a target value of 50,000 and resolution of 15,000 (400 m/z). The maximum injection time for MS/MS was 500 ms. Dynamic exclusion was enabled for 45 s after one MS/MS spectrum acquisition and early expiration was disabled. The isolation window for MS/MS fragmentation was set to 2 m/z.

The RAW mass spectrometric data files were analyzed using Proteome Discoverer software (Thermo Fisher Scientific; version 1.4) with an in-house Mascot search engine (Matrixscience, London, UK; version 2.6) to compare acquired spectra with entries in the UniProtKB Arabidopsis thaliana protein database (version 2017_11; 27567 protein sequences; downloaded from ftp://ftp.uniprot.org/pub/databases/uniprot/current_release/knowledgebase/reference_proteomes/Eukaryota/UP000006548_3702.fasta.gz), cRAP contaminant database (downloaded from http://www.thegpm.org/crap/) and in-house histone database (version 2017_02; 71 protein sequences). Mass tolerances for peptides and MS/MS fragments were 7 ppm and 0.025 Da, respectively. Semi-Arg-C for enzyme specificity allowing up to two missed cleavages was set. For searches against cRAP and UniProtKB Arabidopsis thaliana databases, the variable modification settings were oxidation (M), deamidation (N, Q), acetylation (K, protein N-term) and propionylation (K, N-term), while for histone database searches they were acetylation (K, protein N-term), methylation (K, R), dimethylation (K), trimethylation (K), phosphorylation (S, T), and propionylation (K, N-term, S, T, Y). The abundance of histone peptides was quantified automatically using Proteome Discoverer 1.4 software. Only peptides with statistically significant peptide scores ($p < 0.01$) were considered. The peak area corresponding to each precursor ion was calculated from the extracted ion chromatograms (XICs) using the Precursor Ions Area Detector node. Selected histone peptide identifications were manually verified and quantified

from the peak areas derived from the XICs using Skyline 3.6 software, including identification alignment across the raw files based on retention time and m/z.

The mass spectrometry proteomics data were deposited to the ProteomeXchange Consortium via the PRIDE [36] partner repository with the dataset identifier PXD014739.

4.4. Data Analysis

The peak areas corresponding to post-translationally modified forms of individual histone peptide were treated as compositions and Aitchison's methodology [37] based on log-ratios was applied in the statistical evaluation. First, the missing values were imputed by iterative least trimmed squares regression [38] and areas were transformed to relative abundances (percentages). Then, acetylated and non-acetylated forms of each peptide were amalgamated. All forms of acetylated/non-acetylated histones were processed as follows. The technical replicates were aggregated by geometric mean and closure. In order to fully exploit the statistical significance of differences in relative abundances of individual forms of peptides, multiple transformations, defined for compositional data, were applied. Note that in compositional data, the relative abundances of individual parts were not directly comparable due to the constant sum constraint leading to a spurious negative correlation. The log2 ratio of amalgamated acetylated and non-acetylated forms was calculated (alr-transformation of 2-parts composition) and the t-test was used to compare means of the ratios between corresponding pairs of experimental and control groups. The relative abundances of all individual peptide forms were first ilr-transformed and compared by Hotelling's T2 test to globally assess the differences in the distribution of forms of each peptide. Later, for each peptide, the log2 ratio of relative abundance of one form to the sum of relative abundances of all other forms was calculated and the *t*-test was applied to assess the difference in each individual form. Finally, log2 ratios of all pairs of peptide forms were calculated and compared by *t*-test. The data analysis was performed in R version 3.5.0 [39].

Supplementary Materials: Supplementary materials can be found at http://www.mdpi.com/1422-0067/20/20/5093/s1.

Author Contributions: Conceptualization, Z.Z., M.F. and J.F.; Investigation, G.L., H.K., S.B. and D.Z.; Formal analysis, G.L., I.I. and D.Z.; Validation, G.L. and I.I.; Writing—Original draft preparation, G.L. and M.F.; Writing—Review and editing, Z.Z. and J.F.

Funding: This research was funded by European Regional Development Fund—Project "SINGING PLANT" (No. CZ.02.1.01/0.0/0.0/16_026/0008446). CIISB research infrastructure project LM2015043 funded by MEYS CR is gratefully acknowledged for financially supporting the LC-MS/MS measurements at the Proteomics Core Facility.

Conflicts of Interest: The authors declare no conflict of interest.

Abbreviations

HAT	Histone acetyltransferase
HDA	Histone deacetylase
NaB	Sodium butyrate
MS	Mass spectrometry
PTM	Post-translational modification
TSA	Trichostatin A

References

1. Brownell, J.E.; Allis, C.D. Special HATs for special occasions: Linking histone acetylation to chromatin assembly and gene activation. *Curr. Opin. Genet. Dev.* **1996**, *6*, 176–184. [CrossRef]
2. Kuo, M.H.; Allis, C.D. Roles of histone acetyltransferases and deacetylases in gene regulation. *Bioessays* **1998**, *20*, 615–626. [CrossRef]
3. Chen, Z.J.; Pikaard, C.S. Epigenetic silencing of RNA polymerase I transcription: A role for DNA methylation and histone modification in nucleolar dominance. *Genes Dev.* **1997**, *11*, 2124–2136. [CrossRef] [PubMed]

4. Kadosh, D.; Struhl, K. Targeted recruitment of the Sin3-Rpd3 histone deacetylase complex generates a highly localized domain of repressed chromatin in vivo. *Mol. Cell Biol.* **1998**, *18*, 5121–5127. [CrossRef] [PubMed]
5. Ning, Y.Q.; Chen, Q.; Lin, R.N.; Li, Y.Q.; Li, L.; Chen, S.; He, X.J. The HDA19 histone deacetylase complex is involved in the regulation of flowering time in a photoperiod-dependent manner. *Plant J.* **2019**, *98*, 448–464. [CrossRef] [PubMed]
6. Tanaka, M.; Kikuchi, A.; Kamada, H. The Arabidopsis histone deacetylases HDA6 and HDA19 contribute to the repression of embryonic properties after germination. *Plant Physiol.* **2008**, *146*, 149–161. [CrossRef]
7. Tian, L.; Chen, Z.J. Blocking histone deacetylation in Arabidopsis induces pleiotropic effects on plant gene regulation and development. *Proc. Natl. Acad. Sci. USA* **2001**, *98*, 200–205. [CrossRef]
8. Zheng, M.; Liu, X.B.; Lin, J.C.; Liu, X.Y.; Wang, Z.Y.; Xin, M.M.; Yao, Y.Y.; Peng, H.R.; Zhou, D.X.; Ni, Z.F.; et al. Histone acetyltransferase GCN5 contributes to cell wall integrity and salt stress tolerance by altering the expression of cellulose synthesis genes. *Plant J.* **2019**, *97*, 587–602. [CrossRef]
9. Pandey, R.; Muller, A.; Napoli, C.A.; Selinger, D.A.; Pikaard, C.S.; Richards, E.J.; Bender, J.; Mount, D.W.; Jorgensen, R.A. Analysis of histone acetyltransferase and histone deacetylase families of Arabidopsis thaliana suggests functional diversification of chromatin modification among multicellular eukaryotes. *Nucleic Acids Res.* **2002**, *30*, 5036–5055. [CrossRef]
10. Yang, X.J.; Seto, E. Collaborative spirit of histone deacetylases in regulating chromatin structure and gene expression. *Curr. Opin. Genet. Dev.* **2003**, *13*, 143–153. [CrossRef]
11. Murfett, J.; Wang, X.J.; Hagen, G.; Guilfoyle, T.J. Identification of arabidopsis histone deacetylase HDA6 mutants that affect transgene expression. *Plant Cell* **2001**, *13*, 1047–1061. [CrossRef]
12. Aufsatz, W.; Mette, M.F.; van der Winden, J.; Matzke, M.; Matzke, A.J. HDA6, a putative histone deacetylase needed to enhance DNA methylation induced by double-stranded RNA. *EMBO J.* **2002**, *21*, 6832–6841. [CrossRef] [PubMed]
13. Earley, K.; Lawrence, R.J.; Pontes, O.; Reuther, R.; Enciso, A.J.; Silva, M.; Neves, N.; Gross, M.; Viegas, W.; Pikaard, C.S. Erasure of histone acetylation by Arabidopsis HDA6 mediates large-scale gene silencing in nucleolar dominance. *Genes Dev.* **2006**, *20*, 1283–1293. [CrossRef]
14. Liu, X.C.; Yu, C.W.; Duan, J.; Luo, M.; Wang, K.C.; Tian, G.; Cui, Y.H.; Wu, K.Q. HDA6 Directly Interacts with DNA Methyltransferase MET1 and Maintains Transposable Element Silencing in Arabidopsis. *Plant Physiol.* **2012**, *158*, 119–129. [CrossRef]
15. Probst, A.V.; Fagard, M.; Proux, F.; Mourrain, P.; Boutet, S.; Earley, K.; Lawrence, R.J.; Pikaard, C.S.; Murfett, J.; Furner, I.; et al. Arabidopsis histone deacetylase HDA6 is required for maintenance of transcriptional gene silencing and determines nuclear organization of rDNA repeats. *Plant Cell* **2004**, *16*, 1021–1034. [CrossRef]
16. Chen, L.T.; Luo, M.; Wang, Y.Y.; Wu, K.Q. Involvement of Arabidopsis histone deacetylase HDA6 in ABA and salt stress response. *J. Exp. Bot.* **2010**, *61*, 3345–3353. [CrossRef]
17. Wang, Y.Z.; Hu, Q.; Wu, Z.J.; Wang, H.; Han, S.M.; Jin, Y.; Zhou, J.; Zhang, Z.F.; Jiang, J.F.; Shen, Y.; et al. HISTONE DEACETYLASE 6 represses pathogen defence responses in Arabidopsis thaliana. *Plant Cell Environ.* **2017**, *40*, 2972–2986. [CrossRef] [PubMed]
18. Yu, C.W.; Liu, X.C.; Luo, M.; Chen, C.Y.; Lin, X.D.; Tian, G.; Lu, Q.; Cui, Y.H.; Wu, K.Q. HISTONE DEACETYLASE6 Interacts with FLOWERING LOCUS D and Regulates Flowering in Arabidopsis. *Plant Physiol.* **2011**, *156*, 173–184. [CrossRef]
19. Finnin, M.S.; Donigian, J.R.; Cohen, A.; Richon, V.M.; Rifkind, R.A.; Marks, P.A.; Breslow, R.; Pavletich, N.P. Structures of a histone deacetylase homologue bound to the TSA and SAHA inhibitors. *Nature* **1999**, *401*, 188–193. [CrossRef] [PubMed]
20. Cousens, L.S.; Gallwitz, D.; Alberts, B.M. Different Accessibilities in Chromatin to Histone Acetylase. *J. Biol. Chem.* **1979**, *254*, 1716–1723.
21. Ma, X.J.; Zhang, C.; Zhang, B.; Yang, C.P.; Li, S.J. Identification of genes regulated by histone acetylation during root development in Populus trichocarpa. *BMC Genom.* **2016**, *17*. [CrossRef] [PubMed]
22. Earley, K.W.; Shook, M.S.; Brower-Toland, B.; Hicks, L.; Pikaard, C.S. In vitro specificities of Arabidopsis co-activator histone acetyltransferases: Implications for histone hyperacetylation in gene activation. *Plant J.* **2007**, *52*, 615–626. [CrossRef] [PubMed]
23. Pagano, A.; Araujo, S.D.; Macovei, A.; Dondi, D.; Lazzaroni, S.; Balestrazzi, A. Metabolic and gene expression hallmarks of seed germination uncovered by sodium butyrate in Medicago truncatula. *Plant Cell Environ.* **2019**, *42*, 259–269. [CrossRef] [PubMed]

24. Ledvinová, D.; Mikulášek, K.; Kuchaříková, H.; Brabencová, S.; Fojtová, M.; Zdráhal, Z.; Lochmanová, G. Filter-Aided Sample Preparation Procedure for Mass Spectrometric Analysis of Plant Histones. *Front. Plant Sci.* **2018**, *9*, 1373. [CrossRef]
25. Wu, K.; Zhang, L.; Zhou, C.; Yu, C.W.; Chaikam, V. HDA6 is required for jasmonate response, senescence and flowering in Arabidopsis. *J. Exp. Bot.* **2008**, *59*, 225–234. [CrossRef]
26. Ma, X.; Lv, S.; Zhang, C.; Yang, C. Histone deacetylases and their functions in plants. *Plant Cell Rep.* **2013**, *32*, 465–478. [CrossRef]
27. Ueda, M.; Matsui, A.; Tanaka, M.; Nakamura, T.; Abe, T.; Sako, K.; Sasaki, T.; Kim, J.M.; Ito, A.; Nishino, N.; et al. The Distinct Roles of Class I and II RPD3-Like Histone Deacetylases in Salinity Stress Response. *Plant Physiol.* **2017**, *175*, 1760–1773. [CrossRef]
28. Hartl, M.; Füßl, M.; Boersema, P.J.; Jost, J.O.; Kramer, K.; Bakirbas, A.; Sindlinger, J.; Plöchinger, M.; Leister, D.; Uhrig, G.; et al. Lysine acetylome profiling uncovers novel histone deacetylase substrate proteins in *Arabidopsis*. *Mol. Syst. Biol.* **2017**, *13*, 949. [CrossRef]
29. Činčárová, L.; Lochmanová, G.; Nováková, K.; Šultesová, P.; Konečná, H.; Fajkusová, L.; Fajkus, J.; Zdráhal, Z. A combined approach for the study of histone deacetylase inhibitors. *Mol. Biosyst.* **2012**, *8*, 2937–2945. [CrossRef]
30. Chang, J.; Varghese, D.S.; Gillam, M.C.; Peyton, M.; Modi, B.; Schiltz, R.L.; Girard, L.; Martinez, E.D. Differential response of cancer cells to HDAC inhibitors trichostatin A and depsipeptide. *Br. J. Cancer* **2012**, *106*, 116–125. [CrossRef]
31. Krämer, O.H.; Zhu, P.; Ostendorff, H.P.; Golebiewski, M.; Tiefenbach, J.; Peters, M.A.; Brill, B.; Groner, B.; Bach, I.; Heinzel, T.; et al. The histone deacetylase inhibitor valproic acid selectively induces proteasomal degradation of HDAC2. *EMBO J.* **2003**, *22*, 3411–3420. [CrossRef] [PubMed]
32. Marks, P.A.; Xu, W.S. Histone deacetylase inhibitors: Potential in cancer therapy. *J. Cell Biochem.* **2009**, *107*, 600–608. [CrossRef] [PubMed]
33. Xu, C.R.; Liu, C.; Wang, Y.L.; Li, L.C.; Chen, W.Q.; Xu, Z.H.; Bai, S.N. Histone acetylation affects expression of cellular patterning genes in the Arabidopsis root epidermis. *Proc. Natl. Acad. Sci. USA* **2005**, *102*, 14469–14474. [CrossRef] [PubMed]
34. Chen, D.H.; Huang, Y.; Jiang, C.; Si, J.P. Chromatin-Based Regulation of Plant Root Development. *Front. Plant Sci.* **2018**, *9*, 1509. [CrossRef] [PubMed]
35. Schindelin, J.; Arganda-Carreras, I.; Frise, E.; Kaynig, V.; Longair, M.; Pietzsch, T.; Preibisch, S.; Rueden, C.; Saalfeld, S.; Schmid, B.; et al. Fiji: An open-source platform for biological-image analysis. *Nat. Methods* **2012**, *9*, 676–682. [CrossRef] [PubMed]
36. Vizcaíno, J.A.; Csordas, A.; Del-Toro, N.; Dianes, J.A.; Griss, J.; Lavidas, I.; Mayer, G.; Perez-Riverol, Y.; Reisinger, F.; Ternent, T.; et al. 2016 update of the PRIDE database and its related tools. *Nucleic Acids Res.* **2016**, *44*, 11033. [CrossRef]
37. Aitchison, J. The Statistical-Analysis of Compositional Data. *J. Roy. Stat. Soc. B Met.* **1982**, *44*, 139–177. [CrossRef]
38. Hron, K.; Templ, M.; Filzmoser, P. Imputation of missing values for compositional data using classical and robust methods. *Comput. Stat. Data Anal.* **2010**, *54*, 3095–3107. [CrossRef]
39. R Core Team. R: A Language and Environment for Statistical Computing, R Foundation for Statistical Computing: 2018. Available online: http://www.R-project.org (accessed on 15 May 2019).

International Journal of
Molecular Sciences

MDPI

Article

Nuclear Disposition of Alien Chromosome Introgressions into Wheat and Rye Using 3D-FISH

Veronika Koláčková [1], Kateřina Perničková [1], Jan Vrána [1], Martin Duchoslav [2], Glyn Jenkins [3], Dylan Phillips [3], Edina Turkosi [4], Olga Šamajová [5], Michaela Sedlářová [2], Jozef Šamaj [5], Jaroslav Doležel [1] and David Kopecký [1,*]

1 Institute of Experimental Botany of the Czech Academy of Sciences, Centre of the Region Haná for Biotechnological and Agricultural Research, Šlechtitelů 31, 78371 Olomouc, Czech Republic
2 Department of Botany, Faculty of Science, Palacký University Olomouc, Šlechtitelů 27, 783 71 Olomouc, Czech Republic
3 Institute of Biological, Environmental and Rural Sciences, Aberystwyth University, Aberystwyth, Ceredigion, Wales SY23 3DA, UK
4 Agricultural Institute, Centre for Agricultural Research, Hungarian Academy of Sciences, H-2462 Martonvásár, P.O. Box 19, Hungary
5 Department of Cell Biology, Centre of the Region Haná for Biotechnological and Agricultural Research, Faculty of Science, Palacký University Olomouc, Šlechtitelů 27, 783 71 Olomouc, Czech Republic
* Correspondence: kopecky@ueb.cas.cz; Tel.: +420-5-8523-8723

Received: 2 August 2019; Accepted: 24 August 2019; Published: 25 August 2019

Abstract: During interphase, the chromosomes of eukaryotes decondense and they occupy distinct regions of the nucleus, called chromosome domains or chromosome territories (CTs). In plants, the Rabl's configuration, with telomeres at one pole of nucleus and centromeres at the other, appears to be common, at least in plants with large genomes. It is unclear whether individual chromosomes of plants adopt defined, genetically determined addresses within the nucleus, as is the case in mammals. In this study, the nuclear disposition of alien rye and barley chromosomes and chromosome arm introgressions into wheat while using 3D-FISH in various somatic tissues was analyzed. All of the introgressed chromosomes showed Rabl's orientation, but their relative positions in the nuclei were less clear. While in most cases pairs of introgressed chromosomes occupied discrete positions, their association (proximity) along their entire lengths was rare, and partial association only marginally more frequent. This arrangement is relatively stable in various tissues and during various stages of the cell cycle. On the other hand, the length of a chromosome arm appears to play a role in its positioning in a nucleus: shorter chromosomes or chromosome arms tend to be located closer to the centre of the nucleus, while longer arms are more often positioned at the nuclear periphery.

Keywords: 3D-FISH; barley; chromatin; hybrid; introgression; nucleus; rye; wheat

1. Introduction

During interphase, eukaryotic chromosomes decondense and occupy distinct regions of the nucleus, named chromosome territories or chromosome domains [1,2]. Each chromosome territory (CT) is a complex structure of irregular shape and it appears to be largely stable during the interphase of the cell cycle [3–5]. Although CTs are spatially separated from each other by interchromosomal domains, there are regions where neighboring territories intermingle [6].

Chromosome painting, where whole chromosome probes are used for FISH of single CTs or groups of CTs, showed that interphase chromosomes are radially arranged in human [7,8] primates [9], chicken [10], and mouse [5]. This type of the CT arrangement appears to be evolutionary conserved among vertebrates [11,12]. However, the radial chromosome arrangement has not been observed

in flowering plants. Instead, chromosome territories show two predominant configurations, which are known as Rabl's and Rosette. In the Rabl's orientation [13], centromeres are grouped at, or close to, the nuclear periphery at one pole of the nucleus, while telomeres are dispersed at the opposite pole [14]. This configuration is found in many large-genome plant species and is a remnant of anaphase chromosome movement [15]. A completely different type of nuclear organization has been observed in *Arabidopsis thaliana* (L.) Heynh., where the CTs exhibit rosette-like structures [16]. Centromeres are randomly distributed at the nuclear periphery, while telomeres congregate around the nucleolus. Centromeric heterochromatin forms distinct chromocenters, and euchromatin domains, where the majority of genes are located, create 0.2–2Mb loops that result in rosette-like structures of interphase chromosomes [16–18]. The position of CTs and the arrangement of heterochromatin domains is mostly random in differentiated as well as in meristematic tissues, except for chromosomes with nucleolar organizing regions (NORs), which associate with the nucleolus [16,19].

There is a growing evidence that links nuclear architecture with gene expression. Structural genes are often regulated by loci that are located far from the genes themselves, and sometimes even on different chromosomes. Methodological advances provided a way to map in detail the contacts between genes and their regulators, including promoters and enhancers. The method of chromosome conformation capture (3C) and its modifications, such as 4C and Hi-C, reveal contacts between chromatin fibres [20,21]. Using Hi-C, Dixon et al. [22] found that DNA within each chromosome territory is organized into chromatin domains, which can change their spatial conformation. Chromatin fibres within and between these topologically associated domains (TADs) can interact and affect gene expression via the formation of new contacts between enhancers and promoters, or by interrupting the existing contacts. These interactions are reorganized during growth and development, and in reaction to external factors [23,24].

Merging two genomes via interspecific hybridization may alter chromatin organization, and hence the interactions between genes and their regulatory elements. Gene expression studies on ancient and newly developed allopolyploids reveal substantial changes in gene expression [25]. However, the organization of parental chromatin in interspecific hybrids, as well as its effect on gene expression, remains poorly understood. In Chinese hamster × human hybrid cell lines, the human X chromosome (as the only human chromosome present) is located in a distinct chromatin body [26]. Similarly, Sengupta et al. [27] provided evidence of the stable positioning of gene-poor human chromosomes 7 and 18 on the periphery of human × mouse hybrid nuclei. These results indicate that the location of a CT in a hybrid nucleus might be affected more by its gene content rather than by its parental origin. Even less is known about nuclear architecture in the interspecific hybrids of plants. Chromosome arms of rye (*Secale cereale* L.) introgressed into bread wheat (*Triticum aestivum* L. ssp. *aestivum*) display a typical Rabl's orientation and they appear to be located at the periphery of cell nuclei, while homologous arms are usually spatially separated from each other [28,29]. However, these findings were based on two-dimensional (2D) squash preparations in which the third dimension was compromised.

The studies on spatial CT organization in plants with large genomes, such as wheat, rye, and barley, are hampered by the lack of chromosome-specific painting probes for FISH. A solution is to use alien chromosome introgressions or substitutions and visualize alien chromosomes by genomic *in situ* hybridization (GISH) while using labelled genomic DNA from the donor species. This study employed this approach to shed more light on the spatial organization of parental genomes in the somatic nuclei of interspecific plant hybrids and to compare the nuclei from different cell cycle phases, various tissues, with contrasting relative proportions of parental genomes and varying the lengths of introgressed chromosomes (or arms). A combination of a wide set of various introgression lines (rye introgressions in wheat, barley in wheat and wheat in rye), 3D-GISH, confocal microscopy, and visualization of parental chromatin in software Imaris, made it possible to evaluate the potential impacts of the above-mentioned features on the position of the introgressed alien chromatin.

2. Results

2.1. Morphometric Characteristics of G_1 Nuclei of Wheat-Rye and Wheat-Barley Chromosome Introgression Lines

In total, 481 G_1 nuclei were analyzed, isolated from root tips of plants carrying rye or barley chromatin introgressed into wheat background or wheat chromatin introgressed into rye background (Figures 1 and A1–A3). The parameters that are described in Materials and Methods were evaluated. Generally, the morphology of the G_1 nuclei, which were flow sorted into polyacrylamide gels, ranged from spherical and ellipsoidal to irregular shapes with varying degree of contortion. Only nuclei with spherical and slightly ellipsoidal shapes were selected for analyses. In 3D-GISH, the CTs of introgressed chromosomes or chromosome arms appeared as compact structures of regular shapes that were arranged in a typical Rabl's orientation. Centromeres and telomeres of the host chromosomes also displayed Rabl's configuration. Centromeres were generally close to each other and located at the nuclear periphery at one pole of the nucleus, while the telomeres were located at the opposite pole and usually dispersed over larger volume of the nuclei than the centromeres. In a majority of cases, the centromeres of introgressed chromosomes or chromosome arms were closer to each other than their telomeres and arm mid-points (MA). The distances between the arm mid-points and between their telomeres are similar in a majority of lines (Table 1).

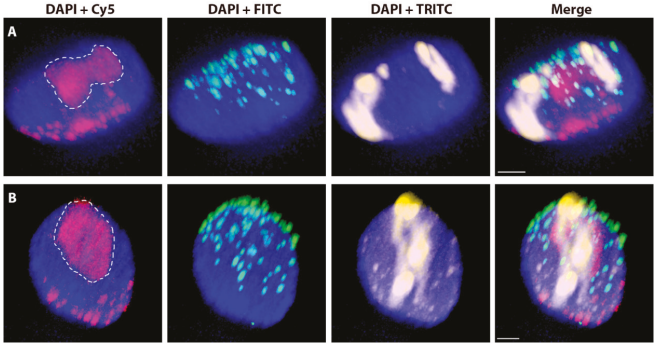

Figure 1. Nuclei (from root tips) with rye chromosomes in wheat background after 3D-FISH. (**A**) Nucleus with a pair of rye 1R chromosomes substituted for wheat chromosomes 1A. (**B**) Nucleus with a pair of rye $_{del}$1RS.1RL chromosomes. Total genomic DNA of rye was labelled with TRITC using Nick translation (yellow), centromeres of both wheat and rye chromosomes were visualized using oligonucleotide probe (magenta), and telomere-specific sequence was PCR-labelled with FITC (green). Nuclear DNA was counterstained with DAPI (blue). Nucleoli areas are indicated by white dashed lines. Scale bar 3 μm.

Among all the analyzed nuclei, there are 315 G_1 nuclei carrying various introgressions of rye chromatin into wheat background (Figures 1 and A1). Volumes of these nuclei range from 753 to 3407 μm^3 (average 1618 μm^3). The lengths of individual rye chromosome arms ranged from 3.7 μm to 20.9 μm. For wheat chromosomes introgressed into rye background, 40 G_1 nuclei were analyzed (Figure A2). Nuclear volumes range from 1029 to 2535 μm^3 (average 1514 μm^3) and lengths of individual wheat chromosome arms range from 1.8 to 12.2 μm. For barley introgressions into wheat background, the total number of analyzed G_1 nuclei is 126 (Figure A3). The nuclear volumes range from 900 to 3872 μm^3 (average 1721 μm^3) and lengths of individual barley chromosome arms range from 1.4 μm to 15.1 μm. In lines 6H and 6HS, the nucleolus is frequently present on the short arm; the secondary constriction, which makes the arm longer: the average length of the 6HS arm, including the nucleolus is 6.7 and 4.1 in complete chromosome 6H and telocentric 6HS; when the nucleolus constriction is excluded from the total measurements, it is 4.2 and 3.5 μm for 6H and 6HS, respectively.

Table 1. Morphometric characteristics of introgressed chromosome arms in wheat-rye and wheat-barley introgression lines.

Introgression	Introgressed Chromosome Arm Length[3] (Mb)	Chromosome Length (Mb)	Arm Ratio	Nuclear Volume (μm^3)	Arm Length (µm)	C-C (µm)	MA1-MA2 (µm)	T-T (µm)	CN-MA (µm)
1AS.1RL	626	902	2.27	1545 ± 228	7.73 ± 1.48	4.01 ± 1.98	5.11 ± 2.28	4.88 ± 1.71	3.55 ± 0.84^{a}
1RS.1BL	423	959	1.27	1501 ± 362	8.21 ± 1.69	3.49 ± 1.50	4.42 ± 1.64	4.18 ± 1.66	3.57 ± 1.01^{a}
1RS.1DL	423	804	0.90	1998 ± 285	6.86 ± 1.31	2.83 ± 1.15	3.55 ± 1.63	3.71 ± 1.74	2.82 ± 0.78^{b}
2RS.2BL	595	1102	0.85	1597 ± 490	8.51 ± 2.58	3.38 ± 1.70	4.38 ± 2.04	4.09 ± 1.95	3.51 ± 1.22^{a}
2BS.2RL	693	1116	1.64	1510 ± 357	8.96 ± 1.62	4.05 ± 1.80	4.99 ± 2.13	4.99 ± 2.25	3.76 ± 0.97^{a}
5RS.5BL	346	928	1.68	1656 ± 329	6.95 ± 1.54	3.06 ± 1.29	3.68 ± 1.47	3.97 ± 1.48	2.99 ± 0.91^{b}
Test statistics	F (dfg, dfe)$^{p\text{-Value}}$	-	-	-	-	-	-	-	13.55 (5, 195.6)***
$_{del}$1RS.1RL	S[1]: 271 L: 626	897	2.31	1986 ± 390	4.04 ± 1.03 7.56 ± 1.67	2.88 ± 1.37	3.52 ± 1.50 3.87 ± 1.74	3.86 ± 1.79 3.56 ± 1.87	2.82 ± 0.98^{a} 3.13 ± 0.87^{A}
1RS.$_{del}$1RL	S: 423 L[2]: 438	861	1.04	2006 ± 500	6.18 ± 1.58 5.21 ± 1.41	3.57 ± 1.69	4.19 ± 1.88 4.06 ± 1.83	4.20 ± 1.92 4.12 ± 1.53	3.05 ± 1.00^{a} 3.09 ± 1.00^{A}
1R(1A)	S: 423 L: 626	1049	1.48	1196 ± 143	8.58 ± 1.79 9.88 ± 1.87	4.09 ± 2.41	5.45 ± 2.27 5.22 ± 2.76	4.99 ± 2.32 4.23 ± 2.47	4.12 ± 1.27^{b} 4.09 ± 1.24^{B}
t1RS	423	423	-	1190 ± 109	8.84 ± 1.77	4.15 ± 1.86	4.94 ± 2.26	4.67 ± 2.09	4.21 ± 1.19^{b}
Test statistics	F (dfg, dfe)$^{p\text{-Value}}$	-	-	-	-	-	-	-	S: 18.76 (3, 93.9.)*** L: 10.57 (2, 82.5)***
3B	S: 433 L: 562	995	1.30	1535 ± 315	5.63 ± 1.47 6.91 ± 1.81	4.30 ± 1.52	5.39 ± 1.7 4.96 ± 1.79	5.35 ± 2.02 4.22 ± 1.93	3.83 ± 0.98 3.76 ± 1.03
5B	S: 290 L: 580	870	2.00	1492 ± 383	4.30 ± 1.67 6.96 ± 1.94	4.48 ± 1.93	4.96 ± 1.86 5.13 ± 1.86	4.82 ± 1.62 3.61 ± 1.77	3.65 ± 1.24 3.60 ± 1.07
Test statistics	F (dfg, dfe)$^{p\text{-Value}}$	-	-	-	-	-	-	-	S: 0.54 (1, 74.2)$^{n.s.}$ L: 0.46 (1, 77.9)$^{n.s.}$
3H	S: 294 L: 406	700	1.38	1316 ± 328	5.74 ± 1.48 6.96 ± 1.94	3.7 ± 2.2	4.54 ± 2.26 3.95 ± 1.98	5.25 ± 2.46 4.36 ± 1.88	3.98 ± 1.43 3.70 ± 1.25
6H	S: 261 L: 322	583	1.23	1848 ± 352	4.13 ± 1.78 (3.46 ± 1.08) 5.68 ± 1.69	3.77 ± 1.59	4.22 ± 1.71 4.29 ± 2.08	4.99 ± 1.76 4.71 ± 1.96	3.18 ± 1.00 3.05 ± 1.08
Test statistics	F (dfg, dfe)$^{p\text{-Value}}$	-	-	-	-	-	-	-	S: 8.30 (1, 69.9)** L: 6.13 (1, 76.4)*
3HL	406	406	-	1419 ± 358	8.19 ± 1.91	2.88 ± 1.49	3.81 ± 2	3.93 ± 2.64	3.65 ± 1.12
3HS	294	294	-	2182 ± 646	4.14 ± 0.97	2.73 ± 1.66	3.08 ± 1.93	3.33 ± 1.99	3.19 ± 1.10
6HL	322	322	-	1695 ± 307	5.46 ± 1.33	2.9 ± 2.06	3.98 ± 2.83	3.97 ± 2.97	3.34 ± 1.29
6HS	261	261	-	1868 ± 609	6.65 ± 1.79 (4.23 ± 1.06)	3.15 ± 1.76	4.26 ± 2.24	4.59 ± 2.45	3.35 ± 1.16
Test statistics	F (dfg, dfe)$^{p\text{-Value}}$	-	-	-	-	-	-	-	1.37 (3, 92.7)$^{n.s.}$

The values (mean ± SD) of arm length, distances between centromeres (C-C), between mid-points of the arms (MA1-MA2), between telomeres (T-T), and arm mid-points to the centre of nucleus (MA-CN) were standardized according to the volume of the nucleus (absolute distance in µm/nuclear volume × 1000). For 6H and 6HS, the arm length without nucleolus is given in brackets. Differences in mean values of centre of the nucleus and the chromosome arm (CN-MA) among introgression lines were tested by general linear models using the F-test. Individual comparison tests were done using the Bonferroni adjusted probability level. Significantly different means of respective characteristic among introgression lines are coded by different letters column-wise and separately for each introgression group and short/long arm, if available (p Value coding: *** $p \leq 0.001$, ** $0.001 < p \leq 0.01$, * $0.01 < p \leq 0.05$, n.s., not significant with $p > 0.05$). [1] deletion of proximal about 36% of 1RS; [2] deletion of proximal about 30% of 1RL; [3] estimated values of chromosome and chromosome arm length and arm ratios were calculated from rye karyotypes of Schlegel et al. [30] and Naranjo [31], from Gill et al. [32], Paux et al. [33] and Salina et al. [34] for wheat, and from Mascher et al. [35] for barley and genome size estimations [36].

In total, 44 G_1 nuclei of triticale were analyzed (Table 2). The CTs of wheat and rye chromatin are readily distinguishable from each other and they do not appear to intermingle (Figure 2, Video S1). All of the chromosomes display Rabl's configuration with their centromeres located close to each other at the nuclear periphery. The nuclear volume of tetraploid triticale ranged from 600 to 1587 μm^3 (average 993 μm^3). On average, 53.6% of this volume is occupied by rye chromatin, while 46.4% is occupied by wheat chromatin. The nuclear volume of hexaploid triticale ranged from 1097 to 2322 μm^3 (average 1412 μm^3), with 37.7% of the nuclear volume belonging to rye chromatin, while 62.3% is occupied by wheat chromatin. These values, for both ploidy levels in triticale, appear to be directly related to the relative DNA contents of the wheat and rye genomes.

Table 2. Characteristics of G_1 nuclei of tetraploid and hexaploid triticale (mean ± SD).

Triticale	Number of Nuclei	Nuclear Volume (μm^3)	Rye Chromatin (%)	Wheat Chromatin (%)
4×	22	993 ± 260	53.6 ± 4.7	46.4 ± 4.7
6×	22	1412 ± 274	37.7 ± 10.0	62.3 ± 10.1

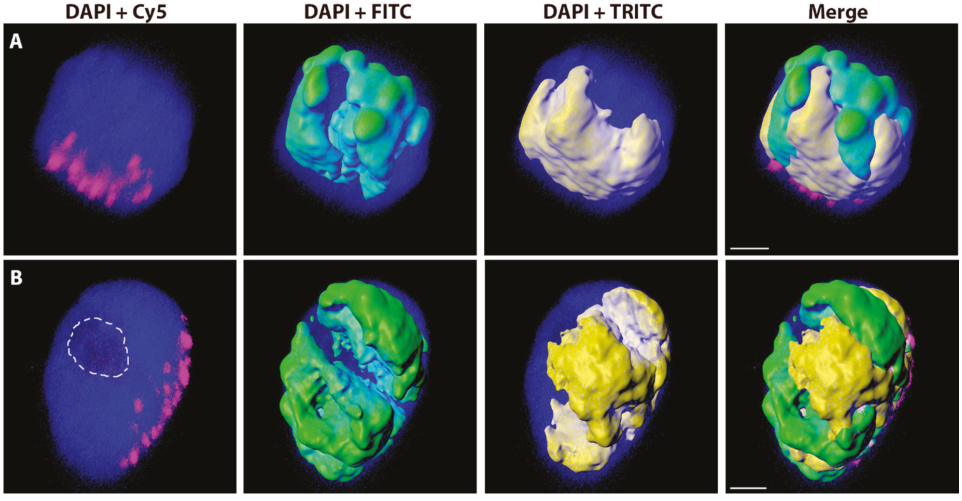

Figure 2. Nuclei of tetraploid (**A**) and hexaploid (**B**) triticale with labelled rye and wheat chromatin. Total genomic DNA of rye was labelled with FITC using Nick translation (green), total genomic DNA of wheat was labelled with TRITC (yellow), and centromeres of both wheat and rye chromosomes were visualized using oligonucleotide probe (magenta). Nuclear DNA was counterstained with DAPI (blue). Wheat and rye chromatin was visualized in Imaris 9.2 using the 'Surfaces' function. The nucleolus area is indicated by a white dashed line. Scale bar 3 μm.

2.2. Variation in the Spatial Arrangements in G_1 Nuclei of Alien Chromosome Arms in Various Wheat-Rye and Wheat-Barley Introgression Lines

There appears to be a relationship between the spatial positioning of a rye chromosome arm and its length. The shortest complete rye chromosome arm, 5RS, tracks most frequently through the inner volume of the nucleus, while the longest arm, 2RL, is more frequently located on the periphery, close to the nuclear envelope. Chromosome arm length and the arm ratio on the spatial positioning of a chromosome arm, the distances between the mid-points of rye arms, and the centres of the nuclei (MA-CN) were compared, after standardization for the nuclear volume to test the possible effect of chromosome length (Table 1). The range of cytogenetic stocks analyzed (centric translocations, deletion lines, additions, and telosomic lines) made it possible to analyze spatial positioning using independent tests involving various configuration of 1R or its arms, with varying chromosome lengths, chromosome

arm lengths and arm ratios (test 1 and 2 for positioning of 1RS and 1RL, respectively), six centric translocations lines (test 3), two addition lines of wheat chromosomes to tetraploid rye (test 4), two whole-chromosome additions of barley chromosomes to wheat (3H, 6H) (test 5), and four telosomic additions of barley chromosome arms to wheat (test 6). Similarly, the arms of the longest wheat chromosome, 3B, present in rye, are more peripherally located than the arms of 5B, a shorter wheat chromosome. Barley introgressions in wheat show a similar pattern: chromosome arms of the longer chromosome 3H occupy more peripheral positions than those of the shorter chromosome 6H (Table 1).

Test 1: Deletion in 1RS in $_{del}$1RS.1RL resulted in a much more central position of this arm than in a normal 1R. Interestingly, separating 1RS from the long arm in t1RS changes the positioning of this arm to the most peripheral among all the 1RS arms analyzed in this study. The MA-CN distances are different for the 1RS arm in different configurations (1R, $_{del}$1RS.1RL, 1RS.$_{del}$1RL, and t1RS). These configurations formed two homogeneous groups: one containing 1R(1A) and t1RS introgressions with significantly higher MA-CN than the second group, containing all the remaining 1RS introgressions (1RS.$_{del}$1RL, $_{del}$1RS.1RL). There is a strong and significant positive correlation between MA-CN and the arm length (r_s = 1.00, $p << 0.001$), a weak positive correlation of MA-CN with the chromosome length (r_s = 0.50, p = 0.67) and a negative correlation with the arm ratio (r_s = −0.50, p = 0.66). As telocentric t1RS only comprises a single chromosome arm, it was excluded from the analysis of correlations between MA-CN and chromosome length and between MA-CN and the arm ratio.

Test 2: Variation in MA-CN among introgression lines was also observed for the 1RL arm. The 1RL arm reduced in length by ca. 30% by a deletion is located in a more central position in the nucleus relative to the complete arm. The short arm appeared to play a role in positioning of the long arm: 1RL displayed the most peripheral location when present in 1R, followed by 1RS.$_{del}$1RL and $_{del}$1RS.1RL (Table 1). Correlations between MA-CN and chromosome length (r_s = 1.00, $p << 0.001$), chromosome arm length (r_s = 1.00, $p << 0.001$), and arm ratio (r_s = 0.50, p = 0.67) are positive and highly significant.

Test 3: Centric translocations significantly differ in the MA-CN distances, and they form two homogeneous groups: one containing 1RS.1DL and 5RS.5BL, with significantly shorter MA-CN than the second group containing all the remaining centric translocations (Table 1). There are weak to strong positive correlations between MA-CN and chromosome length (r_s = 0.71, p = 0.11), the arm length (r_s = 0.83, p = 0.04), and arm ratio (r_s = 0.26, p = 0.62).

Test 4: 3B and 5B introgressions into tetraploid rye do not differ with respect to the MA-CN distance for either the short or long arms (Table 1). There is a clear tendency of MA-CN to increase with the chromosome length and chromosome arm length, and decrease with the arm ratio for the short arms. For the long arms, MA-CN increased with chromosome length and decreased with both the arm length and arm ratio (not tested due to n = 2).

Test 5: 3H, 6H introgressions in wheat significantly differ with respect to the MA-CN distance for both the short and long arms (Table 1). There is a clear tendency for MA-CN to increase with the chromosome length, chromosome arm length, and arm ratio for both short and long arms (not tested due to n = 2).

Test 6: 3HL, 3HS, 6HL, 6HS introgressions in wheat did not differ with respect to the MA-CN distance (Table 1). There is a weak positive correlation between MA-CN and the chromosome arm length (r_s = 0.40, p = 0.60).

All six tests support the hypothesis that chromosome length and chromosome arm length affect spatial positioning of a chromosome arm in a three-dimensional (3D) nucleus. Longer chromosomes and longer chromosome arms tend to be more peripherally located, while shorter chromosomes and chromosome arms are preferentially located in the interior of the nucleus. Regardless of the positioning of the arm in the nuclear volume, all of the chromosomes and arms still display the Rabl's organization.

2.3. The Effect of the Cell Cycle Stages and Tissue-Specificity

To evaluate the possible changes of nuclear characteristics and chromosome positions in various stages of the cell cycle, the 3D-FISH experiments were repeated on the G_2 and S-phases nuclei that

were isolated from root tips of four selected wheat-rye introgression lines (Table 3). Morphologically, the nuclei in G_2 and S were similar to those in G_1 (Figure 3) and so the same shape criteria were used to select nuclei for analyses and the same parameters were measured. As in G_1, introgressed chromosomes or chromosome arms are arranged in Rabl's configuration with their centromeres and telomeres being located on the opposite poles of the nuclei. The fluorescent signal from the genomic probe did not allow for us to distinguish the two chromatids during or after DNA replication in S- or G_2-phase nuclei, respectively.

In total, 85 nuclei in the S phase and 90 nuclei in G_2 were analyzed. Their volumes ranged from 1252 to 3236 μm^3 (average 2076 μm^3) and from 1061 to 4313 μm^3 (average 2456 μm^3) for S and G_2 phases, respectively. The lengths of individual rye chromosome arms in the S-phase ranged from 1.4 to 11.4 μm, and from 2.2 to 9.9 μm in S and G_2, respectively. Relative to the values that were observed in the G_1 nuclei (Table 1), introgressed rye chromosome arms appear to be shorter with the cell cycle progression (they are the longest in G_1 and the shortest in G_2), while the volume of the nucleus increases (it is the smallest in G_1 and the largest in G_2) (Table 3). Introgressed chromosome arms usually display the most peripheral position in G_1 and a more central position in G_2 and S nuclei. Interestingly, the shift to more central positioning of 1RS reduced in length by a deletion in $_{del}$1RS.1RL that is evident in G_1, is not observed in S and G_2.

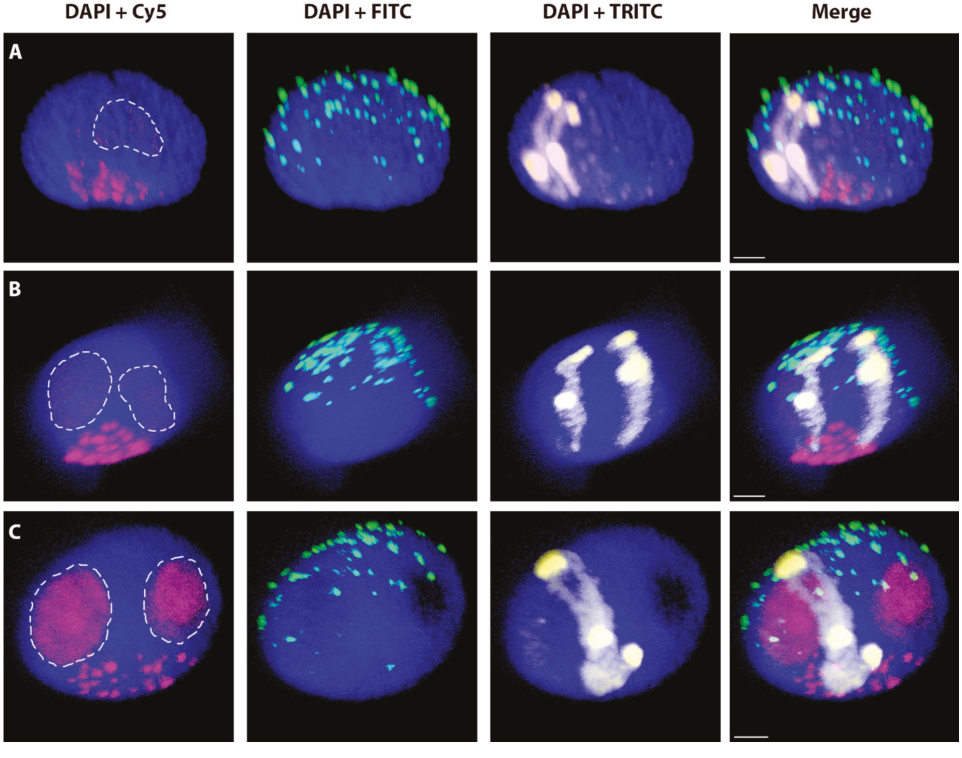

Figure 3. Wheat nuclei with introgressed pair of rye $_{del}$1RS.1RL chromosomes in different cell cycle stages: G_1 phase (**A**), S phase (**B**) and G_2 phase (**C**). Total genomic DNA of rye was labelled with TRITC using Nick translation (yellow), centromeres of both wheat and rye chromosomes were visualized using oligonucleotide probe (magenta), and the telomere-specific sequence was PCR-labelled with FITC (green). Nuclear DNA was counterstained with DAPI (blue). Nucleoli are indicated by white dashed lines. Scale bar = 3 μm. Note more central positioning of rye chromosomes in the progression of cell cycle and no resolution of sister chromatids in G_2.

Table 3. Morphometric characteristics of rye chromosome arms in G_2 and S-phase nuclei of selected wheat-rye introgression lines. The values (mean ± SD) of arm lengths, distances between centromere to centromere (C-C), the mid-point of arm to the mid-point of arm (MA1-MA2), telomere to telomere (T-T), and mid-point of arms to centre of nucleus (MA-CN) were standardized according to the volume of the nucleus (absolute distance in μm/nuclear volume × 1000). Differences in mean values of selected characteristics among the cell cycle stages within each introgression were tested by general linear models using the F-test. Individual tests were done using the Bonferroni adjusted probability level. Significantly different means of respective characteristic among stages are coded by different letters column-wise and separately for each introgression and short/long arm, if available (p value coding: *** $p \leq 0.001$, ** $0.001 < p \leq 0.01$, * $0.01 < p \leq 0.05$, n.s., not significant with $p > 0.05$).

Introgression	Cell Cycle Stage	Nuclear Volume (μm^3)	Arm Length (μm)	C-C (μm)	MA1-MA2 (μm)	T-T (μm)	MA-CN (μm)
1AS.1RL	G_1	1545 ± 228^{a}	7.73 ± 1.48^{a}	4.01 ± 1.98	5.11 ± 2.28	4.88 ± 1.71	3.55 ± 0.84^{a}
	S	1791 ± 400^{b}	7.50 ± 1.60^{a}	3.17 ± 1.24	4.28 ± 1.76	3.73 ± 1.47	3.23 ± 0.95^{a}
	G_2	2562 ± 428^{c}	6.13 ± 1.15^{b}	2.12 ± 0.99	2.28 ± 0.74	2.63 ± 1.27	2.43 ± 0.57^{b}
Test statistics	F (dfg, dfe)^{p}-Value	104.6 (2, 77.2)***	20.8 (2, 85.9)***	-	-	-	33.3 (2, 83.2)***
$_{del}$1RS.1RL[1]	G_1	1986 ± 390^{a}	S: 4.04 ± 1.03^{a} L: 7.56 ± 1.67^{A}	2.88 ± 1.37	3.52 ± 1.50 3.87 ± 1.74	3.86 ± 1.79 3.56 ± 1.87	2.82 ± 0.98 3.13 ± 0.87^{A}
	S	2118 ± 367^{a}	S: 3.68 ± 0.85^{ab} L: 6.26 ± 1.07^{B}	2.74 ± 1.45	3.45 ± 1.58 3.71 ± 1.71	3.91 ± 1.61 3.09 ± 1.13	2.70 ± 0.92 2.87 ± 0.91^{AB}
	G_2	2308 ± 246^{b}	S: 3.38 ± 0.79^{b} L: 6.25 ± 1.12^{B}	2.17 ± 0.91	2.59 ± 1.27 2.75 ± 1.46	2.94 ± 1.54 2.15 ± 1.23	2.54 ± 0.72 2.59 ± 0.67^{B}
Test statistics	F (dfg, dfe)^{p}-Value	12.7 (2, 88.1)***	S: 6 (2, 90.5)** L: 12.1 (2, 89.5)***	-	-	-	S: 1.3 (2, 90.0)$^{n.s.}$ L: 5.72 (2, 89.6)**
1R(1A)	G_1	1196 ± 143^{a}	S: 8.58 ± 1.79^{a} L: 9.88 ± 1.87^{A}	4.09 ± 2.41	5.45 ± 2.27 5.22 ± 2.76	4.99 ± 2.32 4.23 ± 2.47	4.12 ± 1.27 4.09 ± 1.24^{A}
	S	2147 ± 507^{a}	S: 5.88 ± 1.41^{a} L: 6.66 ± 1.59^{B}	2.47 ± 1.08	3.49 ± 1.74 3.38 ± 1.77	3.31 ± 1.83 2.79 ± 1.27	2.74 ± 0.80 2.77 ± 0.85^{AB}
	G_2	2584 ± 450^{b}	S: 5.32 ± 1.15^{b} L: 6.03 ± 1.32^{B}	2.48 ± 1.02	3.29 ± 1.48 3.16 ± 1.37	3.13 ± 1.11 2.46 ± 1.08	2.33 ± 0.74 2.36 ± 0.65^{B}
Test statistics	F (dfg, dfe)^{p}-Value	12.7 (2, 88.1)***	S: 6.0 (2, 90.5)** L: 12.1 (2, 89.5)***	-	-	-	S: 1.3 (2, 90.0)$^{n.s.}$ L: 5.7 (2, 89.6)**
t1RS	G_1	1190 ± 109^{a}	8.84 ± 1.77^{a}	4.15 ± 1.86	4.94 ± 2.26	4.67 ± 2.09	4.21 ± 1.19^{a}
	S	2250 ± 367^{b}	5.72 ± 1.23^{b}	3.38 ± 1.69	3.77 ± 1.67	3.31 ± 1.68	2.59 ± 0.76^{b}
	G_2	2371 ± 402^{b}	5.64 ± 1.19^{b}	2.52 ± 1.3	3.21 ± 1.71	2.96 ± 1.51	2.39 ± 0.86^{b}
Test statistics	F (dfg, dfe)^{p}-Value	323.7 (2, 65.0)***	57.7 (2, 82.8)***	-	-	-	37.4 (2, 83.2)***

[1] deletion of about 36% of 1RS arm (proximal part).

Table 4. Morphometric characteristics of introgressed chromosome arms in embryonic and leaf nuclei of selected wheat-rye introgression lines. The values (mean ± SD) of the arm length, distances centromere to centromere (C-C), mid-point of arm to the mid-point of an arm (MA1-MA2), telomere to telomere (T-T), and mid-point of arms to the centre of nucleus (MA-CN) were standardized according to the volume of the nucleus (absolute distance in µm/nuclear volume x 1000). Differences in mean values of selected characteristics among tissue types within each introgression were tested by general linear models using the F-test. Individual comparison tests were done using the Bonferroni adjusted probability level. Significantly different means of respective characteristic among tissue types are coded by different letters columnwise and separately for each introgression and short/long arm, if available (p Value coding: *** $p \leq 0.001$, ** $0.001 < p \leq 0.01$, * $0.01 < p \leq 0.05$, n.s., not significant with $p > 0.05$).

Introgression	Tissue Type	Nuclear Volume (µm^3)	Arm Length (µm)	C-C (µm)	MA1-MA2 (µm)	T-T (µm)	MA-CN (µm)
1AS.1RL	Root tip	1545 ± 228^a	7.73 ± 1.48^a	4.01 ± 1.98	5.11 ± 2.28	4.88 ± 1.71	3.55 ± 0.84^a
	Embryo	1390 ± 277^b	8.43 ± 1.90^a	3.79 ± 2.00	4.65 ± 2.12	5.25 ± 2.59	3.56 ± 1.07^a
	Leaf	678 ± 73^c	11.69 ± 2.6^b	7.67 ± 3.56	6.79 ± 2.95	6.01 ± 2.8	5.58 ± 1.68^b
Test statistics	F (dfg, dfe)$^{p\text{-Value}}$	428.3 (2, 70.3)***	37.8 (2, 79.9)***	-	-	-	26.6 (2, 78.3)***
$_{del}$1RS.1RL[1]	Root tip	1986 ± 390^a	S: 4.04 ± 1.03^a L: 7.56 ± 1.67^A	2.88 ± 1.37	3.52 ± 1.50 3.87 ± 1.74	3.86 ± 1.79 3.56 ± 1.87	2.82 ± 0.98^a 3.13 ± 0.87^A
	Embryo	1210 ± 188^b	S: 4.45 ± 0.97^a L: 8.78 ± 2.03^B	4.76 ± 2.31	5.13 ± 2.50 4.85 ± 2.58	5.52 ± 2.35 5.40 ± 3.23	4.33 ± 1.06^b 4.23 ± 1.14^B
	Leaf	626 ± 131^c	S: 5.75 ± 1.74^b L: 12.36 ± 2.98^C	7.10± 3.25	8.73 ± 3.07 8.48 ± 3.88	9.46 ± 3.01 7.8± 3.86	6.58 ± 2.30^c 6.21 ± 2.44^C
Test statistics	F (dfg, dfe)$^{p\text{-Value}}$	337.7 (2, 82.3)***	S: 14.9 (2, 79.0)*** L: 41.1 (2, 77.6)***	-	-	-	S: 58.9 (2, 75.6)*** L: 36.6 (2, 72.8)***

[1] deletion of about 36% of 1RS arm (proximal part).

The same 3D-FISH experiments were repeated again, on G_1 nuclei from embryonic and leaf cells of two selected wheat-rye introgressions to assess the possible variability of nuclear characteristics and chromosome positions in various plant tissues (Table 4). The morphology of nuclei that were isolated from both tissues, as well as the general organization of chromosomes in the Rabl's configuration, appeared to be similar to the nuclei that were isolated from root tips (Figure 4).

In total, 44 nuclei from embryonic cells and 41 nuclei from leaf mesophyll were analyzed. The nuclear volumes ranged from 938 to 2064 μm^3 (average 1300 μm^3) in embryonic cells and from 363 to 927 μm^3 (average 651.5 μm^3) in the leaf cells. The lengths of individual rye chromosome arms ranged from 2.8 to 13.7 μm and from 2 to 19.5 μm in nuclei from embryos and from leaves, respectively. When compared to the values that were obtained from the G_1 nuclei from root tips (Table 1), the largest nuclear volume was found in root tips, while the smallest in nuclei from leaf cells. Despite this, the introgressed chromosome arms appeared to be the longest in the root tip nuclei and in embryonic cells, and the shortest in the leaf cell nuclei. In a majority of cases, the distances between introgressed homologous chromosome arms as well as their distances from the centre of the nucleus appear to be the longest in leaf cell nuclei and the shortest in root tip nuclei.

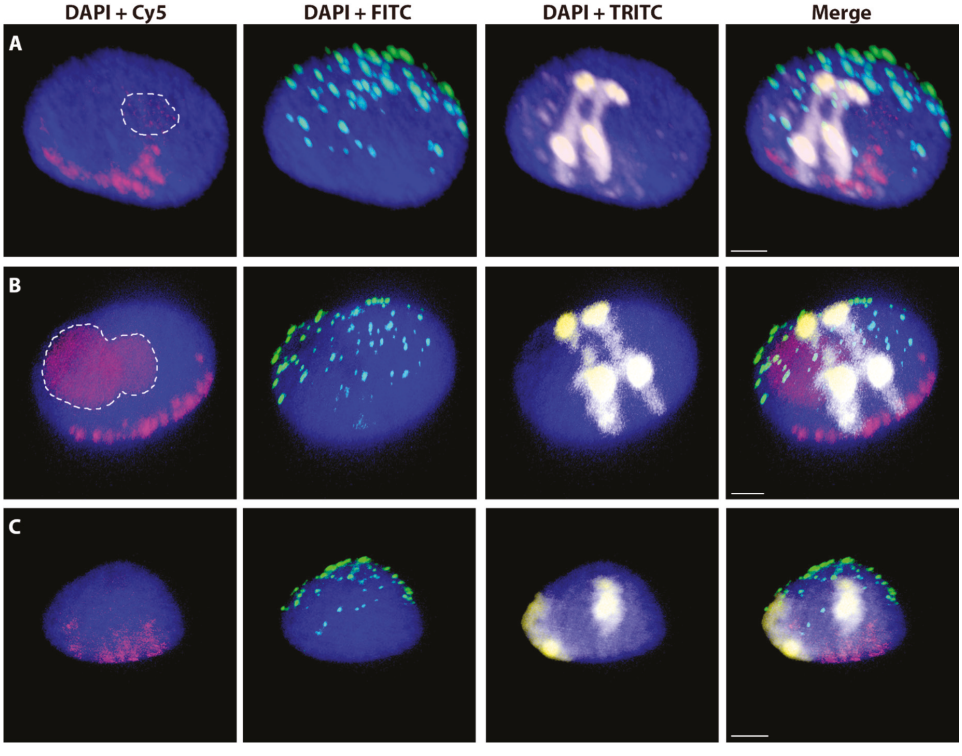

Figure 4. Wheat nuclei with a pair of introgressed rye $_{del}$1RS.1RL chromosomes in various tissues. A nucleus from root tips (**A**), embryos (**B**) and leaf tissue (**C**). Total genomic DNA of rye was labelled with TRITC using Nick translation (yellow), centromeres of both wheat and rye chromosomes were visualized using the oligonucleotide probe (magenta), and telomere-specific sequence was PCR-labelled with FITC (green). Nuclear DNA was counterstained with DAPI (blue). Nucleoli are indicated by white dashed lines. Scale bar 3 μm.

2.4. Spatial Separation vs. Association of Alien Chromosome (Chromosome Arm) Homologues

Visual screening revealed that the territories of pairs of introgressed homologous chromosomes and chromosome arms adopt various types of arrangements (Figure A4). The most frequently observed arrangement across all lines in the G_1 nuclei from root tips (83%) is the complete separation of homologues (Table 5). Complete association along entire homologous arms is evident in only 3.7% of nuclei; 13.3% of nuclei display their partial association. Rye homologues introgressed into the wheat background are completely separated in 82.9% of G_1 nuclei. Partial chromosome association is observed in 14.6% of nuclei, and the complete association of rye homologues was observed in 2.5% of nuclei. Interestingly, in the rye background, not a single nucleus with fully associated wheat homologues was observed; only 5% of such nuclei show partial association, while wheat homologues are completely separated in the remaining nuclei (95%).

Table 5. Numbers of the G_1, S, and G_2 phase nuclei with complete separation, partial association and complete association of introgressed chromosomes or chromosome arms in various tissues of wheat-rye and wheat-barley introgression lines. Unless otherwise stated, the nuclei were in G_1 phase and isolated from root tips.

Introgression	Complete Separation	Partial Association	Complete Association
1AS.1RL (embryo, G_1)	19	1	2
1AS.1RL (leaf, G_1)	16	4	1
1AS.1RL (root tip, G_1)	22	3	
1AS.1RL (root tip, S)	18	3	
1AS.1RL (root tip, G_2)	20	2	1
1RS.1BL	32	7	1
1RS.1DL	37	3	
2RS.2BL	32	8	
2BS.2RL	33	6	1
5RS.5BL	31	7	2
$_{del}$1RS.1RL [1] (embryo, G_1)	16	4	2
$_{del}$1RS.1RL [1] (leaf, G_1)	17		3
$_{del}$1RS.1RL [1] (root tip, G_1)	22	3	
$_{del}$1RS.1RL [1] (root tip, S)	21	1	1
$_{del}$1RS.1RL [1] (root tip, G_2)	15	6	1
1RS.$_{del}$1RL [2]	17	3	1
1R(1A) (G_1)	15	5	2
1R(1A) (S)	15	4	1
1R(1A) (G_2)	18	2	2
t1RS (G_1)	20	1	1
t1RS (S)	20	1	
t1RS (G_2)	19	2	2
3B	20		
5B	18	2	
3H	14	3	3
3HL	18	4	2
3HS	18	2	2
6H	17	2	1
6HL	14	4	2
6HS	19	1	

[1] deletion of proximal about 36% of 1RS arm; [2] deletion of proximal about 30% of 1RL arm.

The frequencies for barley chromosomes or chromosome arms introgressed into wheat are similar to those of rye introgressions. The complete separation of barley homologues is observed in 79.4% of nuclei, while the partial and complete association is displayed by 12.7% and 7.9% of nuclei, respectively.

3D-FISH of embryonic G_1 nuclei from two selected wheat-rye introgression lines shows the complete separation of introgressed homologues in 79.5% of nuclei (Table 5). While 11.4% of embryonic nuclei displayed partial association of rye homologues, complete association is found in 9.1% of nuclei. Similarly, 80.4% of the G_1 nuclei from leaves showed a complete separation of the introgressed chromosomes or chromosome arms. The frequency of both complete and partial associations of rye homologues is the same (9.8% of nuclei). Higher frequencies of complete associations of the introgressed chromosomes or chromosome arms both in leaf and embryonic nuclei, as compared to that obtained from nuclei of root tips were observed.

Rye chromosomes or chromosome arms are completely separated in 80% of G_2 nuclei of four selected wheat-rye introgression lines (Table 5). In 13.3% of the G_2 nuclei, the rye homologues show partial association and only 6.6% of G_2 nuclei showed complete association of rye homologues. In a majority of the S-phase nuclei (87%), rye chromosomes or chromosome arms are completely separated. Partial association is observed in 10.6% of the S-phase nuclei and only 2.4% of S-phase nuclei have completely associated rye chromosomes or chromosome arms. Thus, there are only slight differences when compared to the frequencies that were obtained from the G_1 nuclei.

3. Discussion

The organization of DNA in a nucleus affects many fundamental biological functions, such as replication, gene expression, and chromosome segregation [37]. However, the mechanisms governing spatial organization of CTs in plant cell nuclei, and even chromatin organization itself, are still largely unknown. Large chromosomes in species with large genomes, such as wheat, barley, and rye, assume the Rabl's configuration, while species with small chromosomes and small genomes seem to display different organizations, such as the Rosette observed in *Arabidopsis* [17,29,38–40]. However, genome size *per se* may not be the critical factor in this regard. The current view may be biased toward the species with large genomes, because they are favored as objects of cytogenetic research. Observations in *Brachypodium* have shown that species with small genomes and chromosomes might display the Rabl's configuration: *B. distachyon* (L.) P. Beauv. with a small genome, shows the Rabl's configuration, while *B. stacei* Catalan, Joch.Muell., L.A.J.Mur & T.Langdon and *B. hybridum* Catalán, Joch. Müll., Hasterok & Jenkins with larger genomes appear to have a more random organization of chromosome territories [41]. In the present study, Rabl's orientation of rye chromosome arms was observed in all nuclei. The centromeres were generally more tightly clustered than the telomeres, which is probably a relic of the last anaphase movement. Similarly, Idziak et al. [41] showed that telomeres occupy a larger nuclear space as compared to clusters of centromeric sequences in *Brachypodium*.

The association of homologues or their parts during interphase may facilitate DNA repair via homologous recombination and enable the contacts of genes with their regulatory elements to initiate transcription [42]. However, this study shows that such an association of introgressed homologues is infrequent (~17%). This agrees with a theoretical frequency of random positioning for 42 chromosomes (11.95%) in wheat and with the results of Berr and Schubert [19]. They also found a slightly higher frequency of associations of homologues in the spherical nuclei of various tissues of *Arabidopsis thaliana* than predicted by the SCD (spherical (1Mb) chromatin domain) model of Cremer et al. [8]. Similarly, Mascher et al. [36] identified contacts among chromosomes in barley while using the Hi-C method and found that contacts between homologues only accounted for 13.1–20.9% (16.5%, on average) of all contacts. The spatial association of homologues has been rarely observed in other disomic chromosome introgression lines, using in situ hybridization of squashed tissue samples [43,44]. On the other hand, preferential association of homologues, exceeding random positioning, was observed in the nuclei of *Brachypodium distachyon* and *Drosophila melanogaster* [45,46]. Interestingly, Baroux et al. [47] found the preferential association of one paternal and one maternal homologue in endosperm nuclei of

Arabidopsis (a triploid tissue), leaving one maternal homologue non-associated. In our case, variation in association with homologues among different tissues was also marginal: complete separation ranged from 80% in embryonic and leaf nuclei to 88% in root cells. Similarly, Berr and Schubert [19] found only slight variation in the degree of separation of homologues between spherical nuclei of cotyledon, shoot, stem, and root tissues.

Hiraoka et al. [48] suggested that factors beyond the tissue type, such as the stage of the cell cycle and development, might also affect the spatial alignment of homologues. However, there are no indications that the CT movement occurs during interphase [49,50]. The observations presented here fully support that notion: there were only minor differences among nuclei of four genotypes (rye introgressions in wheat) in different phases of the cell cycle, and in different tissues. Similarly, chromosome arm length was proposed to affect homologue associations, with shorter arms being less likely to be associated than the longer arms [45]. No such correlation was observed in this study. Longer chromosome arms did not associate any more frequently than the shorter ones. Only slight differences were observed among the various stocks tested (wheat chromosomes in rye, barley chromosomes or chromosome arms in wheat, and rye chromosomes or chromosome arms in wheat). This indicates that the organization of chromatin in the 3D space of a nucleus is highly predetermined, at least in the genomes that are involved in this study (wheat, barley, and rye).

On the other hand, considerable variability in the association/separation of homologues among translocation lines may reflect the dynamics of chromatin organization. Variability and movement of chromatin during interphase were observed in several organisms [51]. Chromosomes probably do not actively change their positions, but rather display limited, diffusive movements [52,53], with interstitial chromosome segments generally showing more movement than the centromeres [54]. However, genome organization seems to be flexible enough to allow for the contacts of homologues necessary for DNA repair and initiation of transcription. On the other hand, the general immobility of chromatin plays a key role in the maintenance of genomic stability [55].

It has been reported that cellular differentiation has no major impact on the nuclear organization in various tissues in *A. thaliana* and barley [19,56]. In this study, in the positioning of rye chromosomes during the cell cycle were observed, apart from minor variation in the separation of homologues in nuclei at different phases of the cell cycle, changes. Not surprisingly, the nuclear volume increased during transition through the cell cycle, while the introgressed rye chromosome arms (or chromosomes) became shorter. Interestingly, as they became shorter, they tended to assume more central positions in the nucleus, but were still within Rabl's orientation. This phenomenon was common to all four genotypes tested.

Six independent tests that involved all three types of genotypes (wheat introgression in rye, rye in wheat, and barley in wheat) that were conducted in this study indicated that shorter chromosome arms are more likely to be positioned in the nuclear interior, whereas longer ones are often located at the nuclear periphery. Apart from the chromosome arm length, the total chromosome length also appears to play a role. The same rye chromosome arm 1RS behaved differently when translocated to two different wheat chromosome arms, 1BL and 1DL. The same identical 1RS is more peripheral in 1RS than in 1RS.1DL. Wheat chromosome arm 1BL is considerably longer than 1DL, hence, the translocation chromosome 1RS.1BL is also longer. This difference in positioning of the same chromosome arm present in two translocations of different lengths implies that the position of a chromosome arm in the volume of the nucleus is a function of the chromosome size, and that the length of one arm may affect the position of the entire chromosome. This is further supported by the positioning of the same arms reduced in length by deletions. It appears that the positioning of a chromosome/chromosome arm in the volume of the nucleus, at least in the case of rye introgressions in wheat, is not chromosome-specific (that is, dependent on its gene content), but rather a function of chromosome length. A change in the overall length of a chromosome, such as by translocation to shorter or longer wheat arm, or reduction by deletion, affects the position of the entire chromosome, and not only of the directly affected arm (Table 1). While the general rules of chromosome positioning in the nuclei of plants and animals

appear to be different, Sun et al. [3] and Bolzer et al. [57] reported that smaller human chromosomes were internally positioned and larger chromosomes were close to the nuclear envelope. It is not clear whether or not the length of the chromosome arm itself determines its position. In species with non-Rabl's configuration, it appears that gene density is the critical factor. Gene-dense chromosomes are predominantly positioned close to the nuclear centre while chromosomes with lower gene densities are located towards the nuclear periphery [1,4]. Here, the gene content of all group-1 chromosomes (1A, 1B, 1D, and 1R) is essentially the same, so gene density is a function of the chromosome/chromosome arm length: translocation of the same 1RS to two different wheat arms, both essentially with the same gene content but different length, changes gene density of the entire chromosome. On the other hand, deletions of the gene-poor proximal regions of arms also elevate the gene density of the entire chromosome.

According to Bauer et al. [58], rye chromosome 5R has the highest gene density (3.46 genes per 1Mb), followed by 1R (3.18 genes per 1Mb); gene density in 2R is relatively low (2.83 genes per 1Mb). The physical lengths of the three chromosomes follows the opposite pattern, with 5R being the shortest and 2R the longest in the genome [31]. In this study, 5RS was preferentially located close to the nuclear centre, whereas 2RS more frequently occupied the peripheral positions. However, if there is a general correlation between chromosome length and gene density in rye, there appears no clear way to separate the two factors on chromosome positioning. Different behavior of the same rye arm in two different translocations, 1RS.1DL and 1RS.1BL, each producing a chromosome of different total length, might provide a reasonable approach. There are many clear length differences among homoeologues in wheat. Thus, the same rye chromosome arm translocation to the shortest wheat homoeologue (usually in the D genome) would produce a chromosome of a different total length than translocation to a B-genome homoeologue (usually the largest in the wheat genome). On the other hand, it has not been clarified whether these position effects are of general validity. Random organization of the chromosomes appears to be the case in *Arabidopsis* with the exception of chromosomes 2 and 4. These two chromosomes carry NORs, and since NORs in most cases organize a single nucleolus, these two pairs of chromosomes are physically located more closely to one another than the rest of the genome [16].

Intermingling of the parental genomes in interspecific hybrids with equal proportion of genomes, such as in F1 hybrids of parents with the same numbers of chromosomes (of the same or similar length), is another issue. The pioneering work using sectioned interphase nuclei revealed that genomes of *Hordeum vulgare* and *Secale africanum* Staph. are spatially separated in the *H. vulgare* × *S. africanum* hybrid throughout the cell cycle [59,60]. Moreover, the genome that originates from *H. vulgare* L. tended to be located in a single cluster and positioned centrally in the nucleus. Similarly frequent separation of *Lolium* L. and *Festuca* L. chromatin in interphase nuclei was observed in their F1 hybrids (Kopecký et al., unpublished). On the other hand, not a single nucleus was observed in this study with clear spatial separation of the genomes of wheat and rye (as two hemispheres with the least possible contacts between them), neither in tetraploid nor in hexaploid triticale (Figure 2). Thus, the spatial separation of parental genomes in allopolyploids during the cell cycle is still an open question and more experiments have to be conducted to resolve this issue.

To conclude, this study shows that the chromosome domains of introgressed chromosomes or chromosome arms are highly stable among the tissue types and during the cell cycle phases. Chromosomes uniformly display the Rabl's configuration and homologues are spatially separated, as predicted by the theoretical model. All of the experiments and tests support the hypothesis that shorter chromosomes and chromosome arms are more centrally located in the 3D nucleus, while longer ones are peripherally positioned, close to the nuclear envelope. On the other hand, it appears that the arm ratio itself does not play a role in the positioning of the chromosome and its arms.

4. Materials and Methods

4.1. Plant Material

The plant material consists of a set of lines of common wheat (*Triticum aestivum* L. ssp. *aestivum*, $2n = 6\times = 42$) cv. 'Pavon 76' with introgressions of rye chromosomes or chromosome arms: disomic substitution of rye chromosome 1R for wheat chromosome 1A [1R(1A)], ditelosomic addition line 1RS, a deletion line $_{del}$1RS.1RL(1A), where ca. proximal 36% of the short arm is missing, a deletion line 1RS.$_{del}$1RL(1A) where proximal ca. 30% of the long arm is missing, and homozygotes for centric wheat-rye chromosome translocations 1RS.1BL, 1RS.1DL, 1AS.1RL, 2RS.2BL, 2BS.2RL, and 5RS.5BL. The telosomic line and all centric translocation lines were created by the centric misdivision of complete normal chromosomes of rye and their wheat homoeologues; the deletion chromosomes were identified during selection of centric translocations [61].

Further, a set of alien chromosome addition lines carrying barley (*Hordeum vulgare* L.) cv. 'Manas' chromosomes or chromosome arms in a common wheat (original cross with cv. 'Asakaze', backcrossed to cv. 'Chinese Spring') background (3H, 3HL, 3HS, 6H, 6HL, 6HS) and two lines carrying disomic wheat chromosomes 3B and 5B in a tetraploid rye background was used. Additionally, tetraploid triticale with the genomic constitution AARR and hexaploid triticale cv. 'Rhino' with genomic constitution AABBRR were also involved in the study. All of the materials with rye chromosomes (wheat-rye addition and translocations lines, rye-wheat introgression lines and triticales) were provided by Dr. A.J. Lukaszewski, University of California, Riverside, CA, USA.

Note on terminology: this manuscript uses the original terminology of Bridges (1917) for chromosome aberrations, where "deficiency" is a loss of a terminal chromosome segment and "deletion" indicates a loss of an intercalary segment.

4.2. Isolation of Nuclei by Flow Cytometry Sorting

The isolation of nuclei was performed according to [62]. Nuclei in G_1, G_2, or S phase of the cell cycle were identified and sorted while using a FACSAria II SORP flow cytometer (BD Biosciences, San Jose, CA, USA). About 50,000 nuclei at G_1, G_2, or S phase were obtained for each sample.

Dry seeds were put into water over night to obtain embryonic cells, and after the removal of seed coats they were fixed, as described above. For leaf cells, leaves from mature plants were collected into a tube and fixed in the same way. Seeds and leaves were cut in the meiocyte buffer A to very small pieces by a razor blade. The obtained mixture was filtered through 20 μm nylon mesh into a 5 mL polystyrene tube and processed, as described above.

4.3. Probe Preparation and 3D-FISH

Total genomic DNA of *Secale cereale* L. and *Hordeum vulgare* was labelled with Texas Red or TRITC while using a Nick Translation Kit (Roche Applied Science, Penzberg, Germany) according to manufacturer's instructions, and applied as a probe. A centromeric probe was prepared by PCR using centromere-specific primers [63] and digoxigenin-11-dUTP (Roche Applied Science). The probe was detected with anti-digoxigenin-fluorescein (Roche Applied Science). In some experiments, a combination of telomeric and centromeric probes was used. For the wheat and rye centromeres, an oligonucleotide probe that was based on the sequence of clone pHind258 [63] and directly labelled with Cy5 was used. The telomeric probe was prepared while using PCR and FITC-directly labelled nucleotides. Total genomic DNA of wheat was sheared to 200–500 bp fragments by boiling and used as blocking DNA at a ratio of 1:150 (probe/blocking DNA). To visualize wheat chromosomes in rye background, total genomic DNA of *T. durum* Desf. was labelled with TRITC and then combined with rye blocking DNA (both prepared as described above). For experiments with triticale, rye genomic DNA was labelled with FITC and genomic DNA from *T. durum* was labelled with TRITC (both prepared using a Nick Translation Kit). 3D-FISH experiments were performed, as described in [62].

4.4. Image Acquisition and Analysis

Selected nuclei were optically sectioned while using an inverted laser spinning disk microscope (Axio Observer Z1, Zeiss, Oberkochen, Germany) and ZEN Blue 2012 software; an inverted motorized microscope Olympus IX81 equipped with a Fluoview FV1000 confocal system (Olympus, Tokyo, Japan) and FV10-ASW software; and Axio Imager.Z2 microscope (Zeiss) equipped with confocal Andor DSD2 System and iQ3.6 software (Andor, Belfast, United Kingdom of Great Britain).

For each nucleus, 80–120 optical sections in 160–200 nm steps were taken and then merged into a 3D model. Subsequent analyses were performed while using Imaris 9.2 software (Bitplane, Oxford Instruments, Zurich, Switzerland). Imaris applications 'Contour Surface', 'Spot Detection' and '3D Measurement' were used for the manual analysis of each nucleus. The volume and the centre of the nucleus (CN) were determined from the rendering of primary intensity of DAPI staining while using the function 'Surfaces'. The lengths of introgressed chromosome arms were measured using the 'Polygon' function. The 'Spot' function was used to mark the positions of centromeres (C), telomeres (T), and the mid-points of introgressed chromosome arms (MA). Distances between the centromeres of introgressed homologues (C-C), between their telomeres (T-T) and between their mid-points of arms (MA1-MA2) were measured while using the 'Line' function. For more precise assessment of the distance between the centre of the nucleus and the chromosome arm (CN-MA), distances between three points of the arm (at 25%, 50%, and 75% of the arm length) and the centre of the nucleus for each chromosome arm were measured. Averages of these 3 values were used in subsequent analyses. The nuclear volume of triticale nuclei was calculated as the sum of volumes of the rye and wheat chromatin, both being measured using the 'Surfaces' function. 'Display Adjustment' was used to adjust the channel contrast and, thus, to improve the visualization of all analyzed objects. Between 20 and 40 nuclei were analyzed per genotype.

4.5. Association vs. Separation of Rye Homologous Chromosome Arms in the Wheat Nucleus

The nuclei were visually screened in Imaris to estimate the frequency of association (manifesting itself as physical connection) or separation of targeted chromosomes or chromosome arms, and each nucleus was assigned to one of the categories: 1, complete separation, where no visible connection of the homologous arms was observed; 2, partial association, where a connection in at least a short segment of the chromosome arms was visible; and, 3, complete association, where both homologous chromosomes or chromosome arms were associated along their entire lengths.

4.6. Statistical Data Analysis

The distance between the mid-point of introgressed arms and the centre of nucleus (MA-CN) was used as the main determinant of spatial positioning of introgressed chromosome/chromosome arms in a 3D nucleus. The MA-CN values were compared between the translocation lines while using general linear models (LM) and individual comparison tests were done using Bonferroni adjusted probability level after a significant F test. A similar statistical procedure was used to compare the nuclear volume and arm length. The Spearman correlation coefficient was used to evaluate the relationship between chromosome arm length, chromosome length, arm ratio, and the MA-CN. The MA-CN distances were standardized by nuclear volume as a dependent variable to avoid potential bias caused by nuclear volume variation within and between translocation lines. For statistical evaluation, estimated values of arm ratio, chromosome, and chromosome arm length have been calculated from karyotypes of Schlegel et al. (1987) and Naranjo (2018) for rye, Gill et al. (1991), Paux et al. (2008) and Salina et al. (2018) for wheat, and Mascher et al. (2017) for barley and genome size estimations (Doležel et al., 1998). All statistical analyses were done in NCSS 9 (NCSS 9 Statistical Software; NCSS, LLC; Kaysville, Utah, USA, ncss.com/software/ncss).

Supplementary Materials: Supplementary materials can be found at http://www.mdpi.com/1422-0067/20/17/4143/s1. Video S1. Nucleus of hexaploid triticale with fluorescently labelled rye and wheat chromatin. Total genomic DNA of rye was labelled with FITC using Nick translation (green color), total genomic DNA of wheat was labelled with TRITC (yellow color), and centromeres of both wheat and rye chromosomes were visualized using oligonucleotide probe (magenta color). Nuclear DNA was counterstained with DAPI (blue color). Wheat and rye chromatin was visualized in Imaris 9.2. using 'Surfaces' function.

Author Contributions: Conceptualization, D.K.; Methodology, V.K., K.P. and D.K.; Formal Analysis, V.K., K.P., J.V., M.D., D.P., O.Š. and D.K.; Investigation, V.K., K.P. and D.K.; Resources, J.V., G.J., E.T., O.Š., M.S., J.Š. and J.D.; Data Curation, M.D. and D.K.; Writing—Original Draft Preparation, K.P., M.D. and D.K.; Writing—Review & Editing, V.K., J.V., G.J., E.T., O.Š., M.S., J.Š. and J.D.; Visualization, K.P. and D.K.; Supervision, D.K.; Project Administration, D.K.; Funding Acquisition, J.Š., J.D. and D.K.

Funding: This research was funded by the Czech Science Foundation (grant award 17-13853S) and by the European Regional Development Fund OPVVV project "Plants as a tool for sustainable development" number CZ.02.1.01/0.0/0.0/16_019/0000827 supporting Excellent Research at CRH.

Acknowledgments: We would like to express our thanks to Adam J. Lukaszewski for editing this manuscript and valuable comments.

Conflicts of Interest: The authors declare no conflict of interest.

Abbreviations

3D-FISH	Three-dimensional fluorescent in situ hybridization
CN	Centre of the nucleus
CT	Chromosome territory
GISH	Genomic in situ hybridization
MA	Arm mid-point
NOR	Nucleolar organizing region

Appendix A

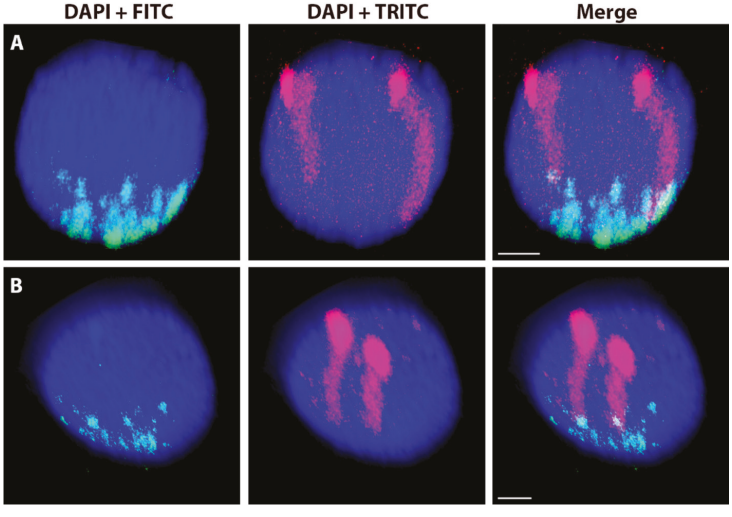

Figure A1. Wheat nuclei with a pair of homologous rye chromosome arms after 3D-FISH. A nucleus of 2BS.2RL (**A**) and 5RS.5BL (**B**) translocation lines. Total genomic DNA of rye was labelled with TRITC using Nick translation (magenta) and the centromere-specific sequence was PCR-labelled with FITC (green). Nuclear DNA was counterstained with DAPI (blue). Scale bar 3 μm.

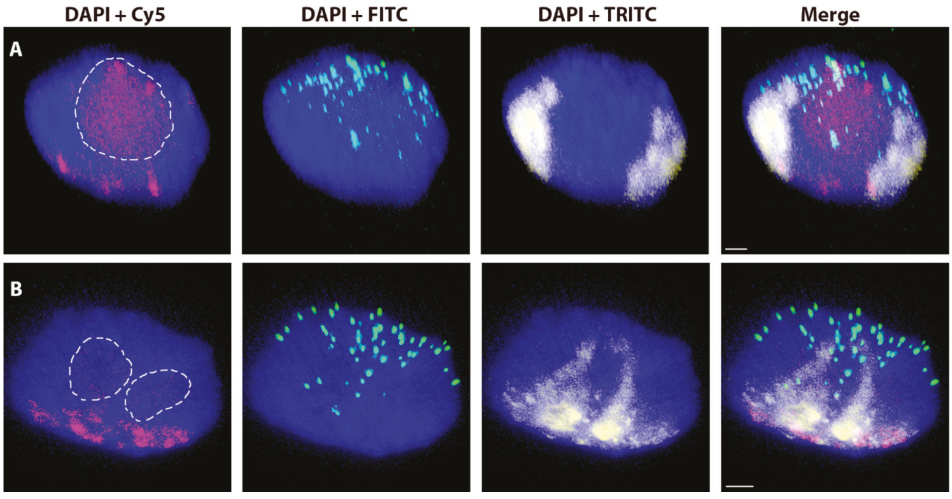

Figure A2. Rye nuclei with a pair of homologous wheat chromosomes. A nucleus carrying chromosome 3B (**A**) and chromosome 5B (**B**). Total genomic DNA of wheat was labelled with TRITC using Nick translation (yellow), centromeres of both wheat and rye chromosomes were visualized using oligonucleotide probe (magenta), and telomere-specific sequence was PCR-labelled with FITC (green). Nuclear DNA was counterstained with DAPI (blue). Nucleoli are indicated by white dashed lines. Scale bar 2 μm.

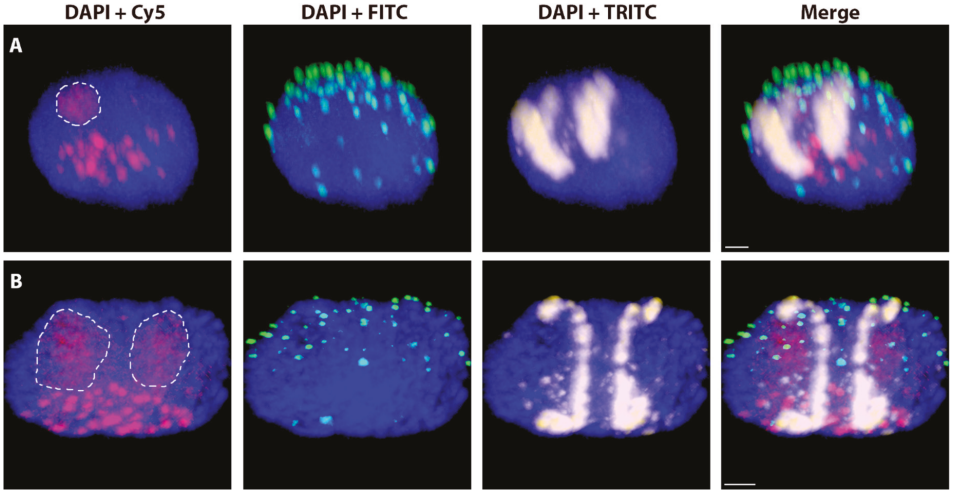

Figure A3. Wheat nuclei with a pair of homologous barley chromosomes. A nucleus carrying chromosome 3H (**A**) and chromosome 6H (**B**). Total genomic DNA of barley was labelled with TRITC using Nick translation (yellow), centromeres of wheat chromosomes were visualized using oligonucleotide probe (magenta), and telomere-specific sequence was PCR-labelled with FITC (green). Nuclear DNA was counterstained with DAPI (blue). Nucleoli are outlined by white dashed lines. Scale bar 3 μm.

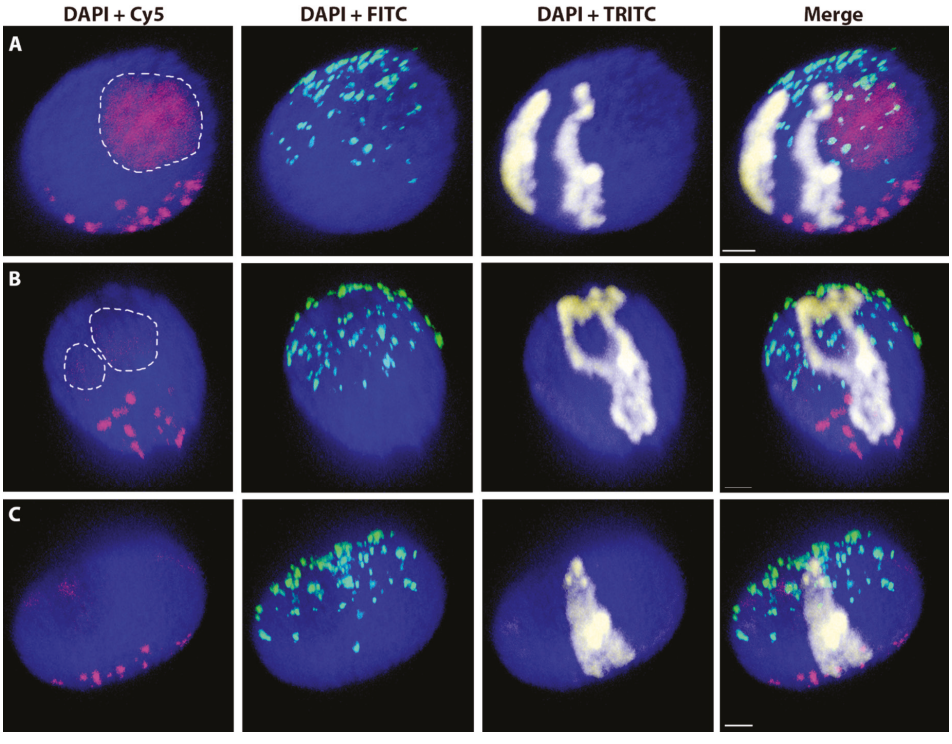

Figure A4. Wheat nuclei with a pair of homologous rye chromosomes $_{del}$1RS.1RL in wheat background. (**A**) Complete separation (**A**), parttaTial association (**B**) and complete association (**C**) of rye homologues. Total genomic DNA of rye was labelled with TRITC using Nick translation (yellow), centromeres of both rye and wheat chromosomes were visualized using oligonucleotide probe (magenta), and telomere-specific sequence was PCR-labelled with FITC (green). Nuclear DNA was counterstained with DAPI (blue). Nucleoli are indicated by white dashed lines. Scale bar 3 μm.

References

1. Cremer, T.; Cremer, C. Chromosome territories, nuclear architecture and gene regulation in mammalian cells. *Nat. Rev. Genet.* **2001**, *2*, 292–301. [CrossRef] [PubMed]
2. Fritz, A.J.; Barutcu, A.R.; Martin-Buley, L.; van Wijnen, A.J.; Zaidi, S.K.; Imbalzano, A.N.; Lian, J.B.; Stein, J.L.; Stein, G.S. Chromosomes at work: Organization of chromosome territories in the interphase nucleus. *J. Cell. Biochem.* **2016**, *117*, 9–19. [CrossRef] [PubMed]
3. Sun, F.L.; Cuaycong, M.H.; Craig, C.A.; Wallrath, L.L.; Locke, J.; Eigin, S.C.R. The fourth chromosome of Drosophila melanogaster: Interspersed euchromatic and heterochromatic domains. *Proc. Natl. Acad. Sci. USA* **2000**, *97*, 5340–5345. [CrossRef] [PubMed]
4. Kozubek, S.; Lukasova, E.; Jirsova, P.; Koutna, I.; Kozubek, M.; Ganova, A.; Bartova, E.; Falk, M.; Pasekova, R. 3D Structure of the human genome: order in randomness. *Chromosoma* **2002**, *111*, 321–331. [CrossRef] [PubMed]
5. Mayer, R.; Brero, A.; von Hase, J.; Schroeder, T.; Cremer, T.; Dietzel, S. Common themes and cell type specific variations of higher order chromatin arrangements in the mouse. *Bmc Cell Biol.* **2005**, *6*, 44. [CrossRef] [PubMed]
6. Gorkin, D.U.; Leung, D.; Ren, B. The 3D genome in transcriptional regulation and pluripotency. *Cell Stem Cell* **2014**, *14*, 762–775. [CrossRef] [PubMed]
7. Croft, J.A.; Bridger, J.M.; Boyle, S.; Perry, P.; Teague, P.; Bickmore, W.A. Differences in the localization and morphology of chromosomes in the human nucleus. *J. Cell Biol.* **1999**, *145*, 1119–1131. [CrossRef]

8. Cremer, M.; von Hase, J.; Volm, T.; Brero, A.; Kreth, G.; Walter, J.; Fischer, C.; Solovei, I.; Cremer, C.; Cremer, T. Non-random radial higher-order chromatin arrangements in nuclei of diploid human cells. *Chromosome Res.* **2001**, *9*, 541–567. [CrossRef]
9. Tanabe, H.; Muller, S.; Neusser, M.; von Hase, J.; Calcagno, E.; Cremer, M.; Solovei, I.; Cremer, C.; Cremer, T. Evolutionary conservation of chromosome territory arrangements in cell nuclei from higher primates. *Proc. Natl. Acad. Sci. USA* **2002**, *99*, 4424–4429. [CrossRef]
10. Habermann, F.A.; Cremer, M.; Walter, J.; Kreth, G.; von Hase, J.; Bauer, K.; Wienberg, J.; Cremer, C.; Cremer, T.; Solovei, I. Arrangements of macro- and microchromosomes in chicken cells. *Chromosome Res.* **2001**, *9*, 569–584. [CrossRef]
11. Manvelyan, M.; Hunstig, F.; Bhatt, S.; Mrasek, K.; Pellestor, F.; Weise, A.; Simonyan, I.; Aroutiounian, R.; Liehr, T. Chromosome distribution in human sperm—A 3D multicolor banding-study. *Mol. Cytogenet.* **2008**, *1*, 25. [CrossRef] [PubMed]
12. Manvelyan, M.; Hunstig, F.; Mrasek, K.; Bhatt, S.; Pellestor, F.; Weise, A.; Liehr, T. Position of chromosomes 18, 19, 21 and 22 in 3D-preserved interphase nuclei of human and gorilla and white hand gibbon. *Mol. Cytogenet.* **2008**, *1*, 9. [CrossRef] [PubMed]
13. Rabl, C. Über Zellteilung. *Morph. Jahrb.* **1885**, *10*, 214–330.
14. Dong, F.G.; Jiang, J.M. Non-Rabl patterns of centromere and telomere distribution in the interphase nuclei of plant cells. *Chromosome Res.* **1998**, *6*, 551–558. [CrossRef] [PubMed]
15. Schubert, I.; Shaw, P. Organization and dynamics of plant interphase chromosomes. *Trends Plant Sci.* **2011**, *16*, 273–281. [CrossRef]
16. Pecinka, A.; Schubert, V.; Meister, A.; Kreth, G.; Klatte, M.; Lysak, M.A.; Fuchs, J.; Schubert, I. Chromosome territory arrangement and homologous pairing in nuclei of Arabidopsis thaliana are predominantly random except for NOR-bearing chromosomes. *Chromosoma* **2004**, *113*, 258–269. [CrossRef]
17. Fransz, P.; de Jong, J.H.; Lysak, M.; Castiglione, M.R.; Schubert, I. Interphase chromosomes in Arabidopsis are organized as well defined chromocenters from which euchromatin loops emanate. *Proc. Natl. Acad. Sci. USA* **2002**, *99*, 14584–14589. [CrossRef]
18. Schubert, V.; Rudnik, R.; Schubert, I. Chromatin associations in arabidopsis interphase nuclei. *Front. Genet.* **2014**, *5*, 389. [CrossRef]
19. Berr, A.; Schubert, I. Interphase chromosome arrangement in Arabidopsis thaliana is similar in differentiated and meristematic tissues and shows a transient mirror symmetry after nuclear division. *Genetics* **2007**, *176*, 853–863. [CrossRef]
20. Dekker, J.; Rippe, K.; Dekker, M.; Kleckner, N. Capturing chromosome conformation. *Science* **2002**, *295*, 1306–1311. [CrossRef]
21. Lieberman-Aiden, E.; van Berkum, N.L.; Williams, L.; Imakaev, M.; Ragoczy, T.; Telling, A.; Amit, I.; Lajoie, B.R.; Sabo, P.J.; Dorschner, M.O.; et al. Comprehensive mapping of long-range interactions reveals folding principles of the human genome. *Science* **2009**, *326*, 289–293. [CrossRef] [PubMed]
22. Dixon, J.R.; Selvaraj, S.; Yue, F.; Kim, A.; Li, Y.; Shen, Y.; Hu, M.; Liu, J.S.; Ren, B. Topological domains in mammalian genomes identified by analysis of chromatin interactions. *Nature* **2012**, *485*, 376–380. [CrossRef] [PubMed]
23. Abney, J.R.; Cutler, B.; Fillbach, M.L.; Axelrod, D.; Scalettar, B.A. Chromatin dynamics in interphase nuclei and its implications for nuclear structure. *J. Cell Biol.* **1997**, *137*, 1459–1468. [CrossRef] [PubMed]
24. Dong, P.; Tu, X.; Li, H.; Zhang, J.; Grierson, D.; Li, P.; Zhong, S. Tissue-specific Hi-C analyses of rice, foxtail millet and maize suggest non-canonical function of plant chromatin domains. *J. Intagr. Plant Biol.* **2019**. [CrossRef] [PubMed]
25. Doyle, J.J.; Flagel, L.E.; Paterson, A.H.; Rapp, R.A.; Soltis, D.E.; Soltis, P.S.; Wendel, J.F. Evolutionary genetics of genome merger and doubling in plants. *Annu. Rev. Genet.* **2008**, *42*, 443–461. [CrossRef]
26. Schardin, M.; Cremer, T.; Hager, H.D.; Lang, M. Specific staining of human-chromosomes in chinese-hamster *x* man hybrid cell-lines demonstrates interphase chromosome territories. *Hum. Genet.* **1985**, *71*, 281–287. [CrossRef] [PubMed]
27. Sengupta, K.; Camps, J.; Mathews, P.; Barenboim-Stapleton, L.; Nguyen, Q.T.; Difilippantonio, M.J.; Ried, T. Position of human chromosomes is conserved in mouse nuclei indicating a species-independent mechanism for maintaining genome organization. *Chromosoma* **2008**, *117*, 499–509. [CrossRef]

28. Heslopharrison, J.S.; Leitch, A.R.; Schwarzacher, T.; Anamthawatjonsson, K. Detection and characterization of 1b/1r translocations in hexaploid wheat. *Heredity* **1990**, *65*, 385–392. [CrossRef]
29. Kopecky, D.; Allen, D.C.; Duchoslav, M.; Dolezel, J.; Lukaszewski, A.J. Condensation of rye chromatin in somatic interphase nuclei of Ph1 and ph1b wheat. *Cytogenet. Genome Res.* **2007**, *119*, 263–267. [CrossRef]
30. Schlegel, R.; Melz, G.; Nestrowicz, R. A Universal reference karyotype in rye, *Secale cereale* L. *Theor. Appl. Genet.* **1987**, *74*, 820–826. [CrossRef]
31. Naranjo, T. Variable patterning of chromatin remodeling, telomere positioning, synapsis, and chiasma formation of individual rye chromosomes in meiosis of wheat-rye additions. *Front. Plant Sci.* **2018**, *9*, 880. [CrossRef] [PubMed]
32. Gill, B.S.; Friebe, B.; Endo, T.R. Standard karyotype and nomenclature system for description of chromosome bands and structural-aberrations in wheat (*Triticum aestivum*). *Genome* **1991**, *34*, 830–839. [CrossRef]
33. Paux, E.; Sourdille, P.; Salse, J.; Saintenac, C.; Choulet, F.; Leroy, P.; Korol, A.; Michalak, M.; Kianian, S.; Spielmeyer, W.; et al. A physical map of the 1-gigabase bread wheat chromosome 3B. *Science* **2008**, *322*, 101–104. [CrossRef] [PubMed]
34. Salina, E.A.; Nesterov, M.A.; Frenkel, Z.; Kiseleva, A.A.; Timonova, E.M.; Magni, F.; Vrana, J.; Safar, J.; Simkova, H.; Dolezel, J.; et al. Features of the organization of bread wheat chromosome 5BS based on physical mapping. *Bmc Genom.* **2018**, *19*, 80. [CrossRef] [PubMed]
35. Mascher, M.; Gundlach, H.; Himmelbach, A.; Beier, S.; Twardziok, S.O.; Wicker, T.; Radchuk, V.; Dockter, C.; Hedley, P.E.; Russell, J.; et al. A chromosome conformation capture ordered sequence of the barley genome. *Nature* **2017**, *544*, 426. [CrossRef] [PubMed]
36. Dolezel, J.; Greilhuber, J.; Lucretti, S.; Meister, A.; Lysak, M.A.; Nardi, L.; Obermayer, R. Plant genome size estimation by flow cytometry: Inter-laboratory comparison. *Ann. Bot.* **1998**, *82*, 17–26. [CrossRef]
37. Sequeira-Mendes, J.; Gutierrez, C. Genome architecture: from linear organisation of chromatin to the 3D assembly in the nucleus. *Chromosoma* **2016**, *125*, 455–469. [CrossRef]
38. Abranches, R.; Beven, A.F.; Aragon-Alcaide, L.; Shaw, P.J. Transcription sites are not correlated with chromosome territories in wheat nuclei. *J. Cell Biol.* **1998**, *143*, 5–12. [CrossRef]
39. Mikhailova, E.I.; Sosnikhina, S.P.; Kirillova, G.A.; Tikholiz, O.A.; Smirnov, V.G.; Jones, R.N.; Jenkins, G. Nuclear dispositions of subtelomeric and pericentromeric chromosomal domains during meiosis in asynaptic mutants of rye (Secale cereale L.). *J. Cell Biol.* **2001**, *114*, 1875–1882.
40. Corredor, E.; Diez, M.; Shepherd, K.; Naranjo, T. The positioning of rye homologous chromosomes added to wheat through the cell cycle in somatic cells untreated and treated with colchicine. *Cytogenet. Genome Res.* **2005**, *109*, 112–119. [CrossRef]
41. Idziak, D.; Robaszkiewicz, E.; Hasterok, R. Spatial distribution of centromeres and telomeres at interphase varies among brachypodium species. *J. Exp. Bot.* **2015**, *66*, 6623–6634. [CrossRef] [PubMed]
42. Parada, L.A.; Misteli, T. Chromosome positioning in the interphase, nucleus. *Trends Cell Biol.* **2002**, *12*, 425–432. [CrossRef]
43. Schwarzacher, T.; Leitch, A.R.; Bennett, M.D.; Heslop-Harrison, J.S. In situ localization of parental genomes in a wide hybrid. *Ann. Bot.* **1989**, *64*, 315–324. [CrossRef]
44. Schubert, I.; Shi, F.; Fuchs, J.; Endo, T.R. An efficient screening for terminal deletions and translocations of barley chromosomes added to common wheat. *Plant J.* **1998**, *14*, 489–495. [CrossRef]
45. Robaszkiewicz, E.; Idziak-Helmcke, D.; Tkacz, M.A.; Chrominski, K.; Hasterok, R. The arrangement of *Brachypodium distachyon* chromosomes in interphase nuclei. *J. Exp. Bot.* **2016**, *67*, 5571–5583. [CrossRef] [PubMed]
46. Fung, J.C.; Marshall, W.F.; Dernburg, A.; Agard, D.A.; Sedat, J.W. Homologous chromosome pairing in *Drosophila melanogaster* proceeds through multiple independent initiations. *J. Cell Biol.* **1998**, *141*, 5–20. [CrossRef]
47. Baroux, C.; Pecinka, A.; Fuchs, J.; Kreth, G.; Schubert, I.; Grossniklaus, U. Non-random chromosome arrangement in triploid endosperm nuclei. *Chromosoma* **2017**, *126*, 115–124. [CrossRef]
48. Hiraoka, Y.; Dernburg, A.F.; Parmelee, S.J.; Rykowski, M.C.; Agard, D.A.; Sedat, J.W. The onset of homologous chromosome-pairing during *Drosophila melanogaster* embryogenesis. *J. Cell Biol.* **1993**, *120*, 591–600. [CrossRef]
49. Bornfleth, H.; Edelmann, P.; Zink, D.; Cremer, T.; Cremer, C. Quantitative motion analysis of subchromosomal foci in living cells using four-dimensional microscopy. *Biophys. J.* **1999**, *77*, 2871–2886. [CrossRef]

50. Lucas, J.N.; Cervantes, E. Significant large-scale chromosome territory movement occurs as a result of mitosis, but not during interphase. *Int. J. Rad. Biol.* **2002**, *78*, 449–455. [CrossRef]
51. Lam, E.; Kato, N.; Watanabe, K. Visualizing chromosome structure/organization. *Annu. Rev. Plant Biol.* **2004**, *55*, 537–554. [CrossRef] [PubMed]
52. Kato, N.; Lam, E. Chromatin of endoreduplicated pavement cells has greater range of movement than that of diploid guard cells in *Arabidopsis thaliana*. *J. Cell Sci.* **2003**, *116*, 2195–2201. [CrossRef] [PubMed]
53. Gartenberg, M.R.; Neumann, F.R.; Laroche, T.; Blaszczyk, M.; Gasser, S.M. Sir-mediated repression can occur independently of chromosomal and subnuclear contexts. *Cell* **2004**, *119*, 955–967. [CrossRef] [PubMed]
54. Tiang, C.L.; He, Y.; Pawlowski, W.P. Chromosome organization and dynamics during Interphase, mitosis, and meiosis in plants. *Plant Physiol.* **2012**, *158*, 26–34. [CrossRef] [PubMed]
55. Soutoglou, E.; Misteli, T. Mobility and immobility of chromatin in transcription and genome stability. *Curr. Opin. Genet. Dev.* **2007**, *17*, 435–442. [CrossRef] [PubMed]
56. Jasencakova, Z.; Meister, A.; Schubert, I. Chromatin organization and its relation to replication and histone acetylation during the cell cycle in barley. *Chromosoma* **2001**, *110*, 83–92. [CrossRef] [PubMed]
57. Bolzer, A.; Kreth, G.; Solovei, I.; Koehler, D.; Saracoglu, K.; Fauth, C.; Muller, S.; Eils, R.; Cremer, C.; Speicher, M.R.; et al. Three-dimensional maps of all chromosomes in human male fibroblast nuclei and prometaphase rosettes. *PLoS Biol.* **2005**, *3*, 826–842. [CrossRef] [PubMed]
58. Bauer, E.; Schmutzer, T.; Barilar, I.; Mascher, M.; Gundlach, H.; Martis, M.M.; Twardziok, S.O.; Hackauf, B.; Gordillo, A.; Wilde, P.; et al. Towards a whole-genome sequence for rye (*Secale cereale* L.). *Plant J.* **2017**, *89*, 853–869. [CrossRef] [PubMed]
59. Schwarzacher-Robinson, T.; Finch, R.A.; Smith, J.B.; Bennett, M.D. Genotypic control of centromere positions of parental genomes in *Hordeum* x *Secale* hybrid metaphases. *J. Cell Sci.* **1987**, *87*, 291–304.
60. Leitch, A.R.; Schwarzacher, T.; Mosgoller, W.; Bennett, M.D.; Heslop-Harrison, J.S. Parental genomes are separated throughout the cell cycle in a plant hybrid. *Chromosoma* **1991**, *101*, 206–213. [CrossRef]
61. Lukaszewski, A.J. Behavior of Centromeres in Univalents and Centric Misdivision in Wheat. *Cytogenet. Genome Res.* **2010**, *129*, 97–109. [CrossRef] [PubMed]
62. Pernickova, K.; Kolackova, V.; Lukaszewski, A.J.; Fan, C.L.; Vrana, J.; Duchoslav, M.; Jenkins, G.; Phillips, D.; Samajova, O.; Sedlarova, M.; et al. Instability of alien chromosome introgressions in wheat associated with improper positioning in the nucleus. *Int. J. Mol. Sci.* **2019**, *20*, 1448. [CrossRef] [PubMed]
63. Ito, H.; Nasuda, S.; Endo, T.R. A direct repeat sequence associated with the centromeric retrotransposons in wheat. *Genome* **2004**, *47*, 747–756. [CrossRef] [PubMed]

International Journal of
Molecular Sciences

MDPI

Article

Identification and Characterization of circRNAs Responsive to Methyl Jasmonate in *Arabidopsis thaliana*

Jingjing Zhang [1,2,†], Ruiqi Liu [1,2,†], Yanfeng Zhu [2], Jiaxin Gong [1,2], Shuwei Yin [1,2], Peisen Sun [1,2], Hao Feng [1,2], Qi Wang [2], Shuaijing Zhao [2], Zhongyuan Wang [2] and Guanglin Li [1,2,*]

1 Key Laboratory of Ministry of Education for Medicinal Plant Resource and Natural Pharmaceutical Chemistry, Shaanxi Normal University, Xi'an 710119, Shaanxi, China; zhangjjg@snnu.edu.cn (J.Z.); ruiqiliu@snnu.edu.cn (R.L.); gongjx@snnu.edu.cn (J.G.); yswdx_anwser@snnu.edu.cn (S.Y.); sps@snnu.edu.cn (P.S.); fenghao@snnu.edu.cn (H.F.)

2 College of Life Sciences, Shaanxi Normal University, Xi'an 710119, Shaanxi, China; hutian@snnu.edu.cn (Y.Z.); wq2017@snnu.edu.cn (Q.W.); jing347431@snnu.edu.cn (S.Z.); wangzhongyuan@snnu.edu.cn (Z.W.)

* Correspondence: glli@snnu.edu.cn; Tel.: +86-139-9285-6645

† These authors contributed equally to this work.

Received: 11 November 2019; Accepted: 23 January 2020; Published: 25 January 2020

Abstract: Circular RNAs (circRNAs) are endogenous noncoding RNAs with covalently closed continuous loop structures that are formed by 3′–5′ ligation during splicing. These molecules are involved in diverse physiological and developmental processes in eukaryotic cells. Jasmonic acid (JA) is a critical hormonal regulator of plant growth and defense. However, the roles of circRNAs in the JA regulatory network are unclear. In this study, we performed high-throughput sequencing of *Arabidopsis thaliana* at 24 h, 48 h, and 96 h after methyl JA (MeJA) treatment. A total of 8588 circRNAs, which were distributed on almost all chromosomes, were identified, and the majority of circRNAs had lengths between 200 and 800 bp. We identified 385 differentially expressed circRNAs (DEcircRNAs) by comparing data between MeJA-treated and untreated samples. Gene Ontology (GO) enrichment analysis of the host genes that produced the DEcircRNAs showed that the DEcircRNAs are mainly involved in response to stimulation and metabolism. Additionally, some DEcircRNAs were predicted to act as miRNA decoys. Eight DEcircRNAs were validated by qRT-PCR with divergent primers, and the junction sites of five DEcircRNAs were validated by PCR analysis and Sanger sequencing. Our results provide insight into the potential roles of circRNAs in the MeJA regulation network.

Keywords: circRNAs; jasmonic acid; *Arabidopsis thaliana*; GO enrichment; miRNA decoys

1. Introduction

Circular RNAs (circRNAs) are a type of noncoding RNA widely found in plants and animals. These molecules have a covalently closed continuous loop structure that typically derives from a backsplicing event in which the upstream 5′ splice acceptor is linked to the downstream 3′ splice donor [1]. Previously, circRNAs were believed to be produced by abnormal splicing [2]. Due to advances in high-throughput sequencing and bioinformatics analysis, many circRNAs have been identified in human, mice, rat, and other species [3–5]. Based on their splice positions in the genome, circRNAs can be divided into exonic circRNAs, intronic circRNAs, exonic-intronic circRNAs, and intergenic circRNAs [6]. Most circRNAs typically have low expression in eukaryotes, but a few are highly expressed in specific cell types, developmental stages or tissues, suggesting that they have key regulatory roles in various biological processes [7].

Increasing evidence indicates that circRNAs play important roles in regulating various biological processes in animals. One of the most common roles of circRNAs in animals is the regulation of gene expression in various biological processes, where they may act as microRNA (miRNA) decoys or sponges to sequester miRNAs [8–12]. Additionally, circRNAs interact with many different RNA binding proteins (RBPs) to function as protein sponges, to recruit proteins to specific locations or subcellular compartments, and to act as scaffolds to mediate complex formation between specific enzymes and substrates [13]. Furthermore, although most circRNAs are considered to be noncoding RNAs, some circRNAs undergo cap-free translation under certain conditions [14]. Recently, increasing numbers of circRNAs have been detected in *Arabidopsis thaliana* [15–17], maize [18–20], rice [15,21], tomato [22–24], wheat [25–27], and grape [28], indicating that circRNAs are widespread in plants. Plant circRNAs are as conserved and tissue specific as animal circRNAs, but their flanking introns do not contain as many repetitive elements and reverse complementary sequences as those in animals [15,16,19,29]. Recent studies have suggested that plant circRNAs play functional roles in developmental processes and stress responses, including the responses to drought, chilling injury, nutrient deficiency, and pathogen invasion [19,20,22,24,25,30]. Based on the functions of animal circRNAs, circRNA-miRNA-mRNA networks have been generated for plants; these networks suggest that plant circRNAs may act as miRNA sponges to regulate functional gene expression [23,25,31]. Additionally, plant circRNAs are involved in the regulation of their parental genes. For example, the expression of some exonic circRNAs and that of their host genes are significantly positively correlated in rice [15], and circRNAs in *Phyllostachys edulis* negatively regulate the expression levels of their cognate linear mRNAs, as evidenced from transcriptome sequencing [32]. Such findings suggest that the regulatory effects of circRNAs on the corresponding parental transcripts are diverse. Additionally, 1569 translated circRNAs have been detected in *A. thaliana* based on ribosome profile databases [33]. However, the mechanisms underlying their regulatory roles are poorly understood. To date, only one report elucidating the molecular mechanisms underlying the regulatory roles of plant circRNAs has been published, in which an exonic circRNA from *SEPALLATA3* in *A. thaliana* was shown to regulate the splicing of its parental mRNA through the formation of an R loop [34].

The phytohormone jasmonic acid (JA) and its derivatives, methyl ester (MeJA) and isoleucine conjugate (JA-Ile), are collectively referred to as jasmonates (JAs) [35]. JAs participate in the regulation of plant growth and developmental processes, such as leaf senescence and the development of roots, shoots, flowers, and seeds [36–39]. In particular, JAs can act as signaling molecules to regulate plant adaptation to abiotic stresses, such as wounding, ultraviolet radiation, and ozone, and biotic stresses, such as pathogen infection and herbivore attack. They do so by inducing the expression of JA-responsive genes and the accumulation of various secondary metabolites in plants [40–43]. However, whether circRNAs participate in plant responses to JA remains to be elucidated.

To explore the potential functions of circRNAs in JA signaling, we performed high-throughput sequencing of MeJA-treated *A. thaliana*. Differentially expressed circRNAs (DEcircRNAs) were identified and then verified by real-time quantitative PCR (qRT-PCR). In addition, DEcircRNAs as miRNA decoys were predicted. Our study reveals the potential functional roles of the circRNAs in the JA signaling network.

2. Results

2.1. Identification and Characterization of circRNAs

To identify circRNAs involved in JA-mediated signaling in *A. thaliana*, we constructed ribosomal (r)RNA-depleted RNA-Seq libraries for seedlings sampled at 24 h, 48 h, and 96 h after MeJA treatment and then conducted IlluminaHiSeq™ X-ten paired-end sequencing. Analysis of the circRNA sequencing data revealed that a total of 489,477,066 reads were generated from 12 samples of *A. thaliana* seedlings, in which the Guanine and Cytosine (GC) content was approximately 42%, and Q30 was greater than 93% (Table S1). We summarized the total numbers of circRNAs identified from the sequencing data

by CIRI2, CIRCexplorer, and find_circ. A total of which 1526 circRNAs were predicted by CIRI2, 3410 circRNAs by CIRCexplorer, and 4564 circRNAs by find_circ; only 12 circRNAs were detected by all three algorithms (Figure S2) [5,44,45]. The expression levels of these 12 circRNAs are different; some are relatively high and some are relatively low, and most of them were expressed at more than one time points, while a few were expressed at only one time point. A total of 8588 unique circRNAs were obtained after the redundant circRNAs were removed by CD-HIT-EST [46,47]. The density distribution of these circRNAs is shown in Figure 1 and indicates that various chromosomal regions can produce circRNAs.

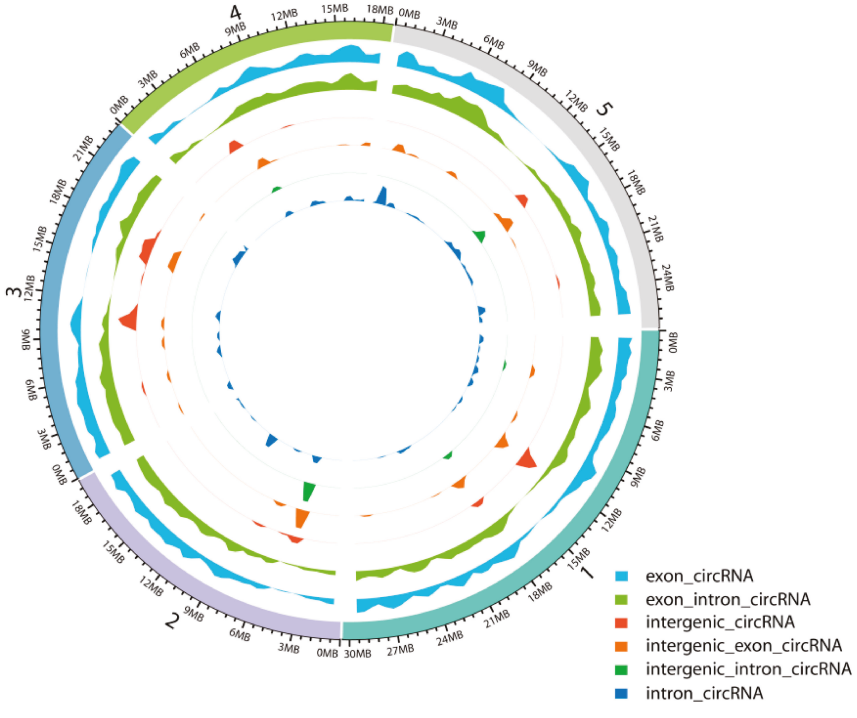

Figure 1. Density distribution of circRNAs on the chromosomes.

According to the start and end positions of circRNAs in the genome (splice site), these unique circRNAs were divided into the following six categories: exon, exon_intron, intergenic, intergenic_exon, intergenic_intron, and intron (Figure 2A). Most circRNAs originated from exons, and a few circRNAs originated from introns, indicating that regions that can produce mRNA are likely to produce circRNAs. The number of circRNAs on each chromosome was counted (Figure 2B). Most circRNAs were located on chromosomes 1 to 5; only a few circRNAs were found in chloroplasts or mitochondria, however, chloroplast chromosomes had the highest ratio of the number of circRNAs to chromosome length. Regarding the number of backspliced junction reads for circRNAs, most of the circRNAs in all samples contained fewer than 10 unique backspliced junction reads, indicating that the expression levels of most circRNAs were low (Figure 2C). In addition, the lengths of the candidate circRNAs were mainly distributed between 200 and 800 bp; a few circRNAs were longer than 1000 bp (Figure 2D). The splicing signal of circRNAs in animals is usually GT-AG; in contrast, the splicing signals at the splice sites of circRNAs in this study were diverse (Figure 2E).

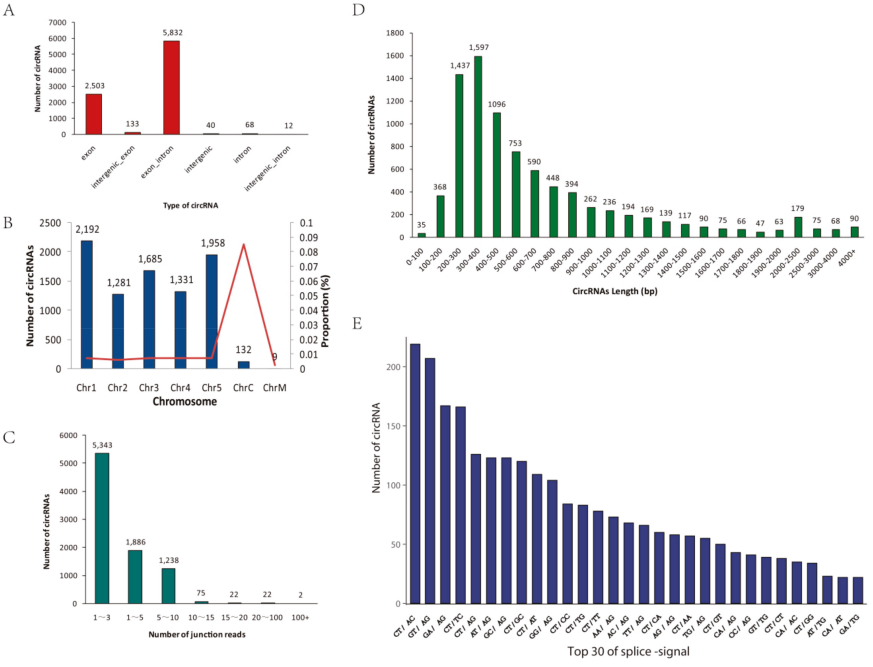

Figure 2. Characterization of circRNAs. (**A**) Classification of circRNAs. (**B**) The number and proportion of circRNAs detected in *A. thaliana* chromosomes. Proportion = (number of circRNAs on chromosome / chromosome length) × 100%. The bars represent the numbers of circRNAs, and the red line represents the proportion. (**C**) The number of junction-reads of circRNAs. (**D**) The length distribution of circRNAs. (**E**) Splicing signals of the circRNAs identified in our circRNA-seq datasets. The histogram shows the top 30 splicing signals of the circRNAs.

Moreover, 7761 circRNAs were derived from 4928 host genes, of which 65.99% produced only one circRNA, and the remainder produced more than one circRNA (Figure 3A). The same host gene produced different circRNAs by alternative splicing, and these alternative circRNAs were unrelated to each other, or one contained the other, or one splice site was identical and the other splice site was different (Figure 3B).

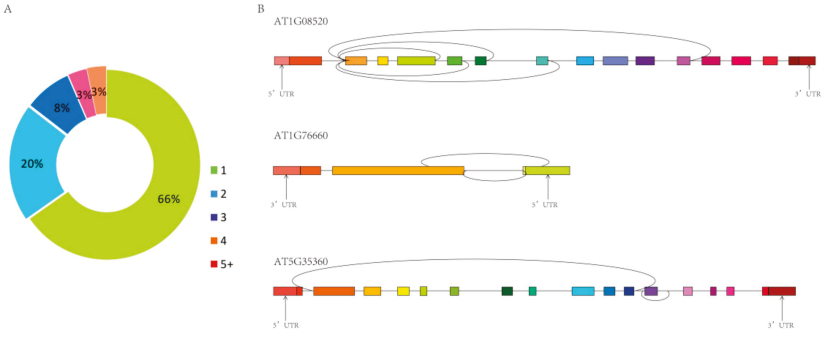

Figure 3. The number of circRNAs produced by the same host genes. (**A**) Percentage of circRNAs produced from the same host gene (7761 circRNAs from 4928 host genes). (**B**) Examples of three host genes that produce more than one circRNA.

2.2. Validation of circRNAs

To confirm our identified circRNAs, we randomly selected six highly expressed circRNAs for experimental validation using polymerase chain reaction (PCR) and Sanger sequencing, and five circRNAs were successfully verified (Figure 4A,B and Figure S3). The structure of circRNAs differs from that of linear RNA, and thus, two sets of primers (convergent and divergent) and two templates (genomic DNA (gDNA) and complementary DNA (cDNA)) were used to verify the circRNAs (Figure 4). For example, circRNA Chr5:359783|360446 was located on the second to the third exon of the mRNA of the gene *AT5G01920* (Figure 4A). To validate this circRNA, we designed convergent and divergent primers on exon 2 and exon 3 and confirmed the sequence by Sanger sequencing after PCR amplification (Figure 4).

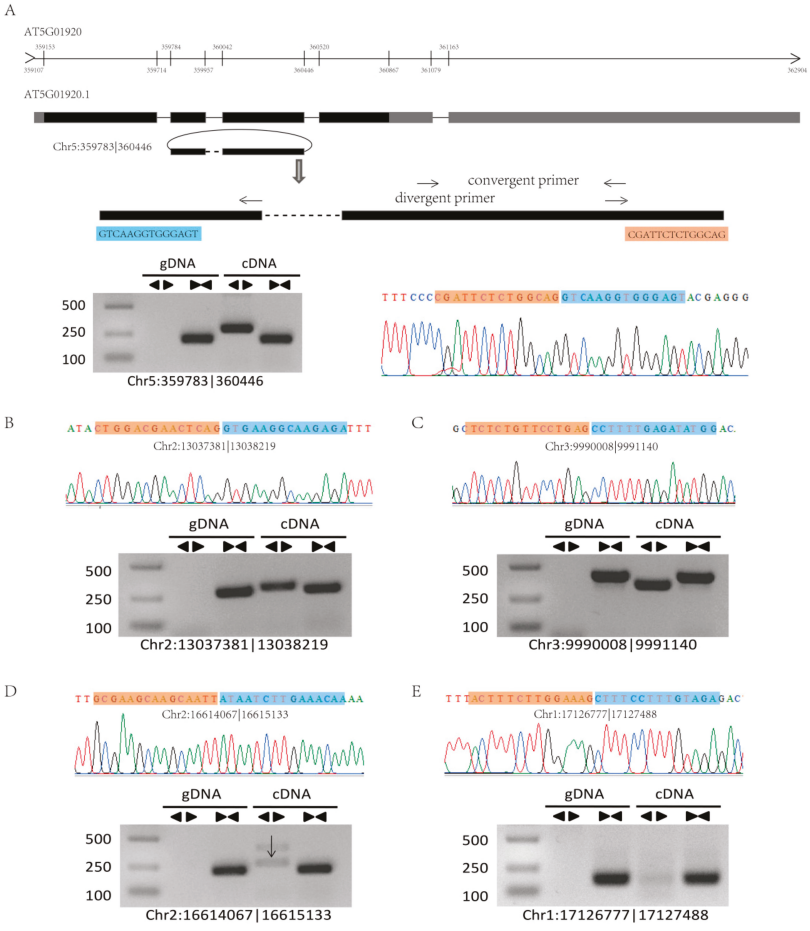

Figure 4. Validation of circRNAs by PCR and Sanger sequencing. (**A**) A circRNA (Chr5:359783|360446) exemplifying the validation strategy. According to the genomic loci, circRNA Chr5:359783|360446 was derived from the gene *AT5901920*. The two sets of arrows indicate two sets of amplification primers on the exon region, which were designed to confirm head-to-tail backsplicing by PCR and Sanger sequencing. (**B**–**E**) Validation of four circRNAs (Chr2:13037381|13038219, Chr3:9990008|9991140, Chr2:16614067|16615133, and Chr1:17126777|17127488) by PCR and Sanger sequencing. Divergent primers successfully amplified the circRNAs in cDNA but not those in gDNA. Convergent primers amplified the circRNAs in both cDNA and gDNA.

2.3. DEcircRNAs Induced by MeJA Treatment

The expression levels of some circRNAs in *A. thaliana* seedlings after MeJA treatment differed from those in controls. In total, 385 DEcircRNAs were detected between MeJA-treated and control seedlings among the three time points (24 h, 48 h, and 96 h) by using the circMeta R packages; among them, 70 circRNAs were differentially expressed at 24 h, 244 circRNAs at 48 h, and 115 circRNAs at 96 h (Figure 5A and Table S2). Moreover, nine circRNAs were differentially expressed at all three time points (Figure 5A). Among the DEcircRNAs, 33 were upregulated and 38 were downregulated at 24 h, 125 were upregulated and 118 were downregulated at 48 h, and 62 were upregulated and 53 were downregulated at 96 h (Figure 5B). In addition, a volcano map indicated that the fold changes of 379 DEcircRNAs were greater than 2 (|log2FoldChange| > 1) (Figure 5C). The expression levels of most DEcircRNAs were very low, with RPKM < 1, but the expression of most DEcircRNAs increased significantly at 24 h and 48 h after MeJA treatment (Figure 5D).

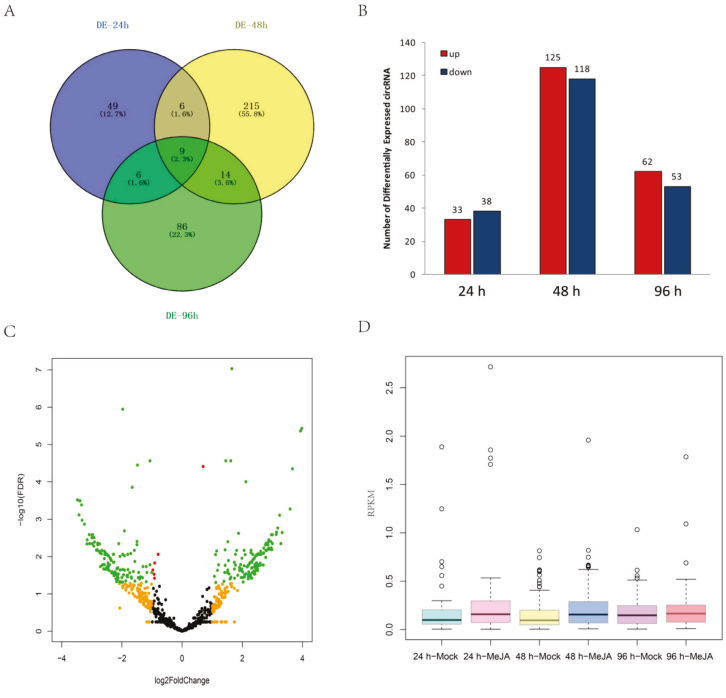

Figure 5. Analysis of DEcircRNAs. (**A**) Venn diagram of DEcircRNAs at three time points. (**B**) Regulation of DEcircRNAs at different time points. (**C**) Volcano map of DEcircRNAs between the control and MeJA treatments. Red nodes represent DEcircRNAs with false discovery rate (FDR) < 0.05, orange nodes represent DEcircRNAs with |log2FoldChange| > 1, and green nodes represent DEcircRNAs with FDR < 0.05 and |log2FoldChange| > 1. (**D**) Relative expression levels of DEcircRNAs after MeJA treatment.

The expression patterns of eight randomly selected DEcircRNAs were detected at different time points by quantitative real-time PCR (qRT-PCR), and the results are shown in Figure 6. We found that two of these eight DEcircRNAs, circRNA Chr4:8756898|8758635 (Figure 6A) and circRNA Chr1:17126777|17127488 (Figure 6E), were differentially expressed at all three time points, while the other six, such as circRNA Chr5:359783|360446 (Figure 6B) and circRNA Chr3:9990008|9991140 (Figure 6F), were differentially expressed at one or two time points. The expression levels of their mRNA were detected, and the results indicated that the expression levels of two circRNAs (Chr4:8756898|8758635 and Chr5:359783|360446) were related to the expression levels of their linear

transcripts (Figure 6A,B; $R^2 > 0.7$), whereas the expression levels of the other circRNAs were not correlated with those of their mRNA (Figure 6C–H).

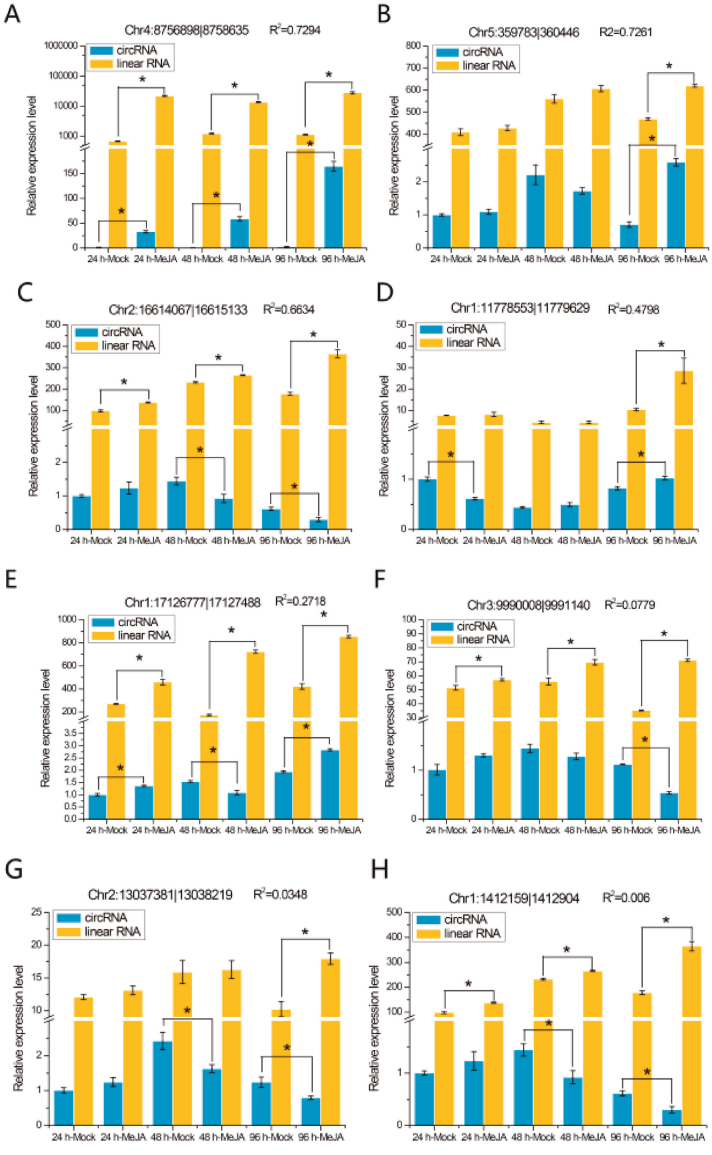

Figure 6. qRT-PCR validation of eight DEcircRNAs and their linear transcripts. (**A**) circRNA Chr4:8756898|8758635; (**B**) circRNA Chr5:359783|360446; (**C**) circRNA Chr2:16614067|16615133; (**D**) circRNA Chr1:11778553|11779629; (**E**) circRNA Chr1:17126777|17127488; (**F**) circRNA Chr3:9990008|9991140; (**G**) circRNA Chr2:13037381|13038219; (**H**) circRNA Chr1:1412159|1412905. Three replicates were established. R^2 represents the correlation of expression level between the circRNAs and linear transcripts. Error bars represent the standard error of the mean. * $p < 0.05$, as determined by Tukey's-b test.

2.4. Functional Prediction of DEcircRNAs by Gene Ontology (GO) Enrichment Analysis

The potential function of a circRNA may depend on the function of its host gene; thus, we analyzed the functions of DEcircRNA host genes [48]. The results of GO enrichment analysis showed that the host genes were involved in three categories: biological process (BP), cellular component (CC), and molecular function (MF) (Figure 7A and Table S6). In the BP category, most circRNAs were enriched in cellular process (GO:0009987), metabolic process (GO:0008152), response to stimulus (GO:0050896), biological regulation (GO:0065007), and developmental process (GO:0032502). In addition, the top 20 significant GO terms, including response to temperature stimulus (GO:0009266), response to abiotic stimulus (GO:0009628), response to stress (GO:0006950), and response to wounding (GO:0009611), are displayed in Figure 7B. These findings indicated that the host genes of the DEcircRNAs were associated with plant responses to stimuli. Thus, these DEcircRNAs might also be involved in the plant responses to stimulation.

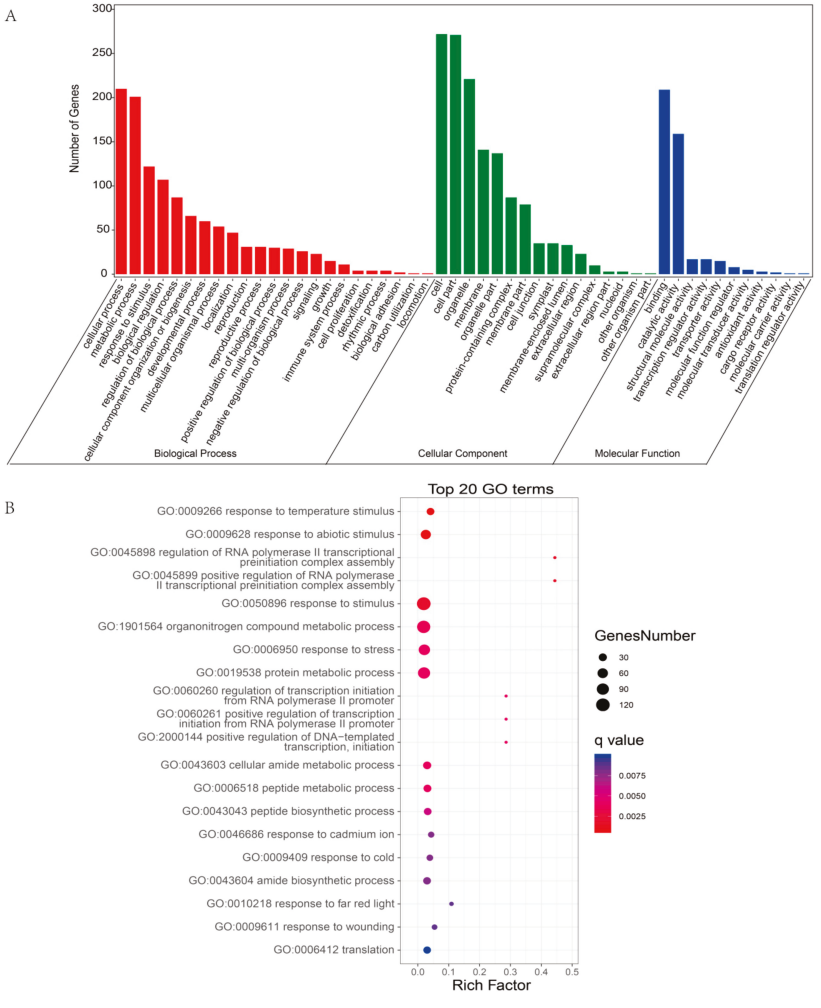

Figure 7. GO enrichment analysis of the host genes of DEcircRNAs. (**A**) The most enriched GO terms of the host genes of DEcircRNAs. (**B**) Top 20 GO enrichment categories of the host genes of DEcircRNAs.

2.5. Functional Prediction of DEcircRNAs Based on the circRNA-miRNA-mRNA Network

Increasing evidence indicates that circRNAs might competitively bind to miRNAs and subsequently regulate their target genes by acting as miRNA decoys or sponges [49–52]. To further explore the functions of DEcircRNAs, we first predicted DEcircRNAs acting as miRNA decoys and mRNAs acting as miRNA targets. Then, a regulatory network of circRNA-miRNA-mRNA was constructed based on potential relationships between these RNAs (Figure 8A). This network was composed of 1698 nodes and 1780 edges, and the nodes included 32 miRNAs, 36 circRNAs (circRNAs acting as miRNA decoys), and 1630 mRNAs (mRNAs acting as miRNA targets) (Figure 8A and Table S3). CircRNAs had one to nine miRNA decoy sites (Figure 8A). For instance, circRNA Chr5:16093397|16096079 might act as a miRNA ath-miR864-5p decoy (Figure 8D). CircRNA Chr3:523385|524409 might act as a decoy for two miRNAs (ath-miRf10261-akr and miRNA ath-miRf10509-akr) (Figure 8C). In addition, multiple circRNAs might act as a decoy for one miRNA, such as circRNA Chr1:24701221|24707801, circRNA Chr1:24702386|24708882, and circRNA Chr1:24701457|24707994, all of which had miRNA ath-miR864-5p decoy sites (Figure 8B).

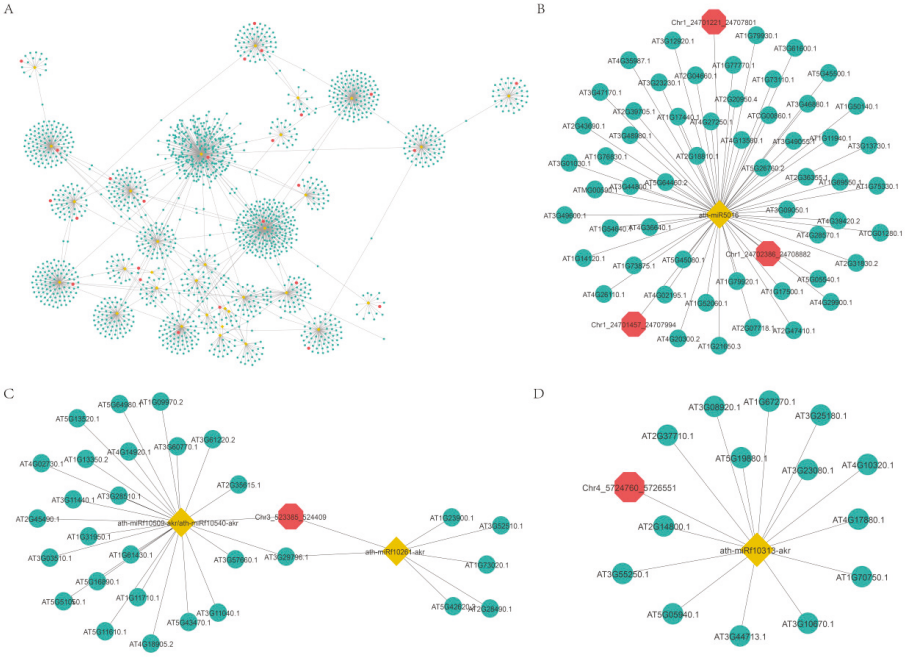

Figure 8. The circRNA-miRNA-mRNA interaction network. Yellow nodes: miRNAs. Red nodes: circRNAs that may be miRNA decoys. Green nodes: mRNAs that may be miRNA targets. (**B**–**D**) were extracted from (**A**).

To further explore the functions of DEcircRNAs, 1630 mRNAs in the regulatory network of circRNA-miRNA-mRNA were subjected to GO analysis. We found that these mRNAs were mainly involved in plant growth and development process, response to various stimuli, response to JA, regulation of the JA-mediated signaling pathway, and JA metabolic process (Figure S1 and Table S4). These results indicated that these circRNAs in the circRNA-miRNA-mRNA network may play roles in JA-mediated signaling.

3. Discussion

CircRNAs are a special class of noncoding RNAs produced by non-linear backsplicing events between downstream splice donors and upstream splice acceptors. Recently, with the development of high-throughput sequencing technology, increasing numbers of circRNAs have been detected in plants and animals. In plants, circRNAs are closely related to plant development and stress responses, including biotic and abiotic stresses [20,22–28,30,53]. However, whether circRNAs participate in the pathways of plant responses to hormones is unclear. In this study, for the first time, circRNAs from *A. thaliana* seedlings at 24, 48, and 96 h after MeJA treatment were profiled. A total of 8588 circRNAs were detected in *A. thaliana* seedlings, of which 1526 circRNAs were predicted by CIRI2, 3410 by CIRCexplorer, and 4564 by find_circ. There was little overlap among the results of the different software programs (Figure S2). Software for the prediction of circRNAs is continually appearing, but different software programs have different advantages and shortcomings regarding sensitivity, precision, and computational cost. Such differences are largely due to the different strategies adopted [54–56]. CircRNAs predicted by all three methods accounted for a small proportion of the total predicted circRNAs, which indicated extensive differences among the prediction algorithms when they were applied to *A. thaliana* circRNA libraries. Thus, several tools should be used in combination to achieve reliable and comprehensive results. Consistent with previous studies, the circRNAs identified in this study were derived from exons, introns, and intergenic regions [13,15]. A large proportion of the circRNAs are derived from individual exons and may be related to the current mechanism of circRNA formation in plants: exon skipping events [34]. We found that although some genes produce more than one circRNA, most produce only one, which is consistent with previous reports in plants [56–58]. In addition, our results showed that many circRNAs were expressed at extremely low levels in *A. thaliana*. This characteristic may be a common basic feature of circRNAs in plants.

Phytohormones are important small signaling molecules in plants and play critical roles in various basic processes in plants [59]. MeJA is a key plant hormone and regulates pivotal processes, including seedling emergence, response to wounding, fertility, and growth-defense balance [60,61]. The biosynthesis, perception, transport, and signal transduction of MeJA have been extensively studied [59]. However, the roles of circRNAs in MeJA-mediated signaling pathways in *A. thaliana* have not been reported. Similar to other stresses in various plants, such as drought stress in maize and *A. thaliana* [20], dehydration stress in wheat [25], and cold stress in grapevine [28], MeJA treatment in *A. thaliana* altered the expression profiles of circRNAs. In this study, among the 8588 identified circRNAs, 385 circRNAs were identified as DEcircRNAs between MeJA-treated and untreated seedlings. The fluctuation of circRNA abundance after MeJA treatment in *A. thaliana* may be related to the possible roles of circRNAs in response to MeJA, such as some putative biomarkers of the JA response, or even some of them as potentials protein coding circRNAs that may be involved in JA signaling. In addition, nine circRNAs that were differentially expressed at three different time points between MeJA treated and controls plants may act as pivotal regulators in MeJA signaling, and the regulatory mechanisms warrant further study.

The circRNAs identified in many plants and animals, including human, have been reported to participate in the regulation of the expression of their host genes [11–13,15,32,34]. For example, some circRNAs regulate the expression of host genes by competing with canonical splicing [12]. In rice, overexpression of the circRNA "Os08circ16564" reduced the expression level of its host gene *AK064900* in both leaf and panicle tissues [21]. Recently, a circRNA from *SEPALLATA3* was shown to regulate splicing of its cognate mRNA through R-loop formation, resulting in transcriptional pausing [34]. In addition, some circRNAs in animals enhance transcription of their host genes by interacting with polymerase II or the U1 small nuclear ribonucleoprotein [11,62]. Therefore, in the present study, GO enrichment analysis of the host genes of DEcircRNAs was performed to investigate the functions of circRNAs in MeJA-mediated signaling. GO analysis showed that these host genes were mainly enriched in the categories cellular process, metabolic process, response to stimulus, and biological regulation. In addition, these host genes were associated with the GO terms developmental process, immune

system process, reproduction, polysaccharide biosynthetic process, and response to reactive oxygen species; these findings are consistent with the reported functions of mRNAs that are differentially expressed after MeJA treatment [63], suggesting that the corresponding circRNAs may play important roles in regulating the expression of their host genes. In this study, we also performed expression pattern analyses of eight DEcircRNAs and their host genes and found that the expression patterns of two circRNAs were correlated with the expression patterns of their corresponding host genes, whereas those of the remaining six circRNAs exhibited no such correlations. The overexpression of the circRNA circR5g05160 in rice did not change the linear transcript accumulation of *LOC_Os05g05160* [63]. These data suggest that the regulatory effects of circRNAs on their host genes are diverse.

Previous studies have shown that circRNAs in animals and human can act as miRNA decoys or sponges to reduce the inhibition of miRNAs on their targets via circRNA-miRNA-mRNA networks [8]. For example, the circRNA hsa_circ_0005105 upregulates *NAMPT* expression via sponging miR-26a, thereby promoting extracellular matrix degradation of chondrocytes [10]. In addition, the circRNA circ_001350 regulates glioma cell proliferation, apoptosis, and metastatic properties by acting as a miRNA sponge [64]. In plants, circRNA-miRNA-mRNA networks have been identified, but they have not been confirmed by experiments [31,65]. To reveal whether DEcircRNAs can target miRNAs and participate in the transcriptional regulation of genes, we identified 385 DEcircRNAs predicted to contain miRNA decoy sites. As expected, 36 of the 385 DEcircRNAs were predicted to have one to nine miRNA decoy sites, which is consistent with other studies in plants [26,27,57]. For instance, circRNA Chr4:12480688|12481259 has nine miRNA decoy sites, indicating that it might regulate various processes through different miRNAs. In addition, three circRNAs (Chr1:24701221|24707801, Chr1:24702386|24708882, and Chr1:24701457|24707994) from the same host gene target the same miRNA, suggesting that plants regulate specific physiological processes through different forms of backsplicing. Moreover, by interacting with miRNAs, circRNAs can regulate the expression of miRNA target genes. In this study, GO enrichment analysis of the corresponding miRNA target genes was performed to identify genes that are regulated by circRNAs as miRNA decoys. These genes were enriched in the terms metabolic process, developmental process, RNA processing, protein phosphorylation, and DNA methylation or demethylation and may play important roles in MeJA-mediated signaling. In addition, we compared mRNAs in our network with transcriptomic data on the response to MeJA in *A. thaliana* from a previous study [63]; the network of mRNAs present in both our network and the previous study is displayed in Figure S4. These results suggest that some circRNAs may act as miRNA decoys to affect the expression of many genes involved in MeJA signaling. However, how these DEcircRNAs perform their functions by acting on their host genes or acting as miRNA sponges in the JA pathway is unclear and awaits further studies.

4. Materials and Methods

4.1. Plant Materials and Treatments

The *A. thaliana* ecotype Col-0 reserved in School of Life Sciences, Shaanxi Normal University was used in this study. Sterilized Col-0 seeds were cultured in 1/2 MS medium and placed in an incubator for two days at 4 °C in the dark for vernalization. Then, the seeds were germinated on 1/2 MS culture medium in an incubator for 6 days with a day/night (16 h/8 h) temperature of 23/16 °C. The seedlings were transferred to mock medium (comprising 9.17 μL of absolute ethanol added to 100 mL of 1/2 MS medium) and 10 μM of MeJA medium (created by diluting 2.5 μL of pure MeJA to 100 μL with absolute ethanol and adding 9.17 μL of diluted MeJA solution to 100 mL of 1/2 MS medium). Seedlings were transplanted into an incubator with a day/night (16/8 h) temperature of 23/16°C. Plant samples were collected at 24, 48, and 96h after transplantation.

4.2. RNA Extraction, cDNA Library Construction, and RNA Sequencing

After treating the seedlings with the control or MeJA medium, plant samples weighing at least 100 mg were collected, and total RNA was extracted using the RNAprep Pure Plant Kit (Tiangen, Beijing, China). The purity, concentration, and integrity of total RNA were detected by the Nanodrop, Qubit 2.0 and Agilent 2100 bioanalyzer respectively. A cDNA library was constructed using 1.5 μg total RNA according to the following steps: (a) rRNA was removed by rRNA probes (Ribo-ZeroTM rRNA Removal Kit, (Plant Leaf); Epicentre, Madison, WI, USA) and (b)linear RNA was removed by RNase R (Epicentre). Then, the rRNA in the remaining RNA was detected by PCR and gel electrophoresis. Next, the remaining RNAs were used to generate circRNA-seq libraries according to Zuo et al. [22]. The cDNA libraries were sequenced on an IlluminaHiSeq™ X-ten platform at Biomarker Technologies Co., Ltd. (Beijing, China), and 2 × 150 bp paired-end reads were obtained according to the standard Illumina protocol. The raw sequencing data were deposited in the US National Center for Biotechnology Information (NCBI) Sequence Read Archive under a Bioproject ID PRJNA597249.

4.3. CircRNA Identification and Differential Expression Analysis

Low-quality reads, including reads with greater than 50% unknown (N) bases or greater than 50% low-quality bases ($Q \leq 20$), and adapters were removed from the sequencing data before circRNA identification by Trim galore (https://github.com/FelixKrueger/TrimGalore). The remaining clean reads were mapped to the *A. thaliana* reference genome TAIR10 using BWA (v0.7.17, mem-T 19) and Bowtie2 (v2.2.9) with default parameters [66,67]. The output of BWA was used to identify the circRNAs by CIRI (v2.0.6) with default parameters and CIRCexplorer with default parameters (v2.3.3), and the output of Bowtie2 was used to identify circRNAs by find_circ with default parameters(v1.0). One or more base differences may be present between the results of different prediction software programs. CD-HIT-EST (v4.6) was used to remove the repeated circRNAs in the prediction results based on the following inclusion criteria: (1) a length difference between the two sequences less than 10 bp and (2) an alignment sequence exceeding 99.7% of the shorter sequence. The other CD-HIT-EST parameters were the default parameters.

DEcircRNAs between the control- and MeJA-treated plants at the three time points were analyzed using the circMeta R package [68]. The results of Poisson-based test (*z*-test) were used to identify DEcircRNAs meeting the following criterion: false discovery rate (FDR) < 0.05. CircRNA expression levels were normalized to the RPKM value [number of circular reads/number of mapped reads (millions) × circRNA length (KB)]. Venn diagrams were generated using online tools (https://bioinfogp.cnb.csic.es/tools/venny/). A volcano plot and boxplot were constructed using the corresponding R packages.

4.4. Validation of circRNAs

Total RNA was extracted from *A. thaliana* seedlings at three time points using Plant RNA kit (Omega, Germany) according to the manufacturer's protocol, and first-strand cDNA was synthesized from total RNA with random hexamer primers using the HiScript®II 1st Strand cDNA Synthesis Kit (+gDNA wiper) (Vazyme, Nanjing, China). To validate the existence of circRNAs, we designed convergent and divergent primers using GeneRunner software. PCR was performed using cDNA and gDNA as templates with two sets of primers. In addition, the PCR products were visualized by agarose gel electrophoresis and confirmed by Sanger sequencing. qRT-PCR was carried out with SYBR Green Master Mix (Vazyme, Nanjing, China) on a CFX 96 Real-Time PCR system (Bio-Rad, Hercules, CA, USA). The qRT-PCR procedure was as follows: 95 °C for 3 min, followed by 45 cycles of 95 °C for 30 s and 60 °C for 30 s. The $2^{-\Delta\Delta Ct}$ method was used to calculate the relative expression of circRNAs [24,69], with GAPDH as the reference gene. The primers are listed in Table S5.

4.5. Functional Prediction of DEcircRNAs

The functions of some DEcircRNAs may depend on their host genes; thus, GO enrichment analysis of the host genes of the DEcircRNAs was performed using the online resource OmicShare (http://www.omicshare.com/).

In addition, the functions of some circRNAs may be independent of their host genes; they may act as miRNA decoys to achieve their effects [8]. To construct the networks among DEcircRNAs, miRNAs, and mRNAs, we obtained miRNA sequences from miRBase (http://mirbase.org/) and the plant microRNA database (PMRD: http://bioinformatics.cau.edu.cn/PMRD/) [70,71], and mRNA sequences were downloaded from Phytozome12 (https://phytozome.jgi.doe.gov/pz/portal.html). The DEcircRNAs sequences were extracted with an in-house Perl script. Next, GSTAr.pl (https://github.com/MikeAxtell/GSTAr) was used to establish the networks between circRNAs and miRNAs and between miRNAs and mRNAs, and the minimum free energy (MFE) of miRNA-circRNA or miRNA-mRNA duplexes was calculated with the RNAhybrid program. Then, the miRNA-targeted mRNA and miRNA-decoyed circRNA were predicted following a method proposed in a previous report [18,51,72]. The general criteria used to define a miRNA decoy were as follows: no more than six mismatched or inserted bases present between the ninth to 20th nucleotides of the miRNA 5′ end, perfect matching of the second to eighth bases of the miRNA 5′ end sequence, and no more than four mismatches or indels in other regions. Finally, the circRNA-miRNA-mRNA network was generated by Cytoscape (v3.7.2) [73].

Supplementary Materials: Supplementary materials can be found at http://www.mdpi.com/1422-0067/21/3/792/s1. Table S1: Quality of the sequence data; Table S2: DEcircRNAs at the three time points; Table S3: DEcircRNAs acting as miRNA decoys; Table S4: GO enrichment analysis of mRNA in the circRNA-miRNA-mRNA network; Table S5: The primers used in this study; Table S6: GO enrichment analysis of the host genes of DEcircRNAs; Figure S1: GO enrichment analysis of mRNA involved in circRNA-miRNA-mRNA networks. (A) The most enriched GO terms of mRNA in circRNA-miRNA-mRNA networks. (B) Top 20 GO enrichment categories of mRNA in circRNA-miRNA-mRNA networks; Figure S2: The Venn diagram of the circRNAs were identified by three algorithms (CIRI2, CIRCexplorer, and find_circ); Figure S3: Un-modified gel photographs of five validated circRNAs. Note: The Sanger sequencing result for the third circRNAis incorrect. For each circRNA, the first column is a 2000bp marker, the second and third columns are gel results that using gDNA as a template, and the primers are divergent and convergent respectively; the fourth and fifth columns are gel results that using cDNA as a template, and the primers are divergent and convergent respectively; Figure S4: Network of mRNAs in both our network and a previous study. Yellow nodes: miRNAs. Red nodes: circRNAs that may be miRNA decoys. Green nodes: mRNAs that may be miRNA targets.

Author Contributions: G.L., J.Z., R.L., and Y.Z. planned the experiments; J.Z., S.Y., and P.S. analyzed the data; J.Z., R.L., Y.Z., J.G., H.F., Q.W., S.Z., and Z.W. performed the experiments; J.Z. and R.L. wrote the paper. All authors have read and agreed to the published version of the manuscript.

Funding: This research was funded by the National Science Foundation of China (grant number 31770333, 31370329, and 11631012), the Program for New Century Excellent Talents in University (NCET-12-0896), and the Fundamental Research Funds for the Central Universities (No. GK201403004).

Conflicts of Interest: The authors declare no conflicts of interest.

References

1. Salzman, J. Circular RNA expression: Its potential regulation and function. *Trends Genet.* **2016**, *32*, 309–316. [CrossRef] [PubMed]
2. Liu, J.; Liu, T.; Wang, X.; He, A. Circles reshaping the RNA world: From waste to treasure. *Mol. Cancer* **2017**, *16*, 58. [CrossRef] [PubMed]
3. Salzman, J.; Gawad, C.; Wang, P.L.; Lacayo, N.; Brown, P.O. Circular RNAs are the predominant transcript isoform from hundreds of human genes in diverse cell types. *PLoS ONE* **2012**, *7*, e30733. [CrossRef] [PubMed]
4. Werfel, S.; Nothjunge, S.; Schwarzmayr, T.; Strom, T.M.; Meitinger, T.; Engelhardt, S. Characterization of circular RNAs in human, mouse and rat hearts. *J. Mol. Cell. Cardiol.* **2016**, *98*, 103–107. [CrossRef] [PubMed]
5. Memczak, S.; Jens, M.; Elefsinioti, A.; Torti, F.; Krueger, J.; Rybak, A.; Maier, L.; Mackowiak, S.D.; Gregersen, L.H.; Munschauer, M.; et al. Circular RNAs are a large class of animal RNAs with regulatory potency. *Nature* **2013**, *495*, 333–338. [CrossRef]
6. Lasda, E.; Parker, R. Circular RNAs: Diversity of form and function. *RNA* **2014**, *20*, 1829–1842. [CrossRef]

7. Barrett, S.P.; Salzman, J. Circular RNAs: Analysis, expression and potential functions. *Development* **2016**, *143*, 1838–1847. [CrossRef]
8. Hansen, T.B.; Jensen, T.I.; Clausen, B.H.; Bramsen, J.B.; Finsen, B.; Damgaard, C.K.; Kjems, J. Natural RNA circles function as efficient microRNA sponges. *Nature* **2013**, *495*, 384–388. [CrossRef]
9. Xu, H.; Guo, S.; Li, W.; Yu, P. The circular RNA Cdr1as, via miR-7 and its targets, regulates insulin transcription and secretion in islet cells. *Sci. Rep.* **2015**, *5*, 12453. [CrossRef]
10. Wu, Y.; Zhang, Y.; Zhang, Y.; Wang, J.J. CircRNA hsa_circ_0005105 upregulates NAMPT expression and promotes chondrocyte extracellular matrix degradation by sponging miR-26a. *Cell Biol. Int.* **2017**, *41*, 1283–1289. [CrossRef]
11. Li, Z.; Huang, C.; Bao, C.; Chen, L.; Lin, M.; Wang, X.; Zhong, G.; Yu, B.; Hu, W.; Dai, L.; et al. Exon-intron circular RNAs regulate transcription in the nucleus. *Nat. Struct. Mol. Biol.* **2015**, *22*, 256–264. [CrossRef] [PubMed]
12. Ashwal-Fluss, R.; Meyer, M.; Pamudurti, N.R.; Ivanov, A.; Bartok, O.; Hanan, M.; Evantal, N.; Memczak, S.; Rajewsky, N.; Kadener, S. circRNA biogenesis competes with pre-mRNA splicing. *Mol. Cell* **2014**, *56*, 55–66. [CrossRef] [PubMed]
13. Kristensen, L.S.; Andersen, M.S.; Stagsted, L.V.W.; Ebbesen, K.K.; Hansen, T.B. The biogenesis, biology and characterization of circular RNAs. *Nat. Rev. Genet.* **2019**, *20*, 675–691. [CrossRef] [PubMed]
14. Granados-Riveron, J.T.; Aquino-Jarquin, G. The complexity of the translation ability of circRNAs. *Biochim. Biophys. Acta-Gene Regul. Mech.* **2016**, *1859*, 1245–1251. [CrossRef]
15. Ye, C.Y.; Chen, L.; Liu, C.; Zhu, Q.H.; Fan, L. Widespread noncoding circular RNAs in plants. *New Phytol.* **2015**, *208*, 88–95. [CrossRef]
16. Sun, X.; Wang, L.; Ding, J.; Wang, Y.; Wang, J.; Zhang, X.; Che, Y.; Liu, Z.; Zhang, X.; Ye, J.; et al. Integrative analysis of *Arabidopsis thaliana* transcriptomics reveals intuitive splicing mechanism for circular RNA. *FEBS letters* **2016**, *590*, 3510–3516. [CrossRef]
17. Chen, G.; Cui, J.; Wang, L.; Zhu, Y.; Lu, Z.; Jin, B. Genome-wide identification of circular RNAs in *Arabidopsis thaliana*. *Front. Plant Sci.* **2017**, *8*, 1678. [CrossRef]
18. Tang, B.; Hao, Z.; Zhu, Y.; Zhang, H.; Li, G. Genome-wide identification and functional analysis of circRNAs in *Zea mays*. *Plos ONE* **2018**, *13*, e0202375. [CrossRef]
19. Chen, L.; Zhang, P.; Fan, Y.; Lu, Q.; Li, Q.; Yan, J.; Muehlbauer, G.J.; Schnable, P.S.; Dai, M.; Li, L. Circular RNAs mediated by transposons are associated with transcriptomic and phenotypic variation in maize. *New Phytol.* **2018**, *217*, 1292–1306. [CrossRef]
20. Zhang, P.; Fan, Y.; Sun, X.; Chen, L.; Terzaghi, W.; Bucher, E. A large-scale circular RNA profiling reveals universal molecular mechanisms responsive to drought stress in maize and *Arabidopsis*. *Plant J.* **2019**, *98*, 697–713. [CrossRef]
21. Lu, T.; Cui, L.; Zhou, Y.; Zhu, C.; Fan, D.; Gong, H.; Zhao, Q.; Zhou, C.; Zhao, Y.; Lu, D.; et al. Transcriptome-wide investigation of circular RNAs in rice. *RNA* **2015**, *21*, 2076–2087. [CrossRef] [PubMed]
22. Zuo, J.; Wang, Q.; Zhu, B.; Luo, Y.; Gao, L. Deciphering the roles of circRNAs on chilling injury in tomato. *Biochem. Biophys. Res. Commun.* **2016**, *479*, 132–138. [CrossRef] [PubMed]
23. Wang, Y.; Wang, Q.; Gao, L.; Zhu, B.; Luo, Y.; Deng, Z.; Zuo, J. Integrative analysis of circRNAs acting as ceRNAs involved in ethylene pathway in tomato. *Physiol. Plant.* **2017**, *16*, 311–321. [CrossRef] [PubMed]
24. Yin, J.; Liu, M.; Ma, D.; Wu, J.; Han, B. Identification of circular RNAs and their targets during tomato fruit ripening. *Postharvest Biol. Technol.* **2018**, *136*, 90–98. [CrossRef]
25. Wang, Y.; Yang, M.; Wei, S.; Qin, F.; Zhao, H.; Suo, B. Identification of circular RNAs and their targets in leaves of *Triticum aestivum* L. under dehydration stress. *Front. Plant Sci.* **2016**, *7*, 2024. [CrossRef]
26. Ren, Y.; Yue, H.; Li, L.; Xu, Y.; Wang, Z.; Xin, Z.; Lin, T. Identification and characterization of circRNAs involved in the regulation of low nitrogen-promoted root growth in hexaploid wheat. *Biol. Res.* **2018**, *51*, 43. [CrossRef]
27. Xu, Y.; Ren, Y. Identification and characterization of CircRNAs involved in the regulation of wheat root length. *Biol. Res.* **2019**, *52*, 19. [CrossRef]
28. Gao, Z.; Li, J.; Luo, M.; Li, H.; Chen, Q.; Wang, L.; Song, S.; Zhao, L.; Xu, W.; Zhang, C.; et al. Characterization and cloning of grape circular RNAs identified the cold resistance-related *Vv-circATS1*. *Plant Physiol.* **2019**, *180*, 966–985. [CrossRef]

29. Huo, L.; Zhang, P.; Li, C.; Rahim, K.; Hao, X.; Xiang, B.; Zhu, X. Genome-wide identification of circRNAs in pathogenic basidiomycetous yeast *Cryptococcus neoformans* suggests conserved circRNA host genes over kingdoms. *Genes* **2018**, *9*, 118. [CrossRef]
30. Wang, Z.; Liu, Y.; Li, D.; Li, L.; Zhang, Q.; Wang, S.; Huang, H. Identification of circular RNAs in kiwifruit and their species-specific response to bacterial canker pathogen invasion. *Front. Plant Sci.* **2017**, *8*, 413. [CrossRef]
31. Liu, S.; Wu, L.; Qi, H.; Xu, M. LncRNA/circRNA–miRNA–mRNA networks regulate the development of root and shoot meristems of *Populus*. *Ind. Crop. Prod.* **2019**, *133*, 333–347. [CrossRef]
32. Wang, Y.; Gao, Y.; Zhang, H.; Wang, H.; Liu, X.; Xu, X.; Zhang, Z.; Kohnen, M.V.; Hu, K.; Wang, H.; et al. Genome-wide profiling of circular RNAs in the rapidly growing shoots of Moso Bamboo (*Phyllostachys edulis*). *Plant Cell Physiol.* **2019**, *60*, 1354–1373. [CrossRef] [PubMed]
33. Sun, P.; Li, G. CircCode: A powerful tool for identifying circRNA coding ability. *Front. Genet.* **2019**, *10*, 981. [CrossRef] [PubMed]
34. Conn, V.M.; Hugouvieux, V.; Nayak, A.; Conos, S.A.; Capovilla, G.; Cildir, G.; Jourdain, A.; Tergaonkar, V.; Schmid, M. A circRNA from *SEPALLATA3* regulates splicing of its cognate mRNA through R-loop formation. *Nat. Plants* **2017**, *3*, 17053. [CrossRef] [PubMed]
35. Reinbothe, C.; Springer, A.; Samol, I.; Reinbothe, S. Plant oxylipins: Role of jasmonic acid during programmed cell death, defence and leaf senescence. *FEBS J.* **2009**, *276*, 4666–4681. [CrossRef] [PubMed]
36. Jiang, J.; Li, J.; Xu, Y.; Han, Y.; Bai, Y.; Zhou, G.; Lou, Y.; Xu, Z.; Chong, K. RNAi knockdown of Oryza sativa root meander curling gene led to altered root development and coiling which were mediated by jasmonic acid signalling in rice. *Plant Cell Environ.* **2007**, *30*, 690–699. [CrossRef]
37. Yuan, Z.; Zhang, D. Roles of jasmonate signalling in plant inflorescence and flower development. *Curr. Opin. Plant Biol.* **2015**, *27*, 44–51. [CrossRef]
38. Wasternack, C.; Forner, S.; Strnad, M.; Hause, B. Jasmonates in flower and seed development. *Biochimie* **2013**, *95*, 79–85. [CrossRef]
39. Sehr, E.M.; Agusti, J.; Lehner, R.; Farmer, E.E.; Schwarz, M.; Greb, T. Analysis of secondary growth in the *Arabidopsis* shoot reveals a positive role of jasmonate signalling in cambium formation. *Plant J.* **2010**, *63*, 811–822. [CrossRef]
40. Wakuta, S.; Suzuki, E.; Saburi, W.; Matsuura, H.; Nabeta, K.; Imai, R.; Matsui, H. OsJAR1 and OsJAR2 are jasmonyl-L-isoleucine synthases involved in wound- and pathogen-induced jasmonic acid signalling. *Biochem. Biophys. Res. Commun.* **2011**, *409*, 634–639. [CrossRef]
41. Zavala, J.A.; Baldwin, I.T. Jasmonic acid signalling and herbivore resistance traits constrain regrowth after herbivore attack in *Nicotiana attenuata*. *Plant Cell Environ.* **2006**, *29*, 1751–1760. [CrossRef] [PubMed]
42. Rao, M.V.; Lee, H.; Creelman, R.A.; Mullet, J.E.; Davis, K.R. Jasmonic acid signaling modulates ozone-induced hypersensitive cell death. *Plant Cell* **2000**, *12*, 1633–1646. [CrossRef] [PubMed]
43. Conconi, A.; Smerdon, M.J.; Howe, G.A.; Ryan, C.A. The octadecanoid signalling pathway in plants mediates a response to ultraviolet radiation. *Nature* **1996**, *383*, 826–829. [CrossRef]
44. Gao, Y.; Wang, J.; Zhao, F. CIRI: An efficient and unbiased algorithm for *de novo* circular RNA identification. *Genome Biol.* **2015**, *16*, 4. [CrossRef] [PubMed]
45. Zhang, X.; Wang, H.; Zhang, Y. Complementary Sequence-Mediated Exon Circularization. *Cell* **2014**, *159*, 134–147. [CrossRef] [PubMed]
46. Li, W.; Godzik, A. Cd-hit: A fast program for clustering and comparing large sets of protein or nucleotide sequences. *Bioinformatics* **2006**, *22*, 1658–1659. [CrossRef] [PubMed]
47. Fu, L.; Niu, B.; Zhu, Z.; Wu, S.; Li, W. CD-HIT: Accelerated for clustering the next generation sequencing data. *Bioinformatics* **2012**, *28*, 3150–3152. [CrossRef] [PubMed]
48. Li, Q.F.; Zhang, Y.C.; Chen, Y.Q.; Yu, Y. Circular RNAs roll into the regulatory network of plants. *Biochem. Biophys. Res. Commun.* **2017**, *488*, 382–386. [CrossRef]
49. Salmena, L.; Poliseno, L.; Tay, Y.; Kats, L.; Pandolfi, P.P. A ceRNA Hypothesis: The Rosetta Stone of a Hidden RNA Language? *Cell* **2011**, *146*, 353–358. [CrossRef]
50. Rubio-Somoza, I.; Weigel, D.; Franco-Zorilla, J.-M.; Garcia, J.A.; Paz-Ares, J. ceRNAs: miRNA Target Mimic Mimics. *Cell* **2011**, *147*, 1431–1432. [CrossRef]
51. Wu, H.J.; Wang, Z.M.; Wang, M.; Wang, X.J. Widespread long noncoding RNAs as endogenous target mimics for microRNAs in plants. *Plant Physiol.* **2013**, *161*, 1875–1884. [CrossRef] [PubMed]

52. Ivashuta, S.; Banks, I.R.; Wiggins, B.E.; Zhang, Y.; Ziegler, T.E.; Roberts, J.K.; Heck, G.R. Regulation of gene expression in plants through miRNA inactivation. *PLoS ONE* **2011**, *6*, e21330. [CrossRef] [PubMed]
53. Zhao, W.; Chu, S.; Jiao, Y. Present scenario of circular RNAs (circRNAs) in plants. *Front. Plant Sci.* **2019**, *10*, 379. [CrossRef] [PubMed]
54. Gao, Y.; Zhao, F. Computational Strategies for Exploring Circular RNAs. *Trends Genet.* **2018**, *34*, 389–400. [CrossRef]
55. Zeng, X.; Lin, W. A comprehensive overview and evaluation of circular RNA detection tools. *PLoS Comput. Biol.* **2017**, *13*, e1005420. [CrossRef]
56. Zhang, X.; Ma, X.; Ning, L.; Li, Z.; Zhao, K.; Li, K.; He, J.; Yin, D. Genome-wide identification of circular RNAs in peanut (*Arachis hypogaea* L.). *BMC Genom.* **2019**, *20*, 653. [CrossRef]
57. Zhang, G.; Diao, S.; Zhang, T.; Chen, D.; He, C.; Zhang, J. Identification and characterization of circular RNAs during the sea buckthorn fruit development. *RNA Biol.* **2019**, *16*, 354–361. [CrossRef]
58. Wang, Y.; Xiong, Z.; Li, Q.; Sun, Y.; Jin, J.; Chen, H.; Zou, Y.; Huang, X.; Ding, Y. Circular RNA profiling of the rice photo-thermosensitive genic male sterile line Wuxiang S reveals circRNA involved in the fertility transition. *BMC Plant Biol.* **2019**, *19*, 1–16. [CrossRef]
59. Ruan, J.; Zhou, Y.; Zhou, M.; Yan, J.; Khurshid, M.; Weng, W.; Cheng, J.; Zhang, K. Jasmonic acid signaling pathway in plants. *Int. J. Mol. Sci.* **2019**, *20*, 2479. [CrossRef]
60. Huang, H.; Liu, B.; Liu, L.; Song, S. Jasmonate action in plant growth and development. *J. Exp. Bot.* **2017**, *68*, 1349–1359. [CrossRef]
61. Wasternack, C. Jasmonates: An update on biosynthesis, signal transduction and action in plant stress response, growth and development. *Ann. Bot.* **2007**, *100*, 681–697. [CrossRef] [PubMed]
62. Zhang, Y.; Zhang, X.O.; Chen, T.; Xiang, J.F.; Yin, Q.F.; Xing, Y.H.; Zhu, S.; Yang, L.; Chen, L.L. Circular intronic long noncoding RNAs. *Mol. Cell* **2013**, *51*, 792–806. [CrossRef] [PubMed]
63. Hickman, R.; Van Verk, M.C. Architecture and dynamics of the jasmonic acid gene regulatory network. *Plant Cell* **2017**, *29*, 2086–2105. [CrossRef] [PubMed]
64. Liu, Y.; Ma, C.; Qin, X.; Yu, H.; Shen, L.; Jin, H. Circular RNA circ_001350 regulates glioma cell proliferation, apoptosis, and metastatic properties by acting as a miRNA sponge. *J. Cell. Biochem.* **2019**, *120*, 15280–15287. [CrossRef]
65. Liang, Y.; Zhang, Y.; Xu, L.; Zhou, D.; Jin, Z.; Zhou, H.; Lin, S.; Cao, J.; Huang, L. CircRNA expression pattern and ceRNA and miRNA-mRNA networks involved in anther development in the CMS line of *Brassica campestris*. *Int. J. Mol. Sci.* **2019**, *20*, 4808. [CrossRef]
66. Li, H.; Durbin, R. Fast and accurate short read alignment with Burrows-Wheeler transform. *Bioinformatics* **2009**, *25*, 1754–1760. [CrossRef]
67. Langmead, B.; Salzberg, S.L. Fast gapped-read alignment with Bowtie 2. *Nat. Methods* **2012**, *9*, 357–359. [CrossRef]
68. Chen, L.; Wang, F.; Bruggeman, E.C.; Li, C.; Yao, B. circMeta: A unified computational framework for genomic feature annotation and differential expression analysis of circular RNAs. *Bioinformatics* **2019**. [CrossRef]
69. Pfaffl, M.W. A new mathematical model for relative quantification in Real-Time RT-PCR. *Nucleic Acids Res.* **2001**, *29*, e45. [CrossRef]
70. Zhang, Z.; Yu, J.; Li, D.; Zhang, Z.; Liu, F.; Zhou, X.; Wang, T.; Ling, Y.; Su, Z. PMRD: Plant microRNA database. *Nucleic Acids Res.* **2010**, *38*, D806–D813. [CrossRef]
71. Kozomara, A.; Birgaoanu, M.; Griffiths-Jones, S. miRBase: From microRNA sequences to function. *Nucleic Acids Res.* **2019**, *47*, D155–D162. [CrossRef] [PubMed]
72. Fan, C.; Hao, Z.; Yan, J.; Li, G. Genome-wide identification and functional analysis of lincRNAs acting as miRNA targets or decoys in maize. *BMC Genom.* **2015**, *16*, 793. [CrossRef] [PubMed]
73. Shannon, P.; Markiel, A.; Ozier, O.; Baliga, N.S.; Wang, J.T.; Ramage, D.; Amin, N.; Schwikowski, B.; Ideker, T. Cytoscape: A software environment for integrated models of biomolecular interaction networks. *Genome Res.* **2003**, *13*, 2498–2504. [CrossRef] [PubMed]

International Journal of
Molecular Sciences

MDPI

Article

Depletion of *KNL2* Results in Altered Expression of Genes Involved in Regulation of the Cell Cycle, Transcription, and Development in *Arabidopsis*

Anastassia Boudichevskaia [1,*], Andreas Houben [1], Anne Fiebig [1], Klara Prochazkova [2], Ales Pecinka [2] and Inna Lermontova [1,3,*]

1 Leibniz Institute of Plant Genetics and Crop Plant Research (IPK) Gatersleben, Corrensstrasse 3, D-06466 Seeland, Germany; houben@ipk-gatersleben.de (A.H.); fiebig@ipk-gatersleben.de (A.F.)
2 Institute of Experimental Botany, Czech Acad Sci, Centre of the Region Haná for Biotechnological and Agricultural Research (CRH), Šlechtitelů 31, CZ-77900 Olomouc, Czech Republic; prochazkova@ueb.cas.cz (K.P.); pecinka@ueb.cas.cz (A.P.)
3 Mendel Centre for Plant Genomics and Proteomics, CEITEC, Masaryk University, Brno CZ-62500, Czech Republic
* Correspondence: boudichevskaia@ipk-gatersleben.de (A.B.); lermonto@ipk-gatersleben.de (I.L.); Tel.: +49/39482 5477 (A.B.); +49/39482 5570 (I.L.)

Received: 10 September 2019; Accepted: 11 November 2019; Published: 15 November 2019

Abstract: Centromeres contain specialized nucleosomes at which histone H3 is partially replaced by the centromeric histone H3 variant cenH3 that is required for the assembly, maintenance, and proper function of kinetochores during mitotic and meiotic divisions. Previously, we identified a KINETOCHORE NULL 2 (KNL2) of *Arabidopsis thaliana* that is involved in the licensing of centromeres for the cenH3 recruitment. We also demonstrated that a knockout mutant for KNL2 shows mitotic and meiotic defects, slower development, reduced growth rate, and fertility. To analyze an effect of *KNL2* mutation on global gene transcription of *Arabidopsis*, we performed RNA-sequencing experiments using seedling and flower bud tissues of *knl2* and wild-type plants. The transcriptome data analysis revealed a high number of differentially expressed genes (DEGs) in *knl2* plants. The set was enriched in genes involved in the regulation of the cell cycle, transcription, development, and DNA damage repair. In addition to comprehensive information regarding the effects of *KNL2* mutation on the global gene expression, physiological changes in plants are also presented, which provides an integrated understanding of the critical role played by KNL2 in plant growth and development.

Keywords: *Arabidopsis*; KNL2; kinetochores; RNA-seq; centromere

1. Introduction

The centromeres are specialized chromosomal domains that are required for proper separation of chromosomes during mitosis and meiosis. The centromere is composed of centromeric DNA, often enriched in satellite repeats, and the large protein complex "kinetochore". In centromeric nucleosomes of most eukaryotes, histone H3 is partially replaced by the centromeric histone H3 variant cenH3 (also known as CENP-A in mammals, CID in *Drosophila*, Cse4 in *Saccharomyces cerevisiae*, and Cnp1 in *Schizosaccharomyces pombe* [1]). Deposition of cenH3 at the centromeric region is a prerequisite of the correct assembly and function of the kinetochore complex. It depends on different cenH3 assembly factors and chaperones [2], the transcription of the centromeric repeats [3–5], and the epigenetic status of centromeric chromatin [6,7]. In mammals, the Mis18 complex composed of Mis18α, Mis18β, and Mis18-binding protein 1 (also known as KNL2) plays an important role in the licensing of centromeres for cenH3 recruitment [8,9]. The human Mis18 protein complex localizes to centromeres

during late telophase and remains associated with the centromere during early G1 phase when new CENP-A is deposited [2,9,10]. It mediates the recruitment of the cenH3 chaperone Holliday junction recognition protein (HJURP) to endogenous centromeres [11,12]. Knockout of murine Mis18a is embryo lethal [7]. Cultured homozygous mutant embryos showed misaligned chromosomes, anaphase bridges, and lagging chromosomes [7].

Up to now, only the cenH3 assembly factor KNL2 has been identified and characterized in plants [13,14]. In contrast to the mammalian cenH3 assembly factor Mis18BP1, the *Arabidopsis* KNL2 protein is present at centromeres during all stages of the mitotic cell cycle, except from metaphase to mid-anaphase [13]. Knockout of *KNL2* in *Arabidopsis* resulted in a reduced amount of cenH3 at centromeres, mitotic and meiotic defects, decreased DNA methylation degree, and lowered growth rate and fertility [13].

All homologs of Mis18BP1 (KNL2) identified up to now contain the conserved SANTA domain [15] at the N-terminus. However, the functional role of this domain still remains obscure. It was suggested that it might be involved in protein–protein interactions due to the presence of many conserved hydrophobic residues. It was shown that an absence of the SANTA domain in *Arabidopsis* KNL2 does not disturb its centromeric localization. Recently, the conserved C-terminal CENPC-k motif [14,16] required for the targeting of Mis18BP1 (KNL2) to centromeres was identified [14,17,18]. It presents in the Mis18BP1 (KNL2) proteins of most eukaryotes excluding therian mammals and *Caenorhabditis elegans* [14,16]. *Arabidopsis* KNL2 binds centromeric repeat *pAL1* and non-centromeric DNA sequences *in vitro*, whereas *in vivo* it associates preferentially with the centromeric repeat *pAL1*. The level and function of the Mis18BP1 protein in human cell culture is regulated by SUMOylation [19], and its centromeric localization is controlled by the phosphorylation in a cell cycle-dependent manner [20]. Whether the KNL2 of plants is regulated in the similar way remains to be elucidated.

Although the Mis18 protein complex is important for the deposition of cenH3 to centromeres in different organisms, its mechanism of function remains to be elucidated in detail. For mammals, it was shown that an interaction of the Mis18 complex with the *de novo* DNA methyltransferases DNMT3A and DNMT3B is required for the regulation of the epigenetic status of centromeric DNA and subsequently the transcription of centromeric repeats [7]. A knockout of mammalian Mis18α resulted in reduced DNA methylation, altered histone modifications, and increased centromeric transcripts in cultured embryos [7]. However, it was not tested whether a knockout of Mis18 complex components has an effect on the methylation status of non-centromeric chromatin and on the expression of other repetitive or gene-coding chromosomal regions. For instance, knockout of *KNL2* resulted in decreased DNA methylation of the marker regions *MEA-ISR* and the *At-SN1* in *Arabidopsis* [13].

In the current study, we used an RNA-sequencing (RNA-seq) approach to address the question of whether the inactivation of KNL2 influences the genome-wide gene expression during seedling and flower bud stages in *Arabidopsis*. This analysis allowed the identification of highly differentially expressed genes (DEGs) in flower buds (n = 1861) and seedlings (n = 459) of the *knl2* mutant. Gene Ontology (GO) term enrichment analysis links the activity of KNL2 to centromere function, DNA repair, DNA methylation as well as regulation of transcription. The specific pattern of gene expression in response to the inactivation of the *KNL2* gene provides a resource for future functional studies to unravel the role of KNL2 in kinetochore assembly and function.

2. Results and Discussion

2.1. Loss of KNL2 Function Leads to Massive Transcriptional Changes

To understand the role of *KNL2* for the kinetochore function, mitotic and meiotic divisions, and subsequently for plant growth and development, we compared the transcriptomes from two tissue types, namely seedlings and flower buds, of wild-type and the *knl2* plants. The experiments in the current study were designed in a way to weaken factors that could introduce experimental noise and would diminish the biological relevance of the data. For the RNA-seq study, we compared control and

mutant plants with the same genetic background (Columbia ecotype) and physical age by performing experiments under the same plant growth conditions. This allowed the identification of DEGs and enriched biological processes. At the same time, the information obtained is limited to a single snapshot of gene expression reflecting the physical age of plants. Further comparative experiments including more time points to study temporal gene expression profiles in the *knl2* mutant line would be desirable, such as the comparison of the transcriptomes of *knl2* and wild-type plants not of the same "physical" but "biological age", since the *knl2* mutant plants showed a delay in growth and development [13].

RNA-seq analysis based on DeSeq2 [21] identified 3261 genes in seedlings (Table S1, Supplementary Materials) that were altered in the *knl2* mutant line (adjusted p-value < 0.05). Among them, 459 genes (Figure 1) were highly differentially expressed (fold change (FC) cutoffs of ≥ 2).

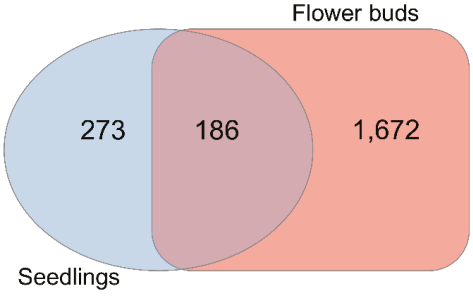

Figure 1. Differential gene expression. Venn diagram showing the number of highly differentially expressed genes (DEGs) (2-fold cutoff, false discovery rate (FDR) corrected p-value < 0.05) obtained by comparing *knl2* versus wild-type ecotype Columbia-0 (Col-0) genes in seedlings and *knl2* versus Col-0 genes in flower buds.

In flower buds, more DEGs were identified in the *knl2* (4750 in total). Out of 1858 highly expressed genes (FC cutoffs of ≥ 2) (Figure 1), 1194 were highly upregulated and 664 were highly downregulated in the *knl2* mutant (adjusted p-value < 0.05). In both tissues, more genes were significantly upregulated than downregulated (Table S1).

In agreement with previously published data [13], which showed absence of the full-length *KNL2* transcript in the *knl2* plants, the mRNA level of *KNL2* was greatly reduced ($\log_2$ FC of −2.63 and −4.57) in seedling and flower bud tissues, respectively, of *knl2* plants, suggesting that the observed transcription responses are the result of *KNL2* depletion.

To explore the distribution of DEGs and to identify the biological consequences of the *KNL2* inactivation, we used the GO::TermFinder [22]. Gene Ontology (GO) enrichment analysis for the "Biological process" was compared for downregulated and upregulated DEGs (adjusted p-value < 0.05) represented in seedlings and, separately, in flower buds. Detailed information about all overrepresented processes is given in a supporting information dataset (Dataset S1, Supplementary Materials). In this paper, we consider in more detail the categories associated with cell division, chromatin status, and plant growth and development. The results of the GO enrichment analysis can shed new light on how *KNL2* depletion leads to plant growth and development alterations.

2.2. Knockout of KNL2 Impairs Expression of Genes Involved in Kinetochore Function

Kinetochores are responsible for the accurate segregation of chromosomes during mitosis and meiosis. Our RNA-seq analysis revealed GO terms related to physical events associated with both types of cell division, such as the "chromosome segregation", "meiosis I", "meiotic chromosome separation", "mitotic metaphase plate congression", "mitotic recombination", and "attachment of mitotic spindle microtubules to kinetochore" in seedlings (Table 1). All DEGs representing these categories were downregulated in the *knl2* plants (Dataset S1, Tables S2 and S3).

Table 1. Assignment of differentially expressed downregulated genes in *knl2* seedlings to different functional categories related to cell processes. Gene Ontologies were analyzed for term enrichment using the Generic Gene Ontology GO::TermFinder tool (cutoff of 5% false discovery rate (FDR)).

GO ID	Biological Process	*p*-Value	FDR Rate, %	Gene Count
GO:0051315	Attachment of mitotic spindle microtubules to kinetochore	0.002143	2.39	2
GO:0007049	Cell cycle	0.003143	2.94	41
GO:0000075	Cell cycle checkpoint	0.004300	3.40	5
GO:0022402	Cell cycle process	0.001001	0.92	30
GO:0007059	Chromosome segregation	0.007086	4.99	11
GO:0051304	Chromosome separation	0.001526	1.15	6
GO:0051103	DNA ligation involved in DNA repair	6.37×10^{-5}	0.06	4
GO:0006310	DNA recombination	4.72×10^{-6}	0.00	20
GO:0006281	DNA repair	0.000745	0.79	26
GO:0006302	Double-strand break repair via homologous recombination	1.79×10^{-5}	0.02	15
GO:0006303	Double-strand break repair via nonhomologous end joining	0.000127	0.15	5
GO:0035825	Homologous recombination	0.001124	0.93	8
GO:0007127	Meiosis I	0.001483	1.10	9
GO:0051307	Meiotic chromosome separation	0.001680	1.31	4
GO:0051310	Metaphase plate congression	0.002143	2.40	2
GO:0007080	Mitotic metaphase plate congression	0.002143	2.44	2
GO:0006312	Mitotic recombination	0.000820	0.82	5
GO:0045786	Negative regulation of cell cycle	0.005582	4.02	7
GO:0000726	Non-recombinational repair	0.000127	0.15	5
GO:0007131	Reciprocal meiotic recombination	0.001124	0.94	8
GO:0071156	Regulation of cell cycle arrest	0.006230	4.82	2

GO terms characterizing the functions of kinetochores, like microtubule binding, chromosome movement, and checkpoint signaling were overrepresented in the downregulated gene list of *knl2* flower bud samples (Table 2).

Table 2. Assignment of differentially expressed downregulated genes in *knl2* flower buds to different functional categories related to cell processes. Gene Ontologies were analyzed for term enrichment using the Generic Gene Ontology GO::TermFinder tool (cutoff of 5% FDR).

GO ID	Biological Process	*p*-Value	FDR Rate, %	Gene Count
GO:0007049	Cell cycle	3.13×10^{-9}	0.00	83
GO:0048468	Cell development	3.30×10^{-8}	0.00	56
GO:0030154	Cell differentiation	$2.36 \times 10–^{5}$	0.08	95
GO:0051301	Cell division	5.97×10^{-7}	0.00	54
GO:0016049	Cell growth	3.06×10^{-6}	0.05	62
GO:0032989	Cellular component morphogenesis	2.59×10^{-8}	0.00	72
GO:0016043	Cellular component organization	2.03×10^{-8}	0.00	261
GO:0070192	Chromosome organization involved in meiotic cell cycle	0.000320	0.52	11
GO:0007059	Chromosome segregation	0.001374	1.31	17
GO:0000910	Cytokinesis	3.63×10^{-5}	0.15	21
GO:0007010	Cytoskeleton organization	6.02×10^{-6}	0.04	33
GO:0061640	Cytoskeleton-dependent cytokinesis	0.000676	0.81	17
GO:0000086	G2/M transition of mitotic cell cycle	0.000205	0.41	7
GO:0048229	Gametophyte development	3.69×10^{-9}	0.00	70
GO:0045143	Homologous chromosome segregation	5.80×10^{-5}	0.18	10
GO:0035825	Homologous recombination	2.30×10^{-5}	0.09	13
GO:0007127	Meiosis I	2.23×10^{-5}	0,09	15
GO:0061982	Meiosis I cell cycle process	7.78×10^{-6}	0.08	16
GO:0051321	Meiotic cell cycle	4.41×10^{-5}	0.15	27
GO:0045132	Meiotic chromosome segregation	1.62×10^{-5}	0.10	14
GO:0051307	Meiotic chromosome separation	0.001212	1.24	5
GO:0140013	Meiotic nuclear division	1.12×10^{-5}	0.07	20
GO:0000226	Microtubule cytoskeleton organization	0.000596	0.78	17
GO:0007018	Microtubule-based movement	0.000235	0.44	10
GO:0000278	Mitotic cell cycle	5.20×10^{-5}	0.19	36
GO:0000281	Mitotic cytokinesis	0.001316	1.29	16
GO:0006312	Mitotic recombination	0.001079	1,20	6
GO:0098813	Nuclear chromosome segregation	0.000706	0.85	16
GO:0000280	Nuclear division	0.000107	0.20	24
GO:0007131	Reciprocal meiotic recombination	2.30×10^{-5}	0.09	13
GO:0051726	Regulation of cell cycle	0.000251	0.45	32
GO:0007129	Synapsis	7.30×10^{-5}	0.19	9

For instance, reduced transcript levels were found for genes with known microtubule-associated functions [23] such as *KINESIN 5* (*ATK5*; AT4G05190), *TITAN1* (*TTN1*; AT3G60740), and *HINKEL* (AT1G18370). The *CELL DIVISION CYCLE 20.1* (*CDC20.1*; AT4G33270), known for its critical role in the spindle assembly checkpoint-dependent meiotic chromosome segregation [24], was also significantly suppressed in the flower buds of *knl2* plants. Another example is the reduced expression of *BUB1* (AT2G20635), a protein kinase containing the Mad3-BUB1-I domain. Being together with CDC20.1 in the same protein–protein interaction network, BUB1 plays an important role in the assembly of the checkpoint proteins at the kinetochore [25]. In our RNA-seq study, it was highly downregulated in both types of tissue. Several other kinetochore associated genes, like *GAMMA-TUBULIN* (*TUBG1*; AT3G61650), *PLEIADE* (*PLE*; AT5G51600), and *AURORA KINASE 1* (AT4G32830) were downregulated in *knl2* flower buds. The expression of the inner kinetochore *CENP-C* (AT1G15660) was decreased in both seedlings and flower buds. Knockout of *KNL2* results in a reduced amount of *cenH3* transcripts of *Arabidopsis* [13]. This result was confirmed by RT-qPCR analysis of the samples used for the current RNA-seq study.

2.3. Reduced DNA Methylation in the knl2 Mutant Might Be Responsible for the Activation of a High Number of Transposons

Knockout of *Arabidopsis KNL2* leads to a reduced level of DNA methylation [13]. In our RNA-seq study, a number of genes related to the DNA and histone methylation showed repressed differential expression in the *knl2* line (in both tissues). For example, histone H3 lysine 9 di-methyltransferase *SUVH4* (AT5G13960), *CHROMOMETHYLASE 2* (*CMT2*; AT4G19020), and *ARGONAUTE 6* (*AGO6*; AT2G32940) were found among differentially downregulated genes in the flower buds (adjusted p-value < 0.05), whereas *DEMETER-LIKE 1* (*DML1*; AT2G36490) showed reduced expression in both tissues used for analysis.

It is known that the activity of transposons is controlled epigenetically through DNA methylation and repressive histone marks (reviewed in [26–28]). It is likely that a reduced level of DNA methylation in the *knl2* mutant results in an altered expression of transposons. Indeed, a considerable number of transposable elements were differentially expressed in *knl2* seedlings (n = 52) and flower buds (n = 89). These elements belonged to the DNA transposons (*CACTA-like*, *hAT-like*, *Mutator-like*) and LTR retrotransposons (*Copia-like*, *Gypsy-like*). In both tissues, more transposons were upregulated in *knl2* plants (Figure 2).

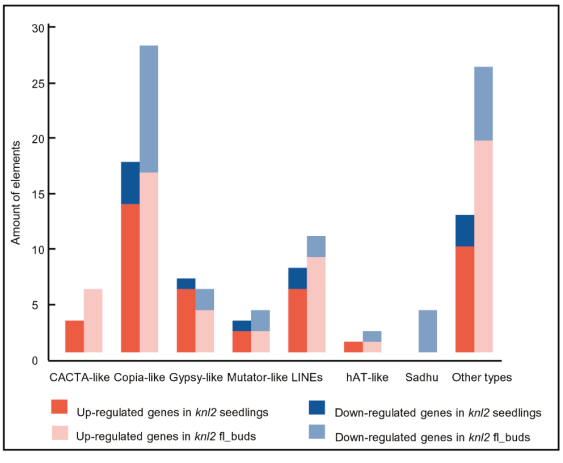

Figure 2. Transposable elements and their amount identified in the *knl2* mutant line. Information is given about transposons up- and downregulated in the *knl2* seedlings and *knl2* flower buds.

In contrast, the non-LTR retrotransposons *Sadhu 1-3* (AT3G44042), *Sadhu 3-1* (AT3G44042), *Sadhu 4-1* (AT5G28913), and *Sadhu 5-1* (AT4G01525) had decreased expression level in the *knl2* flower buds. Depression of *Sadhu 3-1* retroelement was also observed in the epigenetic mutant *suvh4* [29].

2.4. Altered Expression of the Root-related Genes Explains the Slow Root Growth of knl2

Root length was compared between seven-day-old control and the *knl2* mutant seedlings. The average root length of mutant seedlings (0.66 cm) was about 3 times shorter than that of the wild-type (1.82 cm) (Figure 3), and GO terms related to the root development such as "regulation of root development" and "primary root development" were highly overrepresented among the genes downregulated in the *knl2* seedlings (Table 1).

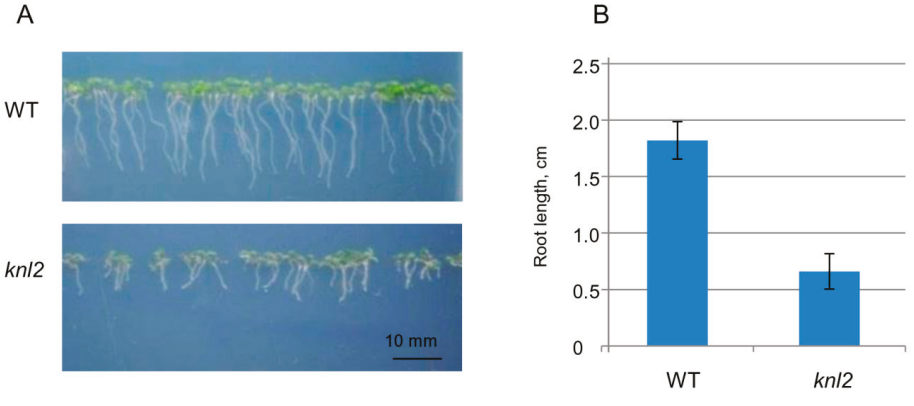

Figure 3. Effect of *KNL2* depletion on the root development. (**A**) Representative phenotypes of wild-type (WT) and *knl2* plants germinated and grown for seven days on $\frac{1}{2}$ Murashige and Skoog (MS) medium. Bar = 10 mm. (**B**) Quantitative data for plants described in (**A**). Data are the means ± standard errors, $n = 20$. Student's *t*-test, $p < 0.01$.

We additionally tested all root-related genes available in TAIR for their overlap with the differentially expressed genes in the *knl2* seedlings. As a result, 119 differentially expressed genes were identified (Table S4, Supplementary Materials). Among them, 14 were highly suppressed (FC cutoffs of ≥ 2). The reduced transcript level was found for *SHORT AND SWOLLEN ROOT 1* (*SSR1*; AT5G02130). The *ssr1-2* plants show reduced root growth [30]. Other downregulated genes encoding the chloroplast/plastid localized GAPDH isoforms are *GAPCp1* (AT1G16300) and *GAPCp2* (AT1G79530). *gapcp* double mutants are characterized by arrested root development, dwarfism, and sterility [31]. The transcription factor *AGAMOUS-like 14*/*XAL2* (AT4G11880) preferentially expressed in roots is highly suppressed in *knl2* seedlings ($\log_2$ FC of −1.05, adjusted *p*-value 0.0001). Several studies demonstrated that *xal2* mutants have short roots [32,33]. In addition, we observed the reduced transcript level of *EMBRYO DEFECTIVE 2757* (*EMB2757*; AT4G29860) in *knl2* seedlings. Genetic analysis of *EMB2757* in *Arabidopsis* has demonstrated that mutations in this gene cause defects in both embryo and seedling development [34]. Upregulated differentially expressed genes in *knl2* seedlings can be further exemplified with *RAPID ALKALINIZATION FACTOR 23 (RALF23*; AT3G16570). Overexpression of *RALF23* leads to slower growing seedlings with roots that have reduced capacity to acidify the rhizosphere [35].

2.5. DNA Damage Repair Genes are Downregulated in the knl2 Plants

The genome stability is maintained by DNA damage responses. The failure to repair DNA damage leads to negative processes related to plant growth, reproduction, and even lethality. We found

that genes representing the GO term "DNA repair" (26 genes) and related categories, such as "double-strand break repair via homologous recombination", "non-recombinational repair", and "DNA ligation involved in DNA repair" were overrepresented among *knl2* DEGs (Table 1). All genes of these categories were downregulated in the mutant. Among downregulated genes were the key players participating in the canonical nonhomologous end joining, such as *KU70* (AT1G16970), *KU80* (AT1G48050), and *LIGASE 4* (AT5G57160). It is known that mutations in these genes lead to increased sensitivity to double-strand DNA breaks (DSB)-inducing factors (reviewed in [36]). AT5G20850, encoding a DNA recombination and repair protein *RAD51*, is another example of a gene with a decreased expression level in *knl2* seedlings ($\log_2$ FC of −0.99, adjusted *p*-value 1.47×10^{-6}). Loss of *RAD51* function does not affect the vegetative development of *Arabidopsis*, probably due to functional redundancy with other genes of the *RAD51* family, but is essential for meiotic repair of DSBs caused by *AtSPO11−1* [37]. In addition, the *RAD51-like* gene, *DISRUPTION OF MEIOTIC CONTROL 1* (*DMC1*; AT3G22880), known to promote interhomolog recombination was strongly downregulated in the *knl2* flower buds ($\log_2$ FC of −1.20, adjusted *p*-value 1.25×10^{-8}). Interestingly, the mammalian kinetochore protein BUB1, playing an important role in chromosome segregation, is also known to participate in the DNA damage response [38]. In human and mouse cells, cenH3/CENP-A accumulates at DSBs together with CENP-N, CENP-T, and CENP-U [39]. Since the induction of DNA damage by radiation resulted in an increased expression of cenH3, the authors proposed a cenH3 function in DNA repair. Further research is needed to unravel the interrelationships between kinetochore genes and the DNA damage response.

To test whether the altered mRNA levels are associated with changed capacity of *knl2* plants for DNA damage repair, we exposed wild-type and mutant plants to 10 μM DNA inter-strand crosslink inducer mitomycin C (MMC), 50 nM DNA strand breaker bleomycin, and 10 nM enzymatic DNA-protein crosslinker camptothecin (Figure S1, Supplementary Materials). This pilot experiment indicated sensitivity of *knl2* plants to MMC, but not other tested drugs (Figure 4).

To validate this result, we treated *knl2* plants with a series of MMC concentrations (2.5 to 15 μM) and found significant reduction in their root growth compared to wild-type plants (Figure 4A,B). Next, we performed propidium iodide (PI) staining of root apices from plants treated for 24 h with 0, 10, and 20 μM MMC. Intense PI staining inside the cells indicates damaged plasma membranes, typical for stressed and dead cells. Under mock conditions, wild-type plant root apical meristems were intact, whereas the meristems of *knl2* plants showed few intensely stained cells. MMC treatment caused dose-dependent accumulation of intensely stained cells in the meristems of wild-type plants, but the increase in the meristem of *knl2* plants was more prominent.

Based on this, we conclude that *knl2* plants fail to properly activate specific DNA damage repair factors, have reduced capacity for repair of DNA inter-strand crosslinks, and suffer from increased cellular damage.

2.6. Knockout of KNL2 Results in Deregulated Expression of a High Number of Transcription Factors

We hypothesized that a large number of DEGs in the *knl2* mutant may be the result of deregulated expression of transcription factors. Therefore, the *knl2* mutant transcriptome was further screened for the presence of differentially expressed transcription factors (TFs). TFs were retrieved from The Plant TF database v.4 [40]. In *knl2* seedlings, 202 TFs were expressed (43 highly differentially expressed), whereas in *knl2* flower buds 330 TFs (137 highly differentially expressed) were detected. The classification of TFs is visualized in the heat map (Figure 5) and is given by the supporting information dataset (Dataset S2, Supplementary Materials). While most of the TF families showed a heterogeneous profile for the single TFs, some of the TF families behaved homogeneously (Figure 5). For example, the TF families B3 and MIKC_MADS and M-type_MADS mostly included downregulated genes in the *knl2* mutant, whereas the TF families ERF, NAC, and WRKY were enriched for upregulated genes. TF families in which many genes were highly differentially expressed were bHLH, C2H2, ERF, HD-ZIP, LBD, MIKC_MADS and M-type_MADS, NAC, and WRKY. The highest expression among TFs was

observed in the NAC family. AT5G14490 encoding for NAC domain-containing protein 85 was highly upregulated in flower buds (log_2 FC of 3.45, adjusted *p*-value 2.69×10^{-12}).

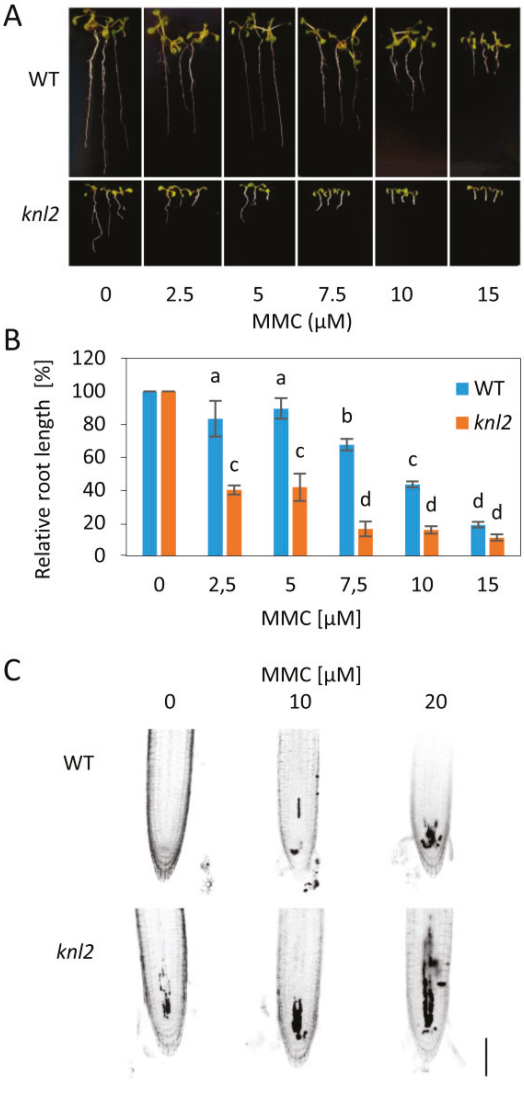

Figure 4. Sensitivity of *knl2* plants to DNA damage. (**A**) Representative phenotypes of wild-type (WT) and *knl2* plants grown for 14 days on mitomycin C (MMC)-containing media. Bar = 10 mm. (**B**) Quantitative data for plants grown as described in (**A**). Error bars represent the standard deviation between the means of three biological replicates, each represented by 15 to 20 plants. Letters above the bars indicate statistically significantly different groups in ANOVA (*p*-value ≤ 0.05) and post hoc Tukey's test. (**C**) Analysis of propidium iodide (PI) uptake (dark sectors) in roots of WT and *knl2* plants. Four-day-old plants were treated with the specified concentration of MMC for 24 h prior to analysis. Bar = 50 µm.

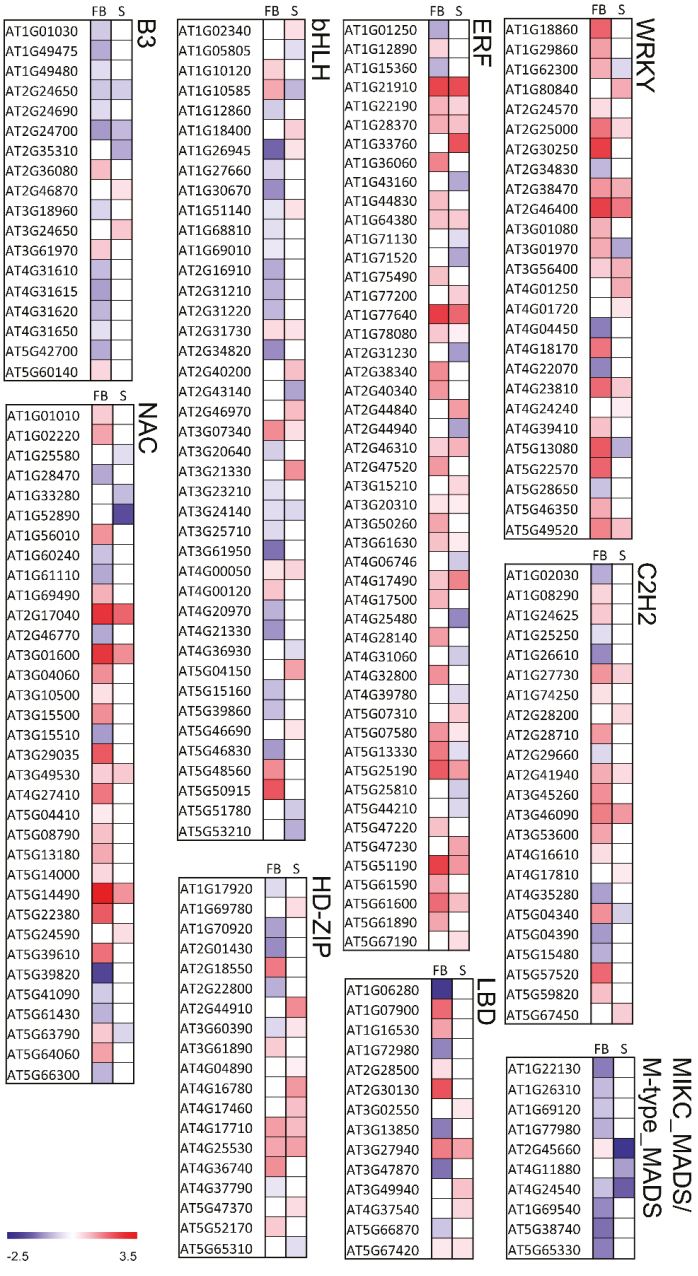

Figure 5. Differentially expressed genes encoding transcription factors in the *knl2* mutant line. Expression in *knl2* flower buds and *knl2* seedlings is depicted as F and S, respectively. Red and blue represent up- and downregulated differentially expressed genes, respectively. All values are $\log_2$ transformed. The gradient color illustrates the expression value.

TFs with an altered expression in the *knl2* mutant are involved in different processes and provide insight into *Arabidopsis* development changes due to the inactivation of the kinetochore gene *KNL2*. There was a striking coordinated downregulation of genes representing the MADS-box family, which are the key regulators of seed and flower development (detailed description is presented below in 3.7). The upregulated TFs can be exemplified by the genes of the WRKY family. The TFs of this family play an important role in plant development and responses to environmental stress stimuli [41–43]. From 74 members of the WRKY TF family, 13 were differentially expressed in seedlings and 26 in the flower buds. The differentially expressed genes *WRKY33* (AT2G38470) and *WRKY46* (AT2G46400), highly upregulated in seedlings and flower buds, are known to play a role in heat stress responses. The expression of these genes was elevated in *MBF1c*-overexpressing plants, which showed enhanced tolerance to heat compared with wild-type plants [44]. *WRKY46* additionally regulates responses to other stresses in *Arabidopsis* [45–47].

Another TF family with overrepresented genes is ERF. The most highly activated genes in flower buds include *DREB19* (AT2G38340; $\log_2$ FC of 1.54, adjusted *p*-value 0.001), *DREB 26* (AT1G21910; $\log_2$ FC of 2.43, adjusted *p*-value 6.77×10^{-7}), and *RAP2.6L* (AT5G13330; $\log_2$ FC of 1.75, adjusted *p*-value 3.54×10^{-10}). A previous study of the *DREB19*, *DREB26*, and *RAP2.6L* effect in *Arabidopsis* demonstrated the participation of the genes in plant developmental processes as well as biotic and/or abiotic stress signaling [48].

The heat map also revealed genes that are differentially expressed in flower buds but not in seedlings and vice versa. We observed that 94 highly differentially expressed genes were present only in flower buds and 18 highly regulated genes were seedling-specific (Dataset S2). The transcriptional repressor of the RAV family *TEMPRANILLO 1* (*TEM1*), known to postpone floral induction [49], is another example of the highly upregulated gene present in the flower buds ($\log_2$ FC of 1.55).

2.7. Late Flowering of the knl2 Plants is Determined by the Altered Expression of Flowering Genes

We observed that flowering of the *knl2* plants delays for 10–14 days compared to wild-type (Figure 6; Figure S2, Supplementary Materials).

From this observation, we could identify a number of enriched GO terms related to the floral development in our RNA-seq data from *knl2* flower buds. These represent such GO categories as "reproduction", "regulation of pollen tube growth", "pollen germination", "pollination", and "pollen development" (Table 3).

Table 3. Assignment of genes differentially expressed in *knl2* flower buds to development-related functional categories based on GO::TermFinder. Genes downregulated in the *knl2* flower buds were included into the GO enrichment analysis (cutoff of 5% FDR).

GO ID	Biological Process	*p*-Value	FDR Rate, %	Gene Count
GO:0048653	Anther development	0.000711	0.84	13
GO:0048589	Developmental growth	0.004788	4.32	54
GO:0060560	Developmental growth involved in morphogenesis	2.06×10^{-5}	0.10	51
GO:0044703	Multi-organism reproductive process	0.002391	2.32	26
GO:0009555	Pollen development	4.10×10^{-11}	0.00	61
GO:0010584	Pollen exine formation	2.12×10^{-5}	0.09	10
GO:0009846	Pollen germination	0.000968	1.15	13
GO:0048868	Pollen tube development	1.57×10^{-6}	0.00	36
GO:0009860	Pollen tube growth	7.09×10^{-9}	0.00	34
GO:0009856	Pollination	2.44×10^{-5}	0.08	44
GO:0010769	Regulation of cell morphogenesis involved in differentiation	0.001673	1.84	9
GO:0080092	Regulation of pollen tube growth	0.000708	0.85	9
GO:0000003	Reproduction	3.55×10^{-4}	0.50	189
GO:0048443	Stamen development	0.002527	2.46	15

Genes representing these and related categories in Table 3 were downregulated in the *knl2* flower buds. Some of the genes belong to the MYB transcription factors and regulate the plant microgamete development. For instance, *AtMYB103* (AT1G63910), important for pollen development [50], is one of the highly suppressed flower bud genes in *knl2*. The expression of other prominent transcription

factors like *AGAMOUS-LIKE 66* (*AGL66;* AT1G77980) and *AGL104* (AT1G22130) involved in pollen maturation and tube growth was significantly reduced. Adamczyk and Fernandez [51] demonstrated that double mutant plants *agl66 agl104* could produce pollen but had severely reduced fertility and aberrant pollen tube growth. Along with *AGL66* and *AGL104*, *AGL94* (AT1G69540) belongs to the MIKC * factors which are highly active in pollen as major regulators of pollen maturation programs [51,52]. These three genes were significantly downregulated in the *knl2* flower buds (adjusted *p*-value < 0.001). This finding might explain the reduced fertility of *knl2* plants in addition to the role of KNL2 in mitosis and meiosis [13].

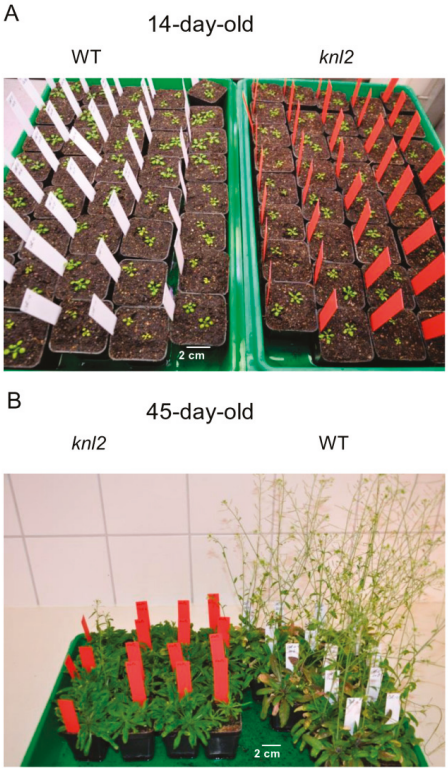

Figure 6. Effect of *KNL2* depletion on the flowering time. (**A**) At early growth stages, no obvious phenotypical differences between wild-type (WT) and the *knl2* mutant were observed. (**B**) The flowering time of the *knl2* mutant delayed by 10–14 days compared to *Arabidopsis* wild-type. Seeds of the *knl2* mutant and wild-type were germinated under short-day conditions, 8 h light/20° C and 16 h dark/18 °C, for two weeks and then plants were transferred to the cultivation room with long-day conditions, 16 h light/20 °C and 8 h dark/18 °C.

The RNA-seq data analysis and observation of the delayed flowering prompted us to inspect the RNA-seq data of the *knl2* seedlings. We asked the questions of whether and, if so, how many flowering-related genes based on the FLOR-ID overlap with the differentially expressed genes in the *knl2* seedlings. From 306 genes, 36 genes could be identified (Dataset S3, Supplementary Materials). There was a striking coordinated downregulation of several prominent flowering-related genes. For example, the floral integrator *Flowering Locus T* (*FT*; AT1G65480), known to be expressed in leaves, was significantly downregulated in *knl2* seedlings. Its reduced expression is in correspondence with the downregulation of *SUPPRESSOR OF OVEREXPRESSION OF CONSTANS 1* (*SOC1*; AT2G45660)

in the *knl2* seedlings ($\log_2$ FC of −2.24, adjusted *p*-value 7.72×10^{-61}). It is known that flowering activator *SOC1* acts in a positive-feedback loop with *AGL24*, which is the important MIKC^c-type transcription factor positively regulating flowering in *Arabidopsis* (reviewed in [53]). In our RNA-seq study, the *AGL24* showed reduced expression in both *knl2* seedlings and flower buds.

GIGANTEA (*GI*; AT1G22770), an important gene in regulating photoperiodic flowering, had a reduced expression in the *knl2* mutant line compared to wild-type. Another regulator of transition to flowering *FKF1* (*ADO3;* AT1G68050) was highly downregulated in the *knl2* mutant line ($\log_2$ FC of −1.70, adjusted *p*-value 2.79×10^{-17}). A member of the MADS-box family *XAANTAL2* (*XAL2/AGL14*; AT4G11880), which is a necessary and sufficient agent to induce flowering [54], showed decreased expression level in the *knl2* seedlings (log2 FC of −1.05, adjusted *p*-value 0.002).

The reduced activity of flower inductive pathway genes observed in the *knl2* seedlings might explain the delay in flower initiation, at least under long-day conditions.

2.8. Knockout of KNL2 Results in Altered Expression of Genes Controlling Seed Development

The loss-of-function *knl2* mutant showed reduced seed production [13]. We used the SeedGenes Project database including 481 genes in order to examine the overlap between these genes and the 4750 genes that we found to be significantly differentially expressed in response to *KNL2* inactivation. From these genes, 42 were differentially expressed in the *knl2* flower bud samples (Table S5, Supplementary Materials). Among downregulated genes, there are those whose disruption causes embryo abortion, such as *CYL 1* (AT5G13690), *EMB 1674* (AT1G58210), *EMB 2184* (AT1G75350), *EMB 3003* (AT1G34430), *EMB 3004* (AT3G06350), and *IMPL 2* (AT4G39120). Highly upregulated genes that include *HSP 17.4* (AT3G46230), *RLP37* (AT3G23110), and *NCED3* (AT3G14440) are known for their expression in seeds and response to abiotic stresses or defense.

2.9. Real-time Quantitative PCR Confirms RNA-seq Analysis

To validate the quality of the RNA-seq data by qRT-PCR, we selected eight genes differentially expressed in seedlings and 11 genes differentially expressed in flower buds (Figure 7; Figure S3, Supplementary Materials). In the case of seedlings, four genes involved in the regulation of root growth (AT4G11880, AT4G28720, AT3G50060, AT2G43140) and two genes involved in the regulation of flowering time (AT2G45660, AT1G68050) were selected for the analysis. In the case of flower buds, an expression of five genes involved in the regulation of flowering time (AT5G48560, AT2G40080, AT5G37770, AT1G10120, AT1G02580) and four genes involved in the regulation of seed development (AT2G01860, AT3G23110, AT5G13690, AT5G23940) was validated. *KNL2* (At5g02520) and *cenH3* (At1g01370) genes were included for the analysis in both types of tissues. Our qRT-PCR confirmed the extreme downregulation of *KNL2* gene expression in the mutant line. All RNA-seq-based determined up- and downregulated genes showed the same qualitative response in both seedlings and flower buds based on qRT-PCR (correlation coefficients between qRT-PCR and RNA-seq data of 0.996 and 0.974, respectively).

2.10. Conclusions

KNL2 of *Arabidopsis* is involved in regulating the centromeric loading of cenH3, and its knockout results in mitotic and meiotic defects and reduced DNA methylation, followed by reduced growth rate and fertility compared to wild-type [13]. Our comparative RNA-seq analysis revealed that these abnormalities were associated with an altered expression of genes regulating corresponding processes. For instance, the reduced growth rate of roots and late flowering of the *knl2* mutant correlate with the altered expression of genes regulating root growth and flowering, respectively. We propose that KNL2 has an essential regulatory function in plant growth and development that is much broader than the regulation of centromeric localization of cenH3 only.

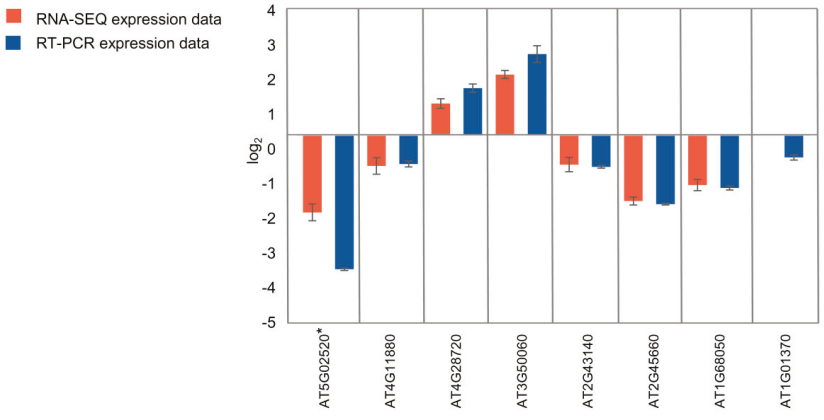

Figure 7. qRT–PCR validation of RNA-seq results. Eight genes were selected from the genes differentially expressed in seedlings according to the RNA-seq data analysis. Detailed annotation of the selected genes is presented in Table S2 (Supplementary Materials). *At5g02520 corresponds to *KNL2*. Error bars indicate the standard error of three biological replicates in qRT-PCR.

3. Materials and Methods

3.1. Plant Materials and Growth Conditions

The *A. thaliana knl2* mutant (SALK_039482) in Col-0 background was described previously [13]. Seeds of *A. thaliana* wild-type and *knl2* were germinated in Petri dishes on half strength Murashige and Skoog (MS) medium (Murashige and Skoog, 1962) for eight days. For harvesting of flower buds, populations of wild-type and *knl2* plants (30 plants per each population) were grown in soil until flowering. In both cases, plants were cultivated with a 16 h photoperiod (21 °C day/18 °C night), 70% relative humidity. Light irradiance at plant level was 130 μmol m^{-2} s^{-1}.

3.2. DNA Damage Sensitivity Assays

For the pilot root length assay experiment, plants were germinated and grown for seven days on $\frac{1}{2}$ strength Murashige and Skoog medium containing 0.01% DMSO and different DNA damage inducers—mitomycin C (MMC) (Duchefa, Haarlem, The Netherlands), bleomycin (Calbiochem, San Diego, CA, USA), and camptothecin (Sigma-Aldrich, Saint Louis, MO, USA) with concentrations specified in the text. For the subsequent analysis, plants were germinated and grown for 14 days on media containing different concentrations of MMC (2.5, 5, 7.5, 10, and 15 μM from Sigma-Aldrich). For PI staining assay, plants were grown on solid $\frac{1}{2}$ Murashige and Skoog medium for four days, then transferred to liquid $\frac{1}{2}$ Murashige and Skoog medium containing 0, 10, and 20 μM MMC and grown for 24 h. Subsequently, the plants were stained with 10 μg/mL propidium iodide solution (Sigma-Aldrich) for 3 min, rinsed with tap water and analyzed using an AxioImager Z2 (Zeiss, Jena, Germany) microscope equipped with the DSD2 confocal module (Andor Technology, Belfast, Great Britain). Plants for all procedures were grown in a Percival growth chamber under long-day (16 h light) conditions and 21 °C.

3.3. RNA Isolation and Illumina Sequencing

Total RNA was extracted from the eight-day-old seedlings of *A. thaliana*. At least 60 seedlings (100 mg) were pooled to produce a biological replicate. For the RNA-seq analysis of flower buds, inflorescences were harvested from three individual plants for each sample (30 mg). Flower buds older than stage 12 and flowers [55] were removed. All tests were performed on three biological

replicates per condition and genotype. Total RNA was isolated from seedlings and flower bud samples using the RNeasy Plant Mini Kit (Qiagen, Hilden, Germany) according to the manufacturer's manual. The RNA preparations were checked for quality using a NanoDrop spectrophotometer and a 2100 Bioanalyzer (Agilent, Santa Clara, CA, USA). In total, 12 RNA samples (1 µg each) were provided to the IPK-Sequencing-Service (IPK, Gatersleben, Germany) for construction of cDNA libraries with the TruSeq RNA Sample Preparation Kit (Illumina, San Diego, CA, USA). The libraries were sequenced in a HiSeq2500 rapid 100-bp single-read run system After sequencing, the adapter sequences and the barcodes were removed.

3.4. RNA-seq Data Processing

Sequencing quality of the reads was examined by using FastQC Read Quality reports, Galaxy Version 0 0.72 [56]. At least 94% of the bases of each read in all samples possessed Illumina Quality >30 and no sequence flagged as poor quality was detected.

Sequences were aligned against the *Arabidopsis* TAIR 10 genome assembly using HISAT2 Galaxy tool version 2.0.3. [57] with default settings. Read counts for each gene were quantified based on the BAM files produced with the HISAT2 by using the tool feature Counts, Galaxy Version 1.4.6.p5 [58]. The advanced setting parameters were strand specificity = "no", GFF feature type filter = "exon", and GFF gene identifier = "Parent". Differentially expressed features were determined based on the feature Counts tables by applying the tool DESeq2, Galaxy Version 2.11.38 [21] with the setting parameter fit type = "parametric". DESeq2 tested for differential expression based on a model using the negative binomial distribution. Differentially expressed genes were identified by comparison of two groups, namely, (1) a mutant line and the wild-type control, condition seedlings and (2) a mutant line and the wild-type control, condition flower buds.

The results of all statistical tests were adjusted for the multiple testing false discovery rate (FDR) with the Benjamini and Hochberg procedure [59]. A cutoff value of adjusted p-values equal to 0.05 was chosen as a threshold to identify significant differentially expressed genes.

3.5. Analysis of Differentially Expressed Genes (DEGs)

Functional characterization of the DEGs showing significant expression changes in response to *KNL2* depletion was done based on the TAIR10 annotation (https://www.arabidopsis.org/). Gene Ontologies were analyzed for term enrichment using the Generic Gene Ontology GO::TermFinder tool ([22]. The analysis was carried out using the Benjamini–Hochberg FDR with a filter p-value of < 0.05.

Information about flowering-related genes was extracted from the Flowering Interactive Database [60]. The appearance of the transcription factors in the analyzed gene sets was confirmed with the Plant Transcription Factor Database v.4.0 [40]. Information about the genes essential for the *Arabidopsis* development from the SeedGenes Project [61] was used to find the corresponding genes among differentially expressed genes.

3.6. Gene Expression Validation by Reverse Transcription Quantitative PCR (RT-qPCR)

Total RNA extraction was performed as described above. The RNA was treated with DNase I (Ambion, Thermo Fisher Scientific, Waltham, MA, USA) according to the manufacturer's protocol to eliminate any residual genomic DNA. Reverse transcription was performed using a first-strand cDNA synthesis kit, oligo dT (18-mer) primer (both Fermentas, Thermo Fisher Scientific, Waltham, MA, USA), and 2 µg of total RNA as a starting material.

The gene-specific primers (Table S6, Supplementary Materials) were designed using the fully automated QuantPrime tool [62]. The amplification of the *UBQ10* (AT4G05320) reference gene [63] was used as an internal control to normalize the data.

Quantitative real-time measurements were performed using POWER SYBR Green Master Mix reagent in a QuantStudio 6 Flex system (Applied Biosystems, Thermo Fisher Scientific, Waltham, MA,

USA), according to the manufacturer's instructions. The cDNA equivalent to 40 ng of total RNA was used in a 10 µL PCR reaction.

The cycling conditions comprised 10 min polymerase activation at 95 °C and 40 cycles at 95 °C for 3 s and 60 °C for 30 s. Three biological replicates per genotype (wild-type and *knl2* mutant line) in both conditions (seedlings and flower buds) were tested. Each biological replicate was represented with three technical replicates, which were analyzed during the same run. Relative gene expression was calculated using the comparative method $2^{-\Delta\Delta CT}$ [64].

3.7. Data Availability

Raw reads are available under the accession number PRJEB32230 at http://www.ebi.ac.uk/ena/data/view/PRJEB32230.

Supplementary Materials: Supplementary materials can be found at http://www.mdpi.com/1422-0067/20/22/5726/s1. Figure S1. *knl2* sensitivity to DNA damaging agents. The plants were grown for seven days on media containing specified drugs. Figure S2. Effect of *KNL2* depletion on the flowering time.The flowering time of the *knl2* mutant delayed by 10–14 days compared to *Arabidopsis* wild-type. Seeds of the *knl2* mutant and wild-type were germinated under short-day conditions, 8 h light/20° C and 16 h dark/18 °C, for two weeks and then plants were transferred to the cultivation room with long-day conditions, 16 h light/20° C and 8 h dark/18 °C. To demonstrate differences in flowering time between the *knl2* mutant and wild-type, images of plant populations were taken with different time intervals. At early growth stages (14-day-old plants), no obvious phenotypical differences between the Col wild-type and the *knl2* mutant were observed. Figure S3. qRT–PCR validation of RNA-seq results. Eleven genes were selected from the genes differentially expressed in flower buds according to the RNA-seq data analysis. Detailed annotation of the selected genes is presented in Table S2. *At5g02520 corresponds to *KNL2*. Error bars indicate the standard error of three biological replicates in qRT-PCR. Table S1. Results of the RNA-seq study based on the DeSeq2 in Col and the *knl2* mutant line. Conditions: seedlings and flower buds. Table S2. Differentially expressed genes in *knl2* seedlings and their annotation. Table S3. Differentially expressed genes in *knl2* flower buds and their annotation. Table S4. Identification of root-related genes in *knl2* seedlings. Table S5. Overlap between seed-related genes from the SeedGenes Project DB and differentially expressed genes in *knl2* flower buds. Table S6. Selected genes and their primers used for qRT-PCR. Dataset S1. GO terms overrepresented in the *knl2* mutant line. Conditions: seedlings and flower buds. Dataset S2. Overlap between TF from The Plant TF database v.4 and differentially expressed genes in the *knl2* mutant line. Dataset S3. Overlap between flowering-related genes from the database FLOR-ID and differentially expressed genes in the *knl2* mutant line.

Author Contributions: A.B., A.P., and I.L. designed the research. A.B., K.P., and I.L. performed experiments. A.B., A.H., A.F., K.P., A.P., and I.L. analyzed the data. A.B. and I.L. wrote the manuscript. All authors read and approved the final manuscript.

Funding: This research was funded by the Deutsche Forschungsgemeinschaft (LE2299/1–2) and the European Regional Development Fund—Project "MSCAfellow@MUNI" (No. CZ.02.2.69/0.0/0.0/17_050/0008496). A.B. was supported by the Deutsche Forschungsgemeinschaft (HO 1779/30–1). A.H. was supported by the German Federal Ministry of Education and Research (Plant 2030, Project 031B0192NN, HaploTools). A.P. and K.P. were supported by a grant from the Czech grant agency (19–13848S). A.P. was further supported by the ERDF project "Plants as a tool for sustainable global development" (No. CZ.02.1.01/0.0/0.0/16_019/0000827).

Acknowledgments: The authors wish to thank Oda Weiss and Heike Kuhlmann for technical assistance. We are grateful to Axel Himmelbach for the RNA-sequencing performed at the IPK Sequencing laboratory (Gatersleben).

Conflicts of Interest: The authors declare no conflict of interest.

References

1. Talbert, P.B.; Henikoff, S. Phylogeny as the basis for naming histones. *Trends Genet.* **2013**, *29*, 499–500. [CrossRef]
2. Silva, M.C.; Jansen, L.E. At the right place at the right time: Novel CENP-A binding proteins shed light on centromere assembly. *Chromosoma* **2009**, *118*, 567–574. [CrossRef] [PubMed]
3. Talbert, P.B.; Henikoff, S. Transcribing centromeres: Noncoding RNAs and kinetochore assembly. *Trends Genet.* **2018**, *34*, 587–599. [CrossRef] [PubMed]
4. Perea-Resa, C.; Blower, M.D. Centromere biology: Transcription goes on stage. *Mol. Cell Biol.* **2018**, *38*, e00263-18. [CrossRef]

5. Bobkov, G.O.M.; Gilbert, N.; Heun, P. Centromere transcription allows CENP-A to transit from chromatin association to stable incorporation. *J. Cell Biol.* **2018**, *217*, 1957–1972. [CrossRef]
6. Bergmann, J.H.; Rodriguez, M.G.; Martins, N.M.; Kimura, H.; Kelly, D.A.; Masumoto, H.; Larionov, V.; Jansen, L.E.; Earnshaw, W.C. Epigenetic engineering shows H3K4me2 is required for HJURP targeting and CENP-A assembly on a synthetic human kinetochore. *EMBO J.* **2011**, *30*, 328–340. [CrossRef]
7. Kim, I.S.; Lee, M.; Park, K.C.; Jeon, Y.; Park, J.H.; Hwang, E.J.; Jeon, T.I.; Ko, S.; Lee, H.; Baek, S.H.; et al. Roles of Mis18alpha in epigenetic regulation of centromeric chromatin and CENP-A loading. *Mol. Cell* **2012**, *46*, 260–273. [CrossRef]
8. Nardi, I.K.; Zasadzinska, E.; Stellfox, M.E.; Knippler, C.M.; Foltz, D.R. Licensing of centromeric chromatin assembly through the Mis18alpha-Mis18beta heterotetramer. *Mol. Cell* **2016**, *61*, 774–787. [CrossRef]
9. Fujita, Y.; Hayashi, T.; Kiyomitsu, T.; Toyoda, Y.; Kokubu, A.; Obuse, C.; Yanagida, M. Priming of centromere for CENP-A recruitment by human hMis18alpha, hMis18beta, and M18BP1. *Dev. Cell* **2007**, *12*, 17–30. [CrossRef]
10. Maddox, P.S.; Hyndman, F.; Monen, J.; Oegema, K.; Desai, A. Functional genomics identifies a Myb domain-containing protein family required for assembly of CENP-A chromatin. *J. Cell Biol.* **2007**, *176*, 757–763. [CrossRef]
11. Foltz, D.R.; Jansen, L.E.; Bailey, A.O.; Yates, J.R., 3rd; Bassett, E.A.; Wood, S.; Black, B.E.; Cleveland, D.W. Centromere-specific assembly of CENP-a nucleosomes is mediated by HJURP. *Cell* **2009**, *137*, 472–484. [CrossRef] [PubMed]
12. Barnhart, M.C.; Kuich, P.H.; Stellfox, M.E.; Ward, J.A.; Bassett, E.A.; Black, B.E.; Foltz, D.R. HJURP is a CENP-A chromatin assembly factor sufficient to form a functional de novo kinetochore. *J. Cell Biol.* **2011**, *194*, 229–243. [CrossRef] [PubMed]
13. Lermontova, I.; Kuhlmann, M.; Friedel, S.; Rutten, T.; Heckmann, S.; Sandmann, M.; Demidov, D.; Schubert, V.; Schubert, I. Arabidopsis KINETOCHORE NULL2 is an upstream component for centromeric histone H3 variant cenH3 deposition at centromeres. *Plant Cell* **2013**, *25*, 3389–3404. [CrossRef]
14. Sandmann, M.; Talbert, P.; Demidov, D.; Kuhlmann, M.; Rutten, T.; Conrad, U.; Lermontova, I. Targeting of arabidopsis KNL2 to centromeres depends on the conserved CENPC-k motif in Its C terminus. *Plant Cell* **2017**, *29*, 144–155. [CrossRef]
15. Zhang, D.; Martyniuk, C.J.; Trudeau, V.L. SANTA domain: A novel conserved protein module in Eukaryota with potential involvement in chromatin regulation. *Bioinformatics* **2006**, *22*, 2459–2462. [CrossRef]
16. Kral, L. Possible identification of CENP-C in fish and the presence of the CENP-C motif in M18BP1 of vertebrates. *F1000Research* **2015**, *4*, 474. [CrossRef]
17. French, B.T.; Westhorpe, F.G.; Limouse, C.; Straight, A.F. Xenopus laevis M18BP1 directly binds existing CENP-A nucleosomes to promote centromeric chromatin assembly. *Dev. Cell* **2017**, *42*, 190e10–199e10. [CrossRef]
18. Hori, T.; Shang, W.H.; Hara, M.; Ariyoshi, M.; Arimura, Y.; Fujita, R.; Kurumizaka, H.; Fukagawa, T. Association of M18BP1/KNL2 with CENP-A nucleosome is essential for centromere formation in non-mammalian vertebrates. *Dev. Cell* **2017**, *42*, 181e3–189e3. [CrossRef]
19. Liebelt, F.; Jansen, N.S.; Kumar, S.; Gracheva, E.; Claessens, L.A.; Verlaan-de Vries, M.; Willemstein, E.; Vertegaal, A.C.O. The poly-SUMO2/3 protease SENP6 enables assembly of the constitutive centromere-associated network by group deSUMOylation. *Nat. Commun.* **2019**, *10*, 3987. [CrossRef]
20. Silva, M.C.; Bodor, D.L.; Stellfox, M.E.; Martins, N.M.; Hochegger, H.; Foltz, D.R.; Jansen, L.E. Cdk activity couples epigenetic centromere inheritance to cell cycle progression. *Dev. Cell* **2012**, *22*, 52–63. [CrossRef]
21. Love, M.I.; Huber, W.; Anders, S. Moderated estimation of fold change and dispersion for RNA-seq data with DESeq2. *Genome Biol.* **2014**, *15*, 550. [CrossRef] [PubMed]
22. Boyle, E.I.; Weng, S.; Gollub, J.; Jin, H.; Botstein, D.; Cherry, J.M.; Sherlock, G. GO: TermFinder—Open source software for accessing Gene Ontology information and finding significantly enriched Gene Ontology terms associated with a list of genes. *Bioinformatics* **2004**, *20*, 3710–3715. [CrossRef] [PubMed]
23. Buschmann, H.; Lloyd, C.W. Arabidopsis mutants and the network of microtubule-associated functions. *Mol. Plant* **2008**, *1*, 888–898. [CrossRef] [PubMed]

24. Niu, B.; Wang, L.; Zhang, L.; Ren, D.; Ren, R.; Copenhaver, G.P.; Ma, H.; Wang, Y. Arabidopsis cell division cycle 20.1 is required for normal meiotic spindle assembly and chromosome segregation. *Plant Cell* **2015**, *27*, 3367–3382. [CrossRef] [PubMed]
25. Kevei, Z.; Baloban, M.; Da Ines, O.; Tiricz, H.; Kroll, A.; Regulski, K.; Mergaert, P.; Kondorosi, E. Conserved CDC20 cell cycle functions are carried out by two of the five isoforms in Arabidopsis thaliana. *PLoS ONE* **2011**, *6*, e20618. [CrossRef]
26. Bucher, E.; Reinders, J.; Mirouze, M. Epigenetic control of transposon transcription and mobility in Arabidopsis. *Curr. Opin. Plant Biol.* **2012**, *15*, 503–510. [CrossRef]
27. Slotkin, R.K.; Martienssen, R. Transposable elements and the epigenetic regulation of the genome. *Nat. Rev. Genet.* **2007**, *8*, 272–285. [CrossRef]
28. Deniz, O.; Frost, J.M.; Branco, M.R. Regulation of transposable elements by DNA modifications. *Nat. Rev. Genet.* **2019**, *20*, 417–431. [CrossRef]
29. Rangwala, S.H.; Richards, E.J. Differential epigenetic regulation within an Arabidopsis retroposon family. *Genetics* **2007**, *176*, 151–160. [CrossRef]
30. Zhang, M.; Wang, C.; Lin, Q.; Liu, A.; Wang, T.; Feng, X.; Liu, J.; Han, H.; Ma, Y.; Bonea, D.; et al. A tetratricopeptide repeat domain-containing protein SSR1 located in mitochondria is involved in root development and auxin polar transport in Arabidopsis. *Plant J. Cell Mol. Biol.* **2015**, *83*, 582–599. [CrossRef]
31. Munoz-Bertomeu, J.; Cascales-Minana, B.; Mulet, J.M.; Baroja-Fernandez, E.; Pozueta-Romero, J.; Kuhn, J.M.; Segura, J.; Ros, R. Plastidial glyceraldehyde-3-phosphate dehydrogenase deficiency leads to altered root development and affects the sugar and amino acid balance in Arabidopsis. *Plant Physiol.* **2009**, *151*, 541–558. [CrossRef] [PubMed]
32. Garay-Arroyo, A.; Ortiz-Moreno, E.; de la Paz Sanchez, M.; Murphy, A.S.; Garcia-Ponce, B.; Marsch-Martinez, N.; de Folter, S.; Corvera-Poire, A.; Jaimes-Miranda, F.; Pacheco-Escobedo, M.A.; et al. The MADS transcription factor XAL2/AGL14 modulates auxin transport during Arabidopsis root development by regulating PIN expression. *EMBO J.* **2013**, *32*, 2884–2895. [CrossRef] [PubMed]
33. Tapia-Lopez, R.; Garcia-Ponce, B.; Dubrovsky, J.G.; Garay-Arroyo, A.; Perez-Ruiz, R.V.; Kim, S.H.; Acevedo, F.; Pelaz, S.; Alvarez-Buylla, E.R. An AGAMOUS-related MADS-box gene, XAL1 (AGL12), regulates root meristem cell proliferation and flowering transition in Arabidopsis. *Plant Physiol.* **2008**, *146*, 1182–1192. [CrossRef] [PubMed]
34. Yamagishi, K.; Nagata, N.; Yee, K.M.; Braybrook, S.A.; Pelletier, J.; Fujioka, S.; Yoshida, S.; Fischer, R.L.; Goldberg, R.B.; Harada, J.J. TANMEI/EMB2757 encodes a WD repeat protein required for embryo development in Arabidopsis. *Plant Physiol.* **2005**, *139*, 163–173. [CrossRef] [PubMed]
35. Srivastava, R.; Liu, J.X.; Guo, H.; Yin, Y.; Howell, S.H. Regulation and processing of a plant peptide hormone, AtRALF23, in Arabidopsis. *Plant J. Cell Mol. Biol.* **2009**, *59*, 930–939. [CrossRef]
36. Manova, V.; Gruszka, D. DNA damage and repair in plants—From models to crops. *Front. Plant Sci.* **2015**, *6*, 885. [CrossRef]
37. Li, W.; Chen, C.; Markmann-Mulisch, U.; Timofejeva, L.; Schmelzer, E.; Ma, H.; Reiss, B. The Arabidopsis AtRAD51 gene is dispensable for vegetative development but required for meiosis. *Proc. Natl. Acad. Sci. USA* **2004**, *101*, 10596–10601. [CrossRef]
38. Yang, C.; Wang, H.; Xu, Y.; Brinkman, K.L.; Ishiyama, H.; Wong, S.T.; Xu, B. The kinetochore protein Bub1 participates in the DNA damage response. *DNA Repair* **2012**, *11*, 185–191. [CrossRef]
39. Zeitlin, S.G.; Baker, N.M.; Chapados, B.R.; Soutoglou, E.; Wang, J.Y.; Berns, M.W.; Cleveland, D.W. Double-strand DNA breaks recruit the centromeric histone CENP-A. *Proc. Natl. Acad. Sci. USA* **2009**, *106*, 15762–15767. [CrossRef]
40. Jin, J.; Tian, F.; Yang, D.C.; Meng, Y.Q.; Kong, L.; Luo, J.; Gao, G. PlantTFDB 4.0: Toward a central hub for transcription factors and regulatory interactions in plants. *Nucleic Acids Res.* **2017**, *45*, D1040–D1045. [CrossRef]
41. Phukan, U.J.; Jeena, G.S.; Shukla, R.K. WRKY transcription factors: Molecular regulation and stress responses in plants. *Front. Plant Sci.* **2016**, *7*, 760. [CrossRef] [PubMed]

42. Jiang, J.; Ma, S.; Ye, N.; Jiang, M.; Cao, J.; Zhang, J. WRKY transcription factors in plant responses to stresses. *J. Integr. Plant Biol.* **2017**, *59*, 86–101. [CrossRef] [PubMed]
43. Finatto, T.; Viana, V.E.; Woyann, L.G.; Busanello, C.; da Maia, L.C.; de Oliveira, A.C. Can WRKY transcription factors help plants to overcome environmental challenges? *Genet. Mol. Biol.* **2018**, *41*, 533–544. [CrossRef] [PubMed]
44. Suzuki, N.; Rizhsky, L.; Liang, H.; Shuman, J.; Shulaev, V.; Mittler, R. Enhanced tolerance to environmental stress in transgenic plants expressing the transcriptional coactivator multiprotein bridging factor 1c. *Plant Physiol.* **2005**, *139*, 1313–1322. [CrossRef] [PubMed]
45. Chen, J.; Nolan, T.M.; Ye, H.; Zhang, M.; Tong, H.; Xin, P.; Chu, J.; Chu, C.; Li, Z.; Yin, Y. Arabidopsis WRKY46, WRKY54, and WRKY70 transcription factors are involved in brassinosteroid-regulated plant growth and drought responses. *Plant Cell* **2017**, *29*, 1425–1439. [CrossRef] [PubMed]
46. Ding, Z.J.; Yan, J.Y.; Xu, X.Y.; Yu, D.Q.; Li, G.X.; Zhang, S.Q.; Zheng, S.J. Transcription factor WRKY46 regulates osmotic stress responses and stomatal movement independently in Arabidopsis. *Plant J. Cell Mol. Biol.* **2014**, *79*, 13–27. [CrossRef]
47. Sheikh, A.H.; Eschen-Lippold, L.; Pecher, P.; Hoehenwarter, W.; Sinha, A.K.; Scheel, D.; Lee, J. Regulation of WRKY46 transcription factor function by mitogen-activated protein kinases in arabidopsis THALIANA. *Front. Plant Sci.* **2016**, *7*, 61. [CrossRef]
48. Krishnaswamy, S.; Verma, S.; Rahman, M.H.; Kav, N.N. Functional characterization of four APETALA2-family genes (RAP2.6, RAP2.6L, DREB19 and DREB26) in Arabidopsis. *Plant Mol. Biol.* **2011**, *75*, 107–127. [CrossRef]
49. Matias-Hernandez, L.; Aguilar-Jaramillo, A.E.; Marin-Gonzalez, E.; Suarez-Lopez, P.; Pelaz, S. RAV genes: Regulation of floral induction and beyond. *Ann. Bot.* **2014**, *114*, 1459–1470. [CrossRef]
50. Higginson, T.; Li, S.F.; Parish, R.W. AtMYB103 regulates tapetum and trichome development in Arabidopsis thaliana. *Plant J. Cell Mol. Biol.* **2003**, *35*, 177–192. [CrossRef]
51. Adamczyk, B.J.; Fernandez, D.E. MIKC* MADS domain heterodimers are required for pollen maturation and tube growth in Arabidopsis. *Plant Physiol.* **2009**, *149*, 1713–1723. [CrossRef] [PubMed]
52. Verelst, W.; Twell, D.; de Folter, S.; Immink, R.; Saedler, H.; Munster, T. MADS-complexes regulate transcriptome dynamics during pollen maturation. *Genome Biol.* **2007**, *8*, R249. [CrossRef] [PubMed]
53. Smaczniak, C.; Immink, R.G.; Angenent, G.C.; Kaufmann, K. Developmental and evolutionary diversity of plant MADS-domain factors: Insights from recent studies. *Development* **2012**, *139*, 3081–3098. [CrossRef] [PubMed]
54. Perez-Ruiz, R.V.; Garcia-Ponce, B.; Marsch-Martinez, N.; Ugartechea-Chirino, Y.; Villajuana-Bonequi, M.; de Folter, S.; Azpeitia, E.; Davila-Velderrain, J.; Cruz-Sanchez, D.; Garay-Arroyo, A.; et al. XAANTAL2 (AGL14) Is an important component of the complex gene regulatory network that underlies Arabidopsis shoot apical meristem transitions. *Mol. Plant* **2015**, *8*, 796–813. [CrossRef] [PubMed]
55. Smyth, D.R.; Bowman, J.L.; Meyerowitz, E.M. Early flower development in Arabidopsis. *Plant Cell* **1990**, *2*, 755–767.
56. Andrews, S. FastQC A Quality Control tool for High Throughput Sequence Data. Available online: http://www.bioinformatics.babraham.ac.uk/projects/fastqc (accessed on 24 November 2010).
57. Kim, D.; Langmead, B.; Salzberg, S.L. HISAT: A fast spliced aligner with low memory requirements. *Nat. Methods* **2015**, *12*, 357–360. [CrossRef]
58. Liao, Y.; Smyth, G.K.; Shi, W. featureCounts: An efficient general purpose program for assigning sequence reads to genomic features. *Bioinformatics* **2014**, *30*, 923–930. [CrossRef]
59. Benjamini, Y.; Hochberg, Y. Controlling the false discovery rate—A practical and powerful approach to multiple testing. *J. R. Stat. Soc. Ser. B* **1995**, *57*, 289–300. [CrossRef]
60. Bouché, F.; Lobet, G.; Tocquin, P.; Périlleux, C. FLOR-ID: An interactive database of flowering-time gene networks in Arabidopsis thaliana. *Nucleic Acids Res.* **2016**, *44*, D1167–D1171. [CrossRef]
61. Meinke, D.; Muralla, R.; Sweeney, C.; Dickerman, A. Identifying essential genes in Arabidopsis thaliana. *Trends Plant Sci.* **2008**, *13*, 483–491. [CrossRef]

62. Arvidsson, S.; Kwasniewski, M.; Riano-Pachon, D.M.; Mueller-Roeber, B. QuantPrime—A flexible tool for reliable high-throughput primer design for quantitative PCR. *BMC Bioinform.* **2008**, *9*, 465. [CrossRef] [PubMed]
63. Czechowski, T.; Stitt, M.; Altmann, T.; Udvardi, M.K.; Scheible, W.R. Genome-wide identification and testing of superior reference genes for transcript normalization in Arabidopsis. *Plant Physiol.* **2005**, *139*, 5–17. [CrossRef] [PubMed]
64. Livak, K.J.; Schmittgen, T.D. Analysis of relative gene expression data using real-time quantitative PCR and the $2^{-\Delta\Delta CT}$ Method. *Methods* **2001**, *25*, 402–408. [CrossRef] [PubMed]

International Journal of
Molecular Sciences

MDPI

Review

Redox Components: Key Regulators of Epigenetic Modifications in Plants

Saravana Kumar R. M., Yibin Wang, Xiaopan Zhang, Hui Cheng, Lirong Sun, Shibin He * and Fushun Hao *

State Key Laboratory of Cotton Biology, Key Laboratory of Plant Stress Biology, School of Life Sciences, Henan University, Kaifeng 475004, China; saravana80@126.com (S.K.R.M.); 18238213127@163.com (Y.W.); xiaopanzhan@163.com (X.Z.); 15194627687@163.com (H.C.); sunlr9208@henu.edu.cn (L.S.)

* Correspondence: sbhe@henu.edu.cn (S.H.); haofsh@henu.edu.cn (F.H.); Tel.: +86-371-23881387 (F.H.)

Received: 27 November 2019; Accepted: 18 February 2020; Published: 19 February 2020

Abstract: Epigenetic modifications including DNA methylation, histone modifications, and chromatin remodeling are crucial regulators of chromatin architecture and gene expression in plants. Their dynamics are significantly influenced by oxidants, such as reactive oxygen species (ROS) and nitric oxide (NO), and antioxidants, like pyridine nucleotides and glutathione in plants. These redox intermediates regulate the activities and expression of many enzymes involved in DNA methylation, histone methylation and acetylation, and chromatin remodeling, consequently controlling plant growth and development, and responses to diverse environmental stresses. In recent years, much progress has been made in understanding the functional mechanisms of epigenetic modifications and the roles of redox mediators in controlling gene expression in plants. However, the integrated view of the mechanisms for redox regulation of the epigenetic marks is limited. In this review, we summarize recent advances on the roles and mechanisms of redox components in regulating multiple epigenetic modifications, with a focus of the functions of ROS, NO, and multiple antioxidants in plants.

Keywords: epigenetic modifications; DNA methylation; histone modification; chromatin remodeling; redox regulation; reactive oxygen species; nitric oxide; antioxidants

1. Introduction

Epigenetic modifications refer to the mitotically- or meiotically-inheritable changes in gene expression that are not affected by the DNA sequence itself, mainly including DNA methylation, histone modifications, chromatin remodeling, and histone variants in plants and other organisms [1,2]. They can change chromatin architecture, affect DNA accessibility, and gene activity, thereby regulating many molecular processes, like the transcription of genes, and replication, repair, and recombination of DNA [1–4]. They play vital roles in controlling growth and development, including cell differentiation, regeneration, reproduction, flowering, and senescence, and governing plant acclimations to various environmental stimuli, such as pathogen infection, drought, high salinity, extreme temperature, heavy metal stresses [1,3–7]. Most epigenetic modifications are reversible, and under the control of multiple factors including different developmental cues, diverse environmental stresses, phytohormone signals [1,8,9]. Among these, redox components are of great importance [10–12].

Redox components consist of numerous oxidants and antioxidants. In plants, the primary oxidants are reactive oxygen species (ROS), for example, hydrogen peroxide (H_2O_2), superoxide radical ($O_2^{\bullet-}$), singlet oxygen ($^1O_2$), and hydroxyl radicals, and reactive nitrogen species, including nitric oxide (NO), peroxynitrite, nitrogen dioxide radicals. [13]. The main antioxidants include enzymatic antioxidants (e.g., superoxide dismutase (SOD), catalase (CAT), ascorbate peroxidase (APX), glutathione peroxidase (GPX), glutathione reductase (GR)), and nonenzymatic antioxidants (e.g., pyridine nucleotides (NAD(P)H), glutathione (GSH), glutaredoxin (GRX), ascorbate (ASC),

and nicotinamide) [14]. These oxidants and antioxidants are able to spatiotemporally change the redox status and influence redox balance, controlling nearly every aspect of cellular processes such as gene expression, biological metabolisms, growth and development, and adaptations to different environmental stresses in plants [13,15–18].

In recent years, many review papers covering the roles and regulatory mechanisms of epigenetic modifications have been published. The relationship between redox metabolites and some epigenetic modifications has also been discussed [8,10–12,19–22]. However, the functions and mechanisms of redox mediators modulating the epigenetic modifications are not comprehensively summarized. In this review, we provide an integrated view how redox components control the epigenetic marks, with a focus of the roles of ROS, NO, and multiple antioxidants in the regulation of DNA methylation, histone methylation, and histone acetylation in plants.

2. Epigenetic Modifications in Plants

2.1. DNA Methylation

DNA methylation typically means the specific post-replication modification over DNA molecules, in which some cytosine bases are methylated at 5′ position to become 5-methyl-cytosine (^{5m}C). In plants, methylation occurs in the C base of "CG", "CHG", and "CHH" (H represents A, C, or T) contexts [23]. DNA methylation favors the maintenance of genome stability, suppresses gene recombination and mutation, and is essential for the silencing of transposable elements and the regulation of gene expression and splicing [3,24]. DNA methylation inhibits transcriptional initiation, and may have little effect on transcriptional elongation within the gene body [25].

In *Arabidopsis thaliana*, de novo DNA methylation is established through RNA-directed DNA methylation (RdDM) pathway, which involves 21-, 22-, and 24- nt small interfering RNAs (siRNAs) production [3,26,27]. DNA methylation is maintained through three pathways: DNA methyltransferase 1 (MET1) for CG methylation, chromomethylase 3 (CMT3) and CMT2 for CHG methylation, and domain rearranged methyltransferase 2 (DRM2), CMT2, and CMT3 for CHH methylation. The methyl donor is S-adenosyl-l-methionine (SAM) [3,23]. Methyl groups can be removed from DNA through DNA demethylation. Active DNA demethylation is mediated by 5-methylcytosine DNA glycosylases through a DNA base excision repair pathway in plants [3,28]. There exist four 5-methylcytosine DNA glycosylases in *A. thaliana*: repressor of silencing 1 (ROS1), demeter (DME), and Demeter-like 2 (DML2) and DML3 [3,28].

2.2. Histone Methylation and Acetylation

Chromatin is the organized nucleoprotein structure in nuclei where nucleosomes are arranged. Each nucleosome is comprised of two copies of H2A, H2B, H3, and H4 histone molecules, and is wrapped by 145~147 bp double-stranded DNA [29]. The N-terminal tails of histones are subject to various post-translational modifications such as methylation, acetylation, phosphorylation, ubiquitinylation, glycosylation, ADP-ribosylation, and sumoylation. These modifications can alter chromatin structure and gene transcription either by affecting the interaction between histones and the surrounding DNA or by modulating the binding of various regulatory proteins to DNA [1,2,7]. Histone methylation and acetylation have been well characterized. They have wide functions in plant evolution, development, and stress acclimations by facilitating or repressing gene expression [22,30–32].

Histone methylation is confined to lysine and arginine residues located at different positions of histone molecules (H3, H4). The transfer of methyls to histone is catalyzed by histone methyltransferase (HMT) families, which include histone lysine methyltransferases (HKMTs) and protein arginine methyltransferases (PRMTs) [22,33]. The donor of methyl groups for histone methylation is also SAM. On the basis of the number of methyls that occurs over histone molecules, histone methylation can be grouped into mono-, di-, and tri-methylation. Different modifications have distinct effects on gene expression [22,33]. For instance, trimethylation of Lys 27 (H3K27me3) leads to the repression of gene expression whereas trimethylation at Lys 4 (H3K4me3) activates gene transcription in *A. thaliana* [34,35]. Methyl groups can be removed by histone demethylases (HDMs). In plants, HDMs are grouped into lysine-specific demethylase 1 (LSD1) and Jumonji C domain-containing proteins (JMJs). Both enzymes follow different pathways to demethylate histones using different cofactors. LSD1 pertains to flavin-dependent amine oxidase family whereas JMJs belong to 2-oxoglutarate-dependent dioxygenase family [33,36].

Histone acetylation is the covalent modification in which acetyl groups are transferred from acetyl CoA to the epsilon-amino group of the lysine residue in histone molecules. Such modification causes the neutralization of the positive charge of the lysine, weakens the interaction between the modified histone and DNA, thus, chromatin becomes relaxed [22,37]. Acetylated histones can also recruit other proteins, which regulate chromatin structure [38,39]. Generally, hyperacetylation of histones favors transcriptional activation whereas hypoacetylation of histones causes gene repression [22,37,40]. The levels of histone acetylation are regulated by the antagonistic activities of histone acetyltransferases (HATs) and histone deacetylases (HDACs) [1,41]. Plant HATs are divided into four classes, including p300/CREB (cAMP responsive element-binding protein)-binding proteins, TATA-binding protein-associated factors, general control nonrepressible 5-related N-terminal acetyltransferases and MOZ, Ybf2/Sas3, Sas2, and Tip60 proteins [41]. HDACs in plants are grouped into three types: reduced potassium dependency 3/histone deacetylase 1 (RDP3/HDA1), silent information regulator 2 (SIR2), and plant-specific histone deacetylase 2 (HD2). SIR2 family proteins (sirtuins) require NAD^+ as cofactor, and other HDACs use Zn or Fe ion as cofactors. There exist 18 HDAC members in *A. thaliana* [41,42].

2.3. Chromatin Remodeling

The regulated change of chromatin structure is termed as chromatin remodeling. It can be changed not only by covalent modifications of histones and DNA, but also by ATP-dependent chromatin remodelers and other chromatin-associated factors. ATP-dependent chromatin remodelers are able to cause the alteration of nucleosome position, destabilization of nucleosomes or displacement of canonical histones by histone variants [43]. Eukaryotic ATP-dependent chromatin remodelers are evolutionarily conserved protein complexes that typically possess a catalytic core: ATPase/helicase of the switching defective2/sucrose non-fermenting2 (SWI2/SNF2) family. They perform functions using the energy provided by ATP hydrolysis [43,44]. In plants, ATP-dependent chromatin remodelers are divided into four major subfamilies, including SWI/SNF subfamily, imitation switch subfamily, chromodomain helicase DNA-binding (CHD) subfamily, and inositol requiring 80/SWI2-related ATPase 1 subfamily [43,44].

3. Redox Components

3.1. ROS and NO

ROS are byproducts of the aerobic metabolism. They act as crucial signaling molecules to mediate and integrate various growth and environmental signals to control plant development, stomatal movement, and acclimation to diverse biotic and abiotic stresses [13,18,45,46]. ROS are generated in distinct organelles or subcellular compartments like chloroplasts, mitochondria, peroxisomes, and apoplasts under normal, especially stressful conditions [18]. Photosynthesis, photorespiration, and mitochondrial electron transport are major sources of ROS. Plasma membrane NADPH oxidase, also known as respiratory burst oxidase (RBOH), is also a key producer of ROS. RBOH-dependent ROS have been demonstrated to be essential regulators of many cellular processes such as seed germination, root formation, tip growth, flowering, stomatal movement, and adaptations to different environmental stimuli in plants [47–52]. Under normal conditions, the concentrations of ROS in tissues are relatively low, and ROS can act as signal molecules. However, under stresses, ROS accumulation in plants increases. When the levels of ROS exceed certain thresholds, oxidative stress occurs. High levels of ROS damage various biological molecules and cell structure, even causing cell death in plants [18,53].

Similar to that of ROS, production of NO is an inevitable process in plant metabolism. NO is synthesized in different compartments of cells including cytosol, chloroplasts, mitochondria, and peroxisomes [54,55]. NO reductases, nitrate reductases, and nitric oxide synthase-like enzyme have been addressed to be important sources of NO in plants. NO is also a key secondary messenger. It independently or synergistically acts with ROS to regulate a wide range of cellular events including vegetative growth, reproductive development, stomatal opening and closure, and responses to diverse biotic and abiotic stresses [16,20,56]. NO and H_2O_2 can easily enter the nucleus through nuclear pores, and react with nuclear proteins, including histones and transcription factors in plants [15,57,58].

3.2. Enzymatic and Nonenzymatic Antioxidants

Cellular redox status constantly undergoes fluctuations that are balanced by different oxidant and antioxidant systems during plant development and in response to stress cues. Of the enzymatic antioxidants, SOD catalyzes the dismutation of $O_2^{\bullet -}$ into O_2 and H_2O_2. CAT, APX, and GPX convert H_2O_2 into O_2 and H_2O, whereas GR is responsible for the conversion of the oxidized glutathione to the reduced one [59,60]. Of the non-enzymatic antioxidants, NAD(P)H, GSH, and ASC are critical soluble redox carrier molecules. They can interchange between the oxidized and reduced states ($NAD(P)^+$/NAD(P)H, GSSG/GSH, and Asc/DAsc). Their capacity to gain or lose electrons also makes them versatile carriers to alter the activities of many enzymes implicated in numerous important metabolic pathways and cellular events. NAD(P)H is vital for the transmission of redox signals. By supplying reducing equivalents to GSH and ASC through the Asada–Foyer–Halliwell cycle [61], NAD(P)H can process ROS and reactive nitrogen species [60]. GSH and ASC directly interact with H_2O_2, and catalyze the conversion of H_2O_2 to H_2O and O_2. Under oxidative conditions, GSH-GSSG equilibrium shifts towards oxidized glutathione, leading to S-glutathionylation of proteins, an important redox-modification in plants [60,62,63].

4. Redox Regulation of Epigenetic Modifications

4.1. Redox Regulation of DNA Methylation

Accumulating evidence indicates that redox intermediates govern DNA methylation levels and gene transcription in plants. In general, increases in ROS accumulation cause DNA hypomethylation. In tobacco, addition of $O_2^{\bullet-}$ inducer paraquat increases the oxidative stress of cells. The expression of *Glycerophosphodiesterase-Like* (*NtGPDL*) is upregulated, and CG sites in the coding regions of *NtGPDL* are selectively demethylated [64]. Similarly, treatment of tobacco suspension cells with jugalone, a toxic plant secondary metabolite 5-hydroxy-1,4-naphthoquinone, increases the ROS levels in nucleus, nucleolus, cytoplasm, and plasma membrane, accompanied with DNA hypomethylation and programmed cell death (PCD) [65]. Additionally, application of 2,2′-azobis (2-amidinopropane) dihydrochloride, a generator of free radicals, in *Pisum sativum* suspension culture clearly decreases the global DNA methylation levels [66].

Similar to ROS, NO negatively modulates DNA methylation in plants. For instance, treatment of rice seedlings with high concentrations of sodium nitroprusside (SNP, a NO donor) leads to DNA hypomethylation predominantly at the CHG sites, and growth inhibition. In addition, the NO-evoked alterations in DNA methylation can be inherited to the next generation [67]. In another study, application of low concentration of SNP to heat-treated *Lablab purpureus* plants causes the reduction in the levels of $O_2^{\bullet-}$ and H_2O_2 and the alteration of DNA demethylation and methylation levels [68]. Additionally, antioxidant nicotinamide, an essential component of NAD(P)H, has shown to induce DNA hypomethylation in *P. sativum* [66].

In plants, three mechanisms for redox regulation of DNA methylation may exist. One mechanism is redox components modulate the synthesis of methyl donor SAM. In plants, SAM synthesis is catalyzed by S-adenosylhomocysteine hydrolase (SAHH)/homologous gene silencing 1 (HOG1), methionine synthase (MS) and S-adenosyl methionine synthase (SAMS)/methionine adenosyltransferases (MAT) [69] (Figure 1). SAHH, MS and SAMS have been demonstrated to be S-nitrosated after treatment with NO donor S-nitrosoglutathione (GSNO) in *A. thaliana*. Activity assay showed that SAMS1 is reversibly inhibited by GSNO [70]. Also, proteomic studies have shown that many of the enzymes involved in SAM synthesis are targets of S-nitrosation and tyrosine nitration [71–73]; and the activity of SAHH is decreased by tyrosine nitration in sunflower [72].

In the SAM cycle, the precursor of SAM is methionine (Met), which is particularly susceptible to oxidation to methionine sulfoxide (MetSo) under stress conditions (Figure 1). Methionine sulfoxide reductases (MSRs) A and B catalyze the reduction of MetSo back to Met [74]. Accordingly, changes in the levels of NAD(H), NADP(H) and GRXs/thioredoxins (TRXs) may affect DNA methylation through controlling the concentrations of Met in cells. NAD(H) and NADP(H) can prevent Met oxidation. In *A. thaliana*, two MSR genes (*MSRB3* and *MSRB8*) are activated under high levels of NAD(H) and NADP(H), and accompanied with an increase in Met content [75]. GRXs/TRXs can donate electrons to MSRs for the catalysis of MetSo reduction [76]. These indicate that NAD(H), NADP(H), GRXs, and TRXs play important roles during the regeneration of Met; accordingly may modulate DNA methylation (Figure 1).

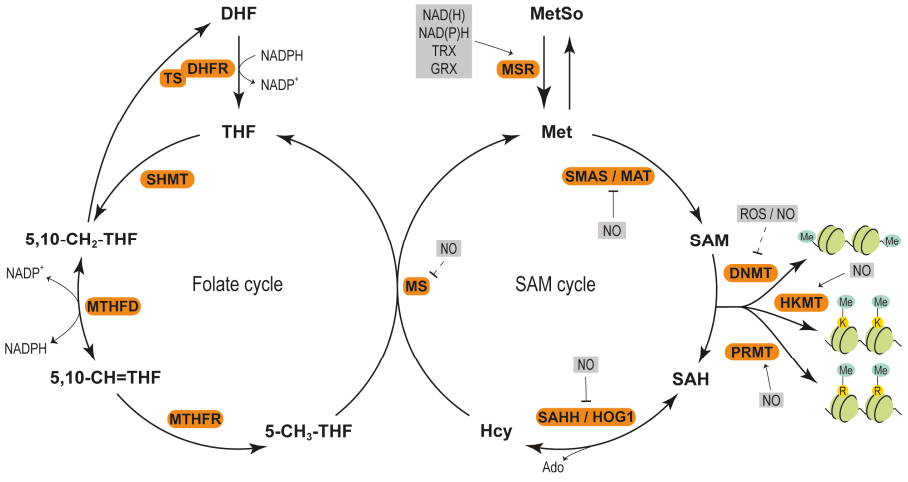

Figure 1. Redox components modulate SAM synthesis through folate cycle in plants. Folate cycle begins with the conversion of DHF to THF through DHFR by utilizing the reducing equivalents from NADPH. Methyls derived from THFs (5,10-CH2-THF, 5,10-CH=THF) are synthesized by SHMT and MTHFD, respectively. 5,10-CH=THF is reduced to 5-CH3-THF by MTHFR. The methyl group from 5-CH3-THF is transferred to Hcy to synthesize Met through MS. The produced Met generates SAM through SAMS. SAM donates methyl groups to DNA or proteins through DNA methyltransferase (DNMT)/HKMT/PRMT, and gets converted to SAH. SAH is further processed to Hcy through SAHH/HOG1. The key enzymes influenced by the cellular redox components are: SAMS/MAT, DNMT/HKMT/PRMT, SAHH/HOG1, MS and MSR. K: lysine; R: arginine; Me: methyl. Dashed lines mean uncharacterized regulation.

Additionally, accumulation of Met is dependent on the metabolism of folate, which provides 5-methyl-tetrahydrofolate (5-CH3-THF) for Met synthesis. In *A. thaliana*, impairment of folate production by sulfamethazine treatment has shown to reduce DNA methylation levels [77]. Folate metabolism can also contribute to the maintenance of redox balance by regulating NADPH production, further modulating DNA methylation in plants [78,79]. As shown in the folate cycle (Figure 1), dihydrofolate reductase-thymidylate synthase (DHFR-TS) is a bifunctional enzyme. Its subunit DHFR is located at the N terminus, and catalyzes the conversion of dihydrofolate (DHF) into tetrahydrofolate (THF) by consuming NADPH. THF and 5,10-CH_2-THF can be interconverted by the enzyme serine hydroxymethyl transferase (SHMT). 5,10-CH_2-THF can also be converted into DHF by TS. Methylenetetrahydrofolate dehydrogenase/methenyltetrahydrofolate cyclohydrolase1 (MTHFD1) is also a bifunctional enzyme, and can convert 5,10-CH_2-THF into 5,10-CH=THF, leading to NADPH formation. Mutation in *MTHFD1* has been demonstrated to disturb folate metabolism and cellular redox state, and lead to loss of DNA methylation in *A. thaliana* [79]. In the *Arabidopsis* genome, three *DHFR-TS* genes exist. DHFR-TS3 inhibits DHFR-TS1 and DHFR-TS2. Overexpression of *DHFR-TS3* leads to decreases of DHFR and MTHFD activities, which in turn cause a drop of NADPH/$NADP^+$ ratio [78], and likely impact DNA methylation. Further, 5,10-CH=THF is converted by methylenetetrahyrofolate reductase (MTHFR) to 5-CH3-THF, which enters the SAM cycle and serves for homocysteine (Hcy) remethylation to Met by MS.

The second mechanism for redox regulation of DNA methylation is that ROS and NO affect the expression and activities of DNA methyltransferases (DNMTs) and DNA demethylases. In *A. thaliana*, ROS mediate the irradiation-triggered DNA demethylation of bystander aerial plants. Irradiation of the roots markedly decreases the expression of *DRM2*, and enhances the transcriptional abundances of *MET1* and *DML3* in bystander aerial plants [80]. Similarly, application of SNP to rice plants induces DNA hypomethylation through down regulation of DNA methyltransferase genes *OsCMT2* and

OsCMT3 and upregulation of the DNA demethylase gene *OsDME* [67]. Yet, it is not clear whether the observed DNA hypomethylation in the SNP-treated plants are due to the regulation of DNA methylase activities or due to the NO-mediated post-translational modification of SAMS.

DNA glycosylases ROS1 and DME have DNA demethylase activity. They catalyze the excision of entire methylated cytosine instead of the methyl group through the base excision repair pathway. ROS1 and DME possess Fe-S cluster assembled structure as their cofactor, and the Fe–S binding motif is essential for their enzymatic activity [81]. Fe-S cluster can gain or lose electrons under different oxidation conditions [82]. Accordingly, redox components may modulate DNA demethylation through impacting the activity of Fe-S cluster assembled DNA demethylases like ROS1 and DEM in plants.

The third mechanism for redox modulation of DNA methylation level is that redox mediators modify the activities of dicer-like4 (DCL4) and RNAse III-like 1 (RTL1), thus affecting the production of siRNAs likely required for DNA methylation through RdDM pathway in plants [83,84]. siRNAs originate from inter- or intramolecular double-stranded RNA (dsRNA) precursors, which are catalyzed by dsRNA-specific endoribonucleases, DCL proteins [85]. In *A. thaliana*, the products of DCL2, DCL3, and DCL4 are 22-, 24- and 21-nt siRNAs, respectively [27,85]. Apart from DCL-mediated dicing activities, RTL1 also influences siRNA production by cleaving the dsRNA before processing by the DCL proteins, and thus acts as a negative regulator of siRNA production [86]. The roles of DCL4 and RTL1 proteins in siRNA production are depicted in Figure 2. In *A. thaliana*, the activity of DCL4 is suppressed by sulfur deficiency. The DCL4 activity can be recovered by supplementation with GSH and TRXs. Moreover, immunopurified DCL4 can be activated by recombinant thioredoxin-h1 with dithiothreitol in vitro, suggesting that DCL4 is under redox regulation. Activation of DCL4 can promote 21-nt siRNA production, and may further promote DNA methylation [83] (Figure 2a). Additionally, Arabidopsis RTL1 has dsRNA binding domains (dsRBD), in which one conserved cysteine (Cys230 in Arabidopsis RTL1) exists. Cys230 has been demonstrated to be crucial for RTL1 cleavage activity. In the presence of GSSG, RTL1 can be glutathionylated at Cys230. Moreover, glutathionylation of RTL1 clearly inhibits its cleavage activity, and the activity of glutathionylated RTL1 can be recovered by two GRX members GRXC1 and GRXC2, indicating that RTL1 is redox regulated (Figure 2b). Moreover, RTL1 negatively regulates siRNA production prior to DCL–mediated cleavage of the siRNA precursors (Figure 2b) [84]. Thus, redox mediators modulate siRNA generation through influencing the activities of DCL4 and RTL1 in plants, and further affect the DNA methylation level.

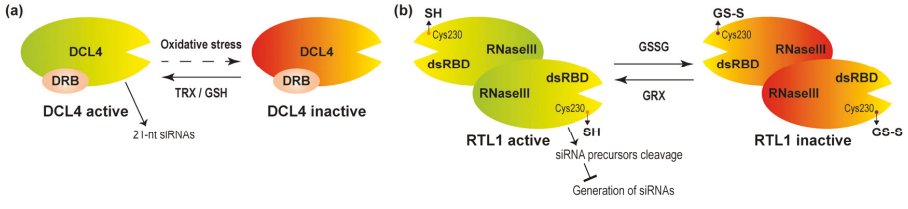

Figure 2. Redox components regulate DCL4 and RTL1 activities. (**a**) Processing of siRNA precursors by DCL4 requires dsRNA-binding protein (DRB), especially DRB4. GSH and TRXs are able to restore DCL4 activity from the inactive state. Activated DCL4 promotes 21 nt siRNA production. (**b**) GSSG/GRXs influence RTL1 activity. RTL1 has RNase III domain and dsRNA binding domains (dsRBD), and acts dimers to perform functions. GSSG treatment results in RTL1 glutathionylation at Cys230 position and inhibits its activity. RTL1 activity is restored by glutaredoxin proteins (GRXs). RTL1 negatively regulates siRNA production prior to DCL–mediated cleavage of the siRNA precursors. The dashed line indicates uncharacterized regulation.

4.2. Redox Adjustment of Histone Methylation

Similar to those of DNA methylation, the methyl groups of histone methylation are also derived from SAM. Thus, redox factors modulating SAM availability also modify histone methylation, as described in the DNA methylation section (Figure 1). In addition to influencing SAM synthesis, redox intermediates also regulate the expression and activity of HMTs and HDMs. For instance, application of S-nitrosocysteine, a NO donor, to *Arabidopsis* leaves upregulates the expression of *Set Domain Group 20*, a gene encoding lysine methyl transferase, and *PcG Histone Methyltransferase Curly Leaf* gene [87], pointing to the important function of NO in modulating the two HMTs. PRMT5 can catalyzes Arg symmetric dimethylation of histones and non-histone proteins in higher eukaryotes [88]. It has been reported that NO positively regulates PRMT5 activity by S-nitrosylation at Cys-125 under NaCl stress in *A. thaliana* [20]. Treatment with NO donor S-nitrosocysteine also prominently promotes JMJs expression in *A. thaliana* [87], implying that JMJs are possibly regulated by NO.

4.3. Redox Regulation of Histone Acetylation

Increasing evidence suggests that redox components regulate histone acetylation through affecting acetyl CoA accumulation. It has been addressed that pyruvate conversion to acetyl CoA is catalyzed by pyruvate dehydrogenase (PDH) complex, which uses NAD^+ as a cofactor for its catalytic activity (Figure 3). Increases in the ratio of NADH to NAD^+ in *Escherchia coli* inhibit PDH activity, and block the acetyl CoA formation [89]. An in vitro study also revealed that elevation in ratio of NADH/NAD^+ is associated with the inhibition of PDH activity in pea [90]. Yet, whether the inhibited PDH activity causes the decreases in levels of acetyl CoA in plants remains to be determined.

Changes in redox reagents also modulate the activities of HATs and HADCs in plants (Figure 3). It has been documented that heat stress promotes the accumulation of $O_2^{\bullet -}$ and induces PCD, followed by histone hyperacetylation due to the elevated expression of genes *HAT-B* and *General Control Nondepressible 5 (GCN5)* in maize seedlings [91]. Dietzel et al. [92] detected the early nuclear target genes of plastidial redox signals in responding to a reduced light-induced signal of the photosynthetic electron transport chain in *A. thaliana*, and found that many nuclear genes are not expressed in the redox compromised state transition 7 (stn7) mutants but expressed in WT. Among these, several are epigenetically regulated. Further studies revealed that the redox signal from chloroplasts of WT rather than stn7 activates the nuclear HAT and HDAC, which promote histone acetylation and deacetylation, respectively [92]. Similarly, *Arabidopsis* mutants accumulated high levels of H_2O_2 (*cat2*) and were defective in GSSG to GSH conversion (*gr1*), showing the differential expression of GCN5-related acetyl transferase gene [93].

In *A. thaliana*, the expression of many pathogensis-related (PR) genes is suppressed by HDA19, which deacetylates the histones on PR protein promoters under nonpathogenic condition. Pathogen attack abolishes HDA19 activity, further resulting in the acetylation of PR protein promoters and increased expression of PR-related genes [94]. Pathogen infection induces oxidative burst at a very early time [95]. Thus, the HDA19 activity affected by pathogen attack is most likely regulated by ROS. Indeed, Liu et al. [96] found that salicylic acid (SA) and flagellin 22 (a bacterial protein) trigger ROS production, leading to the oxidation of HDA9 and HDA19 in *A. thaliana*. The oxidation of the HDACs reduces their activity and further increases the histone acetylation of stress-responsive genes.

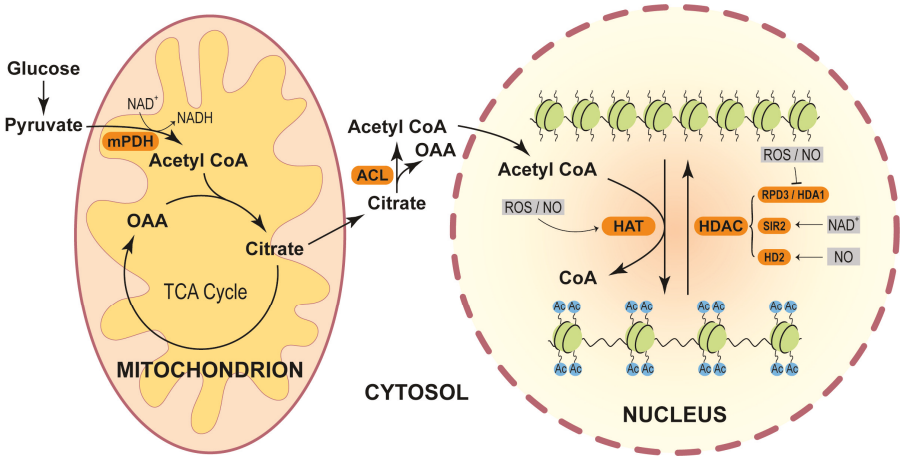

Figure 3. Redox components influence histone acetylations. In the cytoplasm, glucose is broken down to pyruvate, which enters into mitochondria, and is converted to acetyl CoA through mitochondrial pyruvate dehydrogenase (mPDH) by reducing NAD^+. Acetyl CoA combines with oxaloacetate (OAA) produced in the TCA cycle to form citrate, which enters cytoplasm. In cytoplasm, citrate is converted back to OAA and acetyl CoA through ATP-citrate lyase (ACL). Acetyl CoA synthesized in the cytoplasm enters into the nucleus as the source supplier of acetyl group for the histone acetylation process. HAT utilizes the acetyl group from acetyl CoA to introduce acetylation marks (Ac) over the lysine residues of the histone tail, thus weakening the contact between DNA and histone and facilitating gene expression. HDAC removes histone acetyl group, leading to chromatin compaction. Different HAT and HDAC enzymes are affected by ROS, NO, and NAD^+.

In plants, the activities of sirtuin HDACs are dependent on the NAD^+ level and NAD^+/NADH ratio [21]. Thus, oxidative stress alters the redox status of NAD^+, and may further imprint on HDAC activity. In rice, NAD^+-dependent sirtuin OsSRT1 has been reported to play critical roles in suppressing glycolysis by deacetylating histones and glyceraldehyde-3-phosphatedehydrogenase [97]. Redox mediators likely modulate the catalytic activity of OsSRT1 by affecting NAD^+ level.

Mengel et al. [98] found that NO donors GSNO and S-nitroso-N- acetyl-DL-penicillamine and glutathionylating reagent GSSG reversibly suppress HDAC activity in *A. thaliana*. S-nitrosylation has stronger effects than S-glutathionylation on the HDAC activity. In addition, SA has been shown to induce endogenous NO generation, which represses HDAC activity and stimulates histone acetylation [98]. Moreover, GSNO or GSH clearly increases whereas NO scavenger 2-(4-carboxyphenyl)-4,4,5,5-tetramethylimidazoline-1-oxyl-3-oxide decreases acetylation levels of many H3K9/14ac sites, indicating that NO contributes to the GSNO-triggered hyperacetylation. HD2 proteins are plant-specific HDACs. The expression of HD2-like gene *DlHD2* and two ethylene-responsive factor-like genes *DlERF1* and *DlERF2* enhances during longan fruit senescence. Treatment with NO delays the fruit senescence, elevates the transcription of *DlHD2*, but diminishes the expression of *DlERF1* and *DlERF2*. These data imply that NO modulates fruit senescence possibly through affecting the expression of *HD* gene in longan [99]. Additionally, in *A. thaliana*, the HD2 type member HDT2 (histone deacetylase 2) and HDT3 have been identified to be S-nitrosylated [100].

4.4. Redox Affecting Chromatin Remodelers and Other Chromatin-Associated Factors

DNA methylation 1 (DDM1) is an important SWI/SNF2 chromatin remodeler, and can shift nucleosome composition and mediate DNA methylation by allowing MET1, CMT2, and CMT3 to access DNA, especially in heterochromatin regions in plants [101]. Mutation of DDM1 leads to a dramatic decrease in DNA methylation in *A. thaliana* [102]. In rice, exogenous application of SNP results in the downregulation of the expression of *OsDDM1a* and *OsDDM1b*, as well as DNA hypomethylation [67], indicating that NO possibly modulates DNA methylation via impacting chromatin remodeling. PICKLE, a CHD3 remodeler, promotes H3K27me3 in *A. thaliana* [103]. It is identified as a target for tyrosine nitration [73], suggesting that its activity is redox regulated. In *A. thaliana*, topoisomerase VI (Topo VI) A subunit (AtTOP6A), a chromatin-associated factor, has been demonstrated to mediate singlet oxygen signals from the plastid to the nucleus. Under $^1O_2$ accumulation condition, AtTOP6A binds to the promoters of $^1O_2$-responsive *AAA-ATPase* gene and a set of other $^1O_2$-responsive genes, and directly activates the expression of these genes. Topo VI also regulates the transcription of H_2O_2-responsive genes under high light stress. However, changes in the expression of $^1O_2$- and H_2O_2-responsive genes modulated by AtTOP6A are different, suggesting that Topo VI is capable of integrating multiple signals produced by ROS in plants under stress [104].

5. Conclusions

Redox mediators, particularly ROS and NO have been emerging key regulators of chromatin remodeling in plants. They greatly influence not only the transcription and activities of multiple enzymes, catalyzing the addition or removal of methyl and acetyl groups in DNA and histones, but also the biosynthesis and supply of methyl and acetyl donors to DNA and histones. Redox-regulated changes in the epigenetic marks shape chromatin organization, further controlling the expression of many genes and other molecular processes, thereby profoundly affecting plant growth and stress responses. In recent years, much progress has been made on the roles of redox mediators in regulating DNA methylation, and histone modifications in plants. However, many reported actions of redox components on epigenetic marks are indirect effects, and the precise molecular mechanisms underlying the processes are largely unknown. Whether epigenetic modification changes are caused by one oxidant without triggering other antioxidants is also poorly described. Moreover, the research works on redox regulation of other epigenetic marks like phosphorylation, ubiquitinylation, glycosylation, ADP-ribosylation, and sumoylation of histone, chromatin remodeling, and siRNA are quite limited to date.

It has been documented that pathogen attack and diverse abiotic stresses significantly modify epigenetic marks [6,8,9]. ROS, NO and other redox components are also central mediators of these environmental stresses [16,18]. Yet whether the stress triggered chromatin modifications are dominantly mediated by the redox intermediates remains to be determined. Additionally, NADPH oxidase, and multiple antioxidant enzymes contribute to ROS generation and scavenging, respectively, and nitrate reductase and NO synthase-like enzymes are responsible for NO biosynthesis in plants [18,47,54,55]. However, whether these enzymes play important roles in epigenetic modifications is unclear. We believe that these problems will be solved in near future with the rapid development of various biotechnologies, including omics, bioinformatics, and gene editing technologies. We also believe that uncovering the molecular mechanisms for redox control of epigenetic changes will greatly help to understand the strategies of plants adapting to ever-changing environmental conditions, and to facilitate cultivating of elite crop varieties with desired characteristics in the coming days.

Author Contributions: Conceptualization: F.H. and S.H.; writing: S.H., F.H., and S.K.R.M.; visualization: S.K.R.M., H.C., and S.H.; editing: X.Z. and Y.W. L.S. is responsible for editing the MS. All authors have read and agreed to the published version of the manuscript.

Funding: This work was supported by the National Natural Science Foundation of China (31870248 and 31401044), the "111" Project, and the Program for Young Backbone Teachers in Universities of Henan Province (2016GGJS-024).

Conflicts of Interest: The authors declare no conflict of interest.

Abbreviations

ACL	ATP-citrate lyase
APX	Ascorbate peroxidase
ASC	Ascorbate
CAT	Catalase
CHD	Chromodomain helicase DNA-binding
CMT	Chromomethylase
DCL	Dicer-like
DDM1	DNA methylation 1
DHF	Dihydrofolate
DHFR	Dihydrofolate reductase
DME	Demeter
DML	Demeter-like
DNMT	DNA methyltransferase
DRB	dsRNA-binding protein
DRM	Domain rearranged methyltransferase
dsRBD	dsRNA binding domains
GCN5	General Control Nondepressible 5
GPX	Glutathione peroxidase
GR	Glutathione reductase
GRX	Glutaredoxin
GSH	Glutathione
GSNO	S-Nitrosoglutathione
GSSG	Oxidized glutathione
H_2O_2	Hydrogen peroxide
HAT	Histone acetyltransferase
Hcy	Homocysteine
HD2	Histone deacetylase 2
HDAC	Histone deacetylase
HDM	Histone demethylase
HKMT	Histone lysine methyltransferase
HMT	Histone methyltransferase
HDT2	Histone deacetylase 2
JMJ	Jumonji C domain-containing protein
LSD1	Lysine-specific demethylase 1
Met	Methionine
MET1	DNA methyltransferase 1
MetSo	Methionine sulfoxide

MS	Methionine synthase
MSR	Methionine sulfoxide reductase
MTHFD1	Methylenetetrahydrofolate dehydrogenase/methenyltetrahydrofolate cyclohydrolase1
MTHFR	Methylenetetrahyrofolate reductase
NAD(P)H	Pyridine nucleotides
NO	Nitric oxide
OAA	Oxaloacetate
$^1O_2$	Singlet oxygen
$O_2^{\bullet-}$	Superoxide radical
PCD	Programmed cell death
PDH	Pyruvate dehydrogenase
PR	Pathogensis-related
PRMT	Protein arginine methyltransferase
RBOH	Respiratory burst oxidase
RdDM	RNA directed DNA methylation
RDP3/HDA1	Reduced potassium dependency 3/histone deacetylase 1
ROS	Reactive oxygen species
ROS1	Repressor of silencing 1
RTL	RNAse III-like
SA	Salicylic acid
SAM	S-Adenosyl-L-methionine
SAMS/MAT	S-Adenosyl methionine synthase/methionine adenosyl transferases
SAHH/HOG1	S-Adenosylhomocysteine hydrolase/homologous gene gilencing 1
SHMT	Serine hydroxylmethyl transferase
siRNA	Small interfering RNA
SIR2	Silent information regulator 2
SNP	Sodium nitroprusside
SOD	Superoxide dismutase
stn7	State transition 7
SWI/SNF	Switching defective/sucrose non-fermenting
THF	Tetrahydrofolate
Topo VI	Topoisomerase VI
TRX	Thioredoxin
TS	Thymidylate synthase

References

1. Pikaard, C.S.; Mittelsten Scheid, O. Epigenetic regulation in plants. *Cold Spring Harb. Perspect. Biol.* **2014**, *6*, a019315. [CrossRef] [PubMed]
2. Allis, C.; Jenuwein, T. The molecular hallmarks of epigenetic control. *Nat. Rev. Genet.* **2016**, *17*, 487–500. [CrossRef] [PubMed]
3. Zhang, H.M.; Lang, Z.B.; Zhu, J.K. Dynamics and function of DNA methylation in plants. *Nat. Rev. Mol. Cell Biol.* **2018**, *19*, 489–506. [CrossRef] [PubMed]
4. Lebedeva, M.A.; Tvorogova, V.E.; Tikhodeyev, O.N. Epigenetic mechanisms and their role in plant development. *Russ. J. Genet.* **2017**, *53*, 1057–1071. [CrossRef]
5. Lee, K.; Seo, P.J. Dynamic epigenetic changes during plant regeneration. *Trends Plant Sci.* **2018**, *23*, 235–247. [CrossRef]
6. Ramirez-Prado, J.S.; Abulfaraj, A.A.; Rayapuram, N.; Benhamed, M.; Hirt, H. Plant immunity: From signaling to epigenetic control of defense. *Trends Plant Sci.* **2018**, *23*, 833–844. [CrossRef]
7. Chang, Y.N.; Zhu, C.; Jiang, J.; Zhang, H.; Zhu, J.K.; Duan, C.G. Epigenetic regulation in plant abiotic stress responses. *J. Integr. Plant. Biol.* **2019**. [CrossRef]

8. Vriet, C.; Hennig, L.; Laloi, C. Stress-induced chromatin changes in plants: Of memories, metabolites and crop improvement. *Cell. Mol. Life Sci.* **2015**, *72*, 1261–1273. [CrossRef]
9. Yamamuro, C.; Zhu, J.K.; Yang, Z. Epigenetic modifications and plant hormone action. *Mol. Plant* **2016**, *9*, 57–70. [CrossRef]
10. Shen, Y.; Issakidis-Bourguet, E.; Zhou, D.X. Perspectives on the interactions between metabolism, redox, and epigenetics in plants. *J. Exp. Bot.* **2016**, *67*, 5291–5300. [CrossRef]
11. Locato, V.; Cimini, S.; De Gara, L. ROS and redox balance as multifaceted players of cross-tolerance: Epigenetic and retrograde control of gene expression. *J. Exp. Bot.* **2018**, *69*, 3373–3391. [CrossRef] [PubMed]
12. Ageeva-Kieferle, A.; Rudolf, E.E.; Lindermayr, C. Redox-dependent chromatin remodeling: A new function of nitric oxide as architect of chromatin structure in plants. *Front. Plant Sci.* **2019**, *10*, 625. [CrossRef] [PubMed]
13. Del Rio, L.A. ROS and RNS in plant physiology: An overview. *J. Exp. Bot.* **2015**, *66*, 2827–2837. [CrossRef] [PubMed]
14. Gupta, D.K.; Palma, J.M.; Corpas, F.J. *Antioxidants and Antioxidant Enzymes in Higher Plants.*, 1st Ed. ed; Springer International Publishing AG: Gewerbestrasse, Switzerland, 2018; pp. 1–162.
15. He, H.M.; Van Breusegem, F.; Mhamdi, A. Redox-dependent control of nuclear transcription in plants. *J. Exp. Bot.* **2018**, *69*, 3359–3372. [CrossRef]
16. Farnese, F.S.; Menezes-Silva, P.E.; Gusman, G.S.; Oliveira, J.A. When bad guys become good ones: The key role of reactive oxygen species and nitric oxide in the plant response to abiotic stress. *Front. Plant Sci.* **2016**, *7*, 471. [CrossRef]
17. Chan, Z.; Yokawa, K.; Kim, W.Y.; Song, C.P. ROS regulation during plant abiotic stress responses. *Front. Plant Sci.* **2016**, *7*, 1536. [CrossRef]
18. Waszczak, C.; Carmody, M.; Kangasjarvi, J. Reactive oxygen species in plant signaling. *Annu. Rev. Plant Biol.* **2018**, *69*, 209–236. [CrossRef]
19. Shen, Y.; Wei, W.; Zhou, D.X. Histone acetylation enzymes coordinate metabolism and gene expression. *Trends Plant Sci.* **2015**, *20*, 614–621. [CrossRef]
20. Hu, J.L.; Yang, H.J.; Mu, J.Y.; Lu, T.C.; Peng, J.L.; Deng, X.; Kong, Z.S.; Bao, S.L.; Cao, X.F.; Zuo, J.R. Nitric oxide regulates protein methylation during stress responses in plants. *Mol. Cell* **2017**, *67*, 702–710. [CrossRef]
21. Hu, Y.; Lu, Y.; Zhao, Y.; Zhou, D.X. Histone acetylation dynamics integrates metabolic activity to regulate plant response to stress. *Front. Plant Sci.* **2019**, *10*, 1236. [CrossRef]
22. Zhao, T.; Zhan, Z.; Jiang, D. Histone modifications and their regulatory roles in plant development and environmental memory. *J. Genet. Genom.* **2019**. [CrossRef] [PubMed]
23. Law, J.A.; Jacobsen, S.E. Establishing, maintaining and modifying DNA methylation patterns in plants and animals. *Nat. Rev. Genet.* **2010**, *11*, 204–220. [CrossRef] [PubMed]
24. Bartels, A.; Han, Q.; Nair, P.; Stacey, L.; Gaynier, H.; Mosley, M.; Huang, Q.Q.; Pearson, J.K.; Hsieh, T.F.; An, Y.Q.C.; et al. Dynamic DNA methylation in plant growth and development. *Int. J. Mol. Sci.* **2018**, *19*, 2144. [CrossRef] [PubMed]
25. Bewick, A.J.; Schmitz, R.J. Gene body DNA methylation in plants. *Curr. Opin. Plant Biol.* **2017**, *36*, 103–110. [CrossRef]
26. Matzke, M.A.; Mosher, R.A. RNA-directed DNA methylation: An epigenetic pathway of increasing complexity. *Nat. Rev. Genet.* **2014**, *15*, 394–408. [CrossRef]
27. Cuerda-Gil, D.; Slotkin, R.K. Non-canonical RNA-directed DNA methylation. *Nat. Plants* **2016**, *2*, 16163. [CrossRef]
28. Parrilla-Doblas, J.T.; Roldan-Arjona, T.; Ariza, R.R.; Cordoba-Canero, D. Active DNA demethylation in plants. *Int. J. Mol. Sci.* **2019**, *20*, 4683. [CrossRef]

29. Luger, K.; Mader, A.W.; Richmond, R.K.; Sargent, D.F.; Richmond, T.J. Crystal structure of the nucleosome core particle at 2.8 Å resolution. *Nature* **1997**, *389*, 251–260.
30. Ueda, M.; Seki, M. Histone modifications form epigenetic regulatory networks to regulate abiotic stress response. *Plant Physiol.* **2020**, *182*, 15–26. [CrossRef]
31. He, S.B.; Yan, S.H.; Wang, P.; Zhu, W.; Wang, X.W.; Shen, Y.; Shao, K.J.; Xin, H.P.; Li, S.H.; Li, L.J. Comparative analysis of genome-wide chromosomal histone modification patterns in maize cultivars and their wild relatives. *PLoS ONE* **2014**, *9*, e97364. [CrossRef]
32. Tan, J.; He, S.; Yan, S.; Li, Y.; Li, H.; Zhang, H.; Zhao, L.; Li, L. Exogenous EDDS modifies copper-induced various toxic responses in rice. *Protoplasma* **2014**, *251*, 1213–1221. [CrossRef]
33. Liu, C.Y.; Lu, F.L.; Cui, X.; Cao, X.F. Histone methylation in higher plants. *Annu. Rev. Plant Biol.* **2010**, *61*, 395–420. [CrossRef] [PubMed]
34. Zheng, B.; Chen, X. Dynamics of histone H3 lysine 27 trimethylation in plant development. *Curr. Opin. Plant Biol.* **2011**, *14*, 123–129. [CrossRef] [PubMed]
35. Berr, A.; Shafiq, S.; Shen, W.H. Histone modifications in transcriptional activation during plant development. *BBA-Gene Regul. Mech.* **2011**, *1809*, 567–576.
36. Xiao, J.; Lee, U.S.; Wagner, D. Tug of war: Adding and removing histone lysine methylation in *Arabidopsis*. *Curr. Opin. Plant Biol.* **2016**, *34*, 41–53. [CrossRef] [PubMed]
37. Marmorstein, R.; Zhou, M.M. Writers and readers of histone acetylation: Structure, mechanism, and inhibition. *Cold Spring Harbor Perspect. Biol.* **2014**, *6*, a018762. [CrossRef] [PubMed]
38. Zhang, C.J.; Hou, X.M.; Tan, L.M.; Shao, C.R.; Huang, H.W.; Li, Y.Q.; Li, L.; Cai, T.; Chen, S.; He, X.J. The Arabidopsis acetylated histone-binding protein BRAT1 forms a complex with BRP1 and prevents transcriptional silencing. *Nat. Commun.* **2016**, *7*, 11715. [CrossRef]
39. Nie, W.F.; Lei, M.; Zhang, M.; Tang, K.; Huang, H.; Zhang, C.; Miki, D.; Liu, P.; Yang, Y.; Wang, X.; et al. Histone acetylation recruits the SWR1 complex to regulate active DNA demethylation in Arabidopsis. *Proc. Natl. Acad. Sci. USA* **2019**, *116*, 16641–16650. [CrossRef]
40. Zhang, H.; Yue, M.; Zheng, X.; Gautam, M.; He, S.; Li, L. The role of promoter-associated histone acetylation of *Haem Oxygenase-1 (HO-1)* and *Giberellic Acid-Stimulated Like-1 (GSL-1)* genes in heat-induced lateral root primordium inhibition in maize. *Front. Plant Sci.* **2018**, *9*, 1520. [CrossRef]
41. Pandey, R.; Muller, A.; Napoli, C.A.; Selinger, D.A.; Pikaard, C.S.; Richards, E.J.; Bender, J.; Mount, D.W.; Jorgensen, R.A. Analysis of histone acetyltransferase and histone deacetylase families of *Arabidopsis thaliana* suggests functional diversification of chromatin modification among multicellular eukaryotes. *Nucleic Acids Res.* **2002**, *30*, 5036–5055. [CrossRef]
42. Chen, X.; Ding, A.B.; Zhong, X. Functions and mechanisms of plant histone deacetylases. *Sci. China Life Sci.* **2020**, *63*, 206–216. [CrossRef]
43. Ojolo, S.P.; Cao, S.; Priyadarshani, S.V.G.N.; Li, W.; Yan, M.; Aslam, M.; Zhao, H.; Qin, Y. Regulation of plant growth and development: A review from a chromatin remodeling perspective. *Front. Plant Sci.* **2018**, *9*, 1232. [CrossRef]
44. Han, S.K.; Wu, M.F.; Cui, S.; Wagner, D. Roles and activities of chromatin remodeling ATPases in plants. *Plant J.* **2015**, *83*, 62–77. [CrossRef] [PubMed]
45. Song, Y.; Miao, Y.; Song, C.P. Behind the scenes: The roles of reactive oxygen species in guard cells. *New Phytol.* **2014**, *201*, 1121–1140. [CrossRef] [PubMed]
46. Qi, J.; Song, C.P.; Wang, B.; Zhou, J.; Kangasjärvi, J.; Zhu, J.K.; Gong, Z. Reactive oxygen species signaling and stomatal movement in plant responses to drought stress and pathogen attack. *J. Integr. Plant Biol.* **2018**, *60*, 67–88.
47. Marino, D.; Dunand, C.; Puppo, A.; Pauly, N. A burst of plant NADPH oxidases. *Trends Plant Sci.* **2012**, *17*, 9–15. [CrossRef] [PubMed]

48. Ma, L.Y.; Zhang, H.; Sun, L.R.; Jiao, Y.H.; Zhang, G.Z.; Miao, C.; Hao, F.S. NADPH oxidase AtrbohD and AtrbohF function in ROS-dependent regulation of Na^+/K^+ homeostasis in *Arabidopsis* under salt stress. *J. Exp. Bot.* **2012**, *63*, 305–317. [CrossRef]
49. Jiao, Y.H.; Sun, L.R.; Song, Y.L.; Wang, L.M.; Liu, L.P.; Zhang, L.Y.; Liu, B.; Li, N.; Miao, C.; Hao, F.S. AtrbohD and AtrbohF positively regulate abscisic acid-inhibited primary root growth by affecting Ca^{2+} signalling and auxin response of roots in *Arabidopsis*. *J. Exp. Bot.* **2013**, *64*, 4183–4192. [CrossRef]
50. Li, N.; Sun, L.R.; Zhang, L.Y.; Song, Y.L.; Hu, P.P.; Li, C.; Hao, F.S. AtrbohD and AtrbohF negatively regulate lateral root development by changing the localized accumulation of superoxide in primary roots of *Arabidopsis*. *Planta* **2015**, *241*, 591–602. [CrossRef]
51. Chen, Q.; Yang, G. Signal function studies of ROS, especially RBOH dependent ROS, in plant growth, development and environmental stress. *J. Plant Growth Regul.* **2019**. [CrossRef]
52. Sun, L.; Zhao, Z.J.; Hao, F.S. NADPH oxidases, essential players of hormone signalings in plant development and response to stresses. *Plant Signal. Behav.* **2019**, *14*, 1657343. [CrossRef]
53. Czarnocka, W.; Karpinski, S. Friend or foe? Reactive oxygen species production, scavenging and signaling in plant response to environmental stresses. *Free Radic. Biol. Med.* **2018**, *122*, 4–20. [CrossRef]
54. Kolbert, Z.; Barroso, J.B.; Brouquisse, R.; Corpas, F.J.; Gupta, K.J.; Lindermayr, C.; Loake, G.J.; Palma, J.M.; Petřivalský, M.; Wendehenne, D.; et al. A forty year journey: The generation and roles of NO in plants. *Nitric Oxide.* **2019**. [CrossRef]
55. Del Castello, F.; Nejamkin, A.; Cassia, R.; Correa-Aragunde, N.; Fernández, B.; Foresi, N.; Lombardo, C.; Ramirez, L.; Lamattina, L. The era of nitric oxide in plant biology: Twenty years tying up loose ends. *Nitric Oxide.* **2019**, *85*, 17–27. [CrossRef]
56. Sun, L.R.; Yue, C.M.; Hao, F.S. Update on roles of nitric oxide in regulating stomatal closure. *Plant Signal. Behav.* **2019**, *14*, e1649569. [CrossRef] [PubMed]
57. Mengel, A.; Chaki, M.; Shekariesfahlan, A.; Lindermayr, C. Effect of nitric oxide on gene transcription—S-nitrosylation of nuclear proteins. *Front. Plant Sci.* **2013**, *4*, 293. [CrossRef] [PubMed]
58. Martins, L.; Trujillo-Hernandez, J.A.; Reichheld, J.P. Thiol based redox signaling in plant nucleus. *Front. Plant Sci.* **2018**, *9*, 705. [CrossRef] [PubMed]
59. Foyer, C.H.; Noctor, G. Redox signaling in plants. *Antioxid. Redox Signal.* **2013**, *18*, 2087–2090. [CrossRef]
60. Soares, C.; Carvalho, M.E.A.; Azevedo, R.A.; Fidalgo, F. Plants facing oxidative challenges-A little help from the antioxidant networks. *Environ. Exp. Bot.* **2019**, *161*, 4–25. [CrossRef]
61. Foyer, C.H.; Halliwell, B. The presence of glutathione and glutathione reductase in chloroplasts: A proposed role in ascorbic acid metabolism. *Planta* **1976**, *133*, 21–25. [CrossRef]
62. Dalle-Donne, I.; Rossi, R.; Colombo, G.; Giustarini, D.; Milzani, A. Protein S-glutathionylation: A regulatory device from bacteria to humans. *Trends Biochem. Sci.* **2009**, *34*, 85–96. [CrossRef]
63. Zaffagnini, M.; Fermani, S.; Marchand, C.H.; Costa, A.; Sparla, F.; Rouhier, N.; Geigenberger, P.; Lemaire, S.D.; Trost, P. Redox homeostasis in photosynthetic organisms: Novel and established thiol-based molecular mechanisms. *Antioxid. Redox Signal.* **2019**, *31*, 155–210. [CrossRef]
64. Choi, C.S.; Sano, H. Abiotic-stress induces demethylation and transcriptional activation of a gene encoding a glycerophosphodiesterase-like protein in tobacco plants. *Mol. Genet. Genom.* **2007**, *277*, 589–600. [CrossRef]
65. Poborilova, Z.; Ohlsson, A.B.; Berglund, T.; Vildova, A.; Provaznik, I.; Babula, P. DNA hypomethylation concomitant with the overproduction of ROS induced by naphthoquinone juglone on tobacco BY-2 suspension cells. *Environ. Exp. Bot.* **2015**, *113*, 28–39. [CrossRef]
66. Berglund, T.; Wallstrom, A.; Nguyen, T.V.; Laurell, C.; Ohlsson, A.B. Nicotinamide; antioxidative and DNA hypomethylation effects in plant cells. *Plant Physiol. Biochem.* **2017**, *118*, 551–560. [CrossRef] [PubMed]
67. Ou, X.F.; Zhuang, T.T.; Yin, W.C.; Miao, Y.L.; Wang, B.; Zhang, Y.H.; Lin, X.Y.; Xu, C.M.; von Wettstein, D.; Rustgi, S.; et al. DNA methylation changes induced in rice by exposure to high concentrations of the nitric oxide modulator, sodium nitroprusside. *Plant Mol. Biol. Rep.* **2015**, *33*, 1428–1440. [CrossRef]

68. Rai, K.K.; Rai, N.; Rai, S.P. Salicylic acid and nitric oxide alleviate high temperature induced oxidative damage in *Lablab purpureus* L plants by regulating bio-physical processes and DNA methylation. *Plant Physiol. Biochem.* **2018**, *128*, 72–88. [CrossRef] [PubMed]
69. Rahikainen, M.; Alegre, S.; Trotta, A.; Pascual, J.; Kangasjarvi, S. Trans-methylation reactions in plants: Focus on the activated methyl cycle. *Physiol. Plant* **2018**, *162*, 162–176. [CrossRef]
70. Lindermayr, C.; Saalbach, G.; Durner, J. Proteomic identification of S-nitrosylated proteins in Arabidopsis. *Plant Physiol.* **2005**, *137*, 921–930. [CrossRef]
71. Puyaubert, J.; Fares, A.; Reze, N.; Peltier, J.B.; Baudouin, E. Identification of endogenously S-nitrosylated proteins in Arabidopsis plantlets: Effect of cold stress on cysteine nitrosylation level. *Plant Sci.* **2014**, *215–216*, 150–156.
72. Chaki, M.; Valderrama, R.; Fernandez-Ocana, A.M.; Carreras, A.; Lopez-Jaramillo, J.; Luque, F.; Palma, J.M.; Pedrajas, J.R.; Begara-Morales, J.C.; Sanchez-Calvo, B.; et al. Protein targets of tyrosine nitration in sunflower (*Helianthus annuus* L.) hypocotyls. *J. Exp. Bot.* **2009**, *60*, 4221–4234.
73. Lozano-Juste, J.; Colom-Moreno, R.; Leon, J. In vivo protein tyrosine nitration in *Arabidopsis thaliana*. *J. Exp. Bot.* **2011**, *62*, 3501–3517. [CrossRef]
74. Rouhier, N.; Vieira Dos Santos, C.; Tarrago, L.; Rey, P. Plant methionine sulfoxide reductase A and B multigenic families. *Photosynth. Res.* **2006**, *89*, 247–262. [CrossRef]
75. Petriacq, P.; de Bont, L.; Hager, J.; Didierlaurent, L.; Mauve, C.; Guerard, F.; Noctor, G.; Pelletier, S.; Renou, J.P.; Tcherkez, G.; et al. Inducible NAD overproduction in Arabidopsis alters metabolic pools and gene expression correlated with increased salicylate content and resistance to *Pst-AvrRpm1*. *Plant J.* **2012**, *70*, 650–665. [CrossRef]
76. Dos Santos, C.V.; Laugier, E.; Tarrago, L.; Massot, V.; Issakidis-Bourguet, E.; Rouhier, N.; Rey, P. Specificity of thioredoxins and glutaredoxins as electron donors to two distinct classes of Arabidopsis plastidial methionine sulfoxide reductases B. *FEBS Lett.* **2007**, *581*, 4371–4376. [CrossRef]
77. Zhang, H.M.; Deng, X.Y.; Miki, D.; Cutler, S.; La, H.G.; Hou, Y.J.; Oh, J.; Zhu, J.K. Sulfamethazine suppresses epigenetic silencing in Arabidopsis by impairing folate synthesis. *Plant Cell* **2012**, *24*, 1230–1241. [CrossRef]
78. Gorelova, V.; De Lepeleire, J.; Van Daele, J.; Pluim, D.; Mei, C.; Cuypers, A.; Leroux, O.; Rebeille, F.; Schellens, J.H.M.; Blancquaert, D.; et al. Dihydrofolate reductase/thymidylate synthase fine-tunes the folate status and controls redox homeostasis in plants. *Plant Cell* **2017**, *29*, 2831–2853. [CrossRef] [PubMed]
79. Groth, M.; Moissiard, G.; Wirtz, M.; Wang, H.F.; Garcia-Salinas, C.; Ramos-Parra, P.A.; Bischof, S.; Feng, S.H.; Cokus, S.J.; John, A.; et al. MTHFD1 controls DNA methylation in *Arabidopsis*. *Nat. Commun.* **2016**, *7*, 11640. [CrossRef] [PubMed]
80. Xu, W.; Wang, T.; Xu, S.Y.; Xu, S.X.; Wu, L.J.; Wu, Y.J.; Bian, P. Radiation-induced epigenetic bystander effects demonstrated in *Arabidopsis Thaliana*. *Radiat. Res.* **2015**, *183*, 511–524. [CrossRef] [PubMed]
81. Duan, C.G.; Wang, X.G.; Tang, K.; Zhang, H.M.; Mangrauthia, S.K.; Lei, M.G.; Hsu, C.C.; Hou, Y.J.; Wang, C.G.; Li, Y.; et al. MET18 connects the cytosolic iron-sulfur cluster assembly pathway to active DNA demethylation in *Arabidopsis*. *PLoS Genet.* **2015**, *11*, e1005559. [CrossRef]
82. Couturier, J.; Chibani, K.; Jacquot, J.P.; Rouhier, N. Cysteine-based redox regulation and signaling in plants. *Front. Plant Sci.* **2013**, *4*, 105. [CrossRef]
83. Seta, A.; Tabara, M.; Nishibori, Y.; Hiraguri, A.; Ohkama-Ohtsu, N.; Yokoyama, T.; Hara, S.; Yoshida, K.; Hisabori, T.; Fukudome, A.; et al. Post-translational regulation of the dicing activities of Arabidopsis DICER-LIKE 3 and 4 by inorganic phosphate and the redox state. *Plant Cell Physiol.* **2017**, *58*, 485–495. [CrossRef]
84. Charbonnel, C.; Niazi, A.K.; Elvira-Matelot, E.; Nowak, E.; Zytnicki, M.; de Bures, A.; Jobet, E.; Opsomer, A.; Shamandi, N.; Nowotny, M.; et al. The siRNA suppressor RTL1 is redox-regulated through glutathionylation of a conserved cysteine in the double-stranded-RNA-binding domain. *Nucleic Acids Res.* **2017**, *45*, 11891–11907. [CrossRef]

85. Fukudome, A.; Fukuhara, T. Plant dicer-like proteins: Double-stranded RNA-cleaving enzymes for small RNA biogenesis. *J. Plant Res.* **2017**, *130*, 33–44. [CrossRef]
86. Shamandi, N.; Zytnicki, M.; Charbonnel, C.; Elvira-Matelot, E.; Bochnakian, A.; Comella, P.; Mallory, A.C.; Lepere, G.; Saez-Vasquez, J.; Vaucheret, H. Plants encode a general siRNA suppressor that is induced and suppressed by viruses. *PLoS Biol.* **2015**, *13*, e1002326. [CrossRef]
87. Hussain, A.; Mun, B.G.; Imran, Q.M.; Lee, S.U.; Adamu, T.A.; Shahid, M.; Kim, K.M.; Yun, B.W. Nitric oxide mediated transcriptome profiling reveals activation of multiple regulatory pathways in *Arabidopsis thaliana*. *Front. Plant Sci.* **2016**, *7*, 975. [CrossRef]
88. Blanc, R.S.; Richard, S. Arginine methylation: The coming of age. *Mol. Cell* **2017**, *65*, 8–24. [CrossRef]
89. Ojima, Y.; Suryadarma, P.; Tsuchida, K.; Taya, M. Accumulation of pyruvate by changing the redox status in *Escherichia coli*. *Biotechnol. Lett.* **2012**, *34*, 889–893. [CrossRef]
90. Miernyk, J.A.; Randall, D.D. Some kinetic and regulatory properties of the pea mitochondrial pyruvate dehydrogenase complex. *Plant Physiol.* **1987**, *83*, 306–310. [CrossRef]
91. Wang, P.; Zhao, L.; Hou, H.L.; Zhang, H.; Huang, Y.; Wang, Y.P.; Li, H.; Gao, F.; Yan, S.H.; Li, L.J. Epigenetic changes are associated with programmed cell death induced by heat stress in seedling leaves of *Zea mays*. *Plant Cell Physiol.* **2015**, *56*, 965–976. [CrossRef]
92. Dietzel, L.; Glasser, C.; Liebers, M.; Hiekel, S.; Courtois, F.; Czarnecki, O.; Schlicke, H.; Yan, Z.B.; Borner, T.; Mayer, K.; et al. Identification of early nuclear target genes of plastidial redox signals that trigger the long-term response of *Arabidopsis* to light quality shifts. *Mol. Plant* **2015**, *8*, 1237–1252. [CrossRef]
93. Mhamdi, A.; Hager, J.; Chaouch, S.; Queval, G.; Han, Y.; Taconnat, L.; Saindrenan, P.; Gouia, H.; Issakidis-Bourguet, E.; Renou, J.P.; et al. Arabidopsis GLUTATHIONE REDUCTASE1 plays a crucial role in leaf responses to intracellular hydrogen peroxide and in ensuring appropriate gene expression through both salicylic acid and jasmonic acid signaling pathways. *Plant Physiol.* **2010**, *153*, 1144–1160. [CrossRef]
94. Choi, S.M.; Song, H.R.; Han, S.K.; Han, M.; Kim, C.Y.; Park, J.; Lee, Y.H.; Jeon, J.S.; Noh, Y.S.; Noh, B. HDA19 is required for the repression of salicylic acid biosynthesis and salicylic acid-mediated defense responses in Arabidopsis. *Plant J.* **2012**, *71*, 135–146. [CrossRef]
95. Wojtaszek, P. Oxidative burst: An early plant response to pathogen infection. *Biochem. J.* **1997**, *322*, 681–692. [CrossRef]
96. Liu, P.; Zhang, H.; Yu, B.; Xiong, L.; Xia, Y. Proteomic identification of early salicylate- and flg22-responsive redox-sensitive proteins in Arabidopsis. *Sci. Rep.* **2015**, *5*, 8625. [CrossRef]
97. Zhang, H.; Zhao, Y.; Zhou, D.X. Rice NAD^+-dependent histone deacetylase OsSRT1 represses glycolysis and regulates the moonlighting function of GAPDH as a transcriptional activator of glycolytic genes. *Nucleic Acids Res.* **2017**, *45*, 12241–12255. [CrossRef]
98. Mengel, A.; Ageeva, A.; Georgii, E.; Bernhardt, J.; Wu, K.; Durner, J.; Lindermayr, C. Nitric oxide modulates histone acetylation at stress genes by inhibition of histone deacetylases. *Plant Physiol.* **2017**, *173*, 1434–1452. [CrossRef]
99. Kuang, J.F.; Chen, J.Y.; Luo, M.; Wu, K.Q.; Sun, W.; Jiang, Y.M.; Lu, W.J. Histone deacetylase HD2 interacts with ERF1 and is involved in longan fruit senescence. *J. Exp. Bot.* **2012**, *63*, 441–454. [CrossRef]
100. Chaki, M.; Shekariesfahlan, A.; Ageeva, A.; Mengel, A.; von Toerne, C.; Durner, J.; Lindermayr, C. Identification of nuclear target proteins for S-nitrosylation in pathogen-treated *Arabidopsis thaliana* cell cultures. *Plant Sci.* **2015**, *238*, 115–126. [CrossRef]
101. Zemach, A.; Kim, M.Y.; Hsieh, P.H.; Coleman-Derr, D.; Eshed-Williams, L.; Thao, K.; Harmer, S.L.; Zilberman, D. The Arabidopsis nucleosome remodeler DDM1 allows DNA methyltransferases to access H1-containing heterochromatin. *Cell* **2013**, *153*, 193–205. [CrossRef]
102. Jeddeloh, J.A.; Stokes, T.L.; Richards, E.J. Maintenance of genomic methylation requires a SWI2/SNF2-like protein. *Nat. Genet.* **1999**, *22*, 94–97. [CrossRef]

103. Ho, K.K.; Zhang, H.; Golden, B.L.; Ogas, J. PICKLE is a CHD subfamily II ATP-dependent chromatin remodeling factor. *Biochim. Biophys. Acta* **2012**, *1829*, 199–210. [CrossRef]
104. Simkova, K.; Moreau, F.; Pawlak, P.; Vriet, C.; Baruah, A.; Alexandre, C.; Hennig, L.; Apel, K.; Laloi, C. Integration of stress-related and reactive oxygen species-mediated signals by Topoisomerase VI in *Arabidopsis thaliana*. *Proc. Natl. Acad. Sci. USA* **2012**, *109*, 16360–16365. [CrossRef]

MDPI
St. Alban-Anlage 66
4052 Basel
Switzerland
Tel. +41 61 683 77 34
Fax +41 61 302 89 18
www.mdpi.com

International Journal of Molecular Sciences Editorial Office
E-mail: ijms@mdpi.com
www.mdpi.com/journal/ijms

MDPI
St. Alban-Anlage 66
4052 Basel
Switzerland

Tel: +41 61 683 77 34
Fax: +41 61 302 89 18

www.mdpi.com

ISBN 978-3-03936-029-1